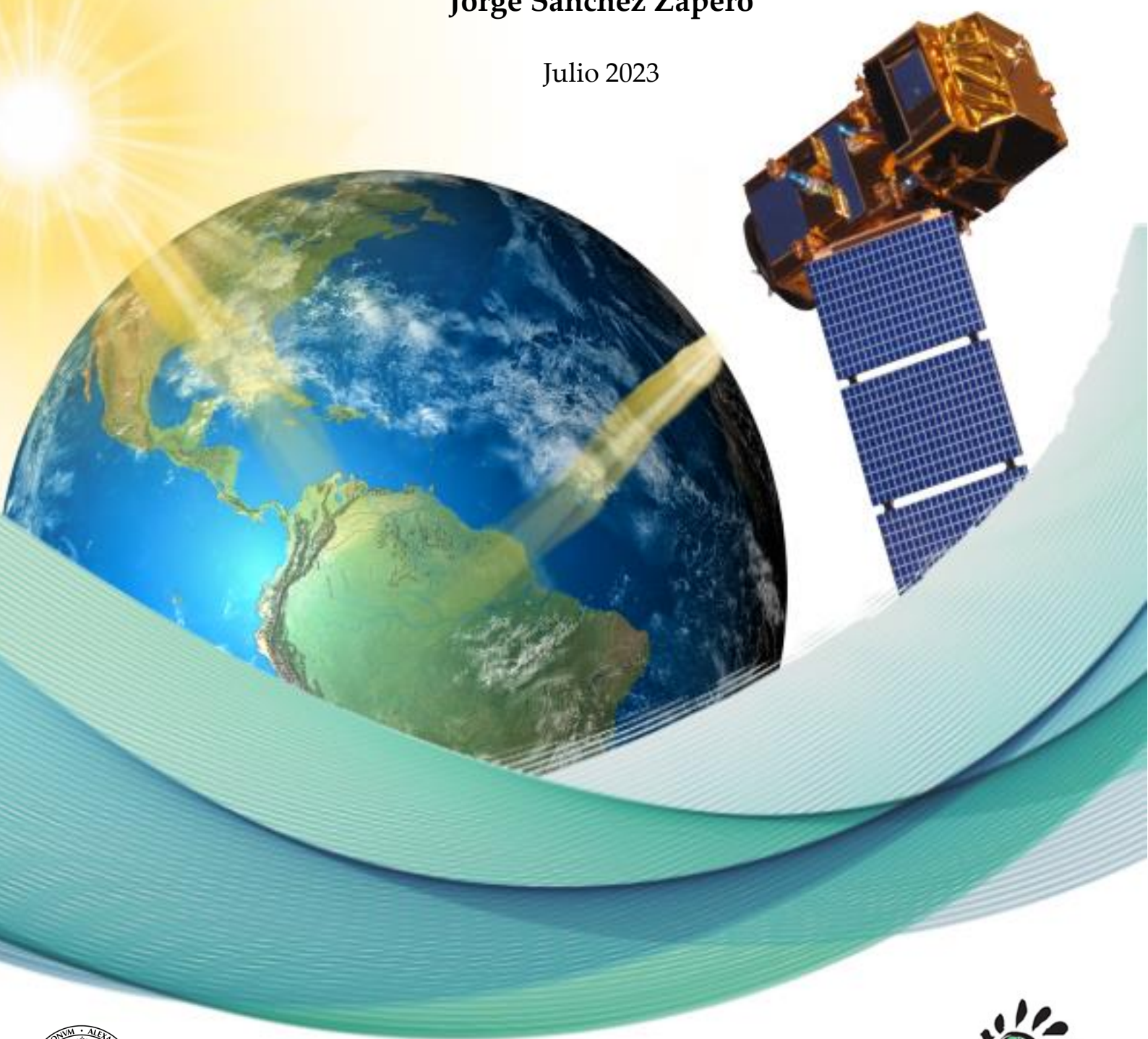


**Desarrollo de un sistema operativo para la validación
estandarizada de productos globales de albedo derivados de satélite.
Aplicación a SPOT/VGT, PROBA-V y Sentinel-3**

Tesis Doctoral

Jorge Sánchez Zapero

Julio 2023



VNIVERSITAT ID VALÈNCIA



VNIVERSITAT DE VALÈNCIA



Facultat de Física

Departament de Física de la Terra i Termodinàmica

**Desarrollo de un sistema operativo para la validación
estandarizada de productos globales de albedo derivados
de satélite. Aplicación a SPOT/VGT, PROBA-V y
Sentinel-3.**

Doctorado en Teledetección

Julio 2023

Jorge Sánchez Zapero

Directores:

Fernando Camacho de Coca

Francisco Javier García Haro

FERNANDO CAMACHO DE COCA, Doctor en Física por la Universidad de Valencia y CEO de la empresa EOLAB.

FRANCISCO JAVIER GARCÍA HARO, Catedrático en el departamento de Física de la Tierra y Termodinámica de la Facultad de Física, Universidad de Valencia.

CERTIFICAN:

Que la tesis doctoral “ Desarrollo de un sistema operativo para la validación estandarizada de productos globales de albedo derivados de satélite. Aplicación a SPOT/VGT, PROBA-V y Sentinel-3.”, presentada por Jorge Sánchez Zaperó ha sido realizada bajo su dirección y es favorable para optar a grado de Doctor por la Universidad de Valencia en el programa de doctorado en Teledetección.

Y para que así conste, firman el presente certificado en Burjassot, a 17 de Julio de 2023.

Fdo.: Fernando Camacho de Coca

Fdo.: Francisco Javier García Haro



Este trabajo ha sido posible gracias a la financiación obtenida de los siguientes proyectos:

- **EC/JRC Copernicus Global Land Service:**
 - Gio Global Land Component - Lot I "Operation of the Global Land Component" Framework Service Contract N° 388533 (JRC)
 - Global Land Operations "Vegetation and Energy" (CGLOPS-1) Framework Service Contract N° 199494 (JRC).
- **EC/ECMWF Copernicus Climate Change Service:**
 - Official reference number service contract: 2018/C3S_312b_Lot5_VITO/SC1
 - Official reference number service contract: 2020/ COP_059_VITO_Albedo

“No sé lo que piensa el mundo de mí, pero a mí me parece haber sido sólo un niño jugando en la orilla del mar, divirtiéndome, encontrando una piedra más lisa o una concha más bonita de lo normal, mientras el gran océano de la verdad yacía ante mis ojos con todo por descubrir.”

Isaac Newton

Agradecimientos

Este trabajo cierra una etapa que no sólo comenzó el 2015, año en el que me matriculé oficialmente del doctorado, sino unos años antes, en 2012 cuando Fernando Camacho me hacía una entrevista de trabajo para hacer las prácticas y el proyecto final de carrera en la empresa EOLAB cuando estaba finalizando mis estudios de ingeniería de telecomunicación. Mi primer gran objetivo fue hacer la validación del primer producto europeo de albedo derivado de satélite. Desde pequeño siempre me motivó el sector espacial y no dudé en aceptar el reto. La temática que me sirvió para completar mi proyecto final de carrera y finalizar mis estudios de ingeniería me ha acompañado también en el desarrollo de esta tesis. Quiero aprovechar esta sección para expresar mi gratitud a mi director de tesis, Fernando Camacho, por darme esa oportunidad laboral en el 2012. Su experiencia, conocimiento y dedicación me han guiado a lo largo de mi carrera profesional y del proceso de investigación. También quiero dar las gracias a mi otro director y tutor en la Universitat de València, Javi, por mostrarse siempre dispuesto a ayudar y colaborar.

Durante este camino he tenido la suerte de conocer a gente maravillosa y quería expresar mi gratitud a todas las personas que han contribuido de manera significativa en la realización de mi tesis doctoral. Muchísimas gracias a todas las personas que han pasado por EOLAB durante todos estos años, algunas durante periodos de tiempo más largos y otras con las que gustaría haber estado trabajando más tiempo. Sin el trabajo y la compañía de Quique esto no habría podido ser posible, pero también gracias a los buenos momentos que he vivido con todos mis compañeros a lo largo de estos: Vicent, Bea, Lorena, Lidia, Xavi, Carol, Carolina, Consuelo, David, Enrica, Silvia, Maria, Ashiro, Piti, Enric, Jesús. *Also thanks to all people involved in CGLS and C3S who is also part of this work: Roselyne, Bruno, Dominique, Jean Louis, Else, Carolien, Iskander, Jonathan, Alexandre, Simon, Tim, Davy. Thank you very much also to CEOS LPV people: Jaime, Mike, Fabrizio, Zhousen, Crystal, Angela. Thank you to all of you for your scientific and technical support.*

Fuera del ámbito profesional también quiero agradecer a mi madre, mi hermana y al resto de familia por su apoyo constante. Con esta tesis puede que os quede un poco más claro lo que vengo haciendo en el trabajo. Durante este tiempo he perdido demasiada gente importante, por lo que este trabajo os lo quiero dedicar con mucho cariño (va por vosotros: abuelitos, suegro y tío Miguel). También han llegado un buen puñado de sobrinos, con su incalculable energía ($E \rightarrow \infty$), que hacen que pueda romper las barreras de la física y consiga viajar en el tiempo.

El agradecimiento más especial se lo quiero dedicar a las dos personas que me aportan esas cosas en mi vida que la ciencia no es capaz de explicar: mi esposa Belén y mi hija Vega. Sois mi mayor fuente de inspiración y motivación en cada paso que doy. Gracias, Belén, por tu apoyo y amor incondicional, comprensión y paciencia infinita conmigo. No podría haber encontrado mejor compañera de viaje. La llegada de nuestra pequeña Vega en 2018 nos ha hecho descubrir, además, el amor desde una perspectiva que nunca habíamos imaginado. Gracias Vega, tú me estás enseñando muchas más cosas de las que seguro puedes aprender de mí. Te pusimos nombre de estrella, una de las más brillantes del universo, pero también tienes nombre de cohete de lanzamiento espacial. Ambas cualidades son, curiosidades del destino, las que mejor te describen. Porque brillas con luz propia y tienes tanta energía que cuando aprendas a canalizarla podrás volar y llegar tan lejos como quieras.

Mi otra dedicatoria especial va destinada a mi ángel de la guardia, mi padre, que hace ya demasiado tiempo que el destino decidió que volara muy alto. Desde entonces eres el satélite que orbita alrededor de mí. Llevas incorporado un sensor que la ciencia y la tecnología jamás podrá implementar, pues haces de guía para que cada día intente ser mejor persona, tal como hacías antes de tu despegue. Os quiero.

Nota introductoria

Esta Tesis doctoral se presenta para obtener el título de Doctorado en Teledetección de la Universidad de Valencia. Según el Reglamento vigente sobre depósito, evaluación y defensa de la Tesis doctoral de la Universidad de Valencia, la Tesis doctoral puede ser presentada de dos formas: 1) Tesis tradicional o 2) Tesis por compendio de publicaciones. En este caso, la Tesis presentada está elaborada por compendio de publicaciones.

La Tesis de acuerdo con esta opción, cumple los siguientes requisitos:

1. El doctorando o la doctoranda tiene que presentar un mínimo de tres artículos, ya publicados o aceptados en revistas indexadas en algún índice internacional como por ejemplo JCR (WoS) y/o SJR (Scopus) en el caso de Ciencias Sociales, y ha de ser el primer firmante de todos los trabajos que presente. En caso contrario, a no ser que en el campo de conocimiento de la tesis se use un convenio específico de ordenación de la firma de los artículos, hace falta que justifique su lugar de firma.
2. La tesis ha de incluir un resumen global de la temática, de los principales resultados y de las conclusiones, que justifique la aportación original del autor o autora, redactado en cualquiera de las lenguas oficiales, con un mínimo de 4000 palabras.
3. Como anexo se incluirá una copia completa de los trabajos publicados o admitidos para su publicación, en la que figuren claramente, el nombre y filiación de todos los coautores de los trabajos y la referencia completa de la revista en la que los trabajos han sido publicados o admitidos para su publicación. En este último caso, debe adjuntarse un justificante de la admisión y la referencia completa de la revista a la que se han enviado.
4. Los trabajos presentados en la tesis doctoral no han sido ni serán utilizados, implícita o explícitamente, para la realización de otra tesis doctoral.

Concretamente, la tesis doctoral está compuesta de las siguientes publicaciones:

1. Roujean, J.L., Leon-Tavares, J., Smets, B., Claes, P., Camacho De Coca, F., **Sánchez-Zapero, J.**, 2018. Surface albedo and toc-r 300m products from PROBA-V instrument in the framework of Copernicus Global Land Service. *Remote Sens. Environ.* 215, 57–73. <https://doi.org/10.1016/j.rse.2018.05.015>
2. **Sánchez-Zapero, J.**, Camacho, F., Martínez-Sánchez, E., Lacaze, R., Carrer, D., Pinault, F., Benhadj, I., Muñoz-Sabater, J., 2020. Quality Assessment of PROBA-V Surface Albedo V1 for the Continuity of the Copernicus Climate Change Service. *Remote Sens.* 2020, Vol. 12, Page 2596 12, 2596. <https://doi.org/10.3390/rs12162596>
3. **Sánchez-Zapero, J.**, Martínez-Sánchez, E., Camacho, F., Wang, Z., Carrer, D., Schaaf, C., García-Haro, F.J., Nickeson, J., Cosh, M., 2023b. Surface ALbedo VALidation (SALVAL) Platform: Towards CEOS LPV Validation Stage 4 - Application to Three Global Albedo Climate Data Records. *Remote Sens.* 2023, Vol. 15, Page 1081 15, 1081. <https://doi.org/10.3390/RS15041081>
4. **Sánchez-Zapero, J.**, Camacho, F., Martínez-Sánchez, E., Gorroño, J., León-Tavares, J., Benhadj, I., Toté, C., Swinnen, E., Muñoz-Sabater, J., 2023a. Global estimates of surface albedo from Sentinel-3 OLCI and SLSTR data for Copernicus Climate Change Service: Algorithm and preliminary validation. *Remote Sens. Environ.* 287, 113460. <https://doi.org/10.1016/J.RSE.2023.113460>

Tabla de contenido

Resumen breve	1
Resumen extenso.....	6
1. Introducción.....	7
1.1. Contexto	7
1.2. Definiciones de albedo	13
1.2.1. Albedo estimado mediante teledetección.....	13
1.2.2. Albedo bajo iluminación real	21
1.3. Marco de Trabajo.....	22
1.4. Motivación y objetivos	24
2. Protocolo de validación.....	29
2.1. Base de datos REALS.....	31
2.2. Muestreo global: LANDVAL	36
2.3. Criterios y métricas de validación	37
2.3.1. Integridad (completeness)	39
2.3.2. Consistencia espacial	40
2.3.3. Consistencia temporal	42
2.3.4. Evaluación del error (exactitud, precisión e incertidumbre)	44
2.3.5. Estabilidad.....	48
3. Resultados	50
3.1. Artículo 1: <i>Surface albedo and toc-r 300m products from PROBA-V instrument in the framework of Copernicus Global Land Service.</i>	51
3.2. Artículo 2: <i>Quality Assessment of PROBA-V Surface Albedo V1 for the Continuity of the Copernicus Climate Change Service.</i>	54

3.3. Artículo 3: <i>Surface ALbedo VALidation (SALVAL) Platform: Towards CEOS LPV Validation Stage 4 – Application to Three Global Albedo Climate Data Records....</i>	57
3.4. Artículo 4: <i>Global estimates of surface albedo from Sentinel-3 OLCI and SLSTR data for Copernicus Climate Change Service: Algorithm and preliminary validation.....</i>	61
4. Discusión general y conclusiones	66
Bibliografía.....	80
Anexo I – Listado informes disponible <i>online</i> publicados en proyectos	97
Anexo II – Copia de publicación 1	101
Anexo III – Copia de publicación 2	118
Anexo IV – Copia de publicación 3	152
Anexo V – Copia de publicación 4.....	190

Lista de Figuras

- Figura 1: Diagrama habitual de un algoritmo para la estimación de albedo mediante teledetección basado en cuatro pasos: corrección atmosférica, inversión de la BRDF, integración angular e integración espectral. 15
- Figura 2: Diagrama de la herramienta de operacional de validación SALVAL, que ofrece resultados de validación estandarizados integrando el protocolo de validación, productos de satélite, datos de campo y requerimientos de usuario. 26
- Figura 3: Distribución global de las 99 localizaciones de REALS y las 720 de LANDVAL para la validación directa y la intercomparación de productos. LANDVAL se representa diferenciando diferentes tipos de bioma: EBF significa 'Evergreen Broadleaved forest', DBF 'Deciduous Broadleaved Forest', NLF Needle-Leaf Forests', OF 'Other Forests', CUL 'CULTivated', HER 'HERbaceous', SHR 'SHRublands', y SBA 'Sparse and Bare Areas'. 30
- Figura 4: Huella espacial (footprint) de la medida de una torre de albedo. 32
- Figura 5: Ejemplo de ajuste de semivariograma y estimadores (ST, RAW) sobre dos estaciones en USA: Desert Rock (DRAK) y Talladega National Forest (TALL). Se muestran las imágenes de Google Earth y Sentinel-2 B8. Fuente: (Sánchez-Zapero et al., 2023b). 34
- Figura 6: Evolución del número de estaciones (arriba-izquierda), número de muestras (arriba-derecha) y RMSD de la comparación MCD43A3 C6.1 versus in situ (abajo) en función del indicador ST para el periodo 2000-2020. 35
- Figura 7: Ejemplo de resultados para evaluar la integridad. a) Distribución global del porcentaje de huecos del producto global C3S PROBA-V V1 para el año 2014; b) Evolución temporal del porcentaje de huecos de los productos C3S PROBA-V V1, C3S SPOT/VGT V1 y MCD43A3 C6 para el año 2014 sobre LANDVAL; y c) histograma de la longitud (en días) de los huecos de los productos C3S PROBA-V V1, C3S SPOT/VGT V1 y MCD43A3 C6 para el periodo de Diciembre 2013 a Mayo 2014 sobre LANDVAL. Fuente: (Sánchez-Zapero et al., 2020). 39

Figura 8: Ejemplo de resultados para evaluar la consistencia espacial entre los productos C3S PROBA-V y SPOT/VGT V1 a) Distribución global de los residuos para la fecha 2014.04.23; b) histogramas de los residuos para el periodo Diciembre 2013 – Mayo 2014 (uno por mes); c) distribución global de residuos entre los requisitos del proyecto C3S para la fecha 2014.04.23; y d) porcentajes de residuos entre los requisitos C3S para el periodo Diciembre 2013 – Mayo 2014. Fuente: ‘Product Quality Assessment Report Surface Albedo v1.0 based on PROBA-V’ (ver Anexo I). 41

Figura 9: Ejemplo de resultados para evaluar la consistencia temporal: a) perfiles temporales de varios productos de albedo (C3SS SPOT/VGT V1, MCD43A3 C6, GlobAlbedo, GLASS) y medidas de campo sobre dos estaciones FLUXNET; y b) Ejemplo de histogramas de correlación cruzada entre pares de productos (C3S SPOT/VGT V1, C3S PROBA-V V1 y MCD43A3 C6) por tipo de bioma. Fuente: ‘Product Quality Assessment Report CDR VGT-based Surface Albedo v1.0’ y ‘Product Quality Assessment Report Surface Albedo v1.0 based on PROBA-V’ (ver Anexo I)..... 43

Figura 10: Panel a: ejemplo de resultados para evaluar el error entre pares de productos. Scatter-plot (izquierda) y métricas asociadas entre C3S Sentinel-3 V3 versus MCD43A3 C6 junto al box-plot del bias para los diferentes rangos de albedo (derecha). Panel b: ejemplo de validación directa (scatter-plots y métricas asociadas) para los productos C3S Sentinel-3 V3 (izquierda) y MCD43A3 C6(derecha). Las líneas verdes, azules y amarillas en los scatter-plots definen los requisitos de usuario (optimal, target, threshold). Fuente: (Sánchez-Zapero et al., 2023a). 46

Figura 11: Ejemplo de resultados para evaluar la precisión de los productos C3S V2, GLASS V4 y MCD43A3 C6.1: a) precisión intra-anual evaluada mediante los histogramas de la suavidad y su valor mediano; y b) precisión inter-anual evaluada con los scatter-plots entre muestras equivalentes de años consecutivos. Fuente: (Sánchez-Zapero et al., 2023b). 47

Figura 12: Ejemplo de resultados para evaluar la estabilidad de los productos C3S V2, GLASS V4 y MCD43A3 C6.1. Perfiles temporales sobre diferentes sitios de calibración para un periodo de 10 años (2001-2010). Las líneas discontinuas representan

la regresión lineal de la tendencia de cada producto. Fuente: (Sánchez-Zapero et al., 2023b)..... 49

Lista de Tablas

Tabla 1. Jerarquía de validación del CEOS/WGCV LPV (Fuente: <https://lpvs.gsfc.nasa.gov/>) 12

Tabla 2. Criterios de selección para los sitios de LANDVAL. 37

Tabla 3. Criterios de calidad, métricas y métodos..... 38

Tabla 4. Métricas para la evaluación del error. 45

Tabla 5. Requerimientos de incertidumbre y estabilidad predefinidos en SALVAL..... 59

Lista de Acrónimos

AL-BH	White-sky albedo (Bi-Hemispherical ALbedo)
AL-BH-BB	White-sky albedo total de onda corta (BB significa BroadBand)
AL-DH	Black-sky albedo (Directional ALbedo)
AL-DH-BB	Black-sky albedo total de onda corta
AVHRR	Advanced Very High Resolution Radiometers
B	mean Bias
BELMANIP	BEenchmark Land Multisite ANalysis & Intercomparison of Products
BNU	Beijing Normal University's
BRDF	Bidirectional Reflectance Distribution Function
BSA	Black-Sky albedo
BSRN	Baseline Surface Radiation Network
CDR	Climate Data Record
CEOS	Committee on Earth Observation Satellites
CV	Coeficiente de Variación espacial
GCOS	Global Climate Observing System
CGLS	Copernicus Global Land Service
GLASS	Global LAnd Surface Satellites
C3S	Copernicus Climate Change Service
ECMWF	European Centre for Medium-Range Weather Forecasts
EC	European Commission
ECV	Essential Climate Variable
EFDC	European Fluxes Database Cluster
EOLAB	Earth Observation LABoratory

ESA	European Space Agency
EUMETSAT	European Organisation for the Exploitation of Meteorological Satellite
EPS	EUMETSAT Polar System
LUXNET	FLUX NETwork
GBOV	Ground-Based Observations for Validation
GLASS	Global LAnd Surface Satellites
GMES	Global Monitoring for Environment and Security
HFOV	Half Field Of View
ICOS	Integrated Carbon Observation System
ICS	International Council for Science
IdePix	Pixel Identification tool
IGARSS	International Geoscience and Remote Sensing Symposium
IOC	Intergovernmental Oceanographic Commission
JCGM	Joint Comitee for Guides in Metrology
JRC	Joint Research Centre
LANDVAL	LAND VALidation network
LP DAAC	Land Processes Distributed Active Archive Center
LPV	Land Product Validation
LSA SAF	Satellite Application Facility on Land Surface Analysis
NASA	National Aeronautics and Space Administration
MAD	Median Absolute Deviation
MAR	Major Axis Regression
MCD43A3	MODIS Terra+Aqua albedo product
MD	Median Deviation
MERIS	Medium Resolution Imaging Spectrometer

METEOSAT	METEOrological SATellite
MI	Moran Index
MISR	Multi-angle Imaging SpectroRadiometer
MODIS	Moderate Resolution Imaging Spectroradiometer
N	Número de muestras
NDSI	Normalized Difference Snow Index
NDVI	Normalized Difference Vegetation Index
NEON	National science foundation's National Ecological Observatory Network
NIR	Near Infra-Red
NOAA	National Oceanic and Atmospheric Administration
OLCI	Ocean and Land Colour Instrument
OLS	Ordinary Least Squares
PAR	Photosynthetically Active Radiation
POLDER	Polarization and Directionality of the Earth's Reflectances
PROBA-V	Project for On-Board Autonomy – Vegetation
QA4ECV	Quality Assurance for Essential Climate Variable
R	Correlation coefficient
RAW	1 st order RAW score of the spatial representativeness
REALS	Representativeness-Evaluated ALbedo Stations
RMSD	Root Mean Squared Deviation
SPOT	Satellite Pour l'Observation de la Terre
SA	Surface ALbedo
SALVAL	Surface ALbedo VALidation tool
SAVS	Surface Albedo Validation Sites
SeaWiFS	Sea-viewing Wide Field-of-view Sensor

SLSTR	Sea and Land Surface Temperature Radiometer
ST	Standard Score of the spatial representativeness
STD	STandard Deviation
SURFRAD	SURFace RADiation Budget
SWIR	Short-Wave Infra-Red
SZA	Sun Zenith Angle
TERN	Australia's Land Ecosystem Observatory or Terrestrial Ecosystem
TOA	Top-Of-Atmosphere
TOC	Top-Of-Canopy
UNEP	United Nations Environment Programme
UNESCO	United Nations Educational Scientific and Cultural Organization
UNFCCC	United Nations Framework Convention on Climate Change
VGT	VEGETATION sensor
WCGV	Working Group on Calibration & Validation
WMO	World Meteorological Organization
WSA	White-Sky Albedo

Resumen breve

El albedo de la superficie terrestre (SA) es una variable climática esencial (ECV), cobrando un papel relevante en el balance energético del planeta. Diferentes agencias espaciales y servicios de observación de la Tierra vienen desarrollando registros de datos climáticos (CDR) de productos de albedo a escala global, derivados con datos procedentes de sensores pasivos a bordo de satélites. Es, por ende, indispensable cuantificar de manera eficiente las incertidumbres asociadas a dichos productos de satélite, proceso que se conoce como validación. La validación también permite establecer en qué medida los productos satisfacen los requerimientos demandados por los usuarios. Por otra parte, la metodología de validación debe seguir unos protocolos y metodologías estandarizados, que ofrezcan a su vez trazabilidad y transparencia en dicho proceso. A nivel internacional, el subgrupo sobre validación de productos terrestres (LPV) del grupo de trabajo sobre calibración y validación (WGCV) del comité de satélites de observación de la Tierra (CEOS) se encarga de la coordinación de las actividades y estandarización de protocolos de validación. El CEOS/WGCV LPV establece, además, una jerarquía de cuatro niveles en función del estado de la validación de los productos dependiendo de varios aspectos como la representatividad global y temporal, el uso de protocolos estandarizados, la publicación de los resultados en revistas científicas (*peer-reviewed*) o la actualización de los resultados cuando la serie temporal se expande. El nivel más alto en la jerarquía (nivel 4) engloba todos estos aspectos.

Todo ello motiva el objetivo principal de esta tesis, que no es otro que el diseño de un sistema operacional de validación estandarizada para llegar al nivel 4, que debe integrar las siguientes cuatro componentes: (1) registros de datos climáticos de albedo a largo plazo derivados con datos de satélite; (2) un conjunto fiable y representativo a nivel global de medidas *in situ*; (3) un protocolo de validación estandarizado que cuente con el acuerdo de la comunidad científica; y (4) una plataforma de validación *online*, de libre acceso, que genere resultados e informes de validación estandarizados y permita actualizar los resultados conforme la serie se expande. En el contexto de esta

tesis se ha trabajado en cada una de estas componentes, llevando cada una al nivel requerido para formar parte del sistema.

Respecto a la primera componente, se ha trabajado en la validación de los productos de albedo desarrollados en el servicio Europeo de observación de la Tierra, denominado *Copernicus*. Los desarrollos iniciales de los algoritmos de albedo se realizaron en el contexto de la componente global del servicio de monitorización de la superficie terrestre de *Copernicus* (CGLS), derivando posteriormente la producción de dichos productos al servicio de cambio climático (C3S) de *Copernicus*. C3S ha desarrollado la serie climática más extensa, cuya calidad e incertidumbre ha sido evaluada en esta tesis para diferentes versiones de algoritmos y sensores utilizados. Por otra parte, también se ha trabajado en el diseño del algoritmo que permite dar continuidad a la serie gracias al uso de los satélites *Copernicus* Sentinel-3, que ofrecen mejoras en cuanto a resolución espacial y espectral. Se ha realizado para ello 4 estudios:

- El punto de partida de esta tesis fue la validación del producto desarrollado en CGLS para la estimación del albedo a partir de datos del sensor *Vegetation* a bordo del minisatélite PROBA (PROBA-V) a 300 m de resolución espacial (Roujean et al., 2018). la validación de dichos productos se realizó sobre Europa, mostrando distribuciones espacial y temporalmente consistentes con los productos de NASA derivados con datos de MODIS a bordo de las plataformas *Terra* y *Aqua* (MCD43A3 C6). La validación directa sobre datos de 10 estaciones representativas mostró una incertidumbre (RMSD) de 0.03 con un sesgo medio (*bias*) de 0.01, mostrando discrepancias similares a las observadas en MCD43A3 C6 (RMSD=0.03, *bias*=0). Se demostró, por tanto, la viabilidad y utilidad del algoritmo.
- En segundo lugar se realizó la validación del producto de albedo de PROBA-V versión 1 (C3S PROBA-V SA V1) que dio continuidad a la serie climática de albedo de C3S a 1 km de resolución espacial (Sánchez-Zapero et al., 2020). Por ello, dicho estudio se centró en la consistencia de los productos C3S en la transición de SPOT a PROBA, donde ambas plataformas incorporan sensores *Vegetation* equivalentes espectralmente (SPOT/VGT y PROBA-V). Se demostró una buena continuidad asociada al cambio de satélite (sesgo medio

típicamente entre $\pm 2\%$). La mayor limitación del producto de PROBA-V respecto al de SPOT/VGT fue su menor número de observaciones válidas. La comparación de C3S PROBA-V SA V1 con el producto MODIS de NASA (MCD43A3 C6) mostró también una buena consistencia, con diferencias sistemáticamente positivas de hasta el 12% (PROBA-V > MODIS). La comparación de PROBA-V con datos *in situ* (20 estaciones) mostró un sesgo positivo (11.5%), con una incertidumbre (RMSD ~ 0.4) similar a la mostrada por MCD43A3 C6.

- El tercer estudio (Sánchez-Zapero et al., 2023b) presenta la validación de 3 series climáticas con más de 20 años de datos usando la herramienta *Surface Albedo Validation* (SALVAL) desarrollada en esta tesis (componente 4 del sistema operacional). Las series climáticas investigadas fueron: la versión 2 del producto de albedo del servicio C3S denominada multi-sensor derivada a partir de datos SPOT/VGT y PROBA-V (C3S V2), el producto de NASA derivado con *Terra+Aqua/MODIS* (MODIS C6.1) y el producto de la Universidad de *Beijing* derivado también con datos MODIS (GLASS V4). Los resultados de validación demostraron que los tres productos de satélite investigados proporcionan series temporales consistentes y realistas a nivel global, mostrando ciertas discrepancias entre ellos principalmente atribuidas a los diferentes algoritmos utilizados y al tipo de sensor.
- Finalmente se realizó el diseño y validación del algoritmo de albedo desarrollado para dar continuidad a la serie climática de C3S basada en SPOT/VGT y PROBA-V usando datos *Copernicus Sentinel-3* a 300 m de resolución espacial (Sánchez-Zapero et al., 2023a). Dicho algoritmo realiza un uso sinérgico de datos de los sensores OCLI y SLSTR a bordo de los satélites Sentinel-3. La validación directa con datos de campo (32 estaciones) mostró resultados similares a los productos NASA MODIS (MCD43A3 C6) pero con un signo en la diferencias opuesto (ligeramente positivo en el caso de Sentinel-3), con una exactitud de 0.005 (3.7%), precisión de 0.016 (11.3%) e incertidumbre de 0.032 (22.7%). Los resultados de validación directa de Sentinel-3 mejoraron los obtenidos por su producto C3S predecesor basado en

PROBA-V. C3S Sentinel-3 SA alcanzó un buen acuerdo espacial y temporal en comparación con otros productos de satélite operacionales derivados con MODIS (MCD43A3 C6) y PROBA-V (C3S PROBA-V SA V1). Se demostró, por tanto, la viabilidad del algoritmo propuesto para la continuidad del CDR del servicio C3S utilizando el uso de datos OLCI+SLSTR de Sentinel-3. La principal limitación del producto fue la subestimación del albedo en la nieve y la transición lenta entre valores bajos y altos en eventos de nieve. Dicha limitación proviene de los datos de entrada (reflectividad de la superficie) proporcionados en CGLS, que usa el clasificador *IdePix* de ESA, donde se confunden los valores de nieve con valores de nube, enmascarando y filtrando dichos valores.

La segunda componente hace referencia a un conjunto fiable y representativo de medidas *in situ* a nivel global. Se ha generado una base de datos de medidas de campo de albedo denominada *Representativeness-Evaluated Albedo Stations* (REALS), integrando los datos procedentes de redes existentes de medidas tales como BSRN, FLUXNET, NEON, EFDC, ICOS o TERN. Se ha evaluado la representatividad espacial de la medida asociada a la estación con el objetivo de determinar si el valor medido por la torre (*footprint*) es representativo a la resolución espacial efectiva de los píxeles de satélite de interés (típicamente de 300 m a 1 km).

La tercera componente implica el desarrollo de unos protocolos y metodologías estandarizados, bajo el consenso de la comunidad científica, que ofrezcan a su vez trazabilidad y transparencia en el proceso de validación. En el desarrollo de esta tesis se ha ido elaborando una metodología de validación en colaboración con el grupo de trabajo del CEOS/WGCV LPV por lo que dicha metodología no sólo es consistente con la buenas prácticas del CEOS/WGCV LPV sino que también ha contribuido a definir criterios y métricas del protocolo de validación del CEOS/WGCV LPV. Se presentan los dos métodos principales y sus particularidades: i) la validación directa, que hace referencia a la comparación de estimaciones de satélite con datos medidos procedentes de estaciones terrestres; y ii) la validación indirecta, también conocida como intercomparación de productos. Se ha definido además un muestreo de 720 localizaciones para la intercomparación de productos (LANDVAL), que ha sido

definido sobre sitios homogéneos con el objetivo de ser representativo a nivel global en cuando a distribución continental y por tipo de bioma.

Finalmente, se ha culminado la integración en un sistema operacional con el desarrollo de una plataforma de validación *online* (SALVAL) que genera resultados de validación estandarizados (Sánchez-Zapero et al., 2023b). La herramienta SALVAL está diseñada para permitir a los productos de albedo alcanzar el nivel máximo (4) en la jerarquía del CEOS/WGCV LPV, contando a su vez con una interfaz amigable para el usuario y permitiendo un ejercicio interactivo de validación que puede ser configurado conforme a los requerimientos definidos por el propio usuario.

Como conclusión, se ha conseguido llevar cada una de las componentes de validación (series climáticas de albedo, base de datos de medidas *in situ*, metodología de validación y herramienta *online*) al nivel necesario para desarrollar un sistema operacional de validación estandarizada. Se han validado, además, los productos de albedo desarrollados en los servicios *Copernicus* CGLS y C3S con los sensores pasivos a bordo de los satélites SPOT, PROBA y Sentinel-3.

Resumen extenso

A continuación se proporciona un resumen extenso global de la temática de la tesis, de los principales resultados y de las conclusiones. En el **capítulo 1** se describe el contexto, y se introducen algunas magnitudes fundamentales, el marco de trabajo y los objetivos marcados. La metodología de validación se presenta en el **capítulo 2**, describiendo el muestreo para la intercomparación (LANDVAL), la base de datos de medidas *in situ* (REALS) y los criterios y métricas de validación.

La parte de resultados (**capítulo 3**) incluye un resumen de los 4 artículos incluidos en esta tesis, presentada como compendio de publicaciones:

- Roujean, J.L., Leon-Tavares, J., Smets, B., Claes, P., Camacho De Coca, F., **Sánchez-Zapero, J.**, 2018. Surface albedo and toc-r 300m products from PROBA-V instrument in the framework of Copernicus Global Land Service. *Remote Sens. Environ.* 215, 57–73. <https://doi.org/10.1016/j.rse.2018.05.015>
- **Sánchez-Zapero, J.**, Camacho, F., Martínez-Sánchez, E., Lacaze, R., Carrer, D., Pinault, F., Benhadj, I., Muñoz-Sabater, J., 2020. Quality Assessment of PROBA-V Surface Albedo V1 for the Continuity of the Copernicus Climate Change Service. *Remote Sens.* 2020, Vol. 12, Page 2596 12, 2596. <https://doi.org/10.3390/rs12162596>
- **Sánchez-Zapero, J.**, Martínez-Sánchez, E., Camacho, F., Wang, Z., Carrer, D., Schaaf, C., García-Haro, F.J., Nickeson, J., Cosh, M., 2023b. Surface ALbedo VALidation (SALVAL) Platform: Towards CEOS LPV Validation Stage 4 - Application to Three Global Albedo Climate Data Records. *Remote Sens.* 2023, Vol. 15, Page 1081 15, 1081. <https://doi.org/10.3390/RS15041081>
- **Sánchez-Zapero, J.**, Camacho, F., Martínez-Sánchez, E., Gorroño, J., León-Tavares, J., Benhadj, I., Toté, C., Swinnen, E., Muñoz-Sabater, J., 2023a. Global estimates of surface albedo from Sentinel-3 OLCI and SLSTR data for Copernicus Climate Change Service: Algorithm and preliminary validation. *Remote Sens. Environ.* 287, 113460. <https://doi.org/10.1016/j.RSE.2023.113460>

Finalmente, en el **capítulo 4** se realiza una discusión general de los resultados y se proporcionan las conclusiones de la tesis, incluyendo las perspectivas futuras.

1. Introducción

1.1. Contexto

El albedo de la superficie terrestre, que se define como la fracción (adimensional) de la radiación solar incidente que es reflejada por la superficie de la Tierra (Dickinson, 1983), está considerado como una ECV de acuerdo con el sistema global de observación del clima (GCOS) (GCOS-244¹). Es una variable de vital importancia pues controla el balance energético de la superficie y es un indicador muy sensible a cambios medioambientales (Dickinson, 1995). Como corolario, el albedo de la superficie determina la fracción de energía solar que es transformada en calor o energía latente, siendo clave para caracterizar el balance energético en el sistema Tierra-atmósfera y constituyendo una entrada indispensable para los modelos que cuantifican la transferencia de energía entre suelo, vegetación y atmósfera (Stephens et al., 2015). También vale la pena señalar que los estudios de sensibilidad climática con modelos de circulación global han confirmado la naturaleza inestable del balance de energía con respecto a pequeños cambios en el albedo de la superficie terrestre (Amut et al., 2007; Henderson-Sellers and Wilson, 1983; Ollinger et al., 2008). El albedo varía en el espacio y el tiempo como resultado tanto de procesos naturales (iluminación solar, deshielo, crecimiento de la vegetación) como de las actividades del ser humano sobre el clima (Lawrence and Chase, 2007), representando un indicador de la vulnerabilidad medioambiental del planeta. Un aumento global del albedo indicaría un enfriamiento del planeta, pues la luz (radiación) absorbida que lo calienta sería menor. Por el contrario, un valor bajo de albedo apuntaría a un calentamiento del planeta, porque la mayor parte de la luz sería absorbida por la superficie del mismo. Las mismas hipótesis son válidas a escala regional. La dinámica estacional también aporta información de interés, ya que el albedo varía notablemente a lo largo del año. A partir de valores altos de albedo podemos identificar la presencia de nieve o hielo en la superficie, así como la presencia de vegetación en valores bajos. La variación temporal del albedo también puede darnos información sobre la fenología de la vegetación o cambios significativos en la superficie por otros fenómenos como incendios, deforestación o inundaciones.

¹ The 2022 GCOS Implementation Plan (GCOS-244): <https://gcos.wmo.int/en/publications/gcos-implementation-plan2022> (acceso online el 02/03/2023).

La observación global de manera regular del sistema climático es un requisito clave para avanzar en el conocimiento científico sobre los cambios que está experimentando nuestro clima. La convención de cambio climático de las Naciones Unidas (UNFCCC), junto a las entidades que la componen (*World Meteorological Organization (WMO)*, *Intergovernmental Oceanographic Commission (IOC) of the United Nations Educational Scientific and Cultural Organization (UNESCO)*, *United Nations Environment Programme (UNEP)*, *International Council for Science (ICS)*) reconoce al GCOS como el organismo responsable de coordinar las observaciones climáticas a nivel internacional. Los planes de implementación del GCOS establecen como requisito el monitorizar sistemáticamente un conjunto de ECVs a nivel global, entre las que está incluido el albedo de la superficie terrestre. En el contexto de cambio climático actual son necesarios, por tanto, registros globales de albedo de la superficie a largo plazo tanto para los modelos climáticos como para modelos biogeoquímicos, hidrológicos o meteorológicos.

Hay dos formas principales de monitorizar las variaciones de albedo. La primera de ellas sería la medición a través estaciones de flujo de manera *in situ*, por ejemplo, con la instalación de piranómetros situados de manera opuesta que miden tanto la radiación incidente que llega al sensor como la que se refleja desde la superficie. Este procedimiento está limitado espacialmente, ya que las medidas se realizan de manera local para un emplazamiento concreto y no podemos medir el albedo para grandes superficies (ni mucho menos a nivel global) ni determinar la variación espacial del mismo. La segunda sería la teledetección, mediante la estimación del albedo a través de datos procedentes de satélites. La tecnología actual de los satélites de observación de la Tierra permite abordar el estudio de forma global, con una alta continuidad tanto a nivel espacial como temporal. Gracias a la adquisición de datos procedentes de sensores pasivos a bordo de dichos satélites que miden la radiación relegada en el rango solar podemos, por ende, obtener registros globales de albedo con una frecuencia temporal alta a diferentes resoluciones espaciales en función del sensor utilizado.

Actualmente, diferentes agencias espaciales e instituciones han implementado servicios que ofrecen datos climáticos de albedo. El servicio precursor es el proporcionado por el *Land Processes Distributed Active Archive Center*² (LP DAAC) de NASA, donde su equipo científico '*Land*'³ tiene como objetivo la monitorización de la cobertura terrestre explotando datos adquiridos a través de sensores MODIS a bordo de los satélites *Terra* y *Aqua*. Por otra parte, el programa europeo de observación de la Tierra, *Copernicus*⁴, es dirigido conjuntamente por la Agencia Espacial Europea (ESA) y por la Comisión Europea (EC) con el objetivo de lograr una capacidad completa, continua y autónoma de observación de la Tierra cuyos resultados sean accesibles libremente por la comunidad científica y el resto de la sociedad. Dicho programa se agrupa en seis áreas temáticas diferentes: la superficie terrestre, los océanos, la respuesta a emergencias, la atmósfera, seguridad y, por último, cambio climático. Dentro de estas temáticas existes varios servicios que ofrecen productos de albedo, como la componente global del servicio de monitorización de la superficie terrestre⁵ (CGLS) o el servicio de cambio climático⁶ (C3S). CGLS desarrolló los primeros algoritmos y cadenas de procesado de productos globales (SA). Posteriormente, los desarrollos de CGLS se trasladaron a C3S, que ofrece actualmente la serie climática más extensa del mercado, proporcionando registros globales de albedo derivados de satélite desde 1981 hasta la actualidad. Existen otras iniciativas que ofrecen productos a los usuarios, como el *Satellite Application Facility on Land Surface Analysis*⁷ (LSA SAF) (Trigo et al., 2011) de la *European Organisation for the Exploitation of Meteorological Satellites*⁸ (EUMETSAT), o el proyecto *Globalbedo*⁹ de la ESA. Fuera de Europa también destacan otras iniciativas, como los productos *Global LAnd Surface Satellites*¹⁰ (GLASS) (Liang et al., 2020) ofrecidos por el centro de procesado y análisis de datos globales de la *Beijing Normal University's* (BNU).

² <https://lpdaac.usgs.gov/> (acceso online el 02/03/2023)

³ <https://modis-land.gsfc.nasa.gov/> (acceso online el 02/03/2023)

⁴ <https://www.copernicus.eu/> (acceso online el 02/03/2023)

⁵ <https://land.copernicus.eu/global/> (acceso online el 02/03/2023)

⁶ <https://climate.copernicus.eu/> (acceso online el 02/03/2023)

⁷ <https://landsaf.ipma.pt/> (acceso online el 02/03/2023)

⁸ <https://www.eumetsat.int/> (acceso online el 02/03/2023)

⁹ <http://www.globalbedo.org/> (acceso online el 02/03/2023)

¹⁰ <http://glass.umd.edu/> (acceso online el 02/03/2023)

Dependiendo de la aplicación y el uso de los productos de albedo, los requisitos pueden variar a diferentes escalas tanto espaciales (que cubren un rango desde pocos metros a 30km) como temporales (desde diario a mensual). Los requisitos locales y regionales varían significativamente según el uso previsto. Sin embargo, GCOS ha especificado un conjunto de requisitos globales que en la mayoría de ocasiones deberían satisfacer las necesidades globales y regionales (GCOS-245¹¹). Además de los requisitos referentes a la resolución, GCOS establece requisitos en cuanto a la estabilidad de la serie climática y la incertidumbre asociada a las estimaciones. A su vez, dada la multitud de productos de albedo existentes, que presentan entre ellos discrepancias tanto temporales como espaciales (Carrer et al., 2010a; Liu et al., 2013, 2017), los usuarios se enfrentan comúnmente a situaciones complejas pues deben conocer cuál de ellos se ajusta mejor a sus necesidades. Es, por tanto, obligatorio cuantificar y medir de manera eficiente las incertidumbres asociadas a los productos globales de albedo derivados mediante teledetección. También se debe evaluar si el producto cumple los requisitos definidos por usuarios (*fitness-for-purpose*), así como determinar en qué medida el producto es adecuado para su aplicación específica (Zeng et al., 2015). Al proceso de determinar la incertidumbre asociada a los productos, así como a la evaluación de su calidad y cumplimiento de los requisitos es lo que conocemos como validación.

La validación se define como el proceso de evaluar, de manera independiente, la calidad de los datos de los productos derivados de la salida de un sistema (Justice et al., 2000). En términos de productos derivados de datos de satélite, la validación es el procedimiento de evaluar su exactitud y cuantificar sus incertidumbres a través de comparaciones analíticas con datos de referencia. Podemos definir dos métodos diferentes de validación: validación directa y validación indirecta.

La validación directa consiste en la comparación del albedo estimado a partir de datos de satélite con medidas de campo (Lewis, P & Barnsley, 1994), siendo el método que permite evaluar las incertidumbres, pues se puede argumentar que es considerado como la validación real en el campo de la teledetección (Mayr et al., 2019). Por lo tanto, la disponibilidad de datos fiables *in situ* para la validación directa de productos de

¹¹ The 2022 GCOS ECVs Requirements (GCOS 245): https://library.wmo.int/index.php?lvl=notice_display&id=22135#.ZACc4XbMJhE (acceso online el 02/03/2023)

teledetección es un requisito científico clave para que los usuarios tomen decisiones efectivas sobre el uso y utilidad de un producto determinado (Nightingale et al., 2019).

Sin embargo, la validación directa está limitada espacialmente por el número de estaciones disponibles, que no representan las variaciones de albedo a nivel global. Por ello, se hace uso de la comparación tanto cuantitativa como cualitativa entre productos de satélite, comúnmente llamada intercomparación de productos o validación indirecta, que se beneficia de la representatividad espacial del estudio dado el carácter global de los productos de satélite. La validación indirecta consiste, por tanto, en comparar el producto de albedo derivado con datos de satélite que estamos evaluando, usando otros productos de satélite como referencia (Carrer et al., 2010b; Qu et al., 2014; Taberner et al., 2010). En general, podemos concluir que la intercomparación de productos ofrece un medio para evaluar las discrepancias (sistemáticas o aleatorias) entre productos. Dicho método es particularmente útil para encontrar desacuerdos espaciales entre productos en áreas extensas y para estratificar la validación en diferentes tipos de cobertura terrestre o áreas geográficas.

Por otra parte, la validación puede estar condicionada y sesgada por el equipo encargada de llevarla a cabo (p.ej., el desarrollador del producto). Es por tanto necesario establecer unos protocolos y metodologías estandarizadas, que ofrezcan a su vez trazabilidad y transparencia en el proceso de validación. El CEOS/WGCV LPV¹² juega un papel clave en las actividades de validación de productos derivados con datos satelitales, coordinando actividades como la estandarización de protocolos de validación de productos derivados con diferentes datos o algoritmos. Cuenta con la presencia de expertos internacionales, prestando la experiencia y conocimientos para garantizar la fiabilidad y precisión de dichos productos de acuerdo a unos estándares comunes. El CEOS/WGCV LPV establece 4 niveles de jerarquía de validación (Nightingale et al., 2011) atendiendo al nivel de calidad del producto y de la madurez de su evaluación (Tabla 1).

¹² <https://lpvs.gsfc.nasa.gov/> (acceso online el 01/03/2023)

Tabla 1. Jerarquía de validación del CEOS/WGCV LPV (Fuente: <https://lpps.gsfc.nasa.gov/>)

Nivel	Definición y estado actual de la validación
0	No se ha validado. La exactitud del producto no ha sido evaluada. El producto se considera como <i>beta</i> .
1	La exactitud del producto se ha evaluado para un pequeño (típicamente < 30) número de localizaciones y periodos temporales por comparación con datos <i>in situ</i> u otro dato de referencia adecuado.
2	La exactitud del producto ha sido estimada sobre un conjunto significativo (típicamente > 30) de localizaciones y periodos de tiempo temporales por comparación con datos <i>in situ</i> u otro dato de referencia adecuado. La consistencia temporal y espacial del producto y su consistencia con productos similares ha sido evaluada sobre una representación global de localizaciones y periodos de tiempo. Los resultados han sido publicados y revisados por pares.
3	Las incertidumbres del producto han sido completamente cuantificadas sobre un conjunto significativo (típicamente > 30) de localizaciones y periodos de tiempo por comparación con datos <i>in situ</i> u otro dato de referencia adecuado. Los procedimientos de validación siguen unas buenas prácticas acordadas por la comunidad. La consistencia temporal y espacial del producto, y su consistencia con productos similares, ha sido evaluada sobre una representación global de localizaciones y periodos de tiempo. Los resultados han sido publicados y revisados por pares.
4	El nivel de validación 3 se actualiza sistemáticamente cuando se lanzan nuevas versiones del producto, o existe una expansión inter-anual de la serie temporal. Cuando sea apropiado para el producto, las incertidumbres se cuantifican mediante comparación con medidas de referencia fiduciarias en una red global de sitios y periodos de tiempo (si están disponibles).

Una reciente revisión de la literatura ha revelado que existen muy pocos ejercicios de validación de productos de albedo a nivel global (Mayr et al., 2019), la mayoría de ellos basados en observaciones de MODIS (Cescatti et al., 2012; Liang et al., 2002; Liu et al., 2013) aunque también basados en otros sensores como PROBA-V, SPOT/VGT o EPS/AVHRR (Lellouch et al., 2020). Este hecho otorga a los productos de albedo un nivel de validación 3, como máximo, de acuerdo a la jerarquía establecida por el CEOS/WGCV LPV (Tabla 1). Además, los resultados de validación existentes no son directamente comparables, ya que los protocolos empleados son diferentes entre los diversos ejercicios en términos de metodologías y métricas, datos de referencia y localizaciones (muestreo), cobertura espacio-temporal y ausencia de transparencia y trazabilidad. Todas estas inconsistencias respaldan la

necesidad de llevar las actividades de validación de productos de albedo hacia un flujo de trabajo de validación operacional (Bayat et al., 2021), que alinearía todos estos diversos aspectos. Esto permitiría, a su vez, alcanzar el máximo nivel de calidad en la jerarquía del CEOS/WGCV LPV (nivel 4), que no ha sido alcanzado en la actualidad para productos de albedo.

Dicho sistema operacional de validación de productos globales de ECVs debe considerar, al menos, cuatro principales componentes (Bayat et al., 2021): (1) registros de datos climáticos o CDRs a largo plazo; (2) un conjunto fiable y representativo a nivel global de medidas de campo; (3) un protocolo de validación estandarizado que cuente con el acuerdo de la comunidad científica; y (4) una plataforma de validación *online*, de libre acceso, que genere resultados e informes de validación estandarizados.

1.2. Definiciones de albedo

1.2.1. Albedo estimado mediante teledetección

Mientras el albedo de la superficie real puede ser medido directamente por estaciones terrestres, este no es el caso de los productos derivados con datos procedentes de instrumentos a bordo de satélites. Existen, por tanto, varias definiciones de productos de albedo de acuerdo al dominio de integración direccional (Pinty et al., 2005; Schaepman-Strub et al., 2006), considerando las dos condiciones más extremas: la radiación solar incidente es completamente directa o completamente difusa.

El **albedo black-sky** (BSA), técnicamente conocido como factor de reflectividad direccional hemisférica (AL-DH), es la reflectividad de la superficie cuando la iluminación proviene de una sola dirección. El BSA se define en ausencia de atmósfera, y depende de la posición angular de la fuente de luz y de las propiedades de la superficie. Dicho modelo considera que toda la energía proviene de radiación solar directa. Dado que el BSA es una función del ángulo cenital solar (SZA), suele calcularse a una hora específica (normalmente al mediodía solar local).

El **albedo white-sky** (WSA), técnicamente conocido como el factor de reflectividad bi-hemisférica (AL-BH), es la reflectividad de la superficie cuando la irradiancia es isotrópica. El albedo de la superficie bajo una cubierta de nubes homogéneas sería una buena

aproximación del WSA, dependiendo únicamente de las propiedades de la superficie. Este modelo considera que la iluminación es completamente difusa.

El albedo, además, suele definirse para dominios espectrales amplios o para bandas espectrales de ancho finito. Esta definición ha sido adoptada por los diferentes grupos internacionales (CEOS WGCV, WMO, GCOS). Para la mayoría de aplicaciones, la cantidad de interés no es espectral, sino de banda ancha. El albedo de banda ancha se define, por tanto, como el ratio del flujo de radiación reflejada e incidente en un determinado intervalo espectral.

La cadena clásica de un algoritmo operacional para la estimación del albedo se ilustra en la Figura 1, y está dividida en los 4 pasos siguientes:

1. **Corrección atmosférica.** Las medidas de las radiancias *Top-Of-Atmosphere* (TOA) que llegan al sensor a bordo del satélite son corregidas de los efectos de la atmósfera, con el objetivo de convertirlas en los correspondientes valores de reflectividades de la superficie o *Top-Of-Canopy* (TOC). En este paso también se realiza el filtrado de los píxeles afectados por contaminación de nubes.
2. **Inversión de la *Bidirectional Reflectance Distribution Function* (BRDF).** Las reflectividades TOC de cada canal espectral sirven como entrada al modelo de inversión de la BRDF, típicamente basado en funciones lineales. Dicho modelo permite describir la dependencia angular de la reflectividad en todas las direcciones.
3. **Integración angular.** Cálculo de los **albedos espectrales** mediante la integración angular de los parámetros de la BRDF.
4. **Integración espectral.** Finalmente, conversión de albedo espectral a **albedo de banda ancha** mediante regresión lineal.

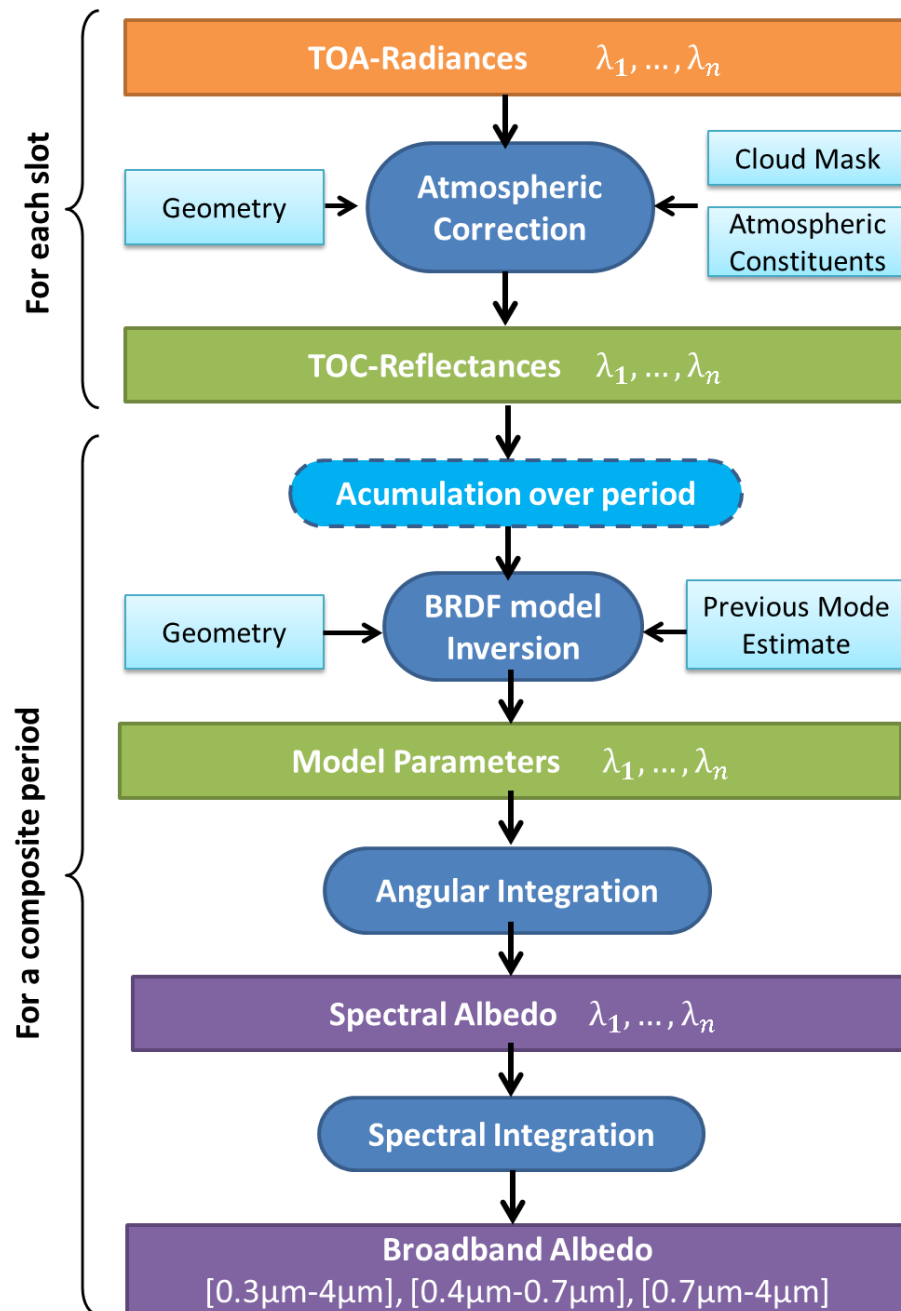


Figura 1: Diagrama habitual de un algoritmo para la estimación de albedo mediante teledetección basado en cuatro pasos: corrección atmosférica, inversión de la BRDF, integración angular e integración espectral.

Hay que tener en cuenta que los diferentes pasos que componen la cadena de procesado para la estimación del albedo con datos de satélite incluyen diferencias significativas que justifican las discrepancias entre productos. A continuación se detalle

punto por punto de qué manera influye cada uno de dichos aspectos en las diferencias entre productos:

- **Características orbitales y tiempo de paso del satélite.**

Las diferencias comienzan en las características de los satélites que llevan a bordo los sensores que nos proporcionan los datos de entrada. El tiempo de paso del satélite determina las condiciones de iluminación de la superficie y, por tanto, la radiancia medida por el satélite.

El calibrado del sensor se realiza bajo unas condiciones de iluminación específicas y la deriva orbital puede tener un efecto importante, pues dichas condiciones de iluminación varían. Satélites como *Terra* y *Aqua* no tienen deriva orbital (hora de paso y órbita constante), pero otros microsátélites como PROBA sí que se ven afectados, pues no llevan ningún sistema de propulsión a bordo, y la órbita se va degradando provocando una variación en la hora de paso durante su periodo de vida operacional. Por otra parte, el satélite SPOT perdió el control de la órbita al final de su misión (desde principios de 2013 hasta mayo de 2014), de manera que la adquisición de las imágenes fue realizándose de manera más temprana (hasta una hora al final de la misión). El incremento gradual del ángulo cenital solar provocó un incremento en el índice de vegetación normalizado (NDVI) que relaciona los canales en el red y NIR, como se mostró en la intercomparación del NDVI entre SPOT/VGT y MODIS (Toté et al., 2017).

- **Muestreo angular del sensor.**

Una de las principales diferencias en la estimación del albedo proviene del diferente muestreo angular usado para la caracterización de la BRDF. Todos los sensores utilizados en los productos estudiados en esta tesis (VGT, OLCI+SLSTR; y MODIS como referencia) tienen un amplio campo de visión, lo que permite la observación de la superficie sobre diferentes condiciones de iluminación solar a lo largo de las diferentes pasadas del satélite.

- **Exactitud geométrica y resolución espacial del sensor.**

La exactitud geométrica y los errores de geolocalización tienen un alto impacto en la calidad del producto, principalmente para superficies y objetivos heterogéneos.

Por otra parte, la resolución efectiva del píxel puede verse afectada dependiendo de la posición de la adquisición del satélite, que varía a lo largo de la franja de observación del sensor junto a la *point spread function* de la cámara (Meyer, 1996). Es, por tanto, una práctica habitual mezclar resoluciones espaciales diferentes, pues los productos se derivan para ventanas de composición de varios días. La resolución nativa de PROBA-V es 100 m al nadir, y 360 m en el borde de la franja de observación. SPOT/VGT alcanza una resolución de 1165 m al nadir, y de 1700 m en el borde. MODIS alcanza una resolución espacial nominal de 250 m para el Red y el NIR, y 500 m para el resto. Para los productos de MODIS de 250 m de resolución nominal al nadir, la resolución efectiva varía entre 344 m y 835 m entre filas y entre 292 m y 523 m entre columnas (Campagnolo and Montano, 2014). En el caso de los productos basados en OLCI+SLSTR, cada sensor tiene una resolución nominal teórica diferente (300 m para OLCI, 500 m para SLSTR). La resolución efectiva puede variar, teóricamente, hasta un valor de 500 m en caso de OLCI y de hasta 800 m en caso de SLSTR. OLCI y SLSTR se embarcan en la misma plataforma (Sentinel-3) y los ángulos de visión son prácticamente idénticos.

- **Canales espectrales del sensor.**

Cada sensor trabaja en diferentes rangos espectrales. Los productos *Copernicus* basados en SPOT/VGT y PROBA-V se derivan con sensores VGT equivalentes espectralmente, con 4 canales. MODIS cuenta con 7 canales espectrales, típicamente más estrechos que los de VGT, por lo que se esperan mayores diferencias en regiones con altas características de absorción como el Red. Por otra parte, el uso sinérgico de OLCI+SLSTR permite una caracterización más completa del espectro solar, con más 20 canales disponibles.

Hay que tener especial atención en la respuesta espectral en el rango de transición de la banda de absorción de clorofila a la banda de reflexión de las hojas (0.68-0.72 μm) (Trishchenko et al., 2002), conocida como *Red-Edge*. Los del Red en los sensores VGT (a bordo de SPOT y PROBA) sobrepasan el límite de 0.7 μm , por lo que este solapamiento con el *Red-Edge* tiene un impacto significativo en la reflectividad en el Red. Para los productos basados en Sentinel-3, las bandas del *Red-Edge* se descartan.

- **Calibración radiométrica del sensor.**

La calibración radiométrica es necesaria para permitir la conversión de las señales medidas por un sensor de satélite en unidades de radiancia absoluta. El rendimiento radiométrico de un sensor tiende a degradarse al degradarse la órbita (Gutman et al., 1999), tal como se ha planteado anteriormente. Los sensores VGT a bordo de SPOT, así como los sensores MODIS y OCLI+SLSTR tienen dispositivos de calibración a bordo, permitiendo una calibración radiométrica precisa (Fougnie et al., 2000; Henry and Meygret, 2000; Xiong and Barnes, 2006). Debido a la ausencia de dispositivos de calibración a bordo en el caso de PROBA-V, la calibración radiométrica se basa únicamente en una calibración vicaria (Sterckx et al., 2013), comprometiendo la estabilidad de las observaciones.

- **Corrección atmosférica.**

Cada cadena de procesamiento utiliza su propio método para corrección atmosférica y enmascaramiento de nubes de acuerdo con las capacidades espaciales y espectrales de cada sensor. Debido a las diferentes características espectrales, la influencia de la perturbación atmosférica será también diferente para los datos provenientes de SPOT/VGT, PROBA-V, MODIS y Sentinel-3/OLCI+SLSTR.

Los productos *Copernicus* derivados con SPOT/VGT, PROBA-V y Sentinel-3/OLCI+SLSTR usan el mismo método de corrección atmosférica (*Simplified Method for Atmospheric Correction*) (Rahman and Dedieu, 1994). Sin embargo, dicho método se apoya en diferentes datos auxiliares de entrada externos referentes a la caracterización de la atmósfera y el espesor óptico de los aerosoles. Sobre superficies densamente cubiertas por vegetación, mayores valores de espesor óptico de los aerosoles se traducen en menores valores de reflectividad en el visible y ligeramente mayores en el NIR, aunque el efecto es mayor en el visible. Las imágenes de MODIS se corrigen de los efectos de la dispersión y absorción de gases y aerosoles, así como de los efectos adyacentes causados por la variación de la cobertura terrestre, los efectos de acoplamiento atmosférico y la contaminación por nubes delgadas (Vermote et al., 2002). Los datos de entradas para la corrección atmosférica de los

productos de MODIS se derivan dentro del propio servicio, sin necesidad de fuentes externas.

El enmascarado de nubes se realiza con diferentes algoritmos para cada producto, dependiendo de las características espectrales de cada sensor. Además, a mayor resolución espacial nativa, mayor ventaja a la hora de detectar pequeñas nubes. Para SPOT/VGT y PROBA-V, sólo se utilizan los canales ópticos para la detección de nubes (Wolters et al., 2018, 2016), por lo que la detección de nubes es menos precisa. Es conocido que la detección de nubes de la colección 1 de PROBA-V muestra grandes errores sobre superficies brillantes y una gran cantidad de errores de omisión en latitudes más altas en los meses de invierno. MODIS cuenta con bandas térmicas, lo que facilita la detección de nubes, nieve y hielo (Ackerman et al., 2010). Por otra parte, los productos basados en Sentinel-3/OLCI+SLSTR usan el clasificador *IdePix* proporcionado por ESA, que tiene una limitación importante, pues clasifica la nieve como nubes.

- **Modelo de BRDF.**

La reflectividad de la superficie varía en función de las condiciones de iluminación y visión por el efecto de la anisotropía de la superficie. La BRDF describe la dependencia de cada superficie para cada píxel, por lo que la corrección de los efectos de la BRDF se considera uno de los requerimientos más importantes para la consistencia entre series climáticas derivadas con diferentes sensores (Cihlar et al., 2004, 1998). Los productos de albedo están corregidos de los efectos de la BRDF, y están definidos bajo las mismas condiciones de iluminación, pues el albedo *black-sky* lo computan todos los productos al mediodía solar local. Sin embargo, las diferencias entre productos se explican, parcialmente, por el diferente modelo usado para parametrizar la BRDF (Carrer et al., 2010b). Por otra parte, el rendimiento del modelo BRDF también depende del número de observaciones libres de nubes disponibles durante el período de síntesis, así como de la distribución angular del muestreo. Las mayores incertidumbres de la BRDF están asociadas con los objetivos de nieve para los cuales ninguno de estos modelos BRDF paramétricos era adecuado (Maignan et al., 2004).

La mayoría de productos de albedo operacionales se basan en modelos semi-empíricos basados en descriptores de la BRDF (paso 2), que han sido desarrollados durante las últimas décadas para modelar la BRDF de un gran número de sensores ópticos (Barnsley et al., 1994; Hu et al., 1997; Lucht et al., 2000; Roujean et al., 1992; Strahler, 1997; Wanner et al., 1997, 1995). El uso de estos modelos está ampliamente extendido, pues pueden representar la firma direccional de la mayoría de los objetivos naturales (Breon and Maignan, 2017; Bréon and Vermote, 2012; Claverie et al., 2015; Franch et al., 2014; Los et al., 2005; Lucht et al., 2000; Roujean et al., 1992, 2018; Roy et al., 2016; Schaaf et al., 2002; Vermote et al., 2009; Wanner et al., 1995). El enfoque se basa en una descomposición del factor de reflectividad bidireccional en una serie de funciones (*kernels*) que están asociadas a los procesos dominantes de dispersión de la luz (p.ej., efectos geométricos o volumétricos), una separación entre suelo y vegetación, o la conjunción entre medios ópticamente gruesos y delgados (Lucht and Roujean, 2000). Tanto las mediciones *in situ* como los experimentos numéricos han apoyado el uso de modelos basados en *kernels*, usados para la mayoría de sensores a bordo de satélites que ofrecen sistemas de adquisición multi-angulares. Ejemplos típicos de estos sensores son los históricos POLDER, SeaWiFS, VGT, MODIS o MERIS (Baret et al., 2007; Justice et al., 1998; Leroy et al., 1997; Muller et al., 2011; Samain et al., 2006; Strahler et al., 1999; Wanner et al., 1997). Estos métodos ofrecen un buen compromiso entre calidad de los resultados, facilidad de implementación y tiempo de computación, siendo una solución pragmática y robusta. Esto explica que sean los más utilizados en contextos operacionales para el desarrollo de productos de albedo.

Existen modelos más rigurosos desde un punto de vista teórico, que tratan el modelo de transferencia radiativa en un sistema que trata la atmósfera y la superficie de forma simultánea. Ejemplos de estos algoritmos se aplicaron a MISR (Diner et al., 2008, 1998) y METEOSAT (Pinty et al., 2000a, 2000b). La característica común de estos algoritmos es la corrección y explotación de las variaciones en la geometría del sensor solar que ocurren como una función de la órbita del satélite, el diseño del sensor, la posición geográfica del objetivo y la hora del año. También existen métodos puramente basados en la observación para la descripción e inversión de la BRDF, como el método de agrupamiento angular utilizado para la generación del producto GLASS (Zhao et al., 2013). Otras investigaciones se

centraron en métodos para obtener albedos de banda ancha directamente a partir de reflectividades TOA (Liang, 2003).

- **Conversión a banda ancha.**

Los productos se definen, habitualmente, en tres rangos espectrales de banda ancha que representan las cantidades más demandadas de albedo: todo el espectro solar o albedo de onda corta (300–4000 nm), el visible (400–700 nm) y el infra-rojo cercano (NIR) (700–3000 nm). En realidad, cualquier cambio en el albedo de onda corta (solar) puede ser tenue debido a la compensación entre el albedo de la superficie del infrarrojo cercano y el visible de banda ancha. Esto justifica plenamente la estimación de los tres productos de albedo de banda ancha, aunque cada uno podría derivarse de los otros dos. Cabe destacar que el rango espectral de la banda ancha visible coincide con el rango de la radiación fotosintéticamente activa (PAR). Como la vegetación absorbe la mayor parte de la radiación PAR, el albedo PAR es particularmente sensible al verdor. Por otro lado, el albedo del infrarrojo cercano es alto para la vegetación frondosa y bajo para el material leñoso en comparación con el albedo visible.

Los productos de albedo de banda ancha se computan a partir de los albedos espectrales de las diferentes bandas de los sensores, que difieren en número de bandas y respuestas espectrales. Además, los albedos de banda ancha se definen, teóricamente, en regiones ligeramente diferentes dependiendo del servicio (*Copernicus*, NASA).

1.2.2. Albedo bajo iluminación real

El **albedo** de la superficie terrestre **bajo iluminación real**, conocido como **albedo blue-sky**, sólo puede medirse mediante la instalación de la instrumentación *in situ* apropiada. Los conjuntos de datos de albedo de referencia se pueden derivar a partir de la relación entre la irradiancia reflejada e incidente en la superficie. Esto se consigue a través de piranómetros, que integran la radiación incidente que alcanza el sensor desde el hemisferio completo. El concepto de “albedómetro” se concibe mediante el acoplamiento de dos de

estos instrumentos, que miden simultáneamente la irradiancia del cielo y la reflectancia de la superficie.

En la práctica, el albedo *blue-sky* suele aproximarse a partir de una combinación lineal de los albedos BSA (iluminación completamente directa) y WSA (iluminación completamente difusa), ponderados por la fracción de radiación difusa (Lucht et al., 2000; Pinty et al., 2005). Dicha cantidad depende, por tanto, de la posición solar, de las condiciones atmosféricas y de las propiedades de la superficie.

$$\text{Blue_sky albedo} = (1 - \text{dif}(\theta_s))\text{BSA}(\theta_s) + \text{dif}(\theta_s)\text{WSA} \quad \text{Eq. 1}$$

donde $\text{dif}(\theta_s)$ es la proporción de radiación difusa a un determinado SZA (θ_s).

La expresión anterior es válida para condiciones libres de nieve. Sin embargo, los efectos de la dispersión múltiple y la anisotropía de la iluminación difusa deben ser considerados de manera más cuidadosa para zonas cubiertas de nieve debido a los altos valores de reflectividad sobre la nieve y al gran ángulo cenital solar a altas latitudes. Entonces, se debería usar una expresión más compleja del albedo *blue-sky* para áreas cubiertas de nieve (Román et al., 2010).

1.3. Marco de Trabajo

Esta tesis doctoral ha sido desarrollada en la empresa *Earth Observation LABORatory*¹³ (EOLAB). EOLAB está especializada en proveer servicios técnicos relacionados con la observación de la Tierra para la observación de la vegetación y las variables de radiación en cuatro áreas principales: (i) diseño de algoritmos para estimar variables geo-biofísicas a partir de datos de teledetección, (ii) evaluación de la calidad de productos de teledetección, (iii) adquisiciones y procesamiento de medidas terrestres, y (iv) consultoría para la asimilación de productos de teledetección en diferentes aplicaciones. EOLAB está estrechamente relacionada con la Universidad de Valencia, pues surgió como *spin-off* de la misma y colabora activamente en la formación de estudiantes de máster y doctorado en la empresa.

¹³ EOLAB Spain S.L. url: <https://eolab.es/> (acceso online el 01/03/2023)

EOLAB destaca a nivel europeo por su posicionamiento en actividades de validación en el programa *Copernicus*, habiendo trabajado en el desarrollo de algoritmos y validación de productos geo-biofísicos en el programa *Global Monitoring for Environment and Security* (GMES), precursor de *Copernicus*. Desde los inicios de los servicios de monitorización de la superficie terrestre (CGLS) y cambio climático (C3S) de *Copernicus*, la empresa es responsable de evaluar la calidad de los productos biofísicos de radiación de la superficie (incluyendo el albedo) y otros parámetros de vegetación. El CGLS, coordinado por el *Joint Research Centre* (JRC) de la comisión europea (EC), produce sistemáticamente una serie de productos geo-biofísicos de calidad, en tiempo casi real, que informan sobre el estado y la evolución de la superficie terrestre a escala global y a medias y bajas resoluciones espaciales (desde 300 m a 1 km). Los productos pueden ser usados para monitorizar la vegetación, el ciclo del agua, el balance energético o la presencia de hielo. Dicho servicio forma parte de la componente de la superficie terrestre de *Copernicus*, siendo operacional desde el año 2013. Por otra parte, el C3S, implementado por el Centro Europeo de Previsiones Meteorológicas a Plazo Medio (ECMWF), proporciona información fiable sobre el clima con observaciones *in situ*, datos de satélite y actividades de re-análisis, contando con herramientas para permitir estrategias de mitigación y adaptación al cambio climático por parte de los responsables políticos y agencias privadas. Cabe destacar que CGLS inicialmente desarrolló las cadenas de procesamiento de productos de albedo con datos de SPOT/VGT, posteriormente adaptándolas a PROBA-V. La producción de dichos productos se trasladó definitivamente al servicio C3S, que produce series climáticas o CDRs de diferentes ECVs. C3S ha extendido la serie climática de albedo derivada con SPOT/VGT (1998-2014) y PROBA-V (2014-2020) hacia el pasado con datos de NOAA/AVHRR (periodo 1981–2005), y continuará la producción tras el fin de PROBA-V (Junio 2020) gracias a las adquisiciones que Sentinel-3 ofrece desde mediados de 2018 en adelante. La actividad en los servicios *Copernicus* ha permitido la definición de los diferentes protocolos y métricas para la validación de productos de albedo, así como la aplicación de los mismos para evaluar la calidad científica de varios productos (ver lista de informes en Anexo I). En este contexto se han realizado las 4 publicaciones en la presente tesis: Anexo II (Roujean et al., 2018), Anexo III (Sánchez-Zapero et al., 2020), Anexo IV (Sánchez-Zapero et al., 2023b) y Anexo V (Sánchez-Zapero et al., 2023a).

A nivel internacional, la compañía viene participando activamente en el CEOS/WGCV LPV (Camacho, 2019), contribuyendo al desarrollo de protocolos de validación de diferentes variables. El director de la empresa, Fernando Camacho, ha ejercido de *chair* (2019-2022) y *vice chair* (2016-2019) del grupo. Desde 2023, el autor de esta tesis está coliderando el CEOS/WGCV LPV en el área temática de la radiación de la superficie, que incluye al producto de albedo. Por este motivo, la presente tesis se enmarca plenamente en la consecución de los objetivos prioritarios del CEOS/WGCV LPV, habiendo contribuido al desarrollo del protocolo de validación de productos globales (Wang et al., 2019), que ha logrado el acuerdo de métricas de expertos internacionales y agencias. También se ha realizado el desarrollo de un sistema estandarizado de validación operacional, respaldado por el CEOS/WGCV LPV y dando lugar a la publicación (Sánchez-Zapero et al., 2023b) incluida en el Anexo IV . Dicha publicación ha presentado también la validación e intercomparación de 3 CDRs de albedo (C3S V2, NASA MCD43A3 C6.1, BNU GLASS V4).

1.4. Motivación y objetivos

Se ha determinado que existe una clara necesidad de cuantificar y medir de manera eficiente las incertidumbres asociadas a los productos globales de albedo derivados con datos de satélite, lo que se conoce como validación. La validación debe permitir, también, evaluar en qué medida el producto satisface los requerimientos del usuario. Dicha validación debe estar estandarizada a nivel metodológico, ofreciendo transparencia y trazabilidad en su proceso. Todo ello impulsa la necesidad de desarrollar un sistema operacional para una validación estandarizada de productos de albedo que permita, a su vez, alcanzar el nivel de validación más alto (nivel 4) en la jerarquía del CEOS/WGCV LPV, lo que representaría un hito sin precedentes en el área de validación de productos globales de albedo. Como se ha comentado, dicho sistema debe considerar, al menos, cuatro principales componentes (Bayat et al., 2021): (1) registros de datos climáticos de albedo derivados de satélite; (2) un conjunto fiable y representativo a nivel global de medidas *in situ*; (3) un protocolo de validación estandarizado que cuente con el acuerdo de la comunidad científica; y (4) una plataforma de validación *online*, de libre acceso, que genere resultados e informes de validación estandarizados.

Respecto a la primera componente, los registros climáticos de albedo los ofrecen los diferentes servicios o agencias. Actualmente en el contexto Europeo, el servicio C3S ha venido desarrollando una serie climática muy extensa, cuya calidad e incertidumbre asociada a las estimaciones debe ser evaluada. Por otra parte, se debe dar continuidad a dicho CDR gracias a la disponibilidad de datos de satélites de nueva generación (Sentinel-3), que ofrecen mejoras en cuanto a resolución espacial y espectral.

En cuanto al conjunto fiable y representativo de medidas *in situ* a nivel global, hay multitud de redes que cuentan con la instrumentación apropiada para la medición del albedo de la superficie terrestre, pero no están directamente diseñadas específicamente para la validación de productos de albedo y dichos datos deben ser homogeneizados y tratados previamente. Por otra parte, los trabajos de validación previamente desarrollados se centran en un número muy limitado de estaciones y periodos temporales por lo que hay una clara necesidad de establecer una red que sea lo más representativa a nivel global. Además, es necesario evaluar la representatividad espacial de la medida *in situ*, que depende de la heterogeneidad de la superficie alrededor de la torre (Román et al., 2009, 2010; Wang et al., 2012, 2014), para determinar si el valor medido por la estación puede representar un área equivalente al píxel de satélite, que suele rondar entre 300 m y 1 km para productos globales con los satélites y sensores actuales.

La tercera componente implica el desarrollo de unos protocolos y metodologías estandarizados, bajo el consenso de la comunidad científica, que ofrezcan a su vez trazabilidad y transparencia en el proceso de validación. La estandarización de protocolos está coordinada internacionalmente por el CEOS/WGCV LPV y previamente al desarrollo de esta tesis no existía un protocolo de buenas prácticas de validación de productos de albedo.

Finalmente, el desarrollo de una plataforma de validación *online* que genere resultados de validación estandarizados representaría un hito sin precedentes en la validación de productos globales de albedo derivados con datos satelitales. Se pretende desarrollar la herramienta SALVAL que integre todas estas componentes para un sistema de validación operacional (ver Figura 2).

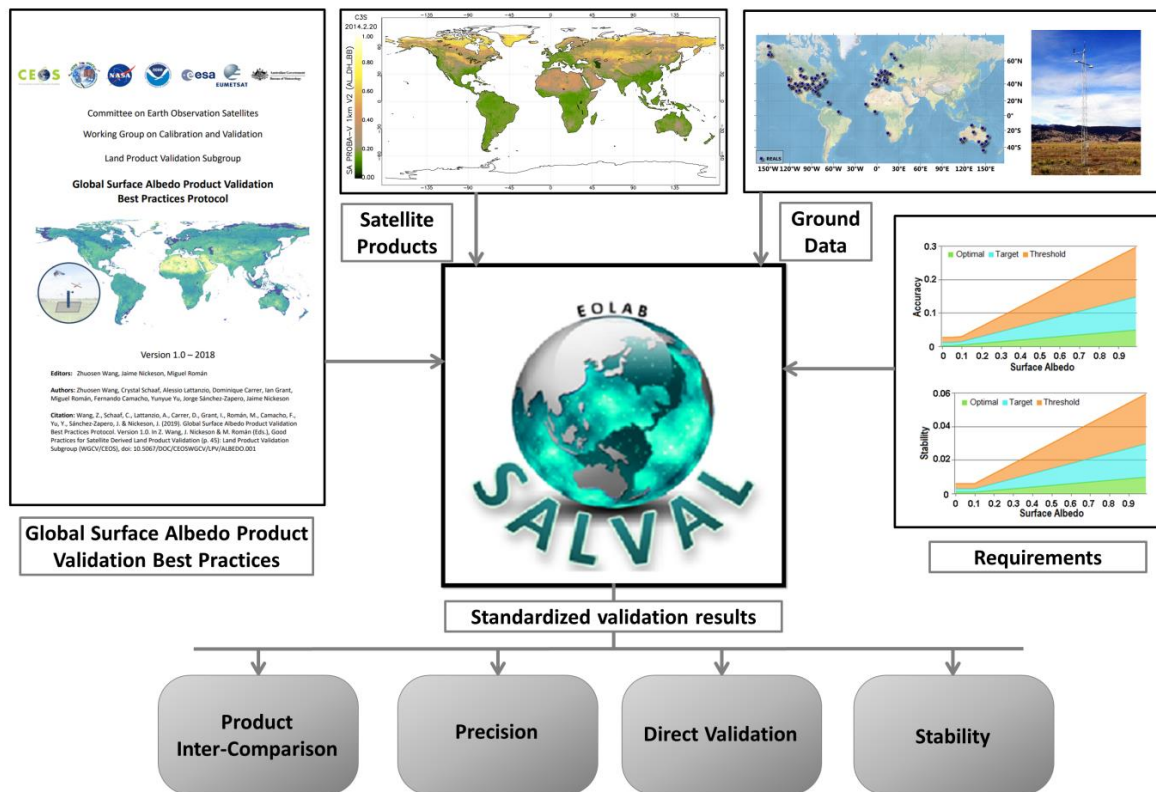


Figura 2: Diagrama de la herramienta de validación SALVAL, que ofrece resultados de validación estandarizados integrando el protocolo de validación, productos de satélite, datos de campo y requerimientos de usuario.

El presente trabajo tiene, por tanto, los siguientes objetivos, que están directamente relacionados con el desarrollo de una metodología de validación de producto de albedo y el desarrollo de un sistema operacional de validación estandarizada, que integra 4 componentes (metodología, series climáticas de albedo, datos de campo y herramienta *online*):

- **OBJETIVO 1:** Desarrollo y propuesta de una metodología propia para la validación estandarizada de productos globales de albedo de la superficie terrestre a diferentes resoluciones.
 - Dicha metodología deberá tratar y desarrollar las métricas necesarias para evaluar la incertidumbre del producto, considerando los diferentes requerimientos expresados por los organismos internacionales (GCOS, WMO).
 - Dicha metodología debe estar estandarizada y contar con el consenso internacional de expertos, desarrolladores de productos y agencias, por lo que se pretende que

- sirva como contribución al protocolo de validación desarrollado por el CEOS/WGCV LPV.
- En cuanto a la intercomparación, se pretende desarrollar estrategias de muestreo común sobre un conjunto representativo de localizaciones a nivel global, permitiendo que los distintos ejercicios de validación indirecta sean comparables entre sí, dando valor al concepto de estandarización.
 - **OBJETIVO 2:** Evaluar la calidad científica, así como determinar la exactitud y la incertidumbre asociada a los productos de albedo a escala global desarrollados dentro del programa *Copernicus*, que se derivan con diferentes sensores satelitales a diferentes resoluciones espaciales.
 - En primer lugar se trabajará en la validación de los prototipos desarrollados en el programa CGLS, que servirán de base para la migración al servicio C3S.
 - Seguidamente se pretende validar la primera versión de los productos de albedo desarrollados en C3S, con el foco en la transición de SPOT/VGT a PROBA-V.
 - Se validará también la segunda versión de la serie climática C3S, que incorpora el concepto '*multi-sensor*' para hacer la serie más consistente entre sensores.
 - Finalmente, se pretende trabajar en el desarrollo y validación de productos C3S de albedo con datos de los satélites *Copernicus* Sentinel-3, haciendo un uso sinérgico de sus sensores OLCI y SLSTR, para la continuidad de la serie climática de albedo.
 - **OBJETIVO 3:** Desarrollo de una base de datos de medidas *in situ* de albedo que sea fiable, integrando datos procesados de redes o iniciativas existente.
 - Se pretende integrar datos del máximo número de estaciones posibles, para que el resultado de la validación sea lo más representativo posible a nivel global.
 - Se evaluará la representatividad espacial de la medida, asegurando que dicha medición sea equivalente a la resolución espacial del píxel de satélite de interés.
 - **OBJETIVO 4:** Desarrollo de una herramienta de software semi-automática, que permita alcanzar una validación operacional continuada en el tiempo a medida que la serie temporal de los productos se expande o se desarrollan nuevas versiones (nivel 4 de validación de acuerdo a la jerarquía del CEOS/WGCV LPV).

- Dicha herramienta deberá permitir a los productos de albedo alcanzar el nivel máximo (4) en la jerarquía del CEOS/WGCV LPV, contando con el respaldo del mismo.
- La herramienta deberá contar con una interfaz amigable para el usuario, permitiendo un ejercicio interactivo de validación que podrá ser configurado en base a los requerimientos del propio usuario (*fitness-for-purpose*).
- La herramienta debe integrar una base de datos de productos y datos *in situ* existentes y permitir al usuario o desarrollador de producto introducir nuevos productos para ser evaluados.

2. Protocolo de validación

Nota: Este capítulo se basa, en parte, en la aportación que se ha hecho al protocolo de validación de productos globales de albedo (Wang et al., 2019) que se ha desarrollado el contexto del CEOS/WGCV LPV: **Global Surface Albedo Product Validation Best Practices Protocol. Version 1.0.**

Referencia: Wang, Z., Schaaf, C., Lattanzio, A., Carrer, D., Grant, I., Roman, M., Camacho, F., Yang, Y., **Sánchez-Zapero, J.**, 2019. Global Surface Albedo Product Validation Best Practices Protocol. Version 1.0. In Z. Wang, J. Nickeson & M. Román (Eds.), Good Practices for Satellite-Derived Land Product Validation (p. 45): Land Product Validation Subgroup (WGCV/CEOS). [WWW Document]. <https://doi.org/doi:10.5067/DOC/CEOSWGCV/LPV/ALBEDO.001>

Así mismo, las métricas y protocolos de validación incorporados en el protocolo CEOS/WGCV LPV, se han ido testando y poniendo en práctica en el programa CGLS y C3S, donde durante el periodo de la tesis doctoral se ha trabajado en la validación de los productos de albedo y reflectividad de la superficie. Así mismo, este capítulo incorpora también métricas y análisis adicionales que se han realizado en los informes de validación de los productos de albedo generados en dichos proyectos (ver listado de informes en Anexo I).

La validación se basa en dos principales enfoques: validación directa (estimación de satélite versus medida *in situ*) y validación indirecta o intercomparación de productos. Para la validación directa entre estimaciones de satélite y medidas reales de albedo, es necesario generar los albedos *blue-sky* (Lewis, P & Barnsley, 1994) de satélite a partir de los valores estimados de BSA y WSA en la banda ancha de onda corta (AL-DH-BB y AL-BH-BB), ponderados por la fracción de difusa medida en la estación terrestre (ver Eq. 1). La intercomparación entre productos, por otra parte, debe tener en cuenta las diferencias en cuanto a características espaciales y temporales de los diferentes conjuntos de datos. Es, por ello, necesario definir un mismo soporte tanto espacial como temporal para la intercomparación. Es recomendable realizar la

comparación de productos ponderando típicamente una ventana de 3x3 píxeles, que reduce las incertidumbres asociadas tanto a los errores de geo-localización como a la resolución efectiva del píxel (Camacho et al., 2013; Sánchez et al., 2015).

Por otra parte, es necesario establecer un muestro de localizaciones común, con el objetivo de llevar el ejercicio a un estado de escalabilidad, trazabilidad y estandarización. De esta manera, los diferentes ejercicios pueden ser comparables entre sí, estando realizados sobre un mismo conjunto de emplazamientos. Se han definido dos redes de localizaciones (Figura 3) para las estrategias tanto de validación directa como de intercomparación de productos, tal como se describe a continuación en los apartados 2.1 y 2.2. Para la validación directa se ha creado la base de datos REALS de medidas *in situ*, generada a partir de datos procedentes de 99 estaciones pertenecientes a redes existentes donde se ha realizado el test de la representatividad espacial de las medidas proporcionadas por las estaciones de acuerdo a protocolos estándares (Román et al., 2010, 2009). Para la intercomparación de productos se ha definido el muestreo global LANDVAL, compuesto por 720 localizaciones y diseñado para representar la variabilidad de tipos de cobertura terrestre y representatividad continental a nivel global. LANDVAL también incluye sitios desérticos de calibración (Lachérade et al., 2013), útiles para la evaluación de la precisión y la estabilidad.

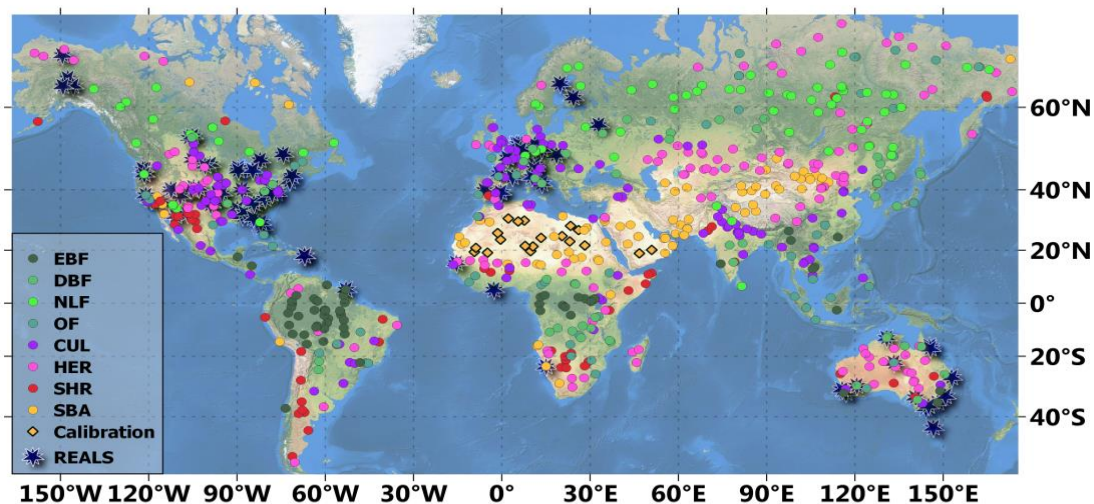


Figura 3: Distribución global de las 99 localizaciones de REALS y las 720 de LANDVAL para la validación directa y la intercomparación de productos. LANDVAL se representa diferenciando diferentes tipos de bioma: EBF significa 'Evergreen Broadleaved forest', DBF 'Deciduous Broadleaved Forest', NLF 'Needle-Leaf Forests', OF 'Other Forests', CUL 'CULTivated', HER 'HERbaceous', SHR 'SHRublands', y SBA 'Sparse and Bare Areas'.

2.1. Base de datos REALS

REALS es una base de datos de medidas *in situ* para la validación directa de productos de albedo de satélite, integrando medidas de una amplia selección de estaciones. Los datos provienen de 99 estaciones con disponibilidad de medidas desde el año 2000 a la actualidad, procedentes de redes o iniciativas existentes, como *Ground-Based Observations for Validation* (GBOV¹⁴) de Copernicus, *Flux Network* (FLUXNET¹⁵), *national science foundation's National Ecological Observatory Network* (NEON¹⁶), *European Fluxes Database Cluster* (EFDC¹⁷), *Integrated Carbon Observation System* (ICOS¹⁸) y *Australia's Land Ecosystem Observatory or Terrestrial Ecosystem* (TERN¹⁹). Muchas de las estaciones GBOV, FLUXNET y EFDC incorporan, a su vez, sus medidas en la red *Baseline Surface Radiation Network* (BSRN²⁰) y su componente norteamericana conocida como *Surface Radiation Budget* (SURFRAD²¹). BSRN se considera como el estándar de calidad de acuerdo al GCOS (GCOS-154, 2011) y a las recomendaciones del CEOS/WGCV LPV (Wang et al., 2019). Es destacable también el hecho de que 23 de las estaciones REALS son consideradas '*Super Sites*' avalados por el CEOS/WGCV LPV, lo que significa que están bien caracterizadas a nivel de estructura y otras variables biofísicas, siguen protocolos de medida de acuerdo a estándares establecidos y vienen estando activas durante largos periodos de tiempo, contando con el respaldo adecuado en cuanto a financiación y capacidades técnicas.

La huella espacial de la medida (*footprint*, ver círculo en la base de la Figura 4) depende de la altura de la torre, por lo que debe evaluarse la representatividad de la misma a la hora de comparar con el tamaño del píxel del producto derivado de satélite.

$$f = 2 H \tan(HFOV) \quad \text{Eq. 2}$$

¹⁴ <https://gbov.acri.fr/> (acceso online el 16/05/2023)

¹⁵ <https://fluxnet.org/> (acceso online el 16/05/2023)

¹⁶ <https://www.neonscience.org/> (acceso online el 16/05/2023)

¹⁷ <http://www.europe-fluxdata.eu/> (acceso online el 16/05/2023)

¹⁸ <https://www.icos-cp.eu/> (acceso online el 16/05/2023)

¹⁹ <https://www.tern.org.au/> (acceso online el 16/05/2023)

²⁰ <https://bsrn.awi.de/> (acceso online el 16/05/2023)

²¹ <https://gml.noaa.gov/grad/surfrad/> (acceso online el 16/05/2023)

donde f [m] es el diámetro de la huella circular de la medida de campo, H [m] es la altura de la torre, y el *Half Field Of View* (*HFOV* [grados]) es la mitad del ángulo de visión del instrumento. Generalmente se usa *HFOV* igual a 40.5° para las medidas *in situ* de albedo (Michalsky et al., 1995) como estándar para la mayoría de instrumentos.

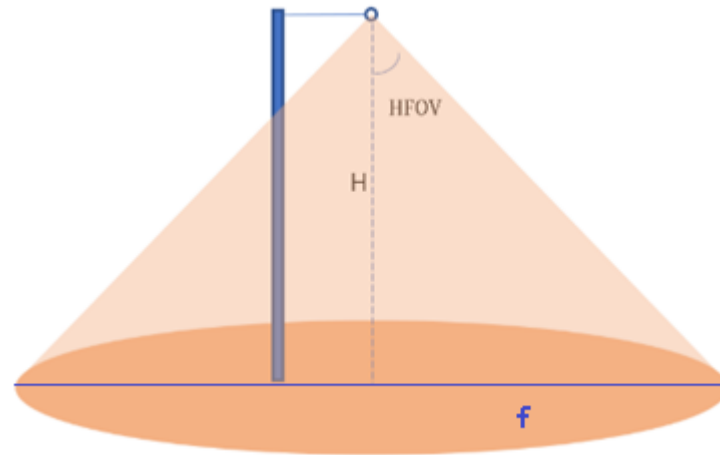


Figura 4: Huella espacial (*footprint*) de la medida de una torre de albedo.

Una de las herramientas más eficientes para describir la representatividad espacial es el uso de semivariogramas (Hohn, 1991). Las características del semivariograma pueden revelar la variabilidad espacial de la superficie y revelar los efectos de escala asociados con los datos de teledetección (Román et al., 2009, 2010; Wang et al., 2012, 2017; Woodcock et al., 1988). Los semivariogramas pueden estimarse a partir de imágenes de satélite de alta resolución (p.ej., Landsat, Sentinel-2) para diferentes periodos del año:

$$\gamma_E(h) = 0.5 \cdot \frac{\sum_{i=1}^{N(h)} (z_{xi} - z_{xi+h})^2}{N(h)} \quad \text{Eq. 3}$$

donde $\gamma_E(h)$ es el semivariograma estimado entre las reflectividades que están dentro de cierta distancia h ; z_{xi} es la reflectividad de la superficie para el píxel x ; z_{xi+h} es la reflectividad de la superficie para otro píxel a una distancia h ; y $N(h)$ es el número de píxeles a una distancia h .

Es práctica habitual ajustar el semivariograma a un modelo esférico, que depende de 3 atributos (*range*, *sill*, *nugget*) fácilmente interpretables (Matheron, 1963):

$$\gamma_E(h) = \begin{cases} c_0 + c \cdot \left(1.5 \cdot \frac{h}{a} - 0.5 \left(\frac{h}{a}\right)^3\right) & \text{for } 0 \leq h \leq a \\ c_0 + c & \text{for } h > a \end{cases} \quad \text{Eq. 4}$$

donde el *range* (a) representa el tamaño promedio de los elementos del paisaje, y corresponde a la distancia a partir de la que se anula la correlación de las propiedades biofísicas asociadas a un punto. El *sill* (c) es el máximo de variancia, siendo el valor de la ordenada del rango en el que el semivariograma se nivela en una asíntota. El *nugget* (c_0) representa el valor que tendría la variancia para una distancia $h = 0$, y puede ser distinto de cero.

Se recomiendan cuatro atributos geo-estadísticos para dicha evaluación (Román et al., 2010, 2009): *Relative Coefficient of Variation* (RCV), *Scale Requirement Index* (RSE), *Relative STrength of the spatial correlation* (RST), y *Relative proportion of Structural Variation* (RSV). Dichos atributos se pueden condensar en un único indicador de la representatividad espacial: *Standard Score* (ST), mientras que aquellas situaciones donde el estimador del semivariograma no proporcione un buen ajuste al modelo esférico, se suele considerar el *score* de primer orden (RAW). Ambos indicadores son directamente proporcionales a la representatividad y la homogeneidad relativa del sitio, por lo que a mayor valor, mayor es la representatividad y la medida es más apropiada para ser comparada con el valor del píxel de satélite.

$$ST = \left(\frac{|R_{CV}| + |R_{ST}| + |R_{SV}|}{3} + R_{SE} \right)^{-1} \quad \text{Eq. 5}$$

$$RAW = |2 R_{CV}|^{-1} \quad \text{Eq. 6}$$

La metodología adoptada para la evaluación de la representatividad espacial de la medida en REALS se basa en la estimación del semivariograma esférico para diferentes resoluciones espaciales (1 km², 1.5 km² y 3 km²). Una vez estimado el semivariograma, se calculan los indicadores geo-estadísticos con el objetivo de cuantificar el nivel de representatividad de las medidas asociadas a cada estación (ST, RAW). La evaluación de la representatividad debe realizarse para varios periodos del año (época de máximo crecimiento de vegetación, época más árida, periodos de nieve, periodos libres de nieve, etc.). En caso de REALS, se ha evaluado la representatividad

para dos situaciones temporales (épocas de mínimo y máximo desarrollo de vegetación) usando imágenes de reflectividad de la superficie de Sentinel-2 (ESA Sentinel-2 mission, n.d.) para la banda B8 (NIR) que es la más representativa del espectro total de onda corta (Bonafoni and Sekertekin, 2020). La Figura 5 muestra un ejemplo del ajuste esférico del semivariograma, y sus indicadores de representatividad especial, para dos estaciones de la base de datos REALS situadas en USA: *Desert Rock (DRAK)* y *Talladega National Forest (TALL)*. El resumen de los indicadores para todas las estaciones REALS se puede encontrar en el apéndice A de la publicación 3 incluida en esta tesis (ver Anexo IV).

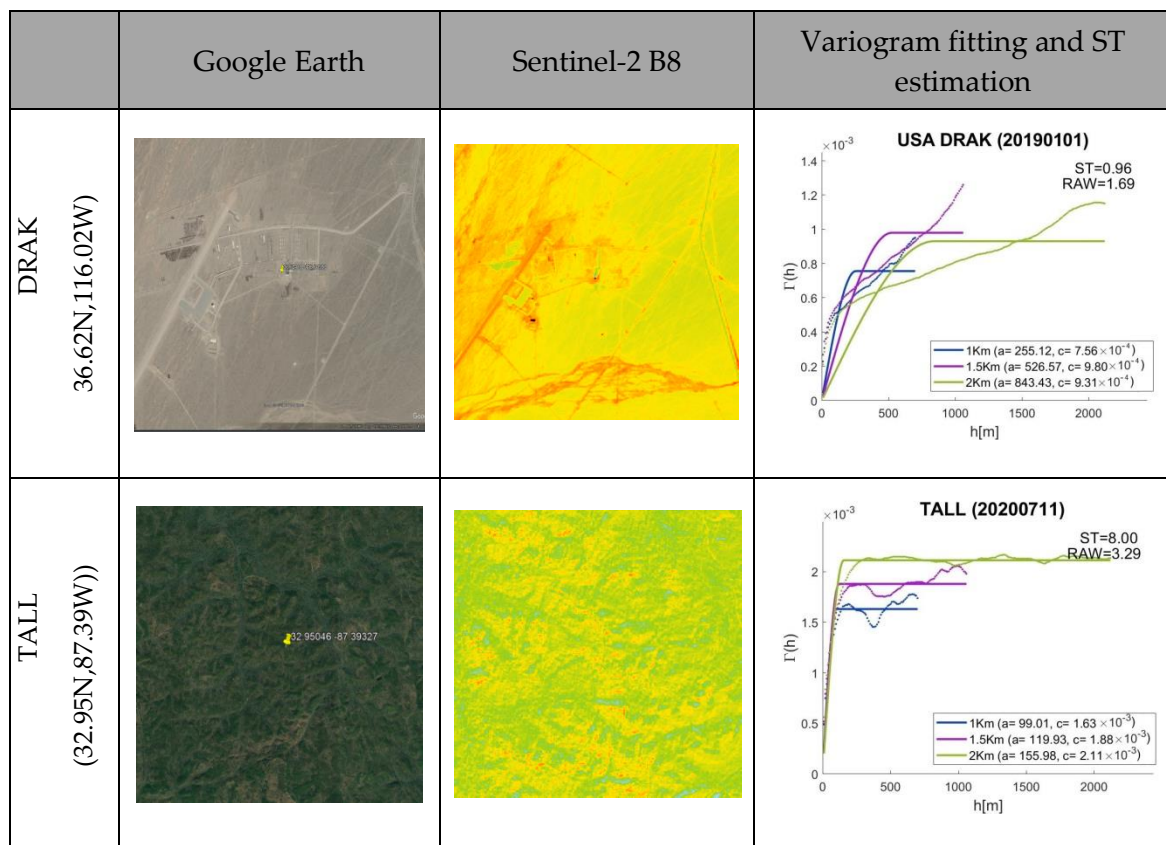


Figura 5: Ejemplo de ajuste de semivariograma y estimadores (ST, RAW) sobre dos estaciones en USA: *Desert Rock (DRAK)* y *Talladega National Forest (TALL)*. Se muestran las imágenes de *Google Earth* y *Sentinel-2 B8*. Fuente: (Sánchez-Zapero et al., 2023b).

Por otra parte, se ha hecho un análisis adicional para determinar un umbral para el indicador ST que diferencie entre sitios no representativos (heterogéneos) y representativos, aptos para la validación directa. Para ello, se ha realizado un análisis

de tres parámetros en función del ST para el periodo 2000-2020: la incertidumbre (RMSD) del producto NASA MCD43A3 C6.1 en comparación con las medidas de *in situ*, el número de estaciones y el número de muestras (ver Figura 6). De acuerdo a este análisis, el RMSD tiende a decrecer cuando el valor ST crece debido a la mayor homogeneidad de los sitios, pero el número de sitios y muestras tiende a decrecer también. Por esta razón, se ha establecido un umbral de ST de 1.5 como filtro dentro de la base de datos REALS ya que ofrece un buen compromiso entre RMSD (tiende a estabilizarse a partir de este umbral) y el número de muestras y sitios descartados. Dicho umbral es similar al usado en otros ejercicios de validación (Cescatti et al., 2012; Sánchez-Zapero et al., 2020).

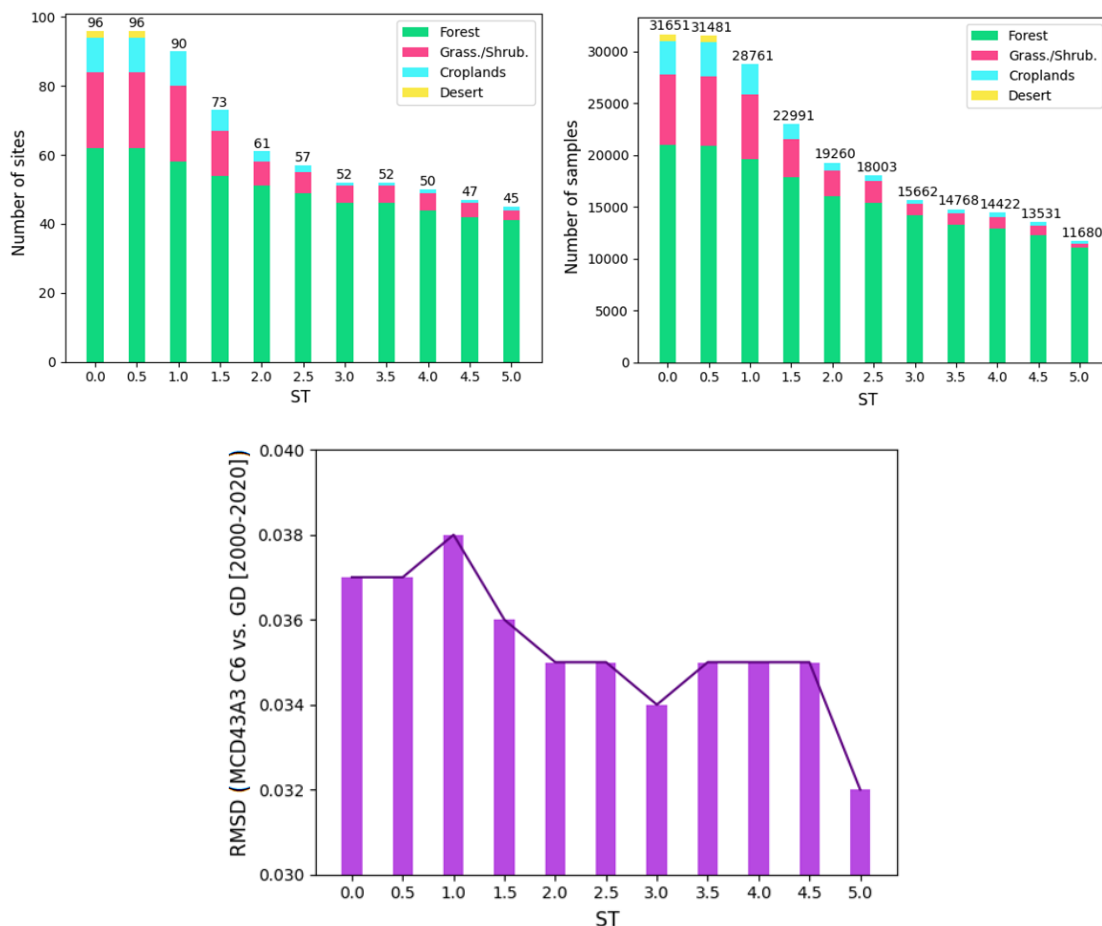


Figura 6: Evolución del número de estaciones (arriba-izquierda), número de muestras (arriba-derecha) y RMSD de la comparación MCD43A3 C6.1 versus *in situ* (abajo) en función del indicador ST para el periodo 2000-2020.

Finalmente, cabe destacar el hecho de que la incertidumbre de la medida de campo depende de la exactitud absoluta del instrumento y de la respuesta no ideal del coseno asociada en sensores ópticos (Michalsky et al., 1995; Vijeta et al., 2021). La mayoría de los errores asociados con la exactitud absoluta del instrumento son similares para los flujos ascendentes y descendentes y, por lo tanto, pueden compensarse. En general, la exactitud esperada es del orden del 4% al 7% en condiciones de cielo despejado, y del 1% al 4% en condiciones nubladas (Cescatti et al., 2012; Pirazzini, 2004; Pirazzini et al., 2006). La estimación de la incertidumbre asociada a las medidas de radiación por un piranómetro comercial se sitúa en torno al 5% (95% de nivel de confianza) bajo condiciones ideales (Reda, 2011). Cabe destacar que la propia incertidumbre de un piranómetro comercial (en torno al 5%) ya es superior al requisito de incertidumbre que establece el GCOS para productos de satélite (nivel óptimo requerido del 3% según la última actualización (GCOS-245, 2022)).

2.2. Muestreo global: LANDVAL

La red de sitios LANDVAL, definida para la intercomparación de productos, cuenta con 720 localizaciones, de las cuales 521 proceden de la red *Surface Albedo Validation Sites* (SAVS 1.0) (Loew et al., 2016), incluyendo 256 de CEOS *Benchmark Land Multisite Analysis and Intercomparison of Products* (BELMANIP) version 2.1 (Weiss et al., 2014). SAVS 1.0²² fue creada en el estudio ALBEDOVAL-2 (Fell et al., 2015) en el marco del proyecto *Quality Assurance for Essential Climate Variable* (QA4ECV), siendo una base de datos estática de más de 2000 potenciales sitios de referencia de los cuales se adjunta información auxiliar con respecto a su homogeneidad espacial y otros datos de interés. Los criterios de selección escogidos se resumen en la Tabla 2, destacando como requisito la homogeneidad en cuanto al mismo tipo de cobertura terrestre en un radio de 5 km alrededor de la coordenada. Adicionalmente, se incluyeron 19 emplazamientos en los desiertos del Sahara y Arabia conocidos por su alta estabilidad temporal, comúnmente utilizados para la calibración de sensores (Lachéradé et al.,

²² disponible en <https://savs.eumetsat.int/> (acceso online el 16/05/2023)

2013). Finalmente, se completó la red hasta los 720 emplazamientos, utilizando los mismos criterios de selección recogidos en la Tabla 2, con el objetivo cubrir regiones (Asia, Africa y Oceanía) o tipos de cobertura (zonas de arbustos, bosques de coníferas o de hoja caducifolia) poco muestreadas por SAVS 1.0. Para ello se hizo uso de localizaciones de otros proyectos o redes conocidas (FP7 Imagines²³, AsiaFlux²⁴, OzFlux²⁵) o mediante la identificación de coordenadas a través de la plataforma Geo-Wiki²⁶.

Tabla 2. Criterios de selección para los sitios de LANDVAL.

Parámetro	Umbral	Comentario
Distancia a cuerpos de agua [km]	5	Evitar píxeles de agua.
Porcentaje mínimo de mismo tipo de cobertura terrestre en un radio de 5 km	60%	Evitar áreas heterogéneas en cuanto al tipo de cobertura terrestre.
Tipo de cobertura mayoritaria	Exclusión cuerpos de agua y áreas urbanas.	
Rango vertical [m] máximo en un radio de 5 km	300	Evitar áreas con una variabilidad del terreno o pendiente significativa cerca del sitio.
Localización (latitud)	60° S a 80°N	Excluir sitios sobre latitudes extremas, donde los productos CGLS y C3S no proporcionan datos.

2.3. Criterios y métricas de validación

A continuación, se describen los criterios de validación, así como los diferentes métodos y métricas propuestos para evaluar cada uno de ellos. El resumen se detalla en la Tabla 3. Las siguientes sub-secciones desarrollan más en detalle la definición de cada criterio, así como las recomendaciones a la hora de evaluar cada uno de ellos. Se muestran, además, gráficas a modo de ejemplo ilustrativo de cada uno de los criterios.

Para evaluar cada criterio, se debe usar una muestra representativa de las condiciones globales para que el resultado sea concluyente, como LANDVAL en el caso de la intercomparación. Además, se recomienda evaluar los criterios, en la medida

²³ <http://www.fp7-imagines.eu/> (acceso online el 16/05/2023)

²⁴ <https://www.asiaflux.net/> (acceso online el 16/05/2023)

²⁵ <https://www.ozflux.org.au/> (acceso online el 16/05/2023)

²⁶ <https://www.geo-wiki.org/> (acceso online el 16/05/2023)

de lo posible, en función del tipo de bioma con el objetivo de proporcionar al usuario una información más detallada de las ventajas y desventajas que tiene el producto en función de la aplicación. Así mismo, hay un especial interés en evaluar si los productos de albedo proporcionan valores realistas sobre superficies con nieve o hielo.

Es recomendable, además, concluir cada ejercicio de validación con un resumen de la conformidad del producto respecto a los requisitos de usuario, donde se indique en qué medida el producto cumple con los mismos (requisitos de incertidumbre, estabilidad, precisión, resoluciones espaciales o temporales, etc.).

Tabla 3. Criterios de calidad, métricas y métodos.

Criterio	Métricas y métodos
Integridad	<ul style="list-style-type: none"> ▪ Mapas globales (anuales, mensuales) del porcentaje de huecos. ▪ Evolución temporal del porcentaje de huecos (global, regional, por tipo de bioma). ▪ Distribución de la longitud temporal de los huecos.
Consistencia espacial	<ul style="list-style-type: none"> ▪ Inspección visual de mapas globales (resolución reducida) y mapas a la máxima resolución sobre zonas de interés. ▪ Mapas e histogramas de residuos. ▪ Auto correlación espacial (CV, MI).
Consistencia temporal	<ul style="list-style-type: none"> ▪ Análisis cualitativo de los perfiles temporales en comparación con datos de referencia (productos validados y datos de campo). ▪ Evaluación cuantitativa de la correlación cruzada de series temporales.
Exactitud	<ul style="list-style-type: none"> ▪ <i>Scatter-plots</i> versus referencias (N, <i>Bias</i>, MD, R, MAR). ▪ <i>Box-plots</i> del <i>Bias</i> por rango de albedo.
Precisión	<ul style="list-style-type: none"> ▪ <i>Scatter-plots</i> (STD, MAD). ▪ <i>Box-plots</i> de la diferencia absoluta por rango de albedo. ▪ Precisión intra-anual. Histogramas de la suavidad (δ) y mediana de δ. ▪ Precisión inter-anual. <i>Scatter-plots</i> (STD, MAD) sobre sitios desérticos de calibración entre años consecutivos.
Incertidumbre	<ul style="list-style-type: none"> ▪ <i>Scatter-plots</i> (RMSD).
Estabilidad	<ul style="list-style-type: none"> ▪ Pendiente/década de la regresión lineal del <i>Bias</i> sobre sitios desérticos de calibración.
Test de conformidad	<ul style="list-style-type: none"> ▪ Evaluación del alcance en el que el producto cumple con los requisitos de usuario.

*N, R, MAR, *Bias*, MD, STD, MAD, RMSD se definen en la Tabla 4 (métricas para la evaluación del error).

2.3.1. Integridad (completeness)

La integridad del producto hace referencia a la proporción de estimaciones válidas sobre un dominio de observación en un momento dado, que a lo largo del tiempo indica su frecuencia y continuidad. La ausencia de datos (huecos) se considera una limitación muy importante de cara al usuario final, y se debe principalmente a la contaminación de nubes, a malas condiciones atmosféricas o a problemas técnicos durante la adquisición de las imágenes. Es, por tanto, imperativo reportar al usuario acerca de la integridad del producto, proporcionando información tanto espacial como temporal de la ausencia de los datos.

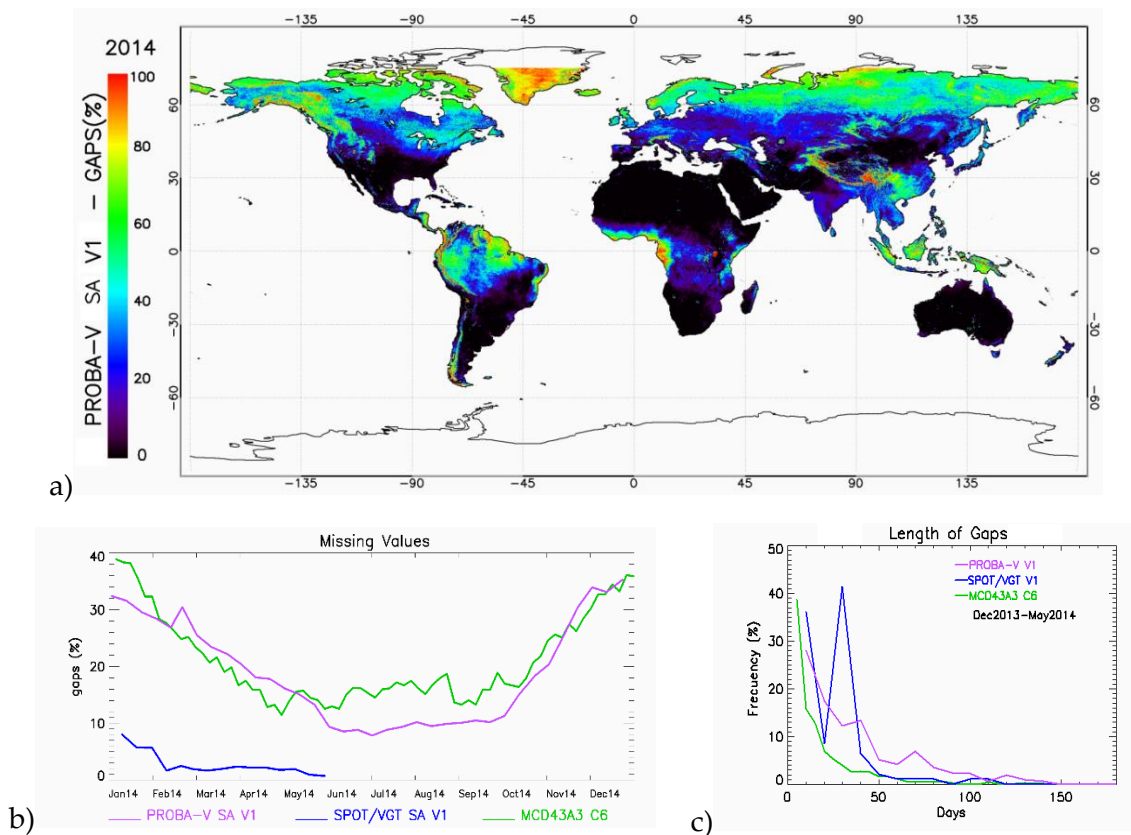


Figura 7: Ejemplo de resultados para evaluar la integridad. a) Distribución global del porcentaje de huecos del producto global C3S PROBA-V V1 para el año 2014; b) Evolución temporal del porcentaje de huecos de los productos C3S PROBA-V V1, C3S SPOT/VGT V1 y MCD43A3 C6 para el año 2014 sobre LANDVAL; y c) histograma de la longitud (en días) de los huecos de los productos C3S PROBA-V V1, C3S SPOT/VGT V1 y MCD43A3 C6 para el periodo de Diciembre 2013 a Mayo 2014 sobre LANDVAL. Fuente: (Sánchez-Zapero et al., 2020).

Los mapas globales (mensuales, anuales) mostrando el porcentaje de huecos ofrecen la mejor perspectiva espacial para identificar las zonas donde se producen la mayor frecuencia de huecos. Un ejemplo de ello es el mapa mostrado en la Figura 7-a, donde se observa el mapa global del porcentaje de huecos para el producto C3S PROBA-V V1 para el año 2014.

Así mismo, es interesante visualizar la evolución del porcentaje de huecos a lo largo del tiempo, que podría estudiarse tanto de manera global (LANDVAL, ver Figura 7-b) como de manera agrupada por tipo de bioma, región o banda latitudinal. Por otra parte, la distribución en forma de histograma de la longitud temporal de los huecos (Figura 7-c) permite comprender mejor el impacto de estos para monitorizar las variaciones temporales.

2.3.2. Consistencia espacial

La consistencia espacial hace referencia al realismo y la repetitividad de las distribuciones espaciales de los valores del producto a lo largo del globo. Para ello, el primer test cualitativo consiste en la inspección visual sistemática de los mapas, basándonos en el conocimiento científico de los expertos, con el objetivo de descartar patrones anómalos o artefactos (p.ej., zonas de huecos, *stripes*, valores poco realistas, etc.). La metodología para la inspección visual debería incluir la visualización de mapas sobre áreas específicas (escala local) a la máxima resolución, así como la visualización de las animaciones de los mapas globales a una resolución reducida en función de la capacidad técnica del equipo informático utilizado para el análisis (p.ej., 1 de cada 16 píxeles).

La consistencia espacial puede ser cuantitativamente evaluada mediante la comparación de las distribuciones espaciales del producto bajo estudio y un producto de referencia validado previamente. Dos productos se consideran espacialmente consistentes cuando los residuos están dentro de los requerimientos de usuario en términos de incertidumbre. Por ello, se deben generar mapas globales de los residuos (ver Figura 8-a) entre pares de productos, lo que servirá a su vez para identificar las

áreas que muestran las inconsistencias espaciales para un análisis más profundo (p.ej., trayectorias temporales). Así mismo, es conveniente generar las distribuciones globales de los píxeles que cumplen los requisitos de usuario (ver Figura 8-c), así como los histogramas de los residuos (ver Figura 8-b) y los porcentajes globales de residuos que cumplen los requisitos (ver Figura 8-d). Los residuos (ε) se estiman a partir de la relación lineal entre dos productos ($Y = aX + b + \varepsilon$). El residuo puede ser estimado, por tanto, como $\varepsilon = Y - aX - b$, y representa las discrepancias que quedan respecto a la tendencia general entre ambos productos. De esta forma, las tendencias sistemáticas no se consideran, representando con mayor claridad patrones asociados a la distribución espacial de los valores estimados. Los histogramas de los valores de los productos y de los residuos por tipo de bioma ofrecen, además, una representación visual de las tendencias que se producen para cada tipo de cubierta terrestre.

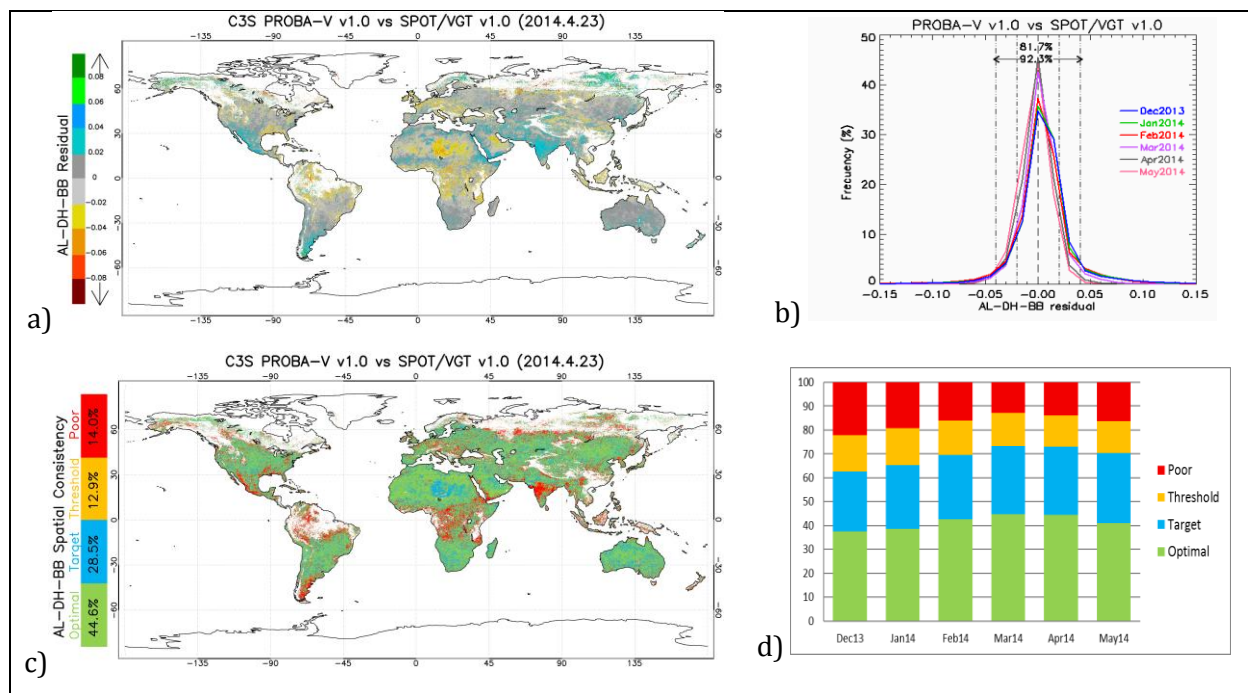


Figura 8: Ejemplo de resultados para evaluar la consistencia espacial entre los productos C3S PROBA-V y SPOT/VGT V1 a) Distribución global de los residuos para la fecha 2014.04.23; b) histogramas de los residuos para el periodo Diciembre 2013 – Mayo 2014 (uno por mes); c) distribución global de residuos entre los requisitos del proyecto C3S para la fecha 2014.04.23; y d) porcentajes de residuos entre los requisitos C3S para el periodo Diciembre 2013 – Mayo 2014. Fuente: 'Product Quality Assessment Report Surface Albedo v1.0 based on PROBA-V' (ver Anexo I).

Además, es recomendable analizar la auto-correlación espacial sobre zonas conocidas por ser homogéneas (p.ej., zonas desérticas, bosques o zonas herbáceas). Para ello, se proponen dos indicadores espaciales: el Coeficiente de Variación espacial (CV) y el Índice de Moran (MI). El CV (Eq. 7) se define como la relación entre la desviación estándar (σ) como porcentaje de la media aritmética (\bar{x}), mostrando una interpretación relativa del grado de la variabilidad espacial y siendo una manera efectiva para medir la dispersión relativa en los datos (Román et al., 2009). Por su parte, MI (Eq. 8) ofrece una medida de la auto correlación espacial (Moran, 1984). Presenta valores entre -1 y 1, indicando auto correlación espacial negativa o positiva, con valores próximos a 0 en el caso de patrones completamente aleatorios. Por otro lado, también se recomienda analizar estos indicadores sobre áreas con gradientes de variación espacial para ver si el producto es capaz de reproducir dicha variabilidad.

$$CV = \frac{\sigma}{\bar{x}} \cdot 100\% \quad \text{Eq. 7}$$

$$MI = \frac{N}{\sum_i \sum_j \omega_{ij}} \frac{\sum_i \sum_j \omega_{ij} (X_i - \bar{X})(X_j - \bar{X})}{\sum_i (X_i - \bar{X})^2} \quad \text{Eq. 8}$$

donde N es el número de unidades espaciales indexadas por i y j; X es la variable de interés; \bar{X} es la media de X; y ω_{ij} es un elemento de una matriz de pesos espaciales.

2.3.3. Consistencia temporal

La consistencia temporal hace referencia al realismo de las variaciones temporales de un producto, y puede analizarse de manera cualitativa comparando la serie temporal con productos de referencia o datos medidos *in situ*. A modo de ejemplo, en la Figura 9-a podemos ver la evolución temporal de varios productos de satélite en comparación con medidas *in situ* procedentes de dos estaciones FLUXNET.

Para analizar cuantitativamente la consistencia temporal entre productos, se mide la correlación cruzada entre las series temporales. La correlación cruzada es el método estándar para estimar el grado en el que dos series están correlacionadas. Considerando dos series $x(i)$ e $y(i)$, donde $i=0, 1, 2, \dots, N-1$, la correlación cruzada con un retraso d se define como:

$$\rho = \frac{\sum_i [(x(i) - mx) \cdot (y(i-d) - my)]}{\sqrt{\sum_i (x(i) - mx)^2} \sqrt{\sum_i (y(i-d) - my)^2}} \quad \text{Eq. 9}$$

donde mx y my son las medias de las correspondientes series. La correlación cruzada se calcula con un retraso $d=0$ con el objetivo de estimar la consistencia entre los perfiles temporales de los diferentes productos usando el mismo soporte temporal.

La Figura 9-b muestra, a modo de ejemplo, los histogramas de la correlación cruzada entre pares de productos (C3S SPOT/VGT V1, C3S PROBA-V V1 y MCD43A3 C6), realizando dicho análisis por tipo de cobertura terrestre.

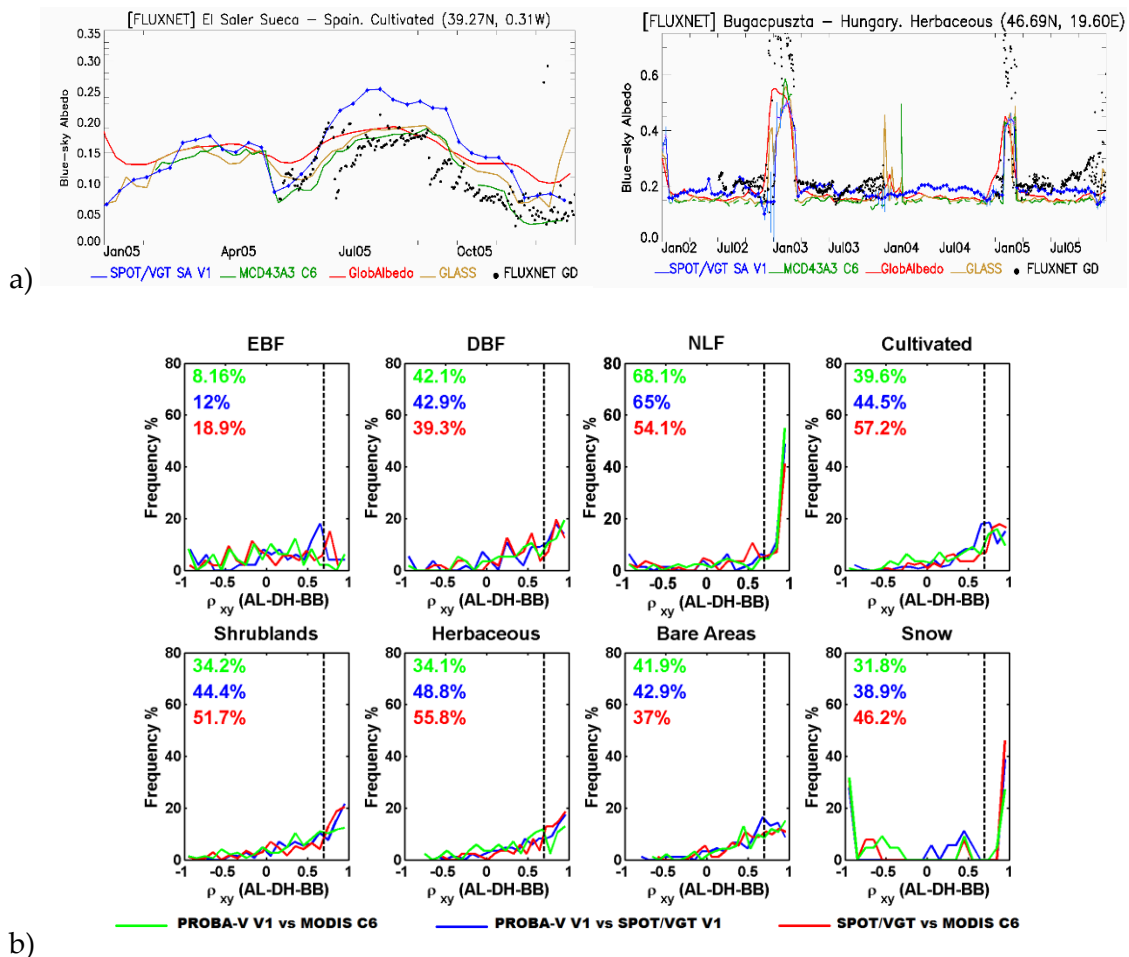


Figura 9: Ejemplo de resultados para evaluar la consistencia temporal: a) perfiles temporales de varios productos de albedo (C3SS SPOT/VGT V1, MCD43A3 C6, GlobAlbedo, GLASS) y medidas de campo sobre dos estaciones FLUXNET; y b) Ejemplo de histogramas de correlación cruzada entre pares de productos (C3S SPOT/VGT V1, C3S PROBA-V V1 y MCD43A3 C6) por tipo de bioma. Fuente: 'Product Quality Assessment Report CDR VGT-based Surface Albedo v1.0' y 'Product Quality Assessment Report Surface Albedo v1.0 based on PROBA-V' (ver Anexo I).

2.3.4. Evaluación del error (exactitud, precisión e incertidumbre)

Las definiciones de los conceptos de error, exactitud, precisión e incertidumbre han sido extraídas de la guía para expresar la incertidumbre en la medida (Lequin, 2004) del *Joint Comitee for Guides in Metrology (JCGM)* (JCGM, 2014).

El **error** (de la medida) es “el resultado de la medida menos el valor real del mesurando”. El valor real (de una cantidad) es el “valor consistente con la definición de una cantidad particular dada”. Dado que normalmente no se puede determinar un valor verdadero, en la práctica se utiliza un valor verdadero convencional. El valor verdadero convencional (de una cantidad) es el “valor atribuido a una cantidad particular y aceptado, a veces por convención, que tiene una incertidumbre apropiada para un propósito dado”. Tradicionalmente, al error se le atribuyen dos componentes: la componente aleatoria (*random*) y la componente sistemática (*bias*). El error aleatorio es “el resultado de una medida menos el valor medio que resultaría de un número infinito de mediciones del mismo mesurando realizadas en condiciones de repetitividad”. Por otra parte, el error sistemático es “la diferencia entre la medida que resultaría de un infinito número de medidas del mismo mesurando, llevada a cabo sobre condiciones de repetitividad, y el valor real del mesurando”.

La **exactitud** es el grado de “cercanía en el acuerdo entre el resultado de una medida y un valor real del mensurando”. Comúnmente, la exactitud viene caracterizada por el *bias* o error sistemático entre el producto de albedo y su referencia estimada, por lo que describe el valor medio de la desviación respecto a la referencia. Se obtiene mediante la diferencia media entre el producto de albedo y la referencia estimada.

La **precisión** o repetitividad es la “proximidad del acuerdo entre los resultados de sucesivas mediciones del mismo mensurando realizadas en las mismas condiciones de medición”. Comúnmente la precisión representa la dispersión de las estimaciones del producto alrededor de su valor esperado y se puede estimar mediante la desviación estándar (STD) de la diferencia entre el albedo estimado y las estimaciones de referencia correspondientes.

La **incertidumbre** es un “parámetro, asociado al resultado de la medida, que caracteriza la dispersión de los valores que podría atribuirse razonablemente al mensurando”. La incertidumbre incluye el sesgo (*bias*) y la precisión, y puede estimarse mediante la Raíz de la Desviación Cuadrática Media (RMSD).

Cabe señalar que los valores atípicos (*outliers*) fuertes y/o múltiples afectan a las métricas clásicas descritas anteriormente (es decir, el *bias* medio y la STD); en tales casos, sería más adecuado usar la desviación mediana (MD) en lugar de la media para estimar el error sistemático, así como la desviación absoluta mediana (MAD) como medida de la precisión (recomendaciones CEOS/WGCV LPV). Además de las métricas citadas, existen otros estadísticos muy valiosos para evaluar el acuerdo entre dos conjuntos de datos, incluido el ajuste lineal. Para este propósito, se propone la regresión del eje mayor (MAR) en lugar de la regresión de mínimos cuadrados ordinarios (OLS) porque está específicamente formulada cuando ambos conjuntos x e y contienen errores (Harper, 2014). El conjunto de métricas se resume en la Tabla 4.

Tabla 4. Métricas para la evaluación del error.

Estadístico	Comentario
N	Número de muestras. Indicativo del alcance de la validación
B	Diferencia (<i>bias</i>) media ($y - x$). Indicativo de la exactitud. B (%) es el valor relativo del <i>bias</i> entre la media de x e y .
MD	Mediana de la diferencia ($y - x$). Indicativo de la exactitud (buenas prácticas del CEOS/WGCV LPV). MD (%) es el MD relativo a la media de entre x e y .
STD	Desviación estándar de la diferencia. Indicativo de la precisión. STD (%) es la STD relativa a la media de entre x e y .
MAD	Mediana de la Desviación Absoluta $ y - x $. Indicativo de la precisión (buenas prácticas del CEOS/WGCV LPV). MAD (%) es el MAD relativo a la media de entre x e y .
RMSD	<i>Root Mean Square Deviation</i> . Indicador de la incertidumbre (error total). RMSD (%) es el RMSD relativo a la media de entre x e y .
R	Coefficiente de correlación. Indica el poder descriptivo de la prueba de precisión lineal. Se utiliza el coeficiente de Pearson.
MAR	Pendiente (<i>slope</i>) y desplazamiento de la ordenada en el origen (<i>offset</i>) de la regresión lineal. Indica algún posible sesgo.

Las métricas recogidas en la Tabla 4 suelen reportarse junto a la gráfica de dispersión (*scatter-plot*) del producto a evaluar (eje y) respecto al conjunto de datos de referencia (eje x). El análisis se puede complementar con los *box-plots* de la diferencia y

de la diferencia absoluta por rangos de albedo. Un ejemplo de todo ello se puede ver en la Figura 10.

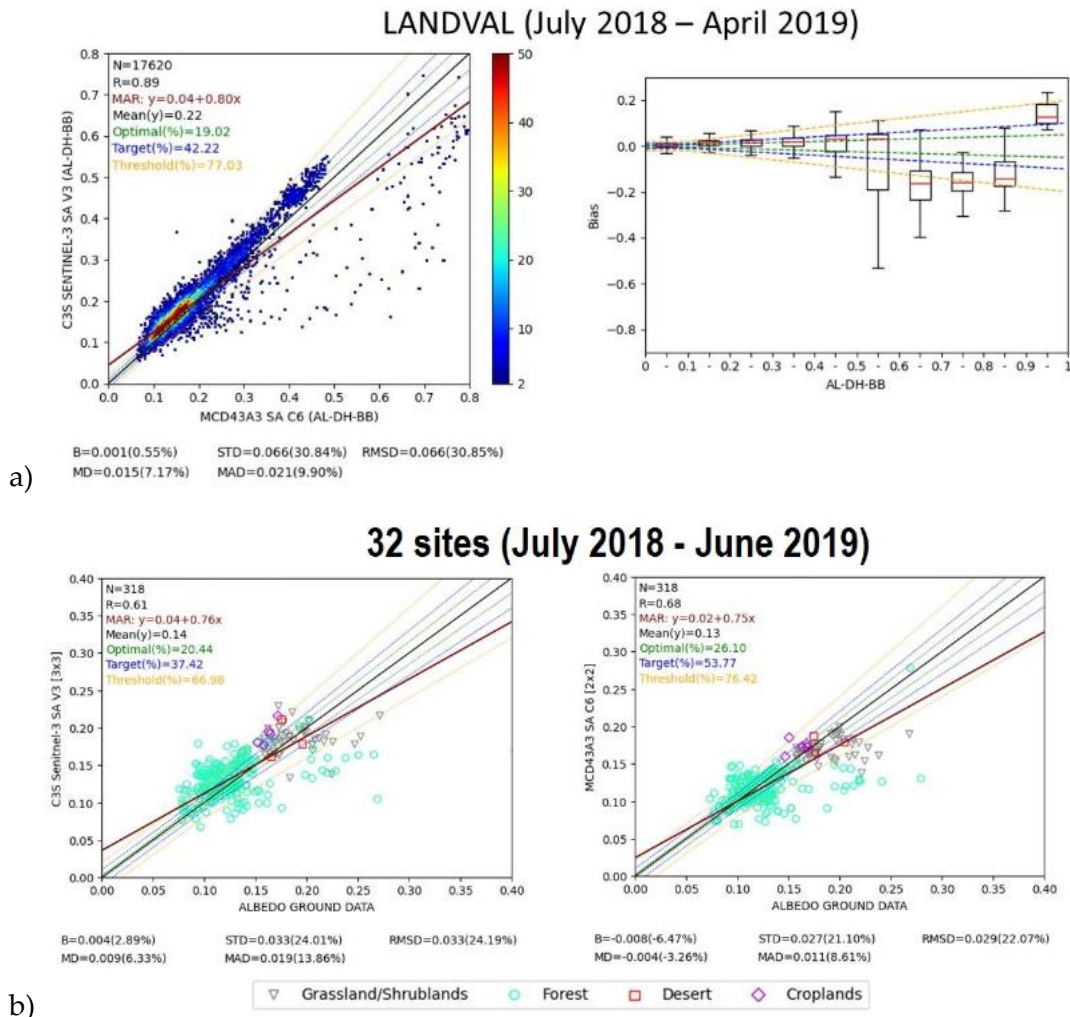


Figura 10: Panel a: ejemplo de resultados para evaluar el error entre pares de productos. Scatter-plot (izquierda) y métricas asociadas entre C3S Sentinel-3 V3 versus MCD43A3 C6 junto al box-plot del bias para los diferentes rangos de albedo (derecha). Panel b: ejemplo de validación directa (scatter-plots y métricas asociadas) para los productos C3S Sentinel-3 V3 (izquierda) y MCD43A3 C6 (derecha). Las líneas verdes, azules y amarillas en los scatter-plots definen los requisitos de usuario (optimal, target, threshold). Fuente: (Sánchez-Zapero et al., 2023a).

Por otra parte, hay dos aspectos de la precisión que conviene ser evaluados: la precisión intra-anual y la inter-anual (ver ejemplos en Figura 11).

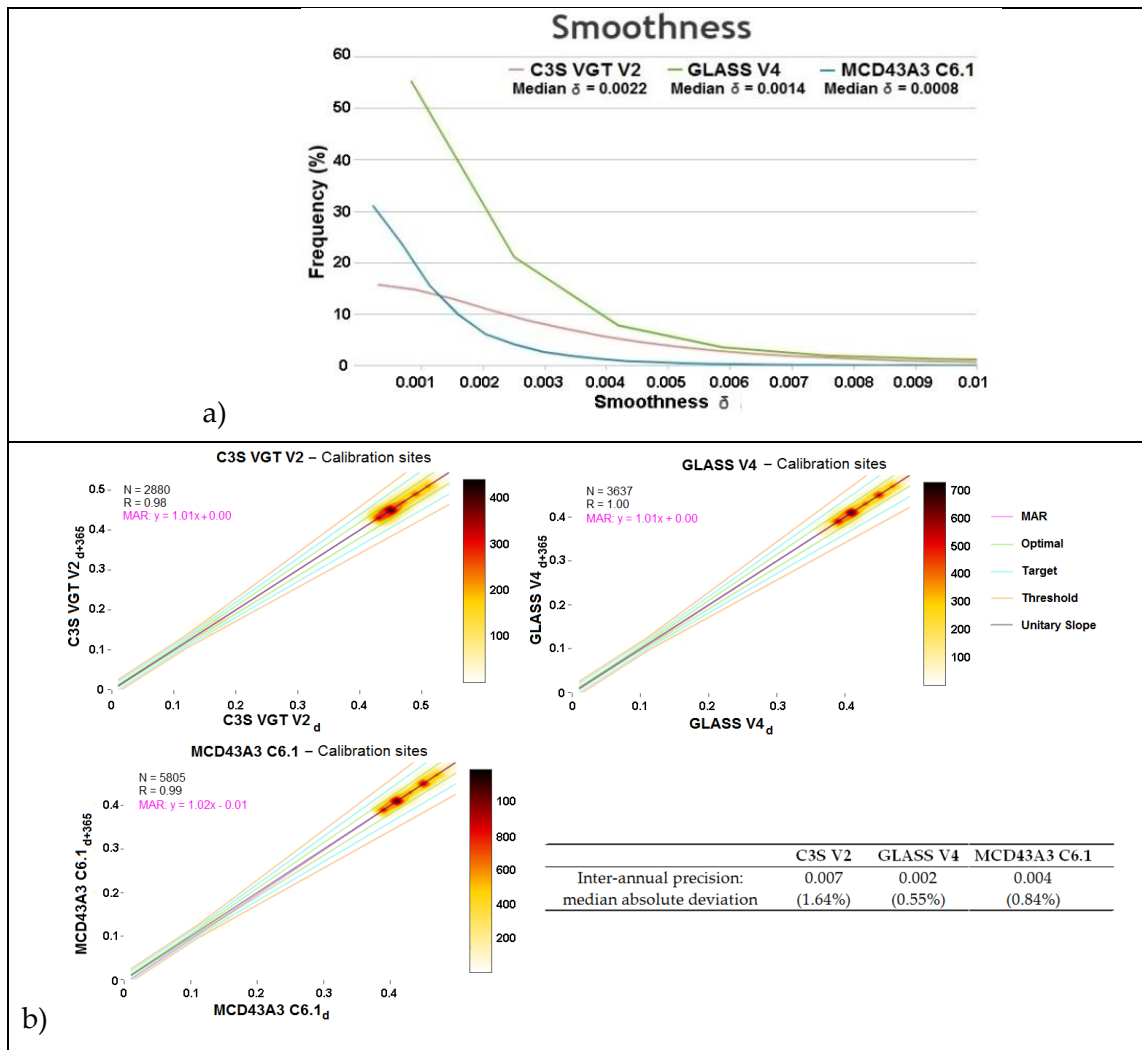


Figura 11: Ejemplo de resultados para evaluar la precisión de los productos C3S V2, GLASS V4 y MCD43A3 C6.1: a) precisión intra-anual evaluada mediante los histogramas de la suavidad y su valor mediano; y b) precisión inter-anual evaluada con los scatter-plots entre muestras equivalentes de años consecutivos. Fuente: (Sánchez-Zapero et al., 2023b).

La **precisión intra-anual** (también conocida como suavidad, δ) se corresponde con el ruido temporal en una escala corta de tiempo. En este caso, se puede considerar como indicador de la precisión intra-anual la anomalía de una muestra respecto a la interpolación lineal de las muestras vecinas. Para calcularla, se toma cada triplete consecutiva de observaciones, y se calcula el valor absoluto de la diferencia entre la observación central $P(d_{n+1})$ y la correspondiente interpolación lineal entre los dos extremos $P(d_n)$ y $P(d_{n+2})$ (Weiss et al., 2007):

$$\delta = \left| P(d_{n+1}) - P(d_n) - \frac{P(d_n) - P(d_{n+2})}{d_n - d_{n+2}} (d_n - d_{n+1}) \right| \quad \text{Eq. 10}$$

Es conveniente evaluar la distribución de δ , tomando la mediana de los valores de δ como indicador cuantitativo de la precisión intra-anual (ver ejemplo en Figura 11-a): cuanto menor sea dicha mediana, mayor será la precisión intra-anual y más suave serán las series temporales del producto.

La **precisión inter-anual** hace referencia a la dispersión de los valores de albedo de un año a otro, por lo que debe evaluarse sobre sitios de calibración (Lachérade et al., 2013). Para ello, se recomienda visualizar los *scatter-plots* entre años consecutivos, usando la STD y MAD como indicadores de la precisión inter-anual (ver ejemplo en Figura 11-b).

2.3.5. Estabilidad

Le estabilidad mide el grado en el que el error de un producto permanece constante durante un periodo de tiempo prolongado, típicamente una década o más. La estabilidad temporal también se puede definir como el cambio en el sesgo durante un periodo de tiempo predefinido (Merchant, 2013), y puede estimarse como la pendiente de la regresión lineal del sesgo (*bias*) en el tiempo (Fell et al., 2015).

Debido a la falta de datos de campo sobre sitios estables durante décadas, se pueden seleccionar sitios de calibración sobre zonas desérticas de reflectividad pseudo-invariante (Lachérade et al., 2013) para la evaluación de la estabilidad. Dado que se esperan variaciones temporales de albedo muy pequeñas o despreciables sobre estos sitios, la variación de los CDR de albedo sobre estas series temporales pueden ser equivalentes a la evaluación del *bias* sobre el tiempo (Sánchez-Zapero et al., 2023b). La Figura 12 muestra un ejemplo del análisis de estabilidad de los productos C3S V2, GLASS V4 y MCD43A3 C6.1, evaluada sobre 10 años en cuatro sitios desérticos de calibración. Se muestra con línea discontinua la tendencia general del producto a lo largo del tiempo, calculando la pendiente de dicha regresión por década como indicador de la estabilidad.

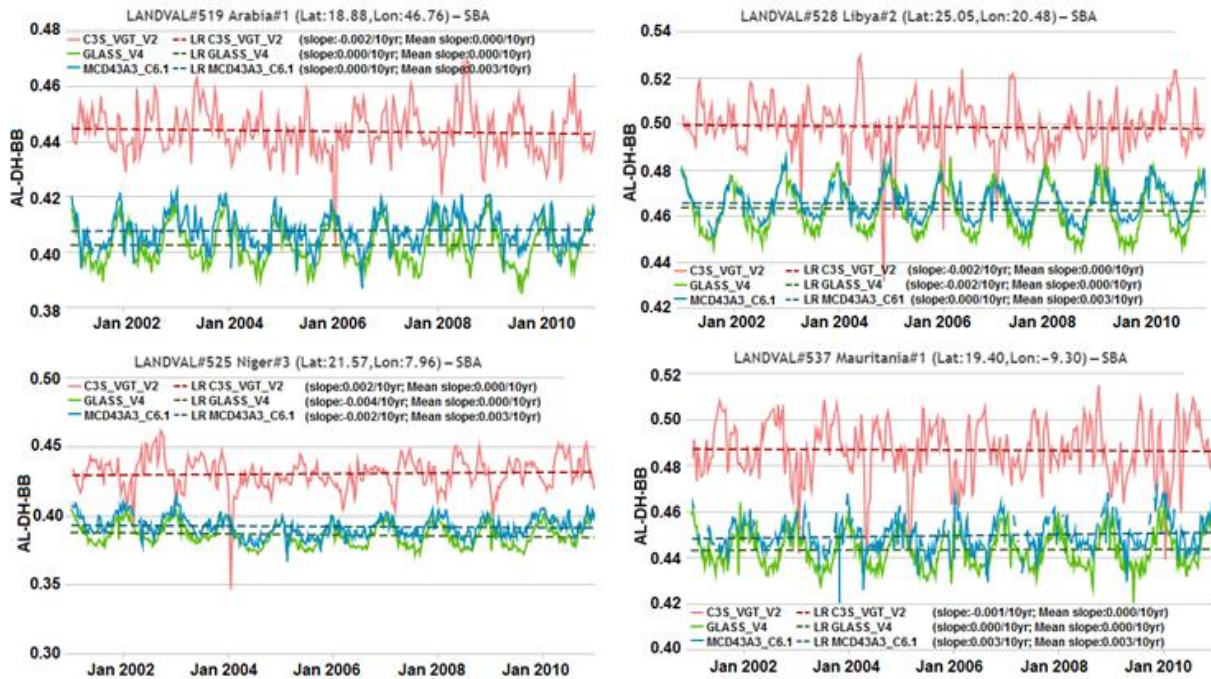


Figura 12: Ejemplo de resultados para evaluar la estabilidad de los productos C3S V2, GLASS V4 y MCD43A3 C6.1. Perfiles temporales sobre diferentes sitios de calibración para un periodo de 10 años (2001-2010). Las líneas discontinuas representan la regresión lineal de la tendencia de cada producto. Fuente: (Sánchez-Zapero et al., 2023b).

3. Resultados

Los resultados de esta tesis corresponden a los cuatro artículos científicos de los que está compuesta, anexados al final de este documento.

En primer lugar, el artículo 1 (Roujean et al., 2018) describe el algoritmo para la estimación del albedo a partir de datos de PROBA-V a 300 m de resolución espacial, que se desarrolló en el servicio CGLS. En el contexto de la tesis se realizó la validación de dichos productos, siendo este el primer prototipo de estimación de albedo que se realizaba a 300 m.

El artículo 2 (Sánchez-Zapero et al., 2020) muestra la validación del producto de albedo de PROBA-V que dio continuidad a la serie climática de albedo de C3S a 1 km de resolución espacial, por lo que se centró el estudio en la consistencia de los productos C3S en la transición de SPOT/VGT a PROBA-V y en el periodo de solapamiento entre ambos satélites.

El artículo 3 (Sánchez-Zapero et al., 2023b) presenta a la comunidad científica la herramienta SALVAL, diseñada para que los productos de albedo puedan alcanzar un nivel 4 de validación estandarizada en la jerarquía de niveles del CEOS/WGCV LPV. Se presentó, además, la validación de 3 series climáticas (C3S V2, MODIS C6.1 y GLASS V4) usando dicha herramienta.

Finalmente, en el trabajo expuesto en el artículo 4 (Sánchez-Zapero et al., 2023a) se trabajó en el desarrollo de los productos de albedo que van a dar continuidad a la serie climática de C3S usando datos de satélites *Copernicus* de nueva generación (Sentinel-3). Dicho artículo describe el algoritmo y la validación preliminar del producto.

A continuación se proporciona un resumen de cada uno de estos artículos.

3.1. Artículo 1: *Surface albedo and toc-r 300m products from PROBA-V instrument in the framework of Copernicus Global Land Service.*

Nota: Basado en el artículo (Roujean et al., 2018), cuya copia completa se adjunta en el Anexo II .

Roujean, J.L., Leon-Tavares, J., Smets, B., Claes, P., Camacho, F., **Sanchez-Zapero, J.**, 2018. Surface albedo and toc-r 300 m products from PROBA-V instrument in the framework of Copernicus Global Land Service. *Remote Sensing of Environment*, 215, 57–73. <https://doi.org/10.1016/j.rse.2018.05.015>

El punto de partida de esta tesis fue la validación de los productos de albedo generados en el contexto del CGLS, proyecto donde se desarrolló la base de protocolos y métricas (ver capítulo 2) de validación, algunas de las cuales fueron incluidas posteriormente en el protocolo de validación de productos de albedo del CEOS/WGCV LPV.

El instrumento PROBA-V se lanzó en 2013 ofreciendo cobertura global diaria a las resoluciones 300 m y 1 km en tres bandas espectrales (*Blue, Red, NIR*) y a 600 m en el infra-rojo de onda corta (SWIR). La misión PROBA-V es la continuación del programa VEGETATION que empezó en el 2000, y ha permitido dar continuidad a las series de productos de 1 km, ofreciendo además una mejora gracias a la resolución de 300 m. El nuevo sensor VEGETATION a bordo de PROBA (PROBA-V) incorpora cámaras orientables y ofrece un amplio campo de visión para el muestreo de la BRDF. Este artículo presenta la metodología y validación de los productos de albedo de la superficie y reflectividad TOC normalizada, diseñados para utilizar observaciones diarias de PROBA-V en el servicio CGLS.

El algoritmo (PROBA-V *Collection 300 m V1*) utiliza la cadena de procesamiento clásica (ver Figura 1), que realiza la discriminación de nubes, las correcciones tanto de atmósfera como de efectos direccionales a nivel de píxel y la integración tanto angular como espectral. La frecuencia temporal de producción es de 10 días, en base a un compuesto temporal de 20 días, siendo una elección que busca un equilibrio entre una alta disponibilidad de escenas claras y una escala de tiempo que permita capturar los

cambios fenológicos. En cuanto al catálogo de productos de albedo, se ofrecen tanto el albedo *black-sky* (BSA) como el *white-sky* (WSA) en tres anchos de banda diferentes (visible, NIR y onda corta total). Se introdujo, además, una técnica recursiva que sirve como relleno de huecos (*gap-filling*) basada en la utilización ponderada de una climatología o datos antiguos (*prior*). Adicionalmente, se proporciona información de la calidad (*Quality Flag*), y la edad de la información (*AGE*), que puede ser utilizada por el usuario para filtrar observaciones de baja calidad o con pocas observaciones.

La validación del producto fue la actividad desarrollada en el contexto de esta tesis. Dicha evaluación se realizó sobre una ventana sub-continental en Europa, cubriendo un área que va de [65°N, 20°W] a [35°N, 30°E], generada para el año 2014. Se evaluaron los siguientes criterios: consistencia espacial, consistencia temporal y evaluación estadística del error. Se usó el producto de NASA basado en los sensores MODIS (MCD43A3 C6) a 500 m de resolución espacial como producto de referencia (al estar validado), así como las medidas procedentes de 10 estaciones de la red EFDC sobre emplazamientos espacialmente homogéneos. Para el análisis estadístico y la consistencia temporal, se definió una red de muestreo de 109 sitios homogéneos distribuidos en la ventana europea, cubriendo las diferentes condiciones en términos de localización y tipo de bioma.

Los productos de albedo PROBA-V *Collection 300 m V1* y MCD43A3 C6 mostraron distribuciones espacialmente consistentes, con incertidumbres generales (RMSD) de 0.03 para la región del visible y de onda corta total, y de 0.04 para el NIR. Se observaron algunas discrepancias espaciales en periodos de invierno. PROBA-V *Collection 300 m V1* mostró, además, evoluciones temporales realistas, ajustándose a las tendencias temporales tanto de MCD43A3 C6 como de las medidas de campo diarias. En particular, dicho producto reprodujo correctamente tanto las transiciones suaves como los cambios pronunciados de albedo. La validación directa sobre datos de 10 estaciones EFDC homogéneas mostró una incertidumbre (RMSD) de 0.03 con un sesgo medio (*bias*) de 0.01, mostrando discrepancias similares a las observadas en MCD43A3 C6 (*bias*=0, RMSD=0.032).

El artículo demostró la utilidad del algoritmo diseñado para estimar el albedo de la superficie usando como entrada la colección 300 m de PROBA-V, identificando algunas limitaciones como la presente en la máscara de nubes de PROBA-V que confunde en algunas ocasiones las nubes con hielo o nieve. A pesar del potencial de este producto desarrollado en CGLS, siendo el primer prototipo de albedo que ofrecía una resolución de 300 m, la Comisión Europea (JRC) no lo incluyó en su catálogo de productos operacionales dentro del servicio, prefiriendo continuar la serie SPOT/VGT con datos PROBA-V a 1 km de resolución espacial.

3.2. Artículo 2: *Quality Assessment of PROBA-V Surface Albedo V1 for the Continuity of the Copernicus Climate Change Service.*

Nota: Basado en el artículo (Sánchez-Zapero et al., 2020), cuya copia completa se adjunta en el Anexo III .

Sánchez-Zapero, J., Camacho, F., Martínez-Sánchez, E., Lacaze, R., Carrer, D., Pinault, F., Benhadj, I., Muñoz-Sabater, J., 2020. Quality Assessment of PROBA-V Surface Albedo V1 for the Continuity of the Copernicus Climate Change Service. *Remote Sensing*, 2020, Vol. 12, Page 2596 12, 2596. <https://doi.org/10.3390/rs12162596>

El servicio C3S ha generado un CDR de productos de albedo a 1 km de resolución espacial basado en las observaciones de SPOT/VGT (Diciembre 1999 - Mayo 2014) y PROBA-V (Diciembre 2013 – Junio 2020), habiendo heredado para ello los algoritmos y líneas de procesado de CGLS y dando como resultado la versión 1 de C3S (C3S SA V1). El principal objetivo del artículo era realizar la validación completa del producto C3S PROBA-V SA V1, con el principal foco en la consistencia con SPOT/VGT para evaluar el impacto del cambio de sensor en la continuidad de la serie C3S SA V1.

La metodología de validación utilizada, expuesta en detalle en el capítulo 2, sigue las recomendaciones recogidas en el protocolo de albedo del grupo CEOS/WGCV LPV (Wang et al., 2019). Se utilizaron los 2 enfoques principales de validación: validación directa e intercomparación de productos. Para la validación directa se usaron medidas de albedo procedentes del servicio *Copernicus* GBOV, donde se analizó la representatividad espacial de las medidas asociada a las 20 estaciones incluidas en GBOV. Los productos de referencia utilizados fueron el producto de C3S SPOT/VGT SA V1 (Sánchez-Zapero, 2018) y el producto de NASA colección 6 (MCD43A3 C6) (Román et al., 2009, 2010; Wang et al., 2012, 2014). La intercomparación se realizó sobre el muestreo global de 720 sitios homogéneos procedentes de la red LANDVAL (ver sección 2.2). Se evaluó la calidad del producto C3S PROBA-V SA V1 considerando diferentes criterios, incluyendo la integridad, la consistencia temporal y la evaluación del error (exactitud, precisión e incertidumbre). Se determinó, además, el nivel en el que los productos de satélite de albedo cumplían los requisitos de usuario en cuanto a

incertidumbre, considerando tanto los requisitos del GCOS (Max [5%; 0.0025]) como los internos del programa C3S (Max [10%; 0.01]).

La comparación del producto C3S PROBA-V SA V1 (píxeles catalogados como de 'alta calidad' según sus bandas de calidad o *Quality Flag*) mostró un sesgo positivo respecto a los datos de campo (*bias*) del 11.5% para el periodo 2014-2018, principalmente para los rangos de albedo menores (<0.2) sobre bosques. C3S PROBA-V SA V1 y MCD43A3 C6 presentaron una incertidumbre similar (RMSD ~ 0.4) en comparación con datos de campo, pero mostrando un signo sistemático opuesto en las diferencias medias. Se determinó que un porcentaje muy bajo de píxeles cumplen los requisitos de usuario (<25% para GCOS y <50% para C3S), por lo que se puso de manifiesto la dificultad de los productos de satélite para cumplir con los requisitos en cuanto a incertidumbre.

Los resultados de la intercomparación revelaron una buena consistencia espacio-temporal entre los productos C3S SPOT/VGT y PROBA-V SA V1, lo que asegura la continuidad del CDR en términos de incertidumbre asociada al cambio de sensor (sesgo medio típicamente entre $\pm 2\%$). La mayor limitación de PROBA-V respecto a SPOT/VGT fue su menor número de observaciones válidas que se debe, en parte a una máscara de nubes más conservadora en el caso de PROBA-V. La comparación de C3S PROBA-V SA V1 y MCD43A3 C6 mostró también una buena consistencia, con diferencias sistemáticamente positivas (PROBA-V > MODIS) del 5%, 8% y 12% para los rangos visible, NIR y de onda corta total respectivamente.

C3S PROBA-V SA V1 mostró una precisión inter-anual alrededor del 1%, similar a MCD43A3 C6 y mejorando los resultados de SPOT/VGT SA V1 (2-3%) ya que estos últimos mostraron cierta inestabilidad sobre sitios desérticos de calibración. Ambos productos C3S muestran peor precisión intra-anual que MCD43A3 C6, principalmente en el dominio espectral del NIR, donde se observó cierto ruido temporal.

Finalmente, se evaluó el rendimiento del uso de la capa adicional de calidad (QFLAG) que proporciona el producto C3S PROBA-V SA V1. Se demostró que el uso de esta capa adicional, en particular el bit 6 (*input status*) y los bits 10-11 (*B2-B0 saturation status*), elimina la mayoría de las estimaciones sobre nieve. En consecuencia,

se recomendó a los usuarios evitar el uso del QFLAG para aplicaciones específicas de nieve.

Como conclusión final, gracias a los resultados de validación y su publicación en la revista científica, el producto C3S PROBA-V SA V1 alcanzó un nivel de validación 3 en la jerarquía del CEOS/WGCV LPV. El artículo se centró en mostrar los resultados de validación más destacados para los albedos de banda ancha. El informe de validación generado en el proyecto C3S (*Product Quality Assessment Report Surface Albedo v1.0 based on PROBA-V* en Anexo I) ofrece un análisis extendido incluyendo otros aspectos como la consistencia espacial, así como los resultados de los albedos espectrales.

3.3. Artículo 3: *Surface ALbedo VALidation (SALVAL) Platform: Towards CEOS LPV Validation Stage 4 – Application to Three Global Albedo Climate Data Records.*

Nota: Basado en el artículo (Sánchez-Zapero et al., 2023b), cuya copia completa se adjunta en el Anexo IV .

Sánchez-Zapero, J., Martínez-Sánchez, E., Camacho, F., Wang, Z., Carrer, D., Schaaf, C., García-Haro, F.J., Nickeson, J., Cosh, M., 2023b. Surface ALbedo VALidation (SALVAL) Platform: Towards CEOS LPV Validation Stage 4 – Application to Three Global Albedo Climate Data Records. *Remote Sensing*, 2023, Vol. 15, Page 1081 15, 1081. <https://doi.org/10.3390/RS15041081>

El trabajo expuesto en este artículo tuvo como principal objetivo el desarrollo de SALVAL, siendo esta una herramienta de software *online* diseñada para validar nuevos productos o realizar una validación operacional y continuada en el tiempo de productos existentes a medida que las series temporales se expanden o se desarrollan nuevas versiones. Dicha herramienta tiene como objetivo alcanzar el nivel 4 de validación de acuerdo a la jerarquía del CEOS/WGCV LPV, permitiendo a los productos de albedo una validación operacional y estandarizada. Se presenta, además, un ejercicio demostrativo usando SALVAL, donde se validaron y compararon tres CDRs de albedo de diferentes servicios operacionales: C3S multi-sensor V2, NASA MODIS MCD43A3 C6.1, y BNU GLASS V4. El objetivo del artículo, por tanto, es doble: (1) presentar la herramienta SALVAL y sus funcionalidades, y (2) mostrar una aplicación de validación e intercomparación sobre tres CDRs existentes de albedo (C3S multi-sensor V2, NASA MCD43A3 C6.1 y BNU GLASS V4).

SALVAL (ver Figura 2) es una plataforma *online* que integra CDRs de productos existentes del albedo sobre un muestreo global (LANDVAL), una base de datos extensa de medidas de *in situ* donde se ha evaluado la representatividad espacial de la medida (REALS, ver sección 2.1) y la metodología y protocolos de validación (descritos en detalle en el capítulo 2) aceptados por la comunidad (CEOS/WGCV LPV). Los resultados se dividen en cuatro categorías: intercomparación de productos, validación

directa, precisión y estabilidad. Cada categoría incorpora diferentes criterios, incluyendo la integridad, consistencia espacial, consistencia temporal, exactitud, precisión o la propia estabilidad. La herramienta SALVAL tiene tres funcionalidades principales: (1) seleccionar el producto a evaluar y los productos de referencia, bien usando los productos existentes integrados en SALVAL o añadiendo un nuevo producto; (2) configurar el ejercicio de validación seleccionando varios parámetros como los requerimientos de usuario, región espectral, dominio espacial y temporal; y (3) ejecución del ejercicio de validación y visualización interactiva de los resultados.

El ejercicio de validación se configuró para un periodo de 20 años (2000-2020), centrándose en los albedos BSA para el ancho de banda de onda corta total para la intercomparación. Para la validación directa, SALVAL sí que toma ambos albedos BSA y WSA de satélite para poder comparar con medidas *in situ* ponderando con la fracción de radiación difusa. Respecto a los productos utilizados, tanto MCD43A3 C6.1 (Schaaf et al., 2002) como C3S V2 (Carrer et al., 2021a, 2021b) usan la cadena de procesado clásica (Figura 1), basándose en descriptores de la BRDF utilizando el mismo modelo tanto para el *kernel* volumétrico (*Ross_Thick*) como para el geométrico (*Li_Sparse Reciprocal*) (Lucht et al., 2000). El producto GLASS V4 (Liang et al., 2020) se basa, sin embargo, en un método de estimación directa usando un modelo de transferencia radiativa. Para el periodo de estudio, NASA MCD43A3 C6.1 y GLASS se basan en el mismo sensor (MODIS) mientras C3S V2 se basan en datos de dos sensores diferentes (SPOT/VGT de 2000 a Mayo 2014, y PROBA-V de Mayo 2014 a 2020). C3S V2 además incorpora el concepto ‘multi-sensor’ en esta segunda versión respecto a la V1 analizada en el artículo anterior (sección 3.2), incorporando un algoritmo recursivo de composición temporal que sirve como relleno de huecos apoyándose en la climatología de los parámetros BRDF de SPOT/VGT. Dicha climatología se usa como dato común auxiliar en todos los productos C3S SA V2 (basados en NOAA/AVHRR, SPOT/VGT, PROBA-V), dando como resultado una mejor consistencia entre las series temporales derivadas con sensores diferentes.

Los requisitos de usuario utilizados corresponden a los predefinidos en la plataforma, resumidos en la Tabla 5, estando basados en revisiones existentes de

requisitos para estimaciones de cambio climático (Ohring et al., 2005), y en los requerimientos del GCOS y WMO.

Tabla 5. Requerimientos de incertidumbre y estabilidad predefinidos en SALVAL.

	<i>Optimal</i>	<i>Target</i>	<i>Threshold</i>
<i>Uncertainty requirement</i>	Max [5%, 0.0025]	Max [10%, 0.01]	Max [15%, 0.015]
<i>Stability requirement</i>	Max [1%, 0.001]	Max [2%, 0.002]	Max [3%, 0.003]

Los resultados de la intercomparación mostraron una integridad similar de los diferentes productos de satélite, pero el producto MCD43A3 C6.1 es mucho más restrictivo si se usa la banda de calidad para descartar píxeles. El mayor porcentaje de huecos se observa principalmente en invierno durante el hemisferio norte. Tanto la consistencia espacial como la evaluación del error mostró un buen acuerdo entre pares de productos (residuos típicamente entre ± 0.015), siendo la comparación entre GLASS V4 y MCD43A3 C6.1 la que mayor porcentaje de residuos cumplía con los requisitos predefinidos (90% *target*, que se corresponde con el Max [10%, 0.01]). El análisis de la precisión (intra en inter-anual) y la consistencia temporal también presentó resultados satisfactorios, mostrando transiciones temporales suaves y un buen acuerdo tanto entre productos como con las observaciones *in situ*, siendo el producto C3S V2 el que manifestó algunas limitaciones (mayor ruido en la señal y dificultades para reproducir algunos episodios espurios de nieve). El análisis de la estabilidad reveló que todos los productos cumplen los requisitos del GCOS (<1% para estabilidad).

La validación directa mostró incertidumbres similares (RMSD = 0.03) en la comparación de píxeles de satélite clasificados como 'alta calidad' con las medidas *in situ* procedentes de estaciones de la base de datos REALS. De nuevo, se detectó que los requisitos de usuario en cuando a incertidumbre son difíciles de cumplir (<30% para *optimal* y <50% para *target*, independientemente del producto evaluado).

En conclusión, los resultados de validación demostraron que los tres productos de satélite investigados proporcionan series temporales consistentes y realistas a nivel global, mostrando ciertas discrepancias entre ellos principalmente asociadas al

algoritmo utilizado y al tipo de sensor (ver sección 1.2.1). Finalmente, se probó que la plataforma SALVAL ofrece una herramienta útil para la validación estandarizada de productos globales de albedo derivados con datos de satélite, permitiendo que alcancen el nivel 4 en la jerarquía del CEOS/WGCV LPV, ofreciendo transparencia, consistencia y trazabilidad en el proceso de validación.

3.4. Artículo 4: *Global estimates of surface albedo from Sentinel-3 OLCI and SLSTR data for Copernicus Climate Change Service: Algorithm and preliminary validation.*

Nota: Basado en el artículo (Sánchez-Zapero et al., 2023a), cuya copia completa se adjunta en el Anexo V .

Sánchez-Zapero, J., Camacho, F., Martínez-Sánchez, E., Gorroño, J., León-Tavares, J., Benhadj, I., Toté, C., Swinnen, E., Muñoz-Sabater, J., 2023a. Global estimates of surface albedo from Sentinel-3 OLCI and SLSTR data for Copernicus Climate Change Service: Algorithm and preliminary validation. *Remote Sensing of Environment* 287, 113460. <https://doi.org/10.1016/j.rse.2023.113460>

Los resultados preliminares de dicho trabajo también se presentaron en el *International Geoscience and Remote Sensing Symposium (IGARSS)*, celebrado en Bruselas (Bélgica) entre el 12 y 16 de Julio de 2021 (Sanchez-Zapero et al., 2021).

Sánchez-Zapero, J., Camacho, F., Leon-Tavares, J., Martinez-Sanchez, E., Gorrone, J., Benhadj, I., Tote, C., Swinnen, E., Munoz-Sabater, J., 2021. Prototype for Surface Albedo Retrieval Based on Sentinel-3 OLCI and SLSTR Data in the Framework of Copernicus Climate Change. *2021 IEEE Int. Geosci. Remote Sens. Symp. IGARSS* 2377–2380. <https://doi.org/10.1109/IGARSS47720.2021.9555099>

Dicho trabajo tuvo como objetivo el desarrollo del algoritmo, cadena de procesado y validación preliminar del producto global de albedo a partir del uso sinérgico de los sensores OLCI y SLSTR de los satélites Sentinel-3 (A y B). Dicho producto se distribuye actualmente en el servicio C3S en modo pre-operacional para dar continuidad a la serie climática de albedo más extensa disponible actualmente por la comunidad internacional, pues comienza en 1981 con datos NOAA/AVHRR (Abril 1981 - Diciembre 2005), prosigue con SPOT/VGT (Diciembre 1999 - Mayo 2014) y PROBA-V (Diciembre 2013 – Junio 2020), y continua con Sentinel-3/OLCI+SLSTR (a partir de Julio 2018). La resolución espacial de la serie climática existente (4 km para

NOAA/AVHRR y 1 km para SPOT/VGT y PROBA-V) se mejora con el uso de datos Sentinel-3 OLCI (~ 300 m) y SLSTR (~ 500 m), en respuesta a los requisitos del GCOS.

El algoritmo utilizado para la estimación de los productos de albedo (ver esquema general en Figura 1) parte de las reflectividades TOC de la superficie (corregidas de efectos atmosféricos). A continuación, se realiza la inversión del modelo de BRDF y, finalmente, se calcula el albedo tanto a nivel espectral (integración angular) como de banda ancha (integración espectral), siendo EOLAB responsable de las integraciones angulares y espectrales.

Respecto a los datos de entrada, se utilizaron las reflectividades TOC proporcionadas por el servicio CGLS, que es el dato de entrada común a las variables biofísicas derivadas en el propio servicio. El uso sinérgico de datos de los sensores OLCI y SLSTR nos permite la caracterización de todo el espectro solar, necesario para la determinación del albedo de banda ancha. Ambos sensores proporcionan información complementaria, pues OLCI ofrece canales en la región del azul (importante para el albedo en el visible) y SLSTR ofrece canales en el SWIR (que juegan un papel muy importante en el albedo de banda ancha en el NIR). Los datos de ambos sensores son ofrecidos por el CGLS en 15 canales de OLCI y 5 de SLSTR en una proyección común, a 300 m de resolución espacial, facilitando el uso sinérgico. Se eligieron 9 canales que cubrieron todo el espectro, 5 de OLCI (Oa03 – 442.5 nm, Oa04 – 490 nm, Oa07 – 620 nm, Oa17 – 865 nm, Oa21 – 1020 nm) y 4 de SLSTR (S1 – 554.27 nm, S2 – 659.47 nm, S5 – 1613.4 nm, S6 – 2255.7 nm). Además, dado que los datos de entrada presentan una limitación en la máscara de nubes y nieve derivada por el método de clasificación *IdePix* proporcionado por ESA, se hizo una clasificación de nieve basada en el *Normalized Difference Snow Index* (NDSI), que permite identificar píxeles de nieve basándose en los canales en el verde (S1) y SWIR (S5) de SLSTR.

Para la caracterización de los descriptores de la BRDF, se usó el procesador *Regularised BRDF inversion for Land Surface reflectance* (ReBeLS), basado en la inversión de un modelo numérico semi-empírico, similar al usado en los productos de MODIS y otros productos previamente derivados en C3S. Dicho procesador fue inicialmente desarrollado en CGLS (Leon-Tavares, 2020) y adaptado para las bandas OCLI y SLSTR

requeridas en C3S para la estimación del albedo. ReBeLS proporciona los descriptores de la BRDF (k_{iso} , k_{vol} , k_{geo}) y sus respectivas varianzas, partiendo de las reflectividades de la superficie junto a su geometría (configuración angular de visión y solar), la información de calidad de las observaciones (*quality flags*) y datos auxiliares (*prior*). La información auxiliar *prior* corresponde a una climatología de la BRDF (Strahler et al., 1999) de productos MODIS C6 (MCD43A1 y MCD43A2), que permite optimizar el proceso de inversión de la BRDF (Muller et al., 2011) cuando no hay observaciones suficientes de Sentinel-3, ofreciendo una técnica de relleno de huecos (*gap-filling*). Para el modelado de la BRDF se usan los modelos de *kernel* más populares (*Ross_Thick* para el volumétrico, *Li_Sparse Reciprocal* para el geométrico (Roujean et al., 1992; Wanner et al., 1995)), conocidos por su uso en los productos de MODIS (MCD43) y otros servicios operacionales (Baret et al., 2013; Geiger et al., 2008; Lucht et al., 2000; Roujean et al., 2018; Schaaf et al., 2002).

Respecto a la integración angular, se ofrecen los albedos tanto BSA como WSA para cada uno de los nueve canales seleccionados. BSA se calcula al mediodía solar mientras que WSA es el albedo compuesto únicamente por iluminación isotrópica difusa (en ausencia de componente directa). En lugar de calcular directamente las integrales respecto a los ángulos, se usa el mismo método pragmático usado en los productos MODIS que se basa en una representación polinómica de dichos albedos (Strahler et al., 1999).

Posteriormente, se realiza la integración espectral mediante una transformación lineal, considerando en el cálculo del albedo espectral coeficientes diseñados específicamente para situaciones de nieve y para observaciones libres de nieve. La metodología para la generación de estos coeficientes se basa en una regresión lineal sobre un conjunto de valores espectrales de bases de datos de albedo y su respectivo espectro (Liang, 2001). El algoritmo diseñado en este artículo incorpora mejoras respecto a lo ya existente, pues diseña específicamente coeficientes para BSA y WSA a diferencia de los productos previos en C3S o los basados en MODIS MCD43, que hacen el cálculo de coeficientes únicamente para BSA (aplicando los mismos a WSA). Otra mejora en este paso del algoritmo es la representatividad de la base de datos utilizada

para la generación de los coeficientes, pues considera una representación global de las propiedades atmosféricas y tipos de bioma.

Con el objetivo de hacer una evaluación inicial del prototipo, el servicio C3S generó un conjunto de datos de prueba de 10 meses (Julio 2018 – Abril 2019). Se evaluó la consistencia temporal del producto y se determinó el error (exactitud, precisión e incertidumbre) mediante validación directa e indirecta. También se realizó el test de conformidad de los requisitos de usuario (GCOS, WMO, C3S) en cuanto a la incertidumbre. Para la validación directa se usó un conjunto de datos *in situ* procedente de 32 estaciones homogéneas (incluidas en REALS), donde se ha evaluado la representatividad espacial de las medidas. También se realizó la intercomparación con NASA MODIS MCD43A3 C6 y con C3S PROBA-V SA V1 (para evaluar la continuidad del servicio C3S), realizada sobre el muestro global de sitios LANDVAL. Adicionalmente se evaluó el rendimiento del producto basado en Sentinel-3 sobre píxeles de nieve, utilizando como referencia el producto MCD43A3 C6 dada su demostrada efectividad para reproducir el albedo en estas condiciones (Wang et al., 2012, 2014).

La comparación con datos de campo mostró resultados similares a MCD43A3 C6 pero con un signo opuesto en la diferencias (ligeramente positivo en el caso de Sentinel-3), con una exactitud de 0.005 (3.7%), precisión de 0.016 (11.3%) e incertidumbre de 0.032 (22.7%). Los resultados de validación del producto C3S basado en Sentinel-3 mejoraron los resultados de validación directa obtenidos con el producto C3S PROBA-V V1. Esta validación preliminar mostró, en términos de consistencia espacial y temporal, que los productos C3S Sentinel-3 alcanzaron un buen acuerdo en comparación con otros productos de satélite operacionales derivados con MODIS (MCD43A3 C6) y PROBA-V (C3S PROBA-V SA V1).

Se demostró, por tanto, la viabilidad del algoritmo propuesto para la continuidad del CDR del servicio C3S utilizando el uso de datos OLCI+SLSTR de Sentinel-3. La principal limitación del producto de albedo C3S de Sentinel-3 fue la subestimación del albedo en la nieve y la transición lenta entre valores bajos y altos en eventos de nieve. Dicha limitación proviene de los datos de entrada proporcionados en CGLS, que usa el

clasificador *IdePix* de la ESA, donde se confunden los valores de nieve con valores de nube, enmascarando y filtrando dichos valores.

NOTA ADICIONAL: Posteriormente al desarrollo del algoritmo se detectó un error de geolocalización en el producto de entrada (Sentinel-3 TOC V1) al algoritmo de albedo, que es proporcionado por el servicio CGLS²⁷. Dicho servicio ha trabajado en la corrección de dicho error y está actualmente generando una nueva versión corregida (Sentinel-3 TOC V2). Una vez estén disponibles los datos de entrada corregidos se espera hacer un reprocesado del producto C3S de albedo basado en Sentinel-3 así como una validación completa y extendida del mismo.

²⁷ Noticia publicada por CGLS sobre el error de geolocalización: <https://land.copernicus.eu/global/content/geolocation-issue-sentinel-3-based-vegetation-products> (acceso *online* el 11/07/2023).

4. Discusión general y conclusiones

El trabajo realizado en esta tesis ha dado respuesta a los cuatro principales objetivos planteados inicialmente (ver sección 1.4). La consecución de dichos objetivos permite alcanzar el principal propósito de la tesis, que es el desarrollo de un sistema operacional de validación estandarizada de productos globales de albedo integrando cuatro componentes principales: metodología de validación respaldada por el consenso de la comunidad (CEOS/WGCV LPV), series climáticas de albedo, datos *in situ* espacialmente representativos y desarrollo de herramienta de validación *online*. Se establecieron diferentes sub-objetivos para cada uno de las cuatro componentes, tal como se desarrolla a continuación.

➔ **OBJETIVO 1: Desarrollo y propuesta de una metodología propia para la validación estandarizada de productos globales de albedo de la superficie terrestre a diferentes resoluciones.**

Dicho objetivo se ha alcanzado con el desarrollo de la metodología de validación descrita en el capítulo 2.

- Se han desarrollado las métricas para evaluar diferentes criterios como la integridad, consistencia espacial, consistencia temporal, evaluación del error (exactitud, precisión, incertidumbre) y estabilidad. Se ha dado respuesta a los requerimientos expresados por organismos internacionales (CGOS, WMO).
- Dicha metodología ha contribuido al protocolo de validación de productos globales de albedo desarrollado por el CEOS/WGCV LPV (Wang et al., 2019) convirtiéndose en un estándar, al contar con el consenso de la comunidad (expertos internacionales en validación, desarrolladores de productos y agencias).
- Se ha desarrollado un muestro representativo de localizaciones a nivel global (LANDVAL, ver sección 2.2) para la intercomparación de productos, permitiendo que los distintos ejercicios de validación indirecta sean

comparables entre sí, dando valor al concepto de estandarización y trazabilidad. Dicho muestreo ha sido usado tanto en los informes de validación realizados en CGLS y C3S (ver listado en Anexo I) como en los artículos de validación global incluidos en esta tesis (Sánchez-Zapero et al., 2023b, 2023a, 2020). Cabe destacar además que también se ha extendido el uso de LANDVAL dentro de los servicios CGLS y C3S para la validación de otros productos globales como índices de vegetación (NDVI) o parámetros biofísicos de vegetación (LAI, FAPAR, FCOVER)(Fuster et al., 2020).

- El muestreo LANDVAL para la intercomparación (720 sitios), junto a la creación de la extensa base de datos REALS (99 estaciones, ver sección 2.1) permite al ejercicio de validación alcanzar un nivel 3 de acuerdo a la jerarquía del CEOS/WGCV LPV (ver Tabla 1), pues la incertidumbre se cuantifica sobre un número de estaciones significativo y la consistencia espacial y temporal con productos de satélite se determina sobre un conjunto representativo a nivel global de localizaciones, permitiendo caracterizar adecuadamente la estructura de la incertidumbre de los productos.

→ **OBJETIVO 2:** Evaluar la calidad científica, así como determinar la exactitud y la incertidumbre asociada a los productos de albedo a escala global desarrollados dentro del programa *Copernicus*, que se derivan con diferentes sensores satelitales a diferentes resoluciones espaciales.

Esta tesis ha contribuido de manera notoria a la validación y el desarrollo de algoritmos para la estimación del albedo dentro del programa *Copernicus*. Se ha evaluado la calidad científica (validación) y monitorizado dicha calidad anualmente para diferentes productos tanto de albedo como de reflectividad de la superficie. Además de haber realizado una validación completa de cada versión de producto (o evolución del algoritmo) y sensor (ver listado de informes de validación en Anexo I), se han realizado las cuatro publicaciones incluidas en esta tesis.

- En el **artículo 1** se realizó la validación del primer prototipo desarrollado en el programa CGLS para estimar el albedo a partir de datos PROBA-V a 300

m de resolución espacial (Roujean et al., 2018). Para la validación del prototipo se procesó y generó el producto sobre una ventana sub-continental en Europa para el año 2014. Se hizo una intercomparación con productos de NASA basados en MODIS (MCD43A3 C6) y una validación directa con datos *in situ* de 10 estaciones homogéneas (EFDC).

- El análisis visual de los mapas reveló patrones espaciales consistentes, con una notable integridad explicada en el beneficio del uso de un compuesto temporal recursivo.
- Se demostró que el producto basado en PROBA-V es consistente espacialmente con el basado en MODIS sobre la ventana Europea, con la mayoría de residuos entre ± 0.025 para el visible y ± 0.05 para el NIR y onda corta total. Cabe resaltar que se descartaron los píxeles de nieve dadas las diferentes estrategias temporales de composición entre productos.
- La consistencia temporal reveló que el producto de PROBA-V es capaz de reproducir los cambios de albedo tanto sobre superficies naturales (p.ej., bosques) como en zonas de cultivos, observados tanto en el producto referencia (MCD43A3 C6) como en las observaciones *in situ*. Sólo en un 40% de casos sobre bosques de coníferas se observaron trayectorias temporales inconsistentes en el dominio NIR (que afecta también al de onda corta total). PROBA-V presentó además mejor integridad (menos huecos) que MCD43A3 C6.
- Los episodios de nieve se reprodujeron por PROBA-V correctamente en un 70% de casos en comparación con MCD43A3 C6 y las observaciones *in situ*. Los eventos no reproducidos, principalmente de poca duración, se pueden explicar por la discriminación entre píxeles de nieve o libres de nieve sobre la amplia ventana de composición temporal del producto.
- La validación directa de PROBA-V reveló una incertidumbre (RMSD) de 0.03, siendo idéntica a la obtenida por MDC43A3 C6. PROBA-V mostró un sesgo medio positivo de 0.01 (9%), mostrando MCD43A3 C6 mejores resultados (diferencias medias en torno a cero y relación lineal óptima).

A pesar de los buenos resultados, se vio que muy pocos píxeles cumplían con los requerimientos de incertidumbre del GCOS (5.9% y 9.2% para PROBA-V y MODIS), lo que evidencia las dificultades de los productos de satélite para satisfacer dichos requisitos.

- Los resultados de validación demostraron el buen rendimiento general del prototipo, pero también evidenciaron algunas limitaciones esperadas por los datos de entrada PROBA-V. Se observó dificultad para reproducir algunos eventos de nieve debida a la máscara de nubes de PROBA-V, que confunde en ocasiones hielo/nieve con nubes. Cabe destacar que PROBA-V no tiene banda térmica (a diferencia de MODIS), de gran utilidad para la detección de hielo y nieve.
- En el **artículo 2** se validó la primera versión (V1) de los productos de albedo desarrollados en C3S con datos PROBA-V (Sánchez-Zapero et al., 2020). Dicho análisis se centró en la transición de SPOT/VGT a PROBA-V dentro de C3S, comparando ambos productos para el periodo de solapamiento de los satélites. Los otros conjuntos de datos de referencia fueron el producto MCD43A3 C6 derivado con datos MODIS y las medidas *in situ* procedentes de GBOV (20 estaciones, donde se evaluó la representatividad espacial de sus medidas).
 - La validación directa con datos medidos por estaciones terrestres mostró que PROBA-V SA V1 tiene una exactitud (MD = +18.2%) similar a SPOT/VGT V1 y peor a que MCD43A3 C6 (MD = -11.2%), mostrando signos opuestos. El signo positivo y sistemático de PROBA-V fue observado principalmente en bosques (albedo < 0.2) y puede deberse, en parte, en el hecho de que el *kernel Roujean* (Roujean et al., 1992) usado para caracterizar la componente geométrica de la BRDF puede presentar limitaciones sobre algunos tipos de cubierta, especialmente sobre bosques densos (Aisheng Wu et al., 1995; Chen and Cihlar, 1997; Liu et al., 2010). Se hizo uso de la banda de calidad auxiliar para descartar estimaciones de baja calidad, que elimina la mayoría de píxeles de nieve

en el caso de PROBA-V, por lo que el ejercicio es prácticamente equivalente a una validación sobre condiciones libres de nieve.

- Los productos de satélite ofrecieron un porcentaje bajo de píxeles que satisfacen los requisitos en cuanto a incertidumbre expresados tanto por el GCOS (<25% de píxeles para Max [5%; 0.0025]) como C3S (<50% para Max [10%; 0.01]). Hay que tener en cuenta que ya los datos de campo presentan incertidumbres en torno al 5% bajo condiciones ideales (Reda, 2011), por lo que dichos requisitos son muy demandantes para productos de satélite.
- La intercomparación de productos determinó la buena consistencia en la versión 1 de C3S asociada al cambio de sensor de SPOT/VGT a PROBA-V, con un sesgo medio típicamente entre $\pm 2\%$. La comparación con MCD43A3 C6 mostró peor consistencia espacio-temporal, con diferencias medias de hasta el 13%. Las diferencias existentes entre diferentes productos se asocian a los diferentes aspectos de la cadena de procesado:
 - i. PROBA-V se diseñó para ser equivalente espectralmente a SPOT/VGT, lo que explica la buena consistencia entre ellos. MODIS tiene bandas equivalentes espectralmente a ellos, pero de un ancho de banda menor dando resultado a diferencias en regiones como el visible, con una alta absorción en vegetación densa.
 - ii. Cada satélite usa un método diferente de discriminación de nubes, corrección atmosférica y clasificación de nieve. PROBA-V usa un algoritmo de detección de nubes más conservador (Iannone et al., 2017), lo que se traslada en mayor cantidad de huecos comparado con SPOT/VGT.
 - iii. Las discrepancias entre productos también están asociadas al uso de diferentes modelos usados en la parametrización de la BRDF (Carrer et al., 2010b) y a los diferentes periodos de composición, que dependen además del número de observaciones libres de

nubes usadas en cada estimación. También se esperan mayores diferencias en la nieve asociadas tanto al periodo de composición como a los modelos de BRDF, que no están propiamente diseñados para estos objetivos (Maignan et al., 2004).

- iv. Las diferentes técnicas de compuestos temporales también influyen en la integridad de los productos. C3S SPOT/VGT V1 usa un compuesto temporal recursivo (Carrer et al., 2018), lo que mejora la continuidad espacio-temporal comparado con C3S PROBA-V V1 y MCD43A3 C6.
 - v. El último paso de la cadena de procesado hace referencia a la conversión a banda ancha. Los productos C3S (PROBA-V y SPOT/VGT) de banda ancha se definen para una misma región espectral, lo que contribuye a un mejor acuerdo. MCD43A3 C6 se define para anchos de banda ligeramente diferentes.
 - vi. Como punto adicional, C3S PROBA-V V1 mostró cierto ruido temporal en la región del NIR, teniendo un impacto directo en la precisión intra-anual, que es ligeramente inferior al resto de productos.
- La publicación de este artículo representó un hito en cuanto a la validación de productos de albedo, pues se habían publicado muy pocos ejercicios de validación sobre condiciones globales y periodos de tiempo representativos hasta la fecha, basados principalmente en MODIS (Cescatti et al., 2012; Liang et al., 2002; Liu et al., 2013). C3S PROBA-V SA V1 alcanzó un nivel de validación 3 en la jerarquía del CEOS/WGCV LPV gracias a esta publicación.
 - El **artículo 3** presentó un ejercicio de validación de tres series climáticas de albedo: C3S multi-sensor V2, NASA MCD43A3 C6.1 y BNU GLASS V4 (Sánchez-Zapero et al., 2023b). C3S V2 incorpora el concepto '*multi-sensor*' para hacer la serie más consistente entre cambios de sensor (NOAA/AVHRR, SPOT/VGT y PROBA-V). Se hizo uso de la herramienta SALVAL para la generación de los resultados de validación, realizando la validación directa

sobre la extensa red REALS. Los resultados de validación demostraron que los 3 productos ofrecen CDRs fiables y altamente consistentes entre ellos a escala global.

- La validación directa mostró un *bias* positivo en torno al 10% en el caso de C3S V2, en línea con lo observado previamente para la versión anterior C3S V1 (Lellouch et al., 2020; Sánchez-Zapero et al., 2020). GLASS V4 y MCD43A3 C6.1 mostraron un signo negativo en las diferencias, contrario a lo observado en C3S V2, pero ofreciendo una exactitud algo mejor (*bias* en torno al -6%).
- De nuevo, la validación directa puso de manifiesto la dificultad de los productos de satélite para satisfacer los requisitos de usuario establecidos actualmente en cuanto a incertidumbre. Típicamente, menos del 20% de píxeles de satélite cumplen con el requisito del GCOS (Max [5%, 0.0025]). Por el contrario, los tres productos cumplieron ampliamente dichos requisitos en cuanto a estabilidad (Max [1%, 0.001]).
- Los tres productos evaluados mostraron una notable integridad debido a las diferentes técnicas incorporadas para mejorar este aspecto: un algoritmo *back-up* en MCD43A3 C6 para observaciones calificadas de baja calidad (potencialmente contaminadas con nubes), un algoritmo de composición temporal recursivo en caso de C3S V2 que usa una climatología de la BRDF como dato '*a priori*', y técnicas de relleno de huecos (*gap-filling*) en el caso de GLASS V4. Cuando se usan las bandas de calidad para descartar píxeles, MCD43A3 C6.1 es el producto con peor integridad.
- En términos de consistencia espacial, todas las combinaciones entre pares de productos cumplieron con un alto porcentaje de casos (>70%) entre los requerimientos óptimos de consistencia. El mejor acuerdo se observó entre MCD43A3 C6.1 y GLASS V4, lo que se explica en parte a que están derivados con datos del mismo sensor (Gu et al., 2021). Se observaron mayores diferencias sobre zonas al norte y áreas

- ecuatoriales, que pueden deberse a una posible contaminación de nubes o a diferencias significativas sobre píxeles de nieve (en el caso del norte).
- Los tres productos mostraron un buen acuerdo temporal, tanto entre sí como en la comparación con medidas *in situ*.
 - La evaluación del error entre pares de productos también reveló un mejor acuerdo en la comparativa de GLASS V4 con MCD43A3 C6.1, ambos basados en MODIS. C3S V2 mostró mayores errores comparados con ambos productos basados en MODIS, pero con resultados satisfactorios (diferencias sistemáticamente positivas en torno al 10%).
 - Como conclusión de la intercomparación, el uso de diferentes sensores es el factor más importante que contribuye a la diferencia entre productos. Sin embargo el resto de factores de la cadena de procesado también contribuye a las diferencias (modelo de BRDF, composición temporal o diferencias en la integración tanto angular como espectral).
- Finalmente, en el **artículo 4** se trabajó en el desarrollo y validación de productos C3S de albedo con datos de satélite de nueva generación Sentinel-3 (C3S Sentinel-3 SA V3), mediante el uso sinérgico de sus sensores OLCI y SLSTR, para la continuidad de la serie climática de albedo (Sánchez-Zapero et al., 2023a).
 - El algoritmo sigue los pasos descritos en la Figura 1, partiendo de las reflectividades de la superficie generadas en CGLS en una proyección común a 300 m de resolución espacial con el objetivo de facilitar la integración de datos de las diferentes fuentes (OLCI y SLSTR). Los siguientes pasos son la inversión del modelo BRDF (que hace uso de un algoritmo temporal recursivo utilizando climatología de MODIS como dato auxiliar), la integración angular y la conversión a banda ancha. Dado que se detectaron dos limitaciones en los datos de entrada (reflectividades de la superficie), se realizaron dos adaptaciones para mitigar efectos negativos en el producto final:
 - i. El procesador *IdePix* proporcionado por la misión Sentinel-3 de la ESA (utilizado por la cadena de pre-procesado de CGLS) no

- identifica correctamente los píxeles de nieve o el hielo, confundiéndolos o enmascarándolos como nubes. Esto da como resultado una carencia de píxeles puros de nieve ingeridos como datos de entrada al procesador BRDF. Se propuso, por tanto una regla alternativa para identificar la nieve basándose en el índice NDSI. A dichos píxeles identificados como nieve se le aplicaron filtrados menos restrictivos con el objetivo tener más datos de entrada puros de nieve.
- ii. Las radiancias de los canales en el SWIR de SLSTR están afectadas por errores de calibración radiométrica, por lo que ESA proporcionó unos coeficientes de calibración para corregir estos efectos (S3_MPC, 2021). Dichos coeficientes no fueron tenidos en cuenta por CGLS, propagando errores a las reflectividades de la superficie. Para mitigar esto, los coeficientes de calibración fueron aplicados directamente a los albedos espectrales de los canales S5 y S6 de SLSTR.
 - o La validación preliminar mostró resultados prometedores sobre un conjunto global de datos limitado temporalmente (10 meses). Se evaluó la consistencia temporal del producto y se determinó el error (exactitud, precisión e incertidumbre) mediante validación directa (32 estaciones REALS) e indirecta (productos MCD43A3 C6 y C3S PROBA-V SA V1, para evaluar la continuidad del servicio C3S). Además se comparó Sentinel-3 SA V3 con MCD43A3 C6 sobre píxeles nieve, ya que este último ha demostrado previamente buena calidad para periodos de nieve (Wang et al., 2014, 2012).
 - i. La consistencia temporal del producto basado en Sentinel-3 fue buena tanto con los productos de referencia como con las medidas *in situ*, reproduciendo bien situaciones tanto para periodos de albedo estable como para variaciones estacionales. Sin embargo, Sentinel-3 SA V3 tiende a reproducir menor número de eventos de nieve o proporciona transiciones más lentas para periodos de

- valores bajos (libre de nieve) a altos de albedo (nieve) comparado con MCD43A3 C6 y las medidas *in situ*. Esto se debe a la baja disponibilidad de datos de entrada para observaciones de nieve; si no hay suficientes observaciones, el modelo no puede reaccionar inmediatamente.
- ii. Se determinó el error respecto al producto C3S PROBA-V SA V1, mostrando altas correlaciones, una exactitud típicamente menor al 5% (con signo negativo: Sentinel-3 < PROBA-V), y una incertidumbre (RMSD) en torno a 0.05. Típicamente, entre un 20% y un 40% de casos (dependiendo del tipo de albedo y región espectral) cumplían los requerimientos de incertidumbre de GCOS, y sobre un 50% los requerimientos de C3S.
 - iii. La comparación con MCD43A3 C6 mostró diferencias positivas para píxeles libres de nieve, y negativas para observaciones de nieve. De nuevo, entre un 20% y 40% de casos (dependiendo del tipo de albedo y región espectral) cumplían los requerimientos de incertidumbre de GCOS, y más de un 50% los requerimientos de C3S.
 - iv. La comparación de Sentinel-3 SA V3 con MCD43A3 C6 sobre nieve mostró diferencias medias negativas: -5% para el visible y hasta del -25% para el NIR y onda corta total. Se observó además gran dispersión para los valores de albedo intermedios, como consecuencia de la heterogeneidad sub-píxel (Jin et al., 2003) debido a mezcla entre zonas de nieve y libres de nieve debido a procesos como el deshielo. Las diferencias en los periodos de composición también juegan un papel clave en las grandes diferencias en la nieve (Wang et al., 2012).
 - v. La validación directa mostró que Sentinel-3 SA V3 proporcionó una exactitud (MD=6.3%) ligeramente inferior a MCD42A3 C6 (MD=-3.3%), con diferente signo en las diferencias. PROBA-V SA V1 mostró mayores diferencias (MD=15.8%), en línea con ejercicios

anteriores (Sánchez-Zapero et al., 2020). Los tres productos mostraron precisión en incertidumbre similar, siendo MCD43A3 C6 el que proporcionó ligeramente mejores resultados (MAD=8.6%, RMSD=0.029).

- La principal limitación del producto es la subestimación de albedo en la nieve (de -14% a -35% comparado con MCD43A3 C6) y la transición lenta de valores bajos (libres de nieve) a altos (píxeles puros de nieve). La regla de decisión alternativa basada en el NDSI para aumentar la adquisición de datos de nieve (dada la limitación de *IdePix*) junto al uso recursivo de climatología BRDF de MODIS en la inversión de la BRDF puede, en parte, corregir las limitaciones en nieve.
- Cabe destacar el hecho de que todos los ejercicios de validación pusieron de manifiesto la dificultad que tienen los productos de satélite de cumplir con los requisitos de usuario existentes en cuanto a la incertidumbre (p.ej., 5% de requisito por parte del GCOS). Dichos requisitos han sido actualizados recientemente, estableciendo un nuevo nivel óptimo de incertidumbre del 3% (GCOS-245, 2022), siendo más demandante que el anterior e incluso superior a la incertidumbre asociada a las medida de estaciones terrestres (5% de error en condiciones ideales (Reda, 2011)).

→ **OBJETIVO 3: Desarrollo de una base de datos de medidas *in situ* de albedo que sea fiable, integrando datos procesados de redes o iniciativas existente.**

El desarrollo de la red REALS (ver sección 2.1) ha dado solución este objetivo.

- Se han integrado datos de un número extenso de estaciones (99) con el objetivo de que el resultado de la validación sea lo más representativo posible a nivel global. Hay que tener en cuenta que el CEOS/WGCV LPV establece un mínimo número de estaciones de 30 para que el resultado sea estadísticamente significativo para llegar a un nivel 3 (ver Tabla 1). REALS, con 99 estaciones, supera largamente estos mínimos requeridos
- Se ha evaluado la representatividad espacial de la medida usando metodologías y estándares internacionales (Román et al., 2010, 2009)

recogidos en el protocolo del CEOS/WGCV LPV, asegurando que dicha medición sea equivalente a la resolución espacial del píxel de satélite de interés. En el caso de REALS, se ha evaluado la representatividad a 1 km², lo que es compatible para los productos globales existentes basados en VGT (1 km), MODIS (500 m) o Sentinel-3 (300 m).

➔ **OBJETIVO 4:** Desarrollo de una herramienta de software semi-automática, que permita alcanzar una validación estandarizada operacional continuada en el tiempo a medida que la serie temporal de los productos se expande o se desarrollan nuevas versiones (nivel 4 de validación de acuerdo a la jerarquía del CEOS/WGCV LPV).

El desarrollo de la herramienta SALVAL, cuya presentación de funcionalidades a la comunidad se ha realizado en el **artículo 3** (Sánchez-Zapero et al., 2023b), ha constituido la consecución de dicho objetivo.

- SALVAL permite a los productos de albedo alcanzar el nivel máximo de validación (4) en la jerarquía del CEOS/WGCV LPV, contando con el respaldo del mismo. Este hecho constituye un hito que no se había alcanzado en el campo de la validación de productos globales de albedo. Como hito adicional, SALVAL está incluida dentro de las herramientas de validación incluidas en el portal de validación y calibración del CEOS²⁸ (CEOS *Cal/Val portal*) gestionado por ESA.
- Gracias a su interfaz de usuario amigable, SALVAL permite una validación interactiva y posibilita configurar cada ejercicio de acuerdo a los requerimientos del propio usuario (*fitness-for-purpose*).
- La herramienta cuenta con una base de datos extensa tanto de productos de satélite existentes como de datos de medidas *in situ*. Además, permite la funcionalidad adicional de importar directamente un producto de nuevo

²⁸ <https://calvalportal.ceos.org/salval> (acceso online el 03/05/2023)

desarrollo con el objetivo de obtener de manera automatizada y estandarizada la validación del mismo.

→ **PERSPECTIVAS FUTURAS:** Se seguirá trabajando en las cuatro áreas principales:

- A nivel de metodologías de validación, el autor de esta tesis ha sido designado por el grupo del CEOS/WGCV LPV para co-liderar el área dedicada a la validación de los productos de radiación de la superficie/albedo, coordinando las actividades a nivel internacional como la definición y estandarización de protocolos. A nivel metodológico este apartado está completo tras la realización del protocolo de validación aunque hay criterios que requieren mayores esfuerzos como la estabilidad, que ha recibido menos atención por parte de los estudios de validación actuales. También se está trabajando en un código que nos permita hacer un muestro global (LANVAL V2) que permita establecer un número de localizaciones definidas por el usuario y que sea representativo a nivel global no sólo en cuanto a localizaciones y zonas continentales (como LANDVAL) sino también por ecorregiones.
- A nivel de productos de satélite, se seguirá trabajando en el programa C3S, donde se van a hacer dos actividades principales como responsables del desarrollo y validación de los productos de albedo en dicho servicio: reprocesado del producto basado en unos datos de entrada mejorados de Sentinel-3 y validación completa sobre un periodo temporal extendido. En base a la validación completa se establecerán unas evoluciones para mejorar el producto. Por otra parte, gracias a SALVAL se podrá ir realizando actualizaciones de la validación, permitiendo atribuir al producto el nivel 4 en la jerarquía del CEOS/WGCV LPV.
- En cuanto a la base de datos de medias *in situ* para la validación directa, se espera ampliar el número de estaciones, principalmente sobre las zonas menos representadas actualmente por REALS (Sudamérica, África o Asia,

ver Figura 3). Las resoluciones medias de los sensores actuales (300 – 500 m) van a ser mejoradas con los futuros satélites de nueva generación (p.ej., Sentinel-3 *Next Generation*), permitiendo ser menos restrictivos con la evaluación de la representatividad espacial de la medida y pudiendo incluir más estaciones a la base de datos.

- Finalmente, se promoverá el uso de SALVAL a través de la comunidad internacional por medio del CEOS/WGCV LPV con el objetivo no sólo de fomentar la estandarización de resultados de validación sino de mejorar la herramienta basándonos en la experiencia y retroalimentación de los usuarios. Se hará una actualización periódica (anualmente) tanto de la base de medidas *in situ* como de productos de satélite, incluyendo nuevos productos (p.ej., Sentinel-3) y extendiendo las series temporales de los ya existentes.

Bibliografía

- Ackerman, S., Frey, R., Strabala, K., Liu, Y., Gumley, L., Baum, B., Menzel, P., 2010. Discriminating clear-sky from cloud with MODIS - Algorithm Theoretical Basis Document (MOD35).
- Aisheng Wu, Zhanqing Li, Cihlar, J., 1995. Effects of land cover type and greenness on advanced very high resolution radiometer bidirectional reflectances: analysis and removal. *J. Geophys. Res.* 100, 9179–9192. <https://doi.org/10.1029/95JD00512>
- Amut, A., Gong, L., Yuan, Z., 2007. Spatial distributions of surface albedo from satellite data in arid oasis. <https://doi.org/10.1117/12.746119> 6679, 550–555. <https://doi.org/10.1117/12.746119>
- Baret, F., Hagolle, O., Geiger, B., Bicheron, P., Miras, B., Huc, M., Berthelot, B., Niño, F., Weiss, M., Samain, O., Roujean, J.L., Leroy, M., 2007. LAI, fAPAR and fCover CYCLOPES global products derived from VEGETATION. Part 1: Principles of the algorithm. *Remote Sens. Environ.* 110, 275–286. <https://doi.org/10.1016/j.rse.2007.02.018>
- Baret, F., Weiss, M., Lacaze, R., Camacho, F., Makhmara, H., Pacholczyk, P., Smets, B., 2013. GEOV1: LAI and FAPAR essential climate variables and FCOVER global time series capitalizing over existing products. Part1: Principles of development and production. *Remote Sens. Environ.* 137, 299–309. <https://doi.org/10.1016/j.rse.2012.12.027>
- Barnsley, M.J., Strahler, A.H., Morris, K.P., Muller, J.P., 1994. Sampling the surface bidirectional reflectance distribution function (BRDF): 1. evaluation of current and future satellite sensors. *Remote Sens. Rev.* 8, 271–311. <https://doi.org/10.1080/02757259409532205>
- Bayat, B., Camacho, F., Nickeson, J., Cosh, M., Bolten, J., Vereecken, H., Montzka, C., 2021. Toward operational validation systems for global satellite-based terrestrial essential climate variables. *Int. J. Appl. Earth Obs. Geoinf.* 95, 102240. <https://doi.org/10.1016/J.JAG.2020.102240>
- Bonafoni, S., Sekertekin, A., 2020. Albedo Retrieval from Sentinel-2 by New Narrow-to-

- Broadband Conversion Coefficients. *IEEE Geosci. Remote Sens. Lett.* 17, 1618–1622. <https://doi.org/10.1109/LGRS.2020.2967085>
- Breon, F.-M., Maignan, F., 2017. A BRDF–BPDF database for the analysis of Earth target reflectances. *Earth Syst. Sci. Data* 9, 31–45. <https://doi.org/10.5194/essd-9-31-2017>
- Bréon, F.-M., Vermote, E., 2012. Correction of MODIS surface reflectance time series for BRDF effects. *Remote Sens. Environ.* 125, 1–9. <https://doi.org/10.1016/j.rse.2012.06.025>
- Camacho, F., 2019. CEOS/WGCV LPV Action Plan 2019-2022. Data Issued: 15.06.2019. Issue 11.00. [WWW Document]. URL https://lpvs.gsfc.nasa.gov/LPV_Meetings/LPV_plenary2019.html (accessed 7.10.23).
- Camacho, F., Cernicharo, J., Lacaze, R., Baret, F., Weiss, M., 2013. GEOV1: LAI, FAPAR essential climate variables and FCOVER global time series capitalizing over existing products. Part 2: Validation and intercomparison with reference products. *Remote Sens. Environ.* 137, 310–329. <https://doi.org/10.1016/j.rse.2013.02.030>
- Campagnolo, M.L., Montano, E.L., 2014. Estimation of effective resolution for daily modis gridded surface reflectance products. *IEEE Trans. Geosci. Remote Sens.* 52, 5622–5632. <https://doi.org/10.1109/TGRS.2013.2291496>
- Carrer, D., Moparthy, S., Lellouch, G., Ceamanos, X., Pinault, F., Freitas, S.C., Trigo, I.F., 2018. Land surface albedo derived on a ten daily basis from Meteosat Second Generation Observations: The NRT and climate data record collections from the EUMETSAT LSA SAF. *Remote Sens.* 10. <https://doi.org/10.3390/rs10081262>
- Carrer, D., Pinault, F., Bigeard, G., Ramon, D., Jolivet, D., Kirches, G., Brockmann, C., Boettcher, M., Benhadj, I., 2021a. Algorithm Theoretical Basis Document Multi sensor CDR Surface Albedo v2.0 (Official reference number service contract: 2018/C3S_312b_Lot5_VITO/SC1). [WWW Document]. URL https://datastore.copernicus-climate.eu/documents/satellite-albedo/D1.3.4-v2.0_ATBD_CDR_SA_MULTI_SENSOR_v2.0_PRODUCTS_v1.1.pdf (accessed 11.10.22).

- Carrer, D., Pinault, F., Lellouch, G., Trigo, I.F., Benhadj, I., Camacho, F., Ceamanos, X., Moparthy, S., Munoz-Sabater, J., Schüller, L., Sánchez-Zapero, J., 2021b. Surface Albedo Retrieval from 40-Years of Earth Observations through the EUMETSAT/LSA SAF and EU/C3S Programmes: The Versatile Algorithm of PYALUS. *Remote Sens.* 13, 372. <https://doi.org/10.3390/rs13030372>
- Carrer, D., Roujean, J.-L., Hautecoeur, O., Elias, T., 2010a. Daily estimates of aerosol optical thickness over land surface based on a directional and temporal analysis of SEVIRI MSG visible observations. *J. Geophys. Res.* 115, D10208. <https://doi.org/10.1029/2009JD012272>
- Carrer, D., Roujean, J., Meurey, C., 2010b. Comparing Operational MSG / SEVIRI Land Surface Albedo Products From Land SAF With Ground Measurements and MODIS. *IEEE Trans. Geosci. Remote Sens.* 48, 1714–1728. <https://doi.org/10.1109/TGRS.2009.2034530>
- Cescatti, A., Marcolla, B., Santhana Vannan, S.K., Pan, J.Y., Román, M.O., Yang, X., Ciais, P., Cook, R.B., Law, B.E., Matteucci, G., Migliavacca, M., Moors, E., Richardson, A.D., Seufert, G., Schaaf, C.B., 2012. Intercomparison of MODIS albedo retrievals and in situ measurements across the global FLUXNET network. *Remote Sens. Environ.* 121, 323–334. <https://doi.org/10.1016/j.rse.2012.02.019>
- Chen, J.M., Cihlar, J., 1997. A hotspot function in a simple bidirectional reflectance model for satellite applications. *J. Geophys. Res. Atmos.* 102, 25907–25913. <https://doi.org/10.1029/97jd02010>
- Cihlar, J., Chen, J., Li, Z., Huang, F., Latifovic, R., Dixon, R., 1998. Can interannual land surface signal be discerned in composite AVHRR data? *J. Geophys. Res.* 103, 23163.
- Cihlar, J., Latifovic, R., Chen, J., Trishchenko, A., Du, Y., Fedosejevs, G., Guindon, B., 2004. Systematic corrections of AVHRR image composites for temporal studies. *Remote Sens. Environ.* 89, 217–233. <https://doi.org/10.1016/j.rse.2002.06.007>
- Claverie, M., Vermote, E., Franch, B., He, T., Hagolle, O., Kadiri, M., Masek, J., 2015. Evaluation of Medium Spatial Resolution BRDF-Adjustment Techniques Using

- Multi-Angular SPOT4 (Take5) Acquisitions. *Remote Sens.* 7, 12057–12075. <https://doi.org/10.3390/rs70912057>
- Dickinson, R.E., 1995. Land processes in climate models. *Remote Sens. Environ.* 51, 27–38. [https://doi.org/10.1016/0034-4257\(94\)00062-R](https://doi.org/10.1016/0034-4257(94)00062-R)
- Dickinson, R.E., 1983. Land surface processes and climate—surface albedos and energy balance. *Adv. Geophys.* 25, 305–353. [https://doi.org/10.1016/S0065-2687\(08\)60176-4](https://doi.org/10.1016/S0065-2687(08)60176-4)
- Diner, D.J., Beckert, J.C., Reilly, T.H., Bruegge, C.J., Conel, J.E., Kahn, R.A., Martonchik, J. V., Ackerman, T.P., Davies, R., Gerstl, S.A.W., Gordon, H.R., Muller, J.P., Myneni, R.B., Sellers, P.J., Pinty, B., Verstraete, M.M., 1998. Multi-angle imaging spectroradiometer (MISR) instrument description and experiment overview. *IEEE Trans. Geosci. Remote Sens.* 36, 1072–1087. <https://doi.org/10.1109/36.700992>
- Diner, D.J., Martonchik, J. V, Borel, C., Gerstl, S.A.W., Gordon, H.R., Knyazikhin, Y., Myneni, R., Pinty, B., Verstraete, M.M., 2008. Level 2 Surface Retrieval Algorithm Theoretical Basis Level 2 Surface Retrieval Algorithm Theoretical Basis Approval.
- ESA Sentinel-2 mission, n.d. Copernicus Sentinel-2 Mission Guide. [WWW Document]. URL <https://sentinel.esa.int/web/sentinel/missions/sentinel-2> (accessed 5.1.23).
- Fell, F., Bennartz, R., Loew, A., 2015. Validation of the EUMETSAT Geostationary Surface Albedo Climate Data Record -2- (ALBEDOVAL-2). [WWW Document]. URL <https://www.eumetsat.int/website/home/Data/TechnicalDocuments/index.html> (accessed 4.12.20).
- Fougnie, B., Henry, P., Cabot, F., Meygret, A., Laubies, M.-C., 2000. VEGETATION : In-flight multi-angular calibration, in: *Proceedings of SPIE*. pp. 331–338.
- Franch, B., Vermote, E.F., Sobrino, J.A., Julien, Y., 2014. Retrieval of Surface Albedo on a Daily Basis: Application to MODIS Data. *IEEE Trans. Geosci. Remote Sens.* 52. <https://doi.org/10.1109/TGRS.2014.2313842>
- Fuster, B., Sánchez-Zapero, J., Camacho, F., García-Santos, V., Verger, A., Lacaze, R., Weiss, M., Baret, F., Smets, B., 2020. Quality Assessment of PROBA-V LAI, fAPAR and fCOVER Collection 300 m Products of Copernicus Global Land Service.

- Remote Sens. 12, 1017. <https://doi.org/10.3390/rs12061017>
- GCOS-154, 2011. Systematic observation requirements for satellite-based data products for climate. Supplemental details to the satellite-based component of the “Implementation Plan for the GCOS in Support of the UNFCCC” [WWW Document]. URL https://library.wmo.int/doc_num.php?explnum_id=3710 (accessed 4.10.22).
- GCOS-245, 2022. The 2022 GCOS ECVs Requirements. [WWW Document]. URL https://library.wmo.int/index.php?lvl=notice_display&id=22135#.Y5eLMofMI2wh https://library.wmo.int/doc_num.php?explnum_id=11318 (accessed 12.20.22).
- Geiger, B., Carrer, D., Franchistéguy, L., Roujean, J.L., Meurey, C., 2008. Land surface albedo derived on a daily basis from meteosat second generation observations. *IEEE Trans. Geosci. Remote Sens.* 46, 3841–3856. <https://doi.org/10.1109/TGRS.2008.2001798>
- Gu, Lingxiao, Shuai, Yanmin, Shao, Congying, Xie, Donghui, Zhang, Qingling, Li, Yaoming, Yang, Jian, Gu, L ;, Shuai, Y ;, Shao, C ;, Xie, D ;, Zhang, Q ;, Li, Y ;, Yang, J, 2021. Angle Effect on Typical Optical Remote Sensing Indices in Vegetation Monitoring. *Remote Sens.* 2021, Vol. 13, Page 1699 13, 1699. <https://doi.org/10.3390/RS13091699>
- Gutman, G., Csiszar, I., Romanov, P., 1999. Using NOAA / AVHRR Products to Monitor El Niño Impacts : Focus on Indonesia in 1997 – 98 1189–1205.
- Harper, W. V., 2014. Reduced Major Axis regression: teaching alternatives to Least Squares. *Proc. Ninth Int. Conf. Teach. Stat.* 1–4. <https://doi.org/10.1016/B978-0-12-420228-3.00013-0>
- Henderson-Sellers, A., Wilson, M.F., 1983. Surface albedo data for climatic modeling. *Rev. Geophys.* 21, 1743–1778. <https://doi.org/10.1029/RG021I008P01743>
- Henry, P., Meygret, A., 2000. Calibration of VEGETATION cameras on board SPOT 4. *Proc. Veg. 2000 Conf. Belgirate, Italy, 3–6 April 2000* 1–9.
- Hohn, M.E., 1991. *An Introduction to Applied Geostatistics*: by Edward H. Isaaks and R. Mohan Srivastava, 1989, Oxford University Press, New York, 561 p., ISBN 0-19-

- 505012-6, ISBN 0-19-505013-4. *Comput. Geosci.* [https://doi.org/10.1016/0098-3004\(91\)90055-I](https://doi.org/10.1016/0098-3004(91)90055-I)
- Hu, B., Lucht, W., Li, X., Strahler, A.H., 1997. Validation of kernel-driven semiempirical models for the surface bidirectional reflectance distribution function of land surfaces. *Remote Sens. Environ.* 62, 201–214. [https://doi.org/10.1016/S0034-4257\(97\)00082-5](https://doi.org/10.1016/S0034-4257(97)00082-5)
- Iannone, R.Q., Niro, F., Goryl, P., Dransfeld, S., Hoersch, B., Stelzer, K., Kirches, G., Paperin, M., Brockmann, C., Gomez-Chova, L., Mateo-Garcia, G., Preusker, R., Fischer, J., Amato, U., Serio, C., Gangkofner, U., Berthelot, B., Iordache, M.D., Bertels, L., Wolters, E., Dierckx, W., Benhadj, I., Swinnen, E., 2017. Proba-V cloud detection Round Robin: Validation results and recommendations., in: 2017 9th International Workshop on the Analysis of Multitemporal Remote Sensing Images, MultiTemp 2017. Institute of Electrical and Electronics Engineers Inc. <https://doi.org/10.1109/Multi-Temp.2017.8035219>
- JCGM, 2014. International Vocabulary of Metrology—Basic and General Concepts and Associated Terms, Chemistry International -- Newsmagazine for IUPAC. Walter de Gruyter GmbH. <https://doi.org/10.1515/ci.2008.30.6.21>
- Jin, Y., Schaaf, C.B., Woodcock, C.E., Gao, F., Li, X., Strahler, A.H., Lucht, W., Liang, S., 2003. Consistency of MODIS surface bidirectional reflectance distribution function and albedo retrievals: 1. Validation. *J. Geophys. Res. D Atmos.* 108, 1–15. <https://doi.org/10.1029/2002jd002804>
- Justice, C., Belward, A., Morisette, J., Lewis, P., Privette, J., Baret, F., 2000. Developments in the 'validation' of satellite sensor products for the study of the land surface. *Int. J. Remote Sens.* 21, 3383–3390.
- Justice, C.O., Vermote, E., Townshend, J.R.G., Defries, R., Roy, D.P., Hall, D.K., Salomonson, V. V., Privette, J.L., Riggs, G., Strahler, A., Lucht, W., Myneni, R.B., Knyazikhin, Y., Running, S.W., Nemani, R.R., Wan, Z., Huete, A.R., Van Leeuwen, W., Wolfe, R.E., Giglio, L., Muller, J.P., Lewis, P., Barnsley, M.J., 1998. The moderate resolution imaging spectroradiometer (MODIS): Land remote sensing for global change research. *IEEE Trans. Geosci. Remote Sens.* 36, 1228–1249.

<https://doi.org/10.1109/36.701075>

Lachérade, S., Fournie, B., Henry, P., Gamet, P., Lacherade, S., Fournie, B., Henry, P., Gamet, P., 2013. Cross calibration over desert sites: Description, methodology, and operational implementation. *IEEE Trans. Geosci. Remote Sens.* 51, 1098–1113. <https://doi.org/10.1109/TGRS.2012.2227061>

Lawrence, P.J., Chase, T.N., 2007. Representing a new MODIS consistent land surface in the Community Land Model (CLM 3.0). *J. Geophys. Res. Biogeosciences* 112. <https://doi.org/10.1029/2006JG000168>

Lellouch, G., Carrer, D., Vincent, C., Pardé, M., C. Frietas, S., Trigo, I.F., 2020. Evaluation of Two Global Land Surface Albedo Datasets Distributed by the Copernicus Climate Change Service and the EUMETSAT LSA-SAF. *Remote Sens.* 12, 1888. <https://doi.org/10.3390/rs12111888>

Leon-Tavares, J., 2020. Copernicus Global Land Operations “Vegetation and Energy”. “CGLOPS-1” Framework Service Contract N° 199494 (JRC) Algorithm Theoretical Basis Document BRDF Model retrieval from Sentinel-3 Collection 300 m Version 1. Issue I1.00 [WWW Document]. URL https://land.copernicus.eu/global/sites/cgls.vito.be/files/products/CGLOPS1_ATB_D_BRDFCorrection300m-V1_I1.10.pdf (accessed 5.24.22).

Lequin, R.M., 2004. Guide to the Expression of Uncertainty of Measurement: Point/Counterpoint. *Clin. Chem.* 50, 977–978. <https://doi.org/10.1373/clinchem.2003.030528>

Leroy, M., Deuzé, J.L., Bréon, F.M., Hautecoeur, O., Herman, M., Buriez, J.C., Tanré, D., Bouffies, S., Chazette, P., Roujean, J.L., 1997. Retrieval of atmospheric properties and surface bidirectional reflectances over land from POLDER/ADEOS. *J. Geophys. Res. Atmos.* 102, 17023–17037. <https://doi.org/10.1029/96jd02662>

Lewis, P & Barnsley, M., 1994. Influence of the sky radiance distribution on various formulations of the earth surface albedo. *Proc. Conf. Phys. Meas. Signatures Remote Sens.* 707–715.

Liang, S., 2003. A direct algorithm for estimating land surface broadband albedos from

- MODIS imagery. *IEEE Trans. Geosci. Remote Sens.* 41, 136–145. <https://doi.org/10.1109/TGRS.2002.807751>
- Liang, S., 2001. Narrowband to broadband conversions of land surface albedo I Algorithms. *Remote Sens. Environ.* 76, 213–238. [https://doi.org/10.1016/S0034-4257\(00\)00205-4](https://doi.org/10.1016/S0034-4257(00)00205-4)
- Liang, S., Cheng, J., Jia, K., Jiang, B., Liu, Q., Xiao, Z., Yao, Y., Yuan, W., Zhang, X., Zhao, X., Zhou, J., 2020. The Global LAnd Surface Satellite (GLASS) product suite. *Bull. Am. Meteorol. Soc.* 1–37. <https://doi.org/10.1175/bams-d-18-0341.1>
- Liang, S., Fang, H., Chen, M., Shuey, C.J., Walthall, C., Daughtry, C., Morisette, J., Schaaf, C., Strahler, A., 2002. Validating MODIS land surface reflectance and albedo products: Methods and preliminary results. *Remote Sens. Environ.* [https://doi.org/10.1016/S0034-4257\(02\)00092-5](https://doi.org/10.1016/S0034-4257(02)00092-5)
- Liu, Q., Wang, L., Qu, Y., Liu, N., Liu, S., Tang, H., Liang, S., 2013. Preliminary evaluation of the long-term GLASS albedo product. *Int. J. Digit. Earth* 6, 69–95. <https://doi.org/10.1080/17538947.2013.804601>
- Liu, S., Liu, Qiang, Liu, Qinhua, Wen, J., Li, X., 2010. The Angular and Spectral Kernel Model for BRDF and Albedo Retrieval. *IEEE J. Sel. Top. Appl. Earth Obs. Remote Sens.* 3, 241–256. <https://doi.org/10.1109/JSTARS.2010.2048745>
- Liu, Y., Wang, Z., Sun, Q., Erb, A.M., Li, Z., Schaaf, C.B., Zhang, X., Román, M.O., Scott, R.L., Zhang, Q., Novick, K.A., Sydonia Bret-Harte, M., Petroy, S., SanClements, M., 2017. Evaluation of the VIIRS BRDF, Albedo and NBAR products suite and an assessment of continuity with the long term MODIS record. *Remote Sens. Environ.* 201, 256–274. <https://doi.org/10.1016/j.rse.2017.09.020>
- Loew, A., Bennartz, R., Fell, F., Lattanzio, A., Doutriaux-Boucher, M., Schulz, J., 2016. A database of global reference sites to support validation of satellite surface albedo datasets (SAVS 1.0). *Earth Syst. Sci. Data* 8, 425–438. <https://doi.org/10.5194/essd-8-425-2016>
- Los, S.O., North, P.R.J., Grey, W.M.F., Barnsley, M.J., 2005. A method to convert AVHRR Normalized Difference Vegetation Index time series to a standard

- viewing and illumination geometry. *Remote Sens. Environ.* 99, 400–411. <https://doi.org/10.1016/j.rse.2005.08.017>
- Lucht, W., Roujean, J.L., 2000. Considerations in the parametric modeling of BRDF and albedo from multiangular satellite sensor observations. *Remote Sens. Rev.* 18, 343–379. <https://doi.org/10.1080/02757250009532395>
- Lucht, W., Schaaf, C.B., Strahler, A.H., 2000. An algorithm for the retrieval of albedo from space using semiempirical BRDF models. *IEEE Trans. Geosci. Remote Sens.* 38, 977–998. <https://doi.org/10.1109/36.841980>
- Maignan, F., Bréon, F.M., Lacaze, R., 2004. Bidirectional reflectance of Earth targets: Evaluation of analytical models using a large set of spaceborne measurements with emphasis on the Hot Spot. *Remote Sens. Environ.* 90, 210–220. <https://doi.org/10.1016/j.rse.2003.12.006>
- Matheron, G., 1963. Principles of geostatistics. *Econ. Geol.* 58, 1246–1266. <https://doi.org/10.2113/gsecongeo.58.8.1246>
- Mayr, S., Kuenzer, C., Gessner, U., Klein, I., Rutzinger, M., 2019. Validation of Earth Observation Time-Series: A Review for Large-Area and Temporally Dense Land Surface Products. *Remote Sens.* 11, 2616. <https://doi.org/10.3390/rs11222616>
- Merchant, C.J., 2013. Thermal remote sensing of sea surface temperature. *Remote Sens. Digit. Image Process.* 17, 287–313. https://doi.org/10.1007/978-94-007-6639-6_15/COVER
- Meyer, D.J., 1996. Estimating the effective spatial resolution of an AVHRR time series. *Int. J. Remote Sens.* 17, 2971–2980. <https://doi.org/10.1080/01431169608949122>
- Michalsky, J.J., Harrison, L.C., Berkheiser, W.E., 1995. Cosine response characteristics of some radiometric and photometric sensors. *Sol. Energy* 54, 397–402. [https://doi.org/10.1016/0038-092X\(95\)00017-L](https://doi.org/10.1016/0038-092X(95)00017-L)
- Moran, P., 1984. “The Interpretation of Statistical Maps.” *Journal of the Royal Statistical Society. Series B (Methodological)*, vol. 10, no. 2, 1948, pp. 243–251. JSTOR. [WWW Document]. URL <https://www.jstor.org/stable/2983777> (accessed 12.3.20).
- Muller, J.-P., Lewis, Philip, Fischer, Jurgen, North, P., Framer, U., López, G., Kennedy,

- T., Lewis, Philip, Fischer, Jürgen, Guanter, L., Preusker, R., Heckel, A., Krämer, U., Danne, O., Brockmann, C., Lewis, P., 2011. The ESA GlobAlbedo Project for mapping the Earth's land surface albedo for 15 years from European sensors, Geophysical Research Abstracts.
- Nightingale, J., Mittaz, J.P.D., Douglas, S., Dee, D., Ryder, J., Taylor, M., Old, C., Dieval, C., Fouron, C., Dubeau, G., Merchant, C., 2019. Ten Priority Science Gaps in Assessing Climate Data Record Quality. *Remote Sens.* 11, 986. <https://doi.org/10.3390/rs11080986>
- Nightingale, J., Schaepman-Strub, G., Nickeson, J., Focus Area leads, L., 2011. Assessing Satellite-Derived Land Product Quality for Earth System Science Applications: Overview of the CEOS LPV Sub-Group. Proc. 34th Int. Symp. Remote Sens. Environ. Sydney, NSW, Aust. 10–15 April 2011.
- Ohring, G., Wielicki, B., Spencer, R., Emery, B., Datla, R., 2005. Satellite Instrument Calibration for Measuring Global Climate Change: Report of a Workshop. *Bull. Am. Meteorol. Soc.* 86, 1303–1314. <https://doi.org/10.1175/BAMS-86-9-1303>
- Ollinger, S. V., Richardson, A.D., Martin, M.E., Hollinger, D.Y., Frolking, S.E., Reich, P.B., Plourde, L.C., Katul, G.G., Munger, J.W., Oren, R., Smith, M.L., Paw U, K.T., Bolsta, P. V., Cook, B.D., Day, M.C., Martin, T.A., Monson, R.K., Schmid, H.P., 2008. Canopy nitrogen, carbon assimilation, and albedo in temperate and boreal forests: Functional relations and potential climate feedbacks. *Proc. Natl. Acad. Sci. U. S. A.* 105, 19336–19341. https://doi.org/10.1073/PNAS.0810021105/SUPPL_FILE/0810021105SI.PDF
- Pinty, B., Lattanzio, A., Martonchik, J. V., Verstraete, M.M., Gobron, N., Taberner, M., Widlowski, J.L., Dickinson, R.E., Govaerts, Y., 2005. Coupling diffuse sky radiation and surface albedo. *J. Atmos. Sci.* 62, 2580–2591. <https://doi.org/10.1175/JAS3479.1>
- Pinty, B., Roveda, F., Verstraete, M.M., Gobron, N., Govaerts, Y., Martonchik, J. V., Diner, D.J., Kahn, R.A., 2000a. Surface albedo retrieval from Meteosat 1. Theory. *J. Geophys. Res. Atmos.* 105, 18099–18112. <https://doi.org/10.1029/2000JD900113>

- Pinty, B., Roveda, F., Verstraete, M.M., Gobron, N., Govaerts, Y., Martonchik, J. V., Diner, D.J., Kahn, R.A., 2000b. Surface albedo retrieval from Meteosat: 2. Applications. *J. Geophys. Res. Atmos.* 105, 18113–18134. <https://doi.org/10.1029/2000JD900114>
- Pirazzini, R., 2004. Surface albedo measurements over Antarctic sites in summer. *J. Geophys. Res.* 109, D20118. <https://doi.org/10.1029/2004JD004617>
- Pirazzini, R., Vihma, T., Granskog, M.A., Cheng, B., 2006. Surface albedo measurements over sea ice in the Baltic Sea during the spring snowmelt period. *Ann. Glaciol.* 44, 7–14. <https://doi.org/10.3189/172756406781811565>
- Qu, Y., Liu, Q., Liang, S., Wang, L., Liu, N., Liu, S., 2014. Direct-estimation algorithm for mapping daily land-surface broadband albedo from modis data. *IEEE Trans. Geosci. Remote Sens.* 52, 907–919. <https://doi.org/10.1109/TGRS.2013.2245670>
- Rahman, H., Dedieu, G., 1994. SMAC: a simplified method for the atmospheric correction of satellite measurements in the solar spectrum. *Int. J. Remote Sens.* 15, 123–143. <https://doi.org/10.1080/01431169408954055>
- Reda, I., 2011. Method to calculate uncertainties in measuring shortwave solar irradiance using thermopile and semiconductor solar radiometers, Tech. Rep. NREL/TP-3B10-52194, 20 pp., Natl. Renewable Energy Lab., Golden, Colo., doi:10.2172/1021250, 2011. [WWW Document]. <https://doi.org/10.2172/1021250>
- Román, M.O., Schaaf, C.B., Lewis, P., Gao, F., Anderson, G.P., Privette, J.L., Strahler, A.H., Woodcock, C.E., Barnsley, M., 2010. Assessing the coupling between surface albedo derived from MODIS and the fraction of diffuse skylight over spatially-characterized landscapes. *Remote Sens. Environ.* 114, 738–760. <https://doi.org/10.1016/j.rse.2009.11.014>
- Román, M.O., Schaaf, C.B., Woodcock, C.E., Strahler, A.H., Yang, X., Braswell, R.H., Curtis, P.S., Davis, K.J., Dragoni, D., Goulden, M.L., Gu, L., Hollinger, D.Y., Kolb, T.E., Meyers, T.P., Munger, J.W., Privette, J.L., Richardson, A.D., Wilson, T.B., Wofsy, S.C., 2009. The MODIS (Collection V005) BRDF/albedo product: Assessment of spatial representativeness over forested landscapes. *Remote Sens.*

- Environ. 113, 2476–2498. <https://doi.org/10.1016/j.rse.2009.07.009>
- Roujean, J.-L., Leroy, M., Deschamps, P.-Y., 1992. A bidirectional reflectance model of the Earth's surface for the correction of remote sensing data. *J. Geophys. Res.* 97, 20455. <https://doi.org/10.1029/92JD01411>
- Roujean, J.L., Leon-Tavares, J., Smets, B., Claes, P., Camacho De Coca, F., Sanchez-Zapero, J., 2018. Surface albedo and toc-r 300 m products from PROBA-V instrument in the framework of Copernicus Global Land Service. *Remote Sens. Environ.* 215, 57–73. <https://doi.org/10.1016/j.rse.2018.05.015>
- Roy, D.P., Zhang, H.K., Ju, J., Gomez-Dans, J.L., Lewis, P.E., Schaaf, C.B., Sun, Q., Li, J., Huang, H., Kovalskyy, V., 2016. A general method to normalize Landsat reflectance data to nadir BRDF adjusted reflectance. *Remote Sens. Environ.* 176, 255–271. <https://doi.org/10.1016/j.rse.2016.01.023>
- S3_MPC, 2021. Sentinel-3 Optical Annual Performance Report - 2020 - Sentinel Online [WWW Document]. URL https://sentinels.copernicus.eu/web/sentinel/user-guides/sentinel-3-olci/document-library/-/asset_publisher/hkf7sg9Ny1d5/content/sentinel-3-optical-annual-performance-report-2020 (accessed 5.2.22).
- Samain, O., Geiger, B., Roujean, J.L., 2006. Spectral normalization and fusion of optical sensors for the retrieval of BRDF and albedo: Application to VEGETATION, MODIS, and MERIS data sets. *IEEE Trans. Geosci. Remote Sens.* 44, 3166–3178. <https://doi.org/10.1109/TGRS.2006.879545>
- Sanchez-Zapero, J., 2018. Product Quality Assessment Report (PQAR) of CDR SPOT/VGT-based Surface Albedo v1.0 (Official reference number service contract: 2018/C3S_312b_Lot5_VITO/SC1). [WWW Document]. URL <https://cds.climate.copernicus.eu/cdsapp#!/dataset/satellite-albedo?tab=doc> (accessed 4.9.20).
- Sanchez-Zapero, J., Camacho, F., Leon-Tavares, J., Martinez-Sanchez, E., Gorrondo, J., Benhadj, I., Tote, C., Swinnen, E., Munoz-Sabater, J., 2021. Prototype for Surface Albedo Retrieval Based on Sentinel-3 OLCI and SLSTR Data in the Framework of

- Copernicus Climate Change. 2021 IEEE Int. Geosci. Remote Sens. Symp. IGARSS 2377–2380. <https://doi.org/10.1109/IGARSS47720.2021.9555099>
- Sánchez-Zapero, J., Camacho, F., Martínez-Sánchez, E., Gorroño, J., León-Tavares, J., Benhadj, I., Toté, C., Swinnen, E., Muñoz-Sabater, J., 2023a. Global estimates of surface albedo from Sentinel-3 OLCI and SLSTR data for Copernicus Climate Change Service: Algorithm and preliminary validation. *Remote Sens. Environ.* 287, 113460. <https://doi.org/10.1016/j.rse.2023.113460>
- Sánchez-Zapero, J., Camacho, F., Martínez-Sánchez, E., Lacaze, R., Carrer, D., Pinault, F., Benhadj, I., Muñoz-Sabater, J., 2020. Quality Assessment of PROBA-V Surface Albedo V1 for the Continuity of the Copernicus Climate Change Service. *Remote Sens.* 2020, Vol. 12, Page 2596 12, 2596. <https://doi.org/10.3390/rs12162596>
- Sánchez-Zapero, J., Martínez-Sánchez, E., Camacho, F., Wang, Z., Carrer, D., Schaaf, C., García-Haro, F.J., Nickeson, J., Cosh, M., 2023b. Surface ALbedo VALidation (SALVAL) Platform: Towards CEOS LPV Validation Stage — Application to Three Global Albedo Climate Data Records. *Remote Sens.* 2023, Vol. 15, Page 1081 15, 1081. <https://doi.org/10.3390/RS15041081>
- Sánchez, J., Camacho, F., Lacaze, R., Smets, B., 2015. Early validation of PROBA-V GEOV1 LAI, FAPAR and FCOVER products for the continuity of the copernicus global land service. *Int. Arch. Photogramm. Remote Sens. Spat. Inf. Sci. - ISPRS Arch.* 40, 93–100. <https://doi.org/10.5194/isprsarchives-XL-7-W3-93-2015>
- Schaaf, C.B., Gao, F., Strahler, A.H., Lucht, W., Li, X., Tsang, T., Strugnell, N.C., Zhang, X., Jin, Y., Muller, J.P., Lewis, P., Barnsley, M., Hobson, P., Disney, M., Roberts, G., Dunderdale, M., Doll, C., D'Entremont, R.P., Hu, B., Liang, S., Privette, J.L., Roy, D., 2002. First operational BRDF, albedo nadir reflectance products from MODIS. *Remote Sens. Environ.* 83, 135–148. [https://doi.org/10.1016/S0034-4257\(02\)00091-3](https://doi.org/10.1016/S0034-4257(02)00091-3)
- Schaepman-Strub, G., Schaepman, M.E., Painter, T.H., Dangel, S., Martonchik, J. V., 2006. Reflectance quantities in optical remote sensing—definitions and case studies. *Remote Sens. Environ.* 103, 27–42. <https://doi.org/10.1016/j.rse.2006.03.002>
- Stephens, G.L., O'Brien, D., Webster, P.J., Pilewski, P., Kato, S., Li, J.L., 2015. The

- albedo of Earth. *Rev. Geophys.* 53, 141–163. <https://doi.org/10.1002/2014RG000449>
- Sterckx, S., Livens, S., Adriaensen, S., 2013. Rayleigh, deep convective clouds, and cross-sensor desert vicarious calibration validation for the PROBA-V mission. *IEEE Trans. Geosci. Remote Sens.* 51, 1437–1452. <https://doi.org/10.1109/TGRS.2012.2236682>
- Strahler, A.H., 1997. Vegetation Canopy Reflectance Modeling-Recent Developments and Remote Sensing Perspectives. *Remote Sens. Rev.* 15, 179–194. <https://doi.org/10.1080/02757259709532337>
- Strahler, A.H., Muller, J.-P., Members, M.S.T., 1999. MODIS BRDF/Albedo Product: Algorithm Theoretical Basis Document Version 5.0.
- Taberner, M., Pinty, B., Govaerts, Y., Liang, S., Verstraete, M.M., Gobron, N., Widlowski, J.L., 2010. Comparison of MISR and MODIS land surface albedos: Methodology. *J. Geophys. Res. Atmos.* 115, 1–13. <https://doi.org/10.1029/2009JD012665>
- Toté, C., Swinnen, E., Sterckx, S., Clarijs, D., Quang, C., Maes, R., 2017. Evaluation of the SPOT/VEGETATION Collection 3 reprocessed dataset: Surface reflectances and NDVI. *Remote Sens. Environ.* 201, 219–233. <https://doi.org/10.1016/j.rse.2017.09.010>
- Trigo, I.F., Dacamara, C.C., Viterbo, P., Roujean, J.-L., Olesen, F., Barroso, C., Camachode-Coca, F., Carrer, D., Freitas, S.C., García-Haro, J., Geiger, B., Gellens-Meulenberghs, F., Ghilain, N., Meliá, J., Pessanha, L., Siljamo, N., Arboleda, A., 2011. The Satellite Application Facility for Land Surface Analysis. *Int. J. Remote Sens.* 32, 2725–2744. <https://doi.org/10.1080/01431161003743199>
- Trishchenko, A.P., Cihlar, J., Li, Z., 2002. Effects of spectral response function on surface reflectance and NDVI measured with moderate resolution satellite sensors. *Remote Sens. Environ.* 81, 1–18. [https://doi.org/10.1016/S0034-4257\(01\)00328-5](https://doi.org/10.1016/S0034-4257(01)00328-5)
- Vermote, E., Justice, C.O., Bréon, F.M., 2009. Towards a generalized approach for correction of the BRDF effect in MODIS directional reflectances. *IEEE Trans.*

- Geosci. Remote Sens. 47, 898–908. <https://doi.org/10.1109/TGRS.2008.2005977>
- Vermote, E.F., Saleous, E., Z, N., Justice, C.O., 2002. Atmospheric correction of MODIS data in the visible to middle infrared: first results. *Remote Sensing of Environment* 83, 97–111.
- Vijeta, Kapri, R.K., Saha, S., Jaiswal, V.K., Sharma, P., 2021. Theoretical Simulation for Evaluating Error in Irradiance Measurement Using Optical Detectors Having Different Cosine Responses. *Mapan - J. Metrol. Soc. India* 36, 473–480. <https://doi.org/10.1007/S12647-021-00486-6/FIGURES/12>
- Wang, Z., Schaaf, C., Lattanzio, A., Carrer, D., Grant, I., Roman, M., Camacho, F., Yang, Y., Sánchez-Zapero, J., 2019. Global Surface Albedo Product Validation Best Practices Protocol. Version 1.0. In Z. Wang, J. Nickeson & M. Román (Eds.), *Good Practices for Satellite-Derived Land Product Validation* (p. 45): Land Product Validation Subgroup (WGCV/CEOS). [WWW Document]. <https://doi.org/doi:10.5067/DOC/CEOSWGCV/LPV/ALBEDO.001>
- Wang, Z., Schaaf, C.B., Chopping, M.J., Strahler, A.H., Wang, J., Román, M.O., Rocha, A. V., Woodcock, C.E., Shuai, Y., 2012. Evaluation of Moderate-resolution Imaging Spectroradiometer (MODIS) snow albedo product (MCD43A) over tundra. *Remote Sens. Environ.* 117, 264–280. <https://doi.org/10.1016/j.rse.2011.10.002>
- Wang, Z., Schaaf, C.B., Strahler, A.H., Chopping, M.J., Román, M.O., Shuai, Y., Woodcock, C.E., Hollinger, D.Y., Fitzjarrald, D.R., 2014. Evaluation of MODIS albedo product (MCD43A) over grassland, agriculture and forest surface types during dormant and snow-covered periods. *Remote Sens. Environ.* 140, 60–77. <https://doi.org/10.1016/j.rse.2013.08.025>
- Wang, Z., Schaaf, C.B., Sun, Q., Kim, J.H., Erb, A.M., Gao, F., Román, M.O., Yang, Y., Petroy, S., Taylor, J.R., Masek, J.G., Morisette, J.T., Zhang, X., Papuga, S.A., 2017. Monitoring land surface albedo and vegetation dynamics using high spatial and temporal resolution synthetic time series from Landsat and the MODIS BRDF/NBAR/albedo product. *Int. J. Appl. Earth Obs. Geoinf.* 59, 104–117. <https://doi.org/10.1016/j.jag.2017.03.008>

- Wanner, W., Li, X., Strahler, A.H., 1995. On the derivation of kernels for kernel-driven models of bidirectional reflectance. *J. Geophys. Res.* 100, 21077–21089. <https://doi.org/10.1029/95jd02371>
- Wanner, W., Strahler, A.H., Hu, B., Lewis, P., Li, X., Barker, C.L., 1997. Global retrieval of bidirectional reflectance and albedo over land from EOS MODIS and MISR data: Theory and algorithm. *J. Geophys. Res.* 102, 143–161.
- Weiss, M., Baret, F., Block, T., Koetz, B., Burini, A., Scholze, B., Lecharpentier, P., Brockmann, C., Fernandes, R., Plummer, S., Myneni, R., Gobron, N., Nightingale, J., Schaepman-Strub, G., Camacho, F., Sanchez-Azofeifa, A., 2014. On line validation exercise (OLIVE): A web based service for the validation of medium resolution land products. application to FAPAR products. *Remote Sens.* 6, 4190–4216. <https://doi.org/10.3390/rs6054190>
- Weiss, M., Baret, F., Garrigues, S., Lacaze, R., 2007. LAI and fAPAR CYCLOPES global products derived from VEGETATION. Part 2: validation and comparison with MODIS collection 4 products. *Remote Sens. Environ.* 110, 317–331. <https://doi.org/10.1016/j.rse.2007.03.001>
- Wolters, E., Dierckx, W., Iordache, M.-D., Swinnen, E., 2018. PROBA-V Products User Manual v3.0. VITO.
- Wolters, E., Swinnen, E., Toté, C., Sterckx, S., 2016. SPOT-VGT Collection 3 Products User Manual. VITO.
- Woodcock, C.E., Strahler, A.H., Jupp, D.L.B., 1988. The use of variograms in remote sensing: I. Scene models and simulated images. *Remote Sens. Environ.* 25, 323–348. [https://doi.org/10.1016/0034-4257\(88\)90108-3](https://doi.org/10.1016/0034-4257(88)90108-3)
- Xiong, X., Barnes, W., 2006. An overview of MODIS radiometric calibration and characterization. *Adv. Atmos. Sci.* 23, 69–79. <https://doi.org/10.1007/s00376-006-0008-3>
- Zeng, Y., Su, Z., Calvet, J.C., Manninen, T., Swinnen, E., Schulz, J., Roebeling, R., Poli, P., Tan, D., Riihelä, A., Tanis, C.M., Arslan, A.N., Obregon, A., Kaiser-Weiss, A., John, V.O., Timmermans, W., Timmermans, J., Kaspar, F., Gregow, H., Barbu,

A.L., Fairbairn, D., Gelati, E., Meurey, C., 2015. Analysis of current validation practices in Europe for space-based climate data records of essential climate variables. *Int. J. Appl. Earth Obs. Geoinf.* 42, 150–161. <https://doi.org/10.1016/j.jag.2015.06.006>

Zhao, X., Liang, S., Liu, S., Yuan, W., Xiao, Z., Liu, Q., Cheng, J., Zhang, Xiaotong, Tang, H., Zhang, Xin, Liu, Q., Zhou, G., Xu, S., Yu, K., 2013. The global land surface satellite (GLASS) remote sensing data processing system and products. *Remote Sens.* 5, 2436–2450. <https://doi.org/10.3390/rs5052436>

Anexo I – Listado informes disponible *online* publicados en proyectos

Copernicus Global Land Service (fecha acceso: 03.05.2023)

- Documentos de validación de albedo:
 - Camacho, F., Sánchez, J. **QUALITY ASSESSMENT REPORT Surface Albedo – Version 1 SPOT/VGT**. Issue 1.10 (date 08.01.2015). Gio Global Land Component - Lot I "Operation of the Global Land Component" Framework Service Contract N° 388533 (JRC). Available online at https://land.copernicus.eu/global/sites/cgls.vito.be/files/products/GIOGL1_VR_SAV1_I1.10.pdf
 - Sánchez-Zapero, J. **SCIENTIFIC QUALITY EVALUATION PROBA-V Surface Albedo Collection 1 km Version 1 (2017 year)**. Issue I1.00 (date 05.06.2018). Copernicus Global Land Operations "Vegetation and Energy" "CGLOPS-1" Framework Service Contract N° 199494 (JRC). Available online at https://land.copernicus.eu/global/sites/cgls.vito.be/files/products/CGLOPS1_SOE2017_SA1km-V1_I1.00.pdf
 - Smets, B., Sánchez-Zapero, J. **PRODUCT USER MANUAL Surface Albedo collection 1 km Version 1**. Issue I1.40 (date 28.06.2018). Copernicus Global Land Operations "Vegetation and Energy" "CGLOPS-1" Framework Service Contract N° 199494 (JRC). Available online at https://land.copernicus.eu/global/sites/cgls.vito.be/files/products/CGLOPS1_PUM_SA1km-V1_I1.40.pdf
 - Sánchez-Zapero, J., de la Madrid, L., Camacho, F. **VALIDATION REPORT Surface Albedo (SA) from PROBA-V Collection 1 km Version 1.5**. Issue I2.21 (date 20.07.2018). Copernicus Global Land Operations "Vegetation and Energy" "CGLOPS-1" Framework Service Contract N° 199494 (JRC). Available online at https://land.copernicus.eu/global/sites/cgls.vito.be/files/products/CGLOPS1_SOE2018_SA1km-V1_I1.00.pdf
 - Sánchez-Zapero, J. **SCIENTIFIC QUALITY EVALUATION PROBA-V Surface Albedo Collection 1 km Version 1 (2018 year)**. Issue I1.00 (date 07.08.2019). Copernicus Global Land Operations "Vegetation and Energy" "CGLOPS-1"

Framework Service Contract N° 199494 (JRC). Available online at https://land.copernicus.eu/global/sites/cgls.vito.be/files/products/CGLOPS1_SOE2018_SA1km-V1_I1.00.pdf

- Documentos de validación de reflectividad de la superficie (TOC reflectance):
 - Sánchez-Zapero, J. **SCIENTIFIC QUALITY EVALUATION PROBA-V TOC-R Collection 1 km Version 1.** Issue I1.00 (date 30.04.2018). Copernicus Global Land Operations “Vegetation and Energy” “ CGLOPS-1” Framework Service Contract N° 199494 (JRC). Available online at https://land.copernicus.eu/global/sites/cgls.vito.be/files/products/CGLOPS1_SOE2017_TOCR1km-V1_I1.00.pdf
 - Smets, B., Ceamanos, J., Sánchez-Zapero, J. **PRODUCT USER MANUAL Top Of Canopy Reflectances (TOC-R) Collection 1 km Version 1.5.** Issue I2.20 (date 26.06.2018). Copernicus Global Land Operations “Vegetation and Energy” “ CGLOPS-1” Framework Service Contract N° 199494 (JRC). Available online at https://land.copernicus.eu/global/sites/cgls.vito.be/files/products/CGLOPS1_PUM_TOCR1km-V1.5_I2.20.pdf
 - Sánchez-Zapero, J., de la Madrid, L., Camacho, F. **QUALITY ASSESSMENT REPORT Normalized Top-Of-Canopy Reflectance (TOC-R) from PROBA-V Collection 1 km Version 1.5.** Issue I2.21 (date 20.07.2018). Available online at https://land.copernicus.eu/global/sites/cgls.vito.be/files/products/CGLOPS1_QAR_TOCR1km-PROBAV-V1.5_I2.21.pdf
 - Sánchez-Zapero, J., Martínez-Sánchez, E., Camacho, F. **QUALITY ASSESSMENT REPORT Sentinel-3 Top Of Canopy (TOC) Reflectance Collection 300 m Version 1.** Issue I1.30 (date 28.07.2022). Available online at https://land.copernicus.eu/global/sites/cgls.vito.be/files/products/CGLOPS1_QAR_S3-TOCr300m-v1_I1.30_Core.pdf

Copernicus Climate Change Service (fecha acceso: 03.05.2023)

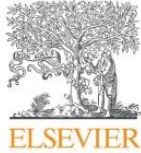
- Documentos de albedo AVHRR V1:
 - Sánchez-Zapero, J., León-Tavares, J., Toté, C. **Product Quality Assurance Document CDR AVHRR-based Surface Albedo v1.0.** Issue v1.1 (date

- 12.09.2019). Official reference number service contract: 2018/C3S_312b_Lot5_VITO/SC1. Available online at https://datastore.copernicus-climate.eu/documents/satellite-albedo/D2.2.1-v1.0_POAD_CDR_SA_AVHRR_v1.0_PRODUCTS_v1.1.pdf
- Sánchez-Zapero, J., Camacho, F., León-Tavares, J. **Product Quality Assessment Report CDR AVHRR-based Surface Albedo v1.0**. Issue v1.0.1 (date 19.11.2019). Official reference number service contract: 2018/C3S_312b_Lot5_VITO/SC1. Available online at https://datastore.copernicus-climate.eu/documents/satellite-albedo/D2.3.1-v1.0_POAR_CDR_SA_AVHRR_v1.0_PRODUCTS_v1.0.1.pdf
 - Documentos de albedo SPOT/VGT V1:
 - Sánchez-Zapero, J. **Product Quality Assessment Report CDR VGT-based Surface Albedo v1.0**. Issue v1.0 (date 10.12.2018). Official reference number service contract: 2018/C3S_312b_Lot5_VITO/SC1. Available online at https://datastore.copernicus-climate.eu/documents/satellite-albedo/D2.3.2-v1.0_POAR_CDR_SA_SPOT-VGT_v1.0_PRODUCTS_v1.0.pdf
 - Sánchez-Zapero, J., Camacho, F., León-Tavares, J., Toté, C. **Product Quality Assurance Document CDR VGT-based Surface Albedo v1.0**. Issue v1.1 (date 03.12.2019). Official reference number service contract: 2018/C3S_312b_Lot5_VITO/SC1. Available online at https://datastore.copernicus-climate.eu/documents/satellite-albedo/D2.2.2-v1.1_POAD_CDR_SA_SPOT-VGT_v1.0_PRODUCTS_v1.1.pdf
 - Documentos de albedo PROBA-V V1:
 - Sánchez-Zapero, J., Camacho, F. **Product Quality Assessment Report Surface Albedo v1.0 based on PROBA-V**. Issue v1.1 (date 19.12.2019). Official reference number service contract: 2018/C3S_312b_Lot5_VITO/SC1. Available online at https://datastore.copernicus-climate.eu/documents/satellite-albedo/D2.3.3-v1.0_POAR_CDR-ICDR_SA_PROBAV_v1.0_PRODUCTS_v1.1.pdf
 - Sánchez-Zapero, J., León-Tavares, J., Toté, C. **Product Quality Assurance Document Surface Albedo V1 based on PROBA-V**. Issue v1.2 (date 19.12.2019). Official reference number service contract: 2018/C3S_312b_Lot5_VITO/SC1. Available online at https://datastore.copernicus-climate.eu/documents/satellite-albedo/D2.2.3-v1.1_POAD_CDR-ICDR_SA_PROBAV_v1.0_PRODUCTS_v1.2.pdf

- Documentos de albedo multi-sensor V2:
 - Sánchez-Zapero, J., Camacho, F. **Product Quality Assurance Document Multi-sensor CDR surface albedo v2.0**. Issue v1.1 (date 03.12.2020). Official reference number service contract: 2018/C3S_312b_Lot5_VITO/SC1. Available online at https://datastore.copernicus-climate.eu/documents/satellite-albedo/D2.2.4-v2.0_POAD_CDR_SA_MULTI_SENSOR_v2.0_PRODUCTS_v1.1.pdf
 - Sánchez-Zapero, J., Martínez-Sánchez, E., Camacho, F., León-Tavares, J. **Product Quality Assessment Report Multi-sensor Surface Albedo v2.0**. Issue v1.1 (date 21.06.2021). Official reference number service contract: 2018/C3S_312b_Lot5_VITO/SC1. Available online at https://datastore.copernicus-climate.eu/documents/satellite-albedo/D2.3.4-v2.0_POAR_CDR_SA_MULTI_SENSOR_v2.0_PRODUCTS_v1.1.pdf
- Documentos de albedo Sentinel-3 V3:
 - Sánchez-Zapero, J., Gorroño, J., Martínez-Sánchez, E., Camacho, F., León-Tavares, J., Benhadj, I., Toté, C. **Algorithm Theoretical Basis Document CDR/ICDR Sentinel-3 Surface Albedo v3.0**. Issue v1.1 (date 22.06.2021). Official reference number service contract: 2020/ COP_059_VITO_Albedo. Available online at https://datastore.copernicus-climate.eu/documents/satellite-albedo/C3S COP 059 D-02 ATBD_CDR-ICDR_SA_SENTINEL3_v3.0_PRODUCTS_v1.1.pdf
 - Sánchez-Zapero, J., Martínez-Sánchez, E., Toté, C. **Preliminary Product Quality Assessment Report CDR/ICDR Sentinel-3 Surface Albedo v3.0**. Issue v1.1 (date 23.06.2021). Official reference number service contract: 2020/COP_059_VITO_Albedo. Available online at https://datastore.copernicus-climate.eu/documents/satellite-albedo/C3S COP 059 D-03_POAR_CDR-ICDR_SA_SENTINEL3_v3.0_PRODUCTS_v1.1.pdf

Anexo II – Copia de publicación 1

Remote Sensing of Environment 215 (2018) 57–73



Contents lists available at [ScienceDirect](#)

Remote Sensing of Environment

journal homepage: www.elsevier.com/locate/rse



Surface albedo and toc-r 300 m products from PROBA-V instrument in the framework of Copernicus Global Land Service



Jean-Louis Roujean^{a,*}, Jonathan Leon-Tavares^b, Bruno Smets^b, Patrick Claes^b,
Fernando Camacho De Coca^c, Jorge Sanchez-Zapero^c

^a UMR3589-CNRM, CNRS/METEO-FRANCE, 42 avenue Coriolis, 31057 Toulouse, France

^b VITO, Boeretang 200, 2400 Mol, Belgium

^c EOLAB, Valencia, Spain

ARTICLE INFO

Keywords:
Albedo
Vegetation
Satellite
Time series

ABSTRACT

PROBA-V instrument launched in 2013 is offering a global daily coverage at pixel resolutions of 333 m and 1 km in three spectral bands (BLUE, RED, NIR) and 600 m for shortwave infrared (SWIR). The PROBA-V mission is the follow-on of the VEGETATION program started in 2000, which allowed generating long-term series at 1 km pixel resolution. The PROBA-V products belong to the Copernicus Global Land Service portfolio (<http://land.copernicus.eu/global/>). The sensor design of PROBA-V with oriented cameras offers a wide field of view (FOV) for sampling the BRDF (Bidirectional Reflectance Distribution Function). This paper details the methodology implemented at the premises of VITO (Flemish Institute for Technological Research) with the aim to disseminate routinely from PROBA-V daily observations for both surface albedo (SA) and top-of-canopy corrected reflectance (TOC-R) products. The method classically operates a selection of cloudless scenes, performs atmospheric corrections, and finally applies a correction of directional effects on a pixel per pixel basis. The synthesis period is the decade and the composite period is 20 days. Such choice is a pointwise sampling as being a trade-off between the availability of clear scenes and the timescale for phenology. Regarding the albedo catalogue, a narrow-band to broadband conversion is stipulated. A recurrent technique serves for gap-filling based on the spread of weighed a priori data. Additional information concerns the quality flag and the age of the product. Preliminary accuracy assessment is performed through a comparison with the Moderate Imaging Spectroradiometer (MODIS) Collection 6. Dependable spatial consistency is reached except for wintertime with deviations in terms of rmse (root mean square errors) about 0.03 for visible and shortwave domains, and 0.04 for near infrared. Besides, both PROBA-V and MODIS C6 exhibit close time profiles, marked by smoothness or rapid transitions. Results over 10 confidence sites reveals rmse values of 0.032 and bias of 0.01 over the 2014 full annual cycle.

1. Introduction

Land surface albedo is the cornerstone for characterizing the energy balance in the coupled surface-atmosphere system and also constitutes an indispensable input quantity for soil-vegetation-atmosphere transfer models. It yields an Essential Climate Variable (ECV) as established by the Global Climate Observing System (GCOS) (GCOS, 2016) with given guidelines for its long-term validation (<http://www.qa4ecv.eu/ecv/albedo>). Knowing the surface albedo, the net radiation at the surface can be estimated and besides the whole energy budget. Heretofore, three spectral broadband ranges, namely the solar spectrum (400–3000 nm), the visible (400–700 nm) and the near- and shortwave-infrared (700–3000 nm), were deemed the relevant quantities. Actually,

any change in the short-wave (solar) albedo can be tenuous because of the counter-balancing between broadband visible and near infrared surface albedo. This fully justifies the dissemination of the three broadband albedo products although one could be derived from the two others. Noteworthy, the spectral range for visible broadband is matching with PAR (Photosynthetically Active Radiation) range to depict the carbon budget. As vegetation absorbs most of the PAR radiation, therefore PAR albedo is particularly sensitive to greenness. On the other hand, near-infrared albedo is high for leafy vegetation and low for woody material comparatively to visible albedo.

Actually, there exists variant definition of albedo products according to the domain of directional integration (Schaepman-Strub et al., 2006). It notably places a regard to the fraction of direct versus

* Corresponding author at: UMR-5126, CESBIO, 18 avenue E. Belin, bpi 2801, 31401 Toulouse, France.
E-mail address: jean-louis.roujean@cesbio.cnes.fr (J.-L. Roujean).

<https://doi.org/10.1016/j.rse.2018.05.015>

Received 22 December 2017; Received in revised form 4 May 2018; Accepted 8 May 2018
Available online 06 June 2018

0034-4257/ © 2018 The Authors. Published by Elsevier Inc. This is an open access article under the CC BY-NC-ND license (<http://creativecommons.org/licenses/by-nc-nd/4.0/>).

diffuse solar radiation. The salient albedo products are the Directional-Hemispherical Reflectance (DHR) – also called Black Sky Albedo (BSA) - and the Bi-Hemispherical Reflectance (BHR) - also called White Sky Albedo (WSA). Their combination relative to the ratio of sky irradiance leads to the so-called Blue Sky Albedo. Actually, the Blue-Sky Albedo is the true albedo to be measured in situ.

The resolution of 333 m offered by PROBA-V sensor will prompt new applications in domains encompassing agriculture, forestry, land use, land cover, hydrology and weather forecasts areas. The point-wise spatial-temporal resolutions of PROBA-V is also prone to leverage geo-engineering activities in order to dampen the effects of a changing climate. The Copernicus Global Land Service (CGLS) operates “a multi-purpose service component” that offers a series of bio-geophysical products on the status and evolution of land surface at global scale (<http://land.copernicus.eu/global>). Timely production and delivery of set of parameters exacerbate the constitution of long term series of satellite-based products elaborated in a coherent manner. The primary objective of CGLS is to continuously monitor the status of land territories and to supply reliable geo-information to decision makers, businesses and citizens to define environmental policies and take right actions. ImagineS (Implementing Multi-scale Agricultural Indicators Exploiting Sentinels) project from FP7 (Framework Program Seventh) was at the root of the development of cutting-edge retrieval methods of key biophysical variables, amongst which the land surface albedo. The algorithm to measure the land surface albedo from PROBA-V is a trimmed methodology previously implemented in operational for Meteosat Second Generation (MSG) (e.g. Geiger et al., 2008). The insurance of the continuity with past product from SPOT/VEGETATION at 1 km is enacted by the follow-on dissemination of 1 km PROBA-V product, owing to CGLS. The algorithm has been fine-tuned with time for the purpose of an enhanced efficient computation and service requirements.

The paper first reviews the background theory about the kernel-driven BRDF (Bidirectional Reflectance Distribution Function) approach. The BRDF model parameters serve to estimate both spectral albedos and TOC-R. A narrow- to broadband conversion is then performed. If most satellite projects adopted the kernel-based approach, a variant was operated for MISR (Multi-angle Imaging Spectro-Radiometer), further assessed in terms of noise (Lucht and Lewis, 2000), then of added-value for MODIS (Jin et al., 2002) and also in virtue of its potential to map snow albedo (Stroeve and Nolin, 2002). Whilst a surface albedo product is useful for surface energy balance and radiation forcing at surface level, TOC reflectance normalized to geometry of reference is more inclined to serve for the monitoring of the surface resources and the derivation of vegetation indices. Section 2 presents the instrument, the calibration accuracy, the levels of data processing and quality. Section 3 tells about the methodology implemented. Section 4 details the tools and criteria for products evaluation. Section 5 provides a preliminary assessment of the products quality. Section 6 concludes the study and stresses future prospects.

2. Characteristics of PROBA-V instrument

2.1. Principle of measurement

PROBA-V payload named VGT was launched in 2013 for 7 years and is fully comparable to the previously VEGETATION sensor embarked on SPOT (Satellite Probatoire d’Observation de la Terre). It is a multi-spectral push-broom spectrometer. The payload consists of three identical cameras, equipped with a very compact Three Mirror Anastigmat (TMA) telescope. Each TMA has a FOV of 34° with four spectral bands. The limit of view zenith angle is 75° (e.g. http://proba-v.vgt.vito.be/sites/proba-v.vgt.vito.be/files/Product_User_Manual.pdf). Three spectral bands belong to the visible range (460 nm for Blue, 658 nm for Red and 834 nm for NIR) plus a SWIR band (1610 nm). VGT is restricted to imaging land and dedicated calibration zones. Each camera owes its own land sea mask that allows removing the sea pixels. About 14 near

polar orbits per day are registered. PROBA-V flies at 820 km altitude. The swath width of 2250 km ensures a daily coverage of land masses above 35° latitude with however a limitation to 75° North and 56° South. About 90% daily coverage is obtained in the equatorial zones. The Ground Sampling Distance is 100 m (VNIR) and 200 m (SWIR) at nadir and 360 m (VNIR) and 690 m (SWIR) at the edge of the swath.

2.2. Data preprocessing and performances

The images are projected in the grid plate carrée for Level 1-b and the geodetic datum is WGS84. The pixel co-ordinates are given for the center of the pixel. For details on the radiometric performances of PROBA-V, we will refer the reader to the dedicated link (<https://earth.esa.int/web/sppa/mission-performance/esa-3rd-party-missions/proba-v/products-and-algorithms/products-information>). To be outlined here that the PROBA-V S1 Top of Canopy (TOC) reflectance values are synthesis of the pixels from the three cameras having harmonized spectral responses functions. Daily PROBA-V composites (S1) of TOC reflectance, at a spatial resolution of 333 m, are the primary sensor data serving as input for both TOC-R and surface albedo algorithms. Note that official references to PROBA-V products indicate 300 m although the true resolution is 333 m. In case of multiple observations per day, the maximum of Normalized Difference Vegetation Index (NDVI) enacts a criterion of selection. The current PROBA-V cloud detection method (implemented in collection 1, C1) identifies the presence of clouds based on land cover class, climatology background surface reflectance per pixel and a set of decision rules (Sterckx et al. (2014), Dierckx et al., 2014, Wolters et al., 2017). The cloud mask is majorly inherited from VEGETATION. The Digital Elevation Model is from GTOPO30 (U.S. Geological Survey). The columnar water vapor and ozone contents, also the atmospheric pressure, are input fields issued from the numerical weather prediction model of the European Centre for Medium-Range Weather Forecasts (ECMWF). The ground segment of PROBA-V applies an atmospheric correction on a pixel-per-pixel basis for cloud-free pixels. The atmospheric correction is performed using the SMAC (Simplified Method for Atmospheric Correction) software (Rahman and Dedieu, 1994). SMAC considers linear parameterizations for the absorption and scattering components of molecules and aerosols based on the physics of the 6S code. These relationships include tunable coefficients depending on aerosol type and PROBA-V channels. However, a continental type is taken everywhere whereas the aerosol optical depth (AOD) at the wavelength of 550 nm is prescribed as a function of latitude. The S1 TOC PROBA-V reflectance is distributed with the Status Map (SM), which tells about the quality of the product (radiometry quality, cloud mask, etc.) (see Table 1). A land sea mask (LSM) is used to delineate the coastline. Note that for time being, the inner water bodies are not masked by the application of LSM.

3. Methodology description

3.1. Algorithm overview

The operational processing scheme of the land surface albedo and TOC-R algorithm is depicted in the flow chart of Fig. 1. It encompasses three successive steps: the spectral TOC reflectance values serve as the input quantities for the inversion of a linear kernel-driven BRDF model, which allows taking into account the angular dependence of the reflectance factor. A well-established approach for an operational computation of the surface albedo is based on semi-empirical BRDF kernel model. Such category of models has received a great deal of attention and effort from the optical remote sensing community in the last decades (Roujean et al., 1992; Barnsley et al., 1994; Wanner et al., 1995; Strahler, 1994; Hu et al., 1997). The approach is based on a decomposition of the bi-directional reflectance factor into a number of kernel functions which are associated to the dominant light scattering processes, e.g. geometric and volumetric effects, a separation between the

Table 1
 Explanation of the pixel quality indicators in the Status Map Dataset. Bits indicated with an asterisk are only available for Level2A data.

Bit	Description	Value	Key
Bits 0–2	Cloud/Ice Snow/Shadow Flag	000	Clear
		001	Shadow
		010	Undefined
		011	Cloud
		100	Ice
Bit 3	Land/Sea	0	Sea
		1	Land
Bit 4	Radiometry quality SWIR flag	0	Bad
		1	Good
Bit 5	Radiometry quality NIR flag	0	Bad
		1	Good
Bit 6	Radiometry quality RED flag	0	Bad
		1	Good
Bit 7	Radiometry quality BLUE flag	0	Bad
		1	Good
Bit 8*	SWIR coverage	0	No
		1	Yes
Bit 9*	NIR coverage	0	No
		1	Yes
Bit 10*	RED coverage	0	No
		1	Yes
Bit 11*	BLUE coverage	0	No
		1	Yes

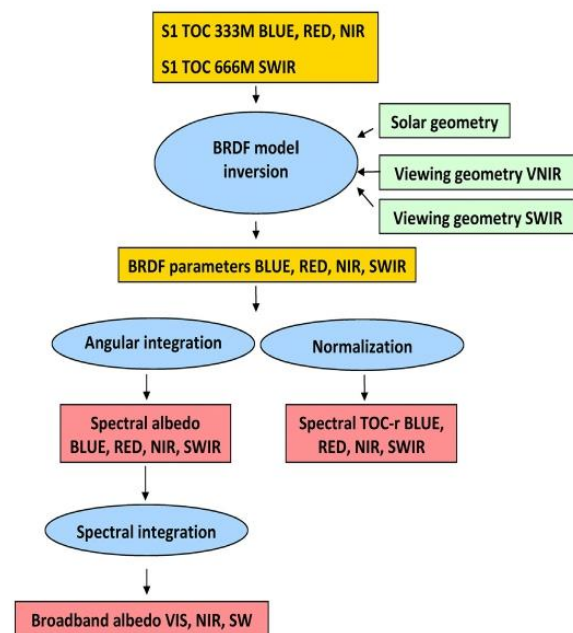


Fig. 1. Flow chart of the algorithm for BRDF model inversion and albedo and TOC-R determination.

soil and vegetation, or the conjunction between media which are optically thick and thin (Lucht and Roujean, 2000).

The kernel-based approach was adopted to map the surface albedo for a number of space-borne sensors like POLDER, SeaWiFS, VEGETATION, MODIS and MERIS (e.g., Leroy et al., 1997; Justice et al., 1998; Wanner et al., 1997; Strahler et al., 1999; Samain et al., 2006; Baret et al., 2007; Muller et al., 2012). The Top-Of-Canopy Reflectance (TOC-R) product is however not always an output product. A TOC-R product is deemed relevant to capture the seasonal cycles of the vegetation mostly as a combination of the spectral signatures to derive in fine the

vegetation indices, which justifies the effort here.

S1 TOC (daily synthesis) products are inputs data valid for each pixel (available from <http://www.vito-eodata.be>). All land target are considered, snow and ice cover inclusive, at the exception of inner seas. The input data sets therefore resume to:

- TOC BLUE, RED, NIR at 1/3 km (VNIR) and SWIR at 2/3 km (SWIR)
- Radiometric quality flag for bands BLUE, RED, NIR, SWIR from Status Map (SM)
- Viewing and solar azimuth angles [0, 360°]
- Viewing Zenith Angles (VZA) and Viewing Azimuth Angles (VAA) are different for VNIR and SWIR

The latitudinal information is foremost ancillary information to estimate the value of the solar zenith angle. This latter corresponds here to noontime in the case of directional albedo and at 10 AM for TOC-R. The semi-empirical BRDF model of Roujean et al. (1992) further adjusted to the measurements reads:

$$R_j(\theta_{vj}, \theta_{sj}, \varphi_j) = \sum_{i=0}^{m-1} k_i f_i(\theta_{vj}, \theta_{sj}, \varphi_j) \quad j = 1, n \quad (1)$$

where n represents the set of surface reflectance values, m stands for the number of kernels, equal to two here to account for the geometric and volume scattering kernels of Roujean et al. (1992), whereas k_i are the model parameters and f_i are the angular kernel functions. The angle ϕ is the relative azimuth between the directions of illumination and scanning. The angles θ_s and θ_v stand for the solar and viewing zenith angles, respectively. The algorithm first estimates the Black-Sky Albedo (BSA) or Directional-Hemispherical Reflectance (DHR) and White-Sky Albedo (WSA) or Bi-directional-Hemispherical Reflectance (BHR) in the four instrument channels by using the retrieved BRDF coefficients from Eq. (1). In the inversion procedure, a weight w_j is assigned to each reflectance value, which is scaled as the inverse of the uncertainty on this reflectance value (e.g. Press et al., 1995). This uncertainty estimate is inherited from a statistical analysis of atmospherically corrected satellite scenes (see Geiger et al., 2008).

The solution to the linear least square inverse problem is stated as.

$$\mathbf{R} = \mathbf{F}\mathbf{k}. \quad (2)$$

The reflectance vector $b_j = R_j w_j$ is the solution of the following equation.

$$(\mathbf{A}^T \mathbf{A}) \mathbf{k} = \mathbf{A}^T \mathbf{b}. \quad (3)$$

The design matrix $A_{ji} = F_{ji} w_j$ tailors the uncertainty covariance matrix:

$$\mathbf{C}_k = (\mathbf{A}^T \mathbf{A})^{-1}. \quad (4)$$

Provided few PROBA-V measurements and poor angular sampling scenario, more robust techniques like singular value decomposition (SVD) and QR-decomposition are advised to minimize numerical errors. The system can be better conditioned by adding constraints (e.g., Li et al., 2001; Hagolle et al., 2004; Pokrovsky et al., 2003). A priori information is given on the BRDF coefficients in terms of the first and second moments (average and standard deviation, respectively) of their a priori probability distribution function (PDF). That is:

$$k_i = k_{i,ap} \pm \sigma_{ap} [k_i] \quad (5)$$

Therefore, Eq. (3) is rewritten in the form.

$$(\mathbf{A}^T \mathbf{A} + \mathbf{c}_{ap}^{-1}) \mathbf{k} = \mathbf{A}^T \mathbf{b} + \mathbf{c}_{ap}^{-1} \mathbf{k}_{ap} \quad (6)$$

The covariance matrix \mathbf{C}_{ap} for a priori information reduces to diagonal matrix terms by making the assumption of uncorrelated a priori information. Such matrix reads:

$$\mathbf{C}_{ap} = \mathbf{C}_k^{in} (1 + \Delta)^{(t_0 - t_{in})/\Delta t} \quad (7)$$

J.-L. Roujean et al.

Remote Sensing of Environment 215 (2018) 57–73

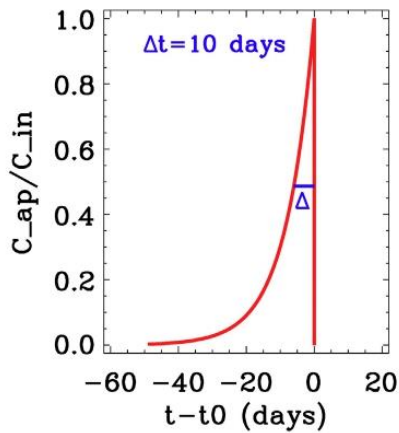


Fig. 2. Effective temporal weight function in the recursive composition scheme.

where the quantity $t_0 - t_{in}$ measures the elapsed time between two successive runs of the algorithm, with $\Delta t = 10$ days. The characteristic time scale Δ is the full width at half mean of the weighing function (Fig. 2). Based on Eq. (7), the BRDF model inversion assigns less importance to observations as they get away from day t_0 . Once the BRDF from the vector k is known, the spectral albedo values are computerized by performing an angular integral of the kernel functions, f . Finally, a spectral integration of the spectral albedo leads to broadband albedos. For more about the algorithm, we will refer the reader to the implemented method for Spinning Enhanced Visible and InfraRed Imager (SEVIRI) onboard MSG (Meteosat Second Generation) as described in Geiger et al. (2008) from which the algorithm is basically derived.

3.2. Uncertainty estimate

The uncertainty estimate reports on the model performance by paying attention to the angular sampling and to the number of data. It is assumed that the probability distribution functions (PDF) of the errors of the TOC reflectance values are Gaussian and mutually uncorrelated. Using linear expressions, the albedo uncertainty estimate is obtained by propagating those of the model parameters as shown in Eq. (8) with the appropriate angular kernel integrals, I :

$$\sigma[a] = \sqrt{I^T C_k I} \quad (8)$$

Any residual cloud contamination will have an impact in the contribution of outliers in the PDF of the TOC reflectance errors, then on inversion results and surface albedo quality. To be outlined Eq. (8) remains valid for TOC-R.

3.3. Age of the product

The accumulation of information over days is mandatory for polar orbiting systems. The longer is the composite period, the more data to be stored for further exploitation. This is a trade-off process. Herein, PROBA-V land surface albedo and TOC-R products are reduced to 20-

Table 2
Albedo product quality flag information.

Bit	Description	Value	Key
Bits 0–1	Land Sea Mask	00	Sea
		01	Land
		10	Corrupted
		11	Inland water
Bit 2	Input data	0	No
		1	Yes
Bit 3	Majority Rule for snow or snow-free	0	No
		1	Yes
Bit 4	A Priori Information	0	No
		1	Yes
Bit 5	Snow	0	No
		1	Yes
Bit 6	Aerosol correction	0	Climatology
		1	Near real time
Bit 7	Algorithm Failure	0	No
		1	Yes

days composite period against 30-days for 1 km VEGETATION program because the 333 m resolution of PROBA-V permits a better cloud removal. The product frequency is still 10 days. The synthetic period ends at days 10, 20, and last day of the month (Fig. 3). The true age of the product, Z_{Age} , is given to the user per pixel as a novelty. It is the median date value of clear sky dates over the composite period. Smoothness is slightly enhanced by assigning weight to the a priori information. Duration of cloudiness entails the propagation of a priori information and gap-filling.

3.4. Quality flag

The Quality Flag (Q-Flag) integrates all uncertainty assessments that led to the elaboration of the product (see Table 2). It reports merely information about a priori, snow coverage, and land pixel. If snow pixels are present during the composite period, the majority rule will apply. It means snow and snow-free pixels will compete in number to make an unmerged albedo product. The Bit 3 informs the user about the procedure application, with the risk for a merged albedo according to snow detection. The Bit 4 indicates that less than three observations were available. A priori estimate is reported in this case as a remedy to the gap-filling procedure. The Bit 6 is always 0 since a climatology is hitherto adopted for aerosol compound.

3.5. Narrow to broadband conversion

The narrow to broadband conversion is approximated as a weighted sum of the integrand at discrete values of the integration variable. The SWIR channel shows a coarser resolution compared to other channels and therefore a same SWIR pixel may be considered for neighboring pixels of other channels. Broadband albedo estimate at spectral interval γ is derived from the spectral quantities by applying a linear transformation where a_γ and a_β stand for broadband and spectral albedos, respectively. Viz:

$$a_\gamma = c_{0\gamma} + \sum_{\beta} c_{\beta\gamma} a_\beta \quad (9)$$

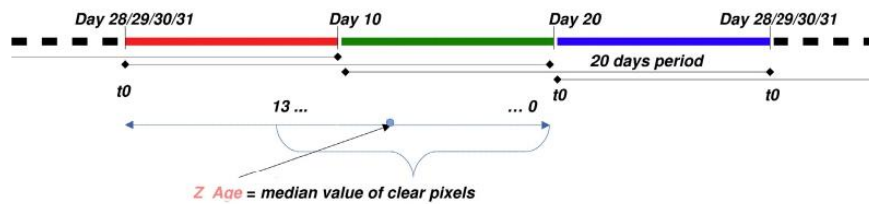


Fig. 3. Illustration of the achievement of Z_{Age} information.

Table 3
Narrow- to broadband conversion coefficients for PROBA-V channels and uncertainty estimates.

Broad-band	NDVI	$c_{0\gamma}$	$c_{\beta\gamma}$ Blue	$c_{\beta\gamma}$ Red	$c_{\beta\gamma}$ NIR	$c_{\beta\gamma}$ SWIR	RMSE
Visible [0.4–0.7 μm]	[–1.,1.]	0.0010	0.5039	0.4923	–	–	0.0067
	< 0.2 & snow	0.0284	0.5736	0.3837	–	–	0.0199
Near Infrared [0.7 - 4 μm]	[–1.,1.]	0.0140	–	0.0068	0.5677	0.3481	0.0135
	< 0.2 & snow	0.0212	–	0.0438	0.5509	0.3633	0.0128
Total [0.3–4 μm]	[–1.,1.]	0.0097	0.1863	0.2212	0.3434	0.1817	0.0089
	< 0.2 & snow	0.0248	0.1196	0.2764	0.3566	0.07	0.0154

Table 4
Uncertainty metrics for product validation.

Gaussian Statistics	Comment
Scatter plot of ground versus product	Qualitative assessment of agreement.
N: Number of samples	Indicative of the power of the validation
RMSE: Root Mean Square Error	RMSE computed between ground and product values should be compared to the RMSE value corresponding to ground measurements. Indicates the Accuracy (Total Error). Relative values between the average of x and y were also computed.
B: MeanBias	Difference between average values of ground and product. Indicative of accuracy and possible offset. Relative values between the average of x and y were also computed.
S: Standard deviation	Standard deviation of the pair differences. Indicates precision.
R ² : Correlation coefficient	Indicates descriptive power of the linear accuracy test. Pearson coefficient was used.
Major Axis Regression (slope, offset)	Indicates some possible bias
p-Value	Test on whether the slope is significantly different to 1 (Null hypothesis: slope = 1). (p > 0.05 accepted)
% GCOS requirements	Percentage of pixels matching the GCOS requirements [*] .

* The GCOS requirements on accuracy were used: Max(5%; 0.0025). Furthermore, an additional target level of Max(10%; 0.005) was used.

Table 5
Summary of the Quality Assessment procedure.

Quality Criteri	Product evaluated	Reference Product	Coverage
Spatial Consistency	PROBA-V SA Collection 300 m	MODIS C6	European Region
		Visual inspection of global maps. Difference maps & global Scatter-plots (R ² , RMSE, Bias, Scattering).	
Temporal Consistency	PROBA-V SA Collection 300 m	MODIS C6 Ground measurements	EUVAL Validation sites
		Qualitative inspection of temporal variations.	
Overall Statistical Consistency	PROBA-V SA Collection 300 m	MODIS C6	EUVAL (section 0)
		Scatter-plots (R ² , RMSE, Bias, Scattering) between pair of products.	
Accuracy Assessment (Error)	PROBA-V SA Collection 300 m & MODIS C6	Ground measurements	Validation sites
		Scatter-plots, Pearson's correlation, Root Mean Square Error (RMSE), bias, linear fit (offset and slope, MAR).	

with coefficients $c_{0\gamma}$ and $c_{\beta\gamma}$ shown in Table 3. Three different broadband albedo intervals are considered: the total short-wave range from 300 nm to 4000 nm (BB), the visible wavelength range from 400 nm to 700 nm (VI), as well as the near infrared range from 700 nm to 4000 nm (NI). Negative NDVI values combining RED and NIR PROBA-V channels served to distinguish snow from snow-free pixels. The values in Table 3 were initially determined by van Leeuwen and Roujean (2002) for VEGETATION, further adapted to PROBA-V by VITO. Linear relationships were calibrated using synthetic data sets generated by the SAIL (Scattering by Arbitrarily Inclined Leaves) radiation transfer code (Verhoef, 1984), plus ASTER spectral library (Hook, 1998). They hold for both DHR (AL-DH) and BHR (AL-BH) products by assuming a spectral irradiance regardless to atmospheric effects. The errors of the spectral albedo estimates are supposed uncorrelated (see Table 3).

4. Tools of quality protocol for accuracy assessment

4.1. Information on product distribution

The processing chain is operated at the premises of VITO within the context of the EU Copernicus Global Land Service (CGLS). New land surface albedo and TOC-R products are proposed every ten days. They are distributed within three days after the last scene acquisition. For time being, they are available from the year 2014. The products are distributed as global files, combining the relevant layers into one single multi-band netCDF4-CF1.6 compliant format. To keep the file sizes to a reasonable size, not all layers are combined into one single file. Instead the TOC-R products are provided per band as well as the albedo products. The products can be downloaded from <http://land.copernicus.eu/global> and can be reformatted, cropped or subset through an on-line customization tool.

4.2. Methodology for quality assessment of the product

Preliminary Quality Assessment of the PROBA-V 1 Collection 300 m was focused on the surface albedo product merely. The evaluation is carried on over a European region covering the area from 35° to 65° of latitude and from –20° to 30° of longitude. The harnessing lumps together a cross-comparison with MODIS C6 products and then a direct validation using available ground observations coming from European Fluxes Data Cluster (EFDC) stations. The following main criteria were devised: spatial consistency, temporal consistency, and statistical assessment of discrepancies with similar products and accuracy. Surface albedo products receive regularly updated specifications (e.g. GCOS, 2016) as it is the case for an ECV (Essential Climate Variable). For surface albedo values lower than 0.05, the accuracy required is 0.0025. Therefore, a relative accuracy of 5% is still considered. Additional requirements come from the “WMO Rolling Requirement Review” that aids the setting of the priorities to be agreed by WMO (World Meteorological Organization) members and their space agencies. The GCOS requirements are only partly consistent with this process in that they provide only target but not “breakthrough” or “threshold” (i.e. minimum) requirements. But GCOS provides requirements on stability

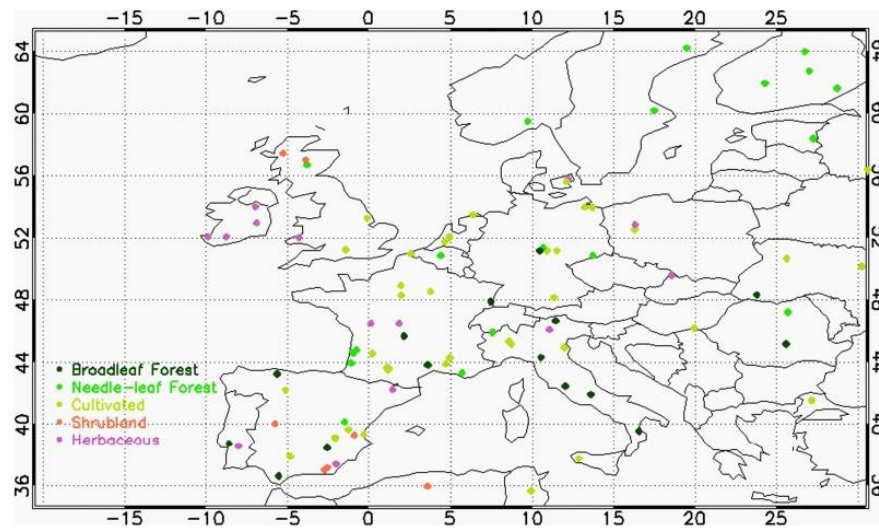


Fig. 4. Location of the 109 selected European validation (EUVAL) sites and their classification into the main biome type. Red square delineates the region under study. (For interpretation of the references to colour in this figure legend, the reader is referred to the web version of this article.)

Table 6

Selected 10 EFDC sites for Accuracy Assessment providing field albedo and diffuse measurements. The typical tower height used in this study is 10 m and then the footprint of the albedo measurements is 127 m (see Román et al., 2009).

Code	Site name	Country	Land Cover	Lat (deg)	Lon (deg)	Diffuse Method
CZ-BK1	Bily Kriz Forest	Czech Rep.	NLF	49.50472	18.54111	Direct
DE-Obe	Oberbärenburg	Germany	NLF	50.78362	13.71963	Indirect
ES-CPa	Cortes de Pallas	Spain	Shrublands	39.22417	-0.90305	Direct
ES-LMa	Majadas del Tietar	Spain	Savanna	39.9415	-5.77336	Direct
FR-Pue	Puechabon	France	EBF	43.74139	3.595833	Direct
IT-Col	Collelongo	Italy	BDF	41.84936	13.58814	Direct
IT-MBo	Monte Bondone	Italy	Herbaceous	46.01468	11.04583	Direct
IT-Tor	Torgnon	Italy	Shrublands	45.84444	7.578055	Indirect
DE-Tha	Tharandt	Germany	Mixed Forest	50.96361	13.56694	Direct
PL-Brd	Brody ^a	Poland	Crop	52.43418	16.29952	Direct

^a For PL-Brd Cropland site. Only Leaf-Off season (fall and winter) was considered for the accuracy assessment, due to the spatial homogeneity is not ensured during the Leaf-On season (spring and summer).

Table 7

Additional 7 EFDC sites for temporal realism.

Code	Site name	Country	Land Cover	Lat (deg)	Lon (deg)
DE-Akm	Anklam	Germany	Shrublands	53.866170	13.683420
ES-ES	El Saler-Sueca	Spain	Crop	39.275550	-0.315278
IT-CA1	Castel d'Asso1	Italy	Crop	42.38041	12.02656
IT-CA2	Castel d'Asso2	Italy	Crop	42.37722	12.02604
IT-CA3	Castel d'Asso 3	Italy	Crop	42.38	12.0222
DE-Kli	Klingenberg	Germany	Crop	50.89288	13.52251
PL-Tuc	Tuczno	Poland	Wetland	53.192944	16.097472

that are not currently included in the WMO requirements database. The “WMO Observing Requirements Database” specifies requirements on the surface albedo for climatologic applications at three uncertainty quality levels: Goal (5%), Breakthrough (7%) and Threshold (10%).

Quality Assessment exercise follows here a procedure with prevalent protocols and metrics defined to be consistent with the recommendations of the Land Product Validation (LPV) group of the Committee on Earth Observation Satellite (CEOS) for the validation of satellite-derived land products. Spatial consistency mirrors the level of truth and repeatability of the spatial distribution of retrievals in the lack of spurious patterns or other artifacts (e.g., missing values, stripes, unrealistic low values, etc.). It is achieved through systematic visual

inspection analysis of the global maps, using the maps difference at a monthly basis. Temporal consistency reports on the degree of realism of the temporal variations. Temporal courses of satellite products were investigated over the confident sites of the EUVAL network and other selected stations. This supposes high frequency data are available like daily ground observations. Statistical analysis was performed over a selection of representative European sites for validation (EUVAL) based on uncertainties metrics associated to the scatter-plots between pairs of products (Table 4). To be outlined that only sites that are spatially representative at the kilometer scale were put in valor. Table 5 summarizes the number of validation metrics used to verify the consistency between PROBA-V SA Collection 300 m for the whole 2014 year, using as references MODIS C6 product and ground data coming from EFDC stations.

A trimmed analysis of the spatial and statistical consistency was performed at 1 km resolution. PROBA-V SA 300 m products were re-sampled using an average value over a 3 × 3 pixels window (from 1/3 km to 1 km spatial resolution). MODIS C6 data were re-sampled using an average over 2 × 2 pixels window (from 1/2 km to 1 km). Twofold analysis based on temporal consistency and accuracy assessment relied on the native spatial resolution of each product. The comparison is carried on 10-days periods defined as the closest to the center of the temporal composite window, being 20 days (PROBA-V SA 300 m) and

J.-L. Roujean et al.

Remote Sensing of Environment 215 (2018) 57–73

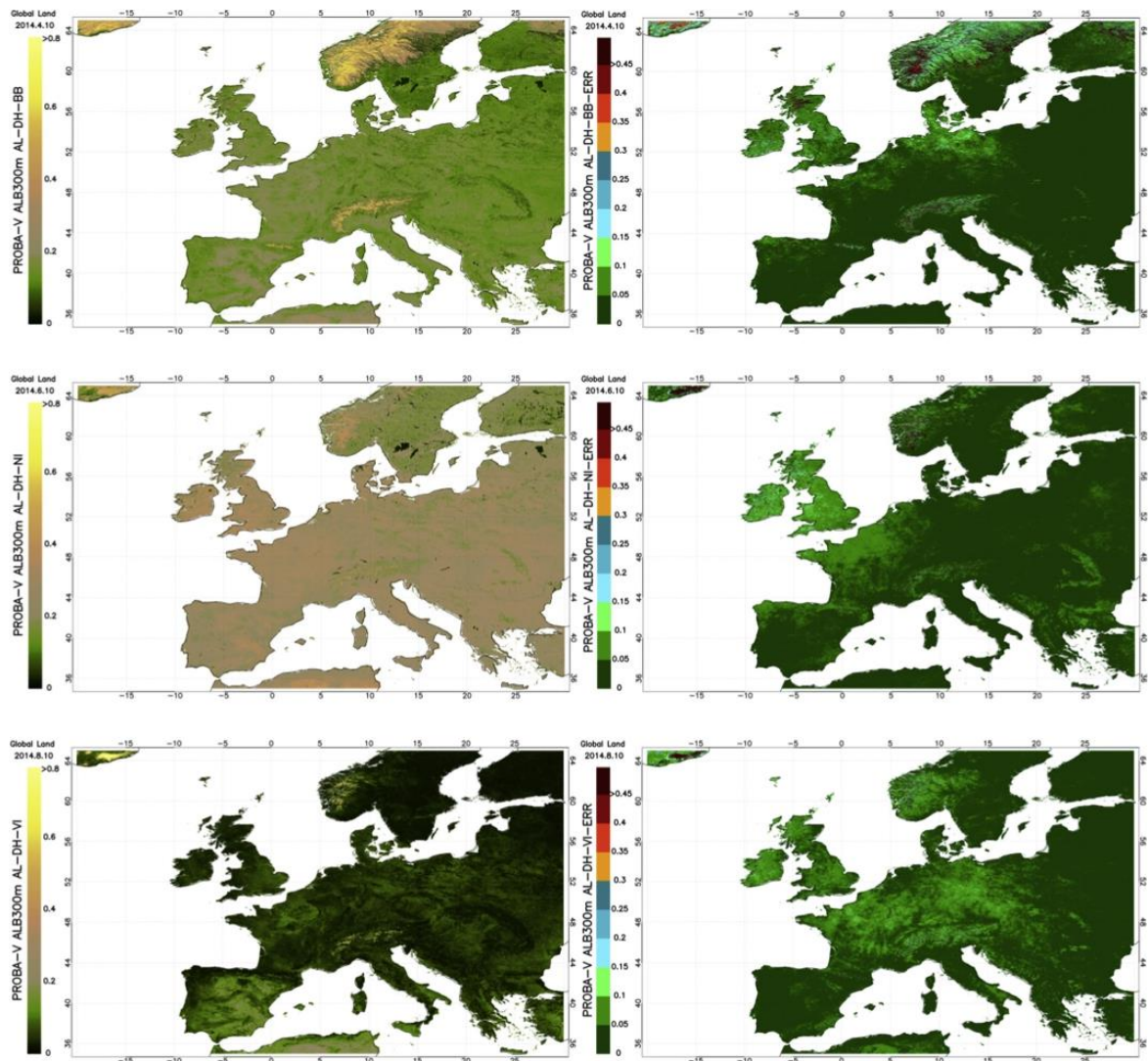


Fig. 5. Maps of AL-DH (Left side) and AL-DH error estimates (right side) for several spectral domains and selected dates: AL-DH-BB for 2014.04.10 (Top), AL-DH-NI for 2014.06.10 (Middle) and AL-DH-VI for 2014.08.10 (Bottom).

16 days (MODIS C6). Only pixels with Z_Age values beyond 10 days have been retained. This offers more realistic results of comparison by discarding products from sensors too far away in time. The date assigned to a PROBA-V pixel was established as the date given in the product file name - ending the composite window frame - less the Z_Age value.

4.3. Data sets for validation

4.3.1. PROBA-V data sets

The quality assessment is performed against a data set of PROBA-V SA V1 Collection 300m images covering 15 tiles encompassing a wide European region from 35° to 65° of latitude and from -20° to 30° of longitude. The dataset is available at 10 days frequency covering the whole year 2014. For each tile, files in HDF5 format were considered with the content of black-sky and white-sky albedos in visible, NIR and

shortwave domains, plus ancillary information (error estimate, Quality Flag, Z_Age).

4.3.2. MODIS collection 6

For the cross-comparison, it is considered the MODIS BRDF/Albedo (MCD43A3) Collection 6 (DOI: <https://doi.org/10.5067/MODIS/MCD43A3.006>) at 500-meter spatial resolution, which achieved validation stage 3 in the CEOS/LPV hierarchy (Wang et al., 2018). Collection 6 provides improved quality compared with previous Collection 5, as well as more retrieval at high latitudes from use of all available observations. Only high quality MODIS products were retained for further analysis. It includes notably both directional hemispherical reflectance (black-sky albedo) at local solar noon and bi-hemispherical reflectance (white-sky albedo) for three broad-bands (visible: 0.3–0.7 μm, NIR: 0.7–5.0 μm, and Total: 0.3–5.0 μm). The MCD43A3 albedo quantities are disseminated on a sinusoidal grid, with temporal

J.-L. Roujean et al.

Remote Sensing of Environment 215 (2018) 57–73

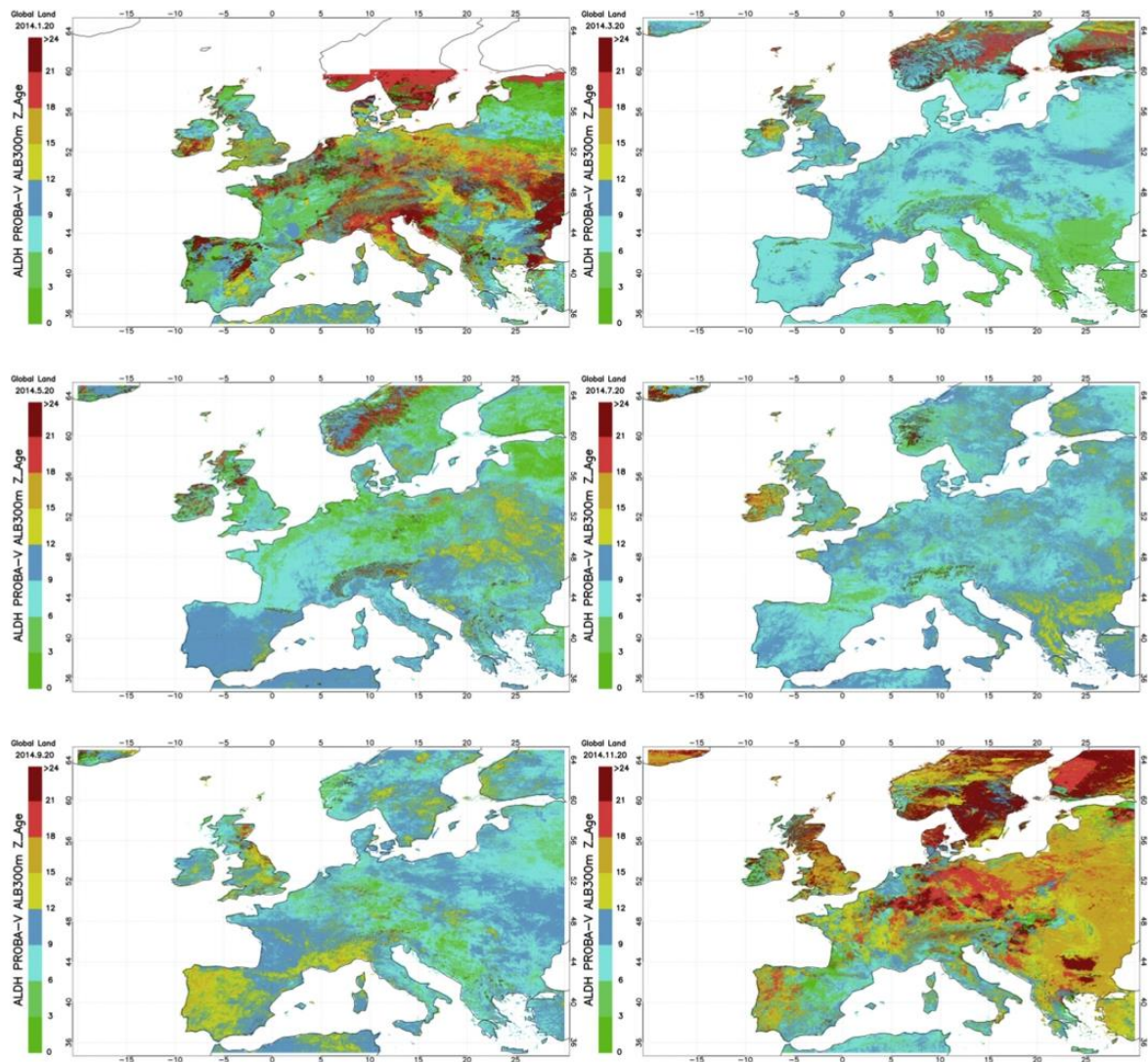


Fig. 6. Maps of ALDH Z_Age for several dates. From Top to Bottom and from Left to Right: 2014.01.20, 2014.03.20, 2014.05.20, 2014.07.20, 2017.09.20 and 2014.11.20.

composite period of 16 days. Both Terra and Aqua data are used in the generation of this product. As a quick remind, MODIS albedo algorithm uses atmospherically corrected reflectance data (MOD09 product with flags about “cloud”, “cirrus high” and “aerosol high”) to best fit the kernel-driven BRDF model Ross Thick Li Sparse-Reciprocal (RTLSR) (Lucht and Lewis, 2000). Only periods with 7 clear observations lead to full inversion. Otherwise it makes use of a backup algorithm with prior information for a magnitude inversion in the MODIS BRDF products. A gap filling occurs for less than three clear observations. To be outlined here that the MODIS albedo team provides separated snow-free gap filled products: https://www.umb.edu/spectralmass/terra_aqua_modis/v006/mcd43gf_cmg_gap_filled_snow_free_products (Sun et al., 2017). Integrating BRDF model parameters lead to spectral albedos further converted into broadband albedos (Liang et al., 1999). A well-behaved agreement ($r^2 = 0.82$) was found between the comparison of mean yearly MODIS albedo Collection 5 retrievals with ground measurements

taken at 53 FLUXNET homogeneous sites (Cescatti et al., 2012).

4.3.3. Sites selection from European validation (EUVAL)

The temporal and statistical consistency was computed over 109 sites from the European Validation (EUVAL) network (Fig. 4). Only homogeneous sites covering at least 3 km² were deemed dependable based on previous study based on the biome type classification (GLC2000 (e.g. https://land.copernicus.eu/global/sites/cgls.vito.be/files/products/GIOGL1_QAR_LAI300m-V1_J1.10.pdf). The percentage of EUVAL sites per main biome is decomposed as follows: 14.37% for Broadleaf Forest, 21.56% for Needle-leaf forest, 32.68% for Cultivated areas, 9.8% for Shrublands, 11.76% for Herbaceous, and 9.80% for bare soils.

4.3.4. Accuracy assessment from EFDC

The accuracy assessment of PROBA-V SA Collection 300 m products

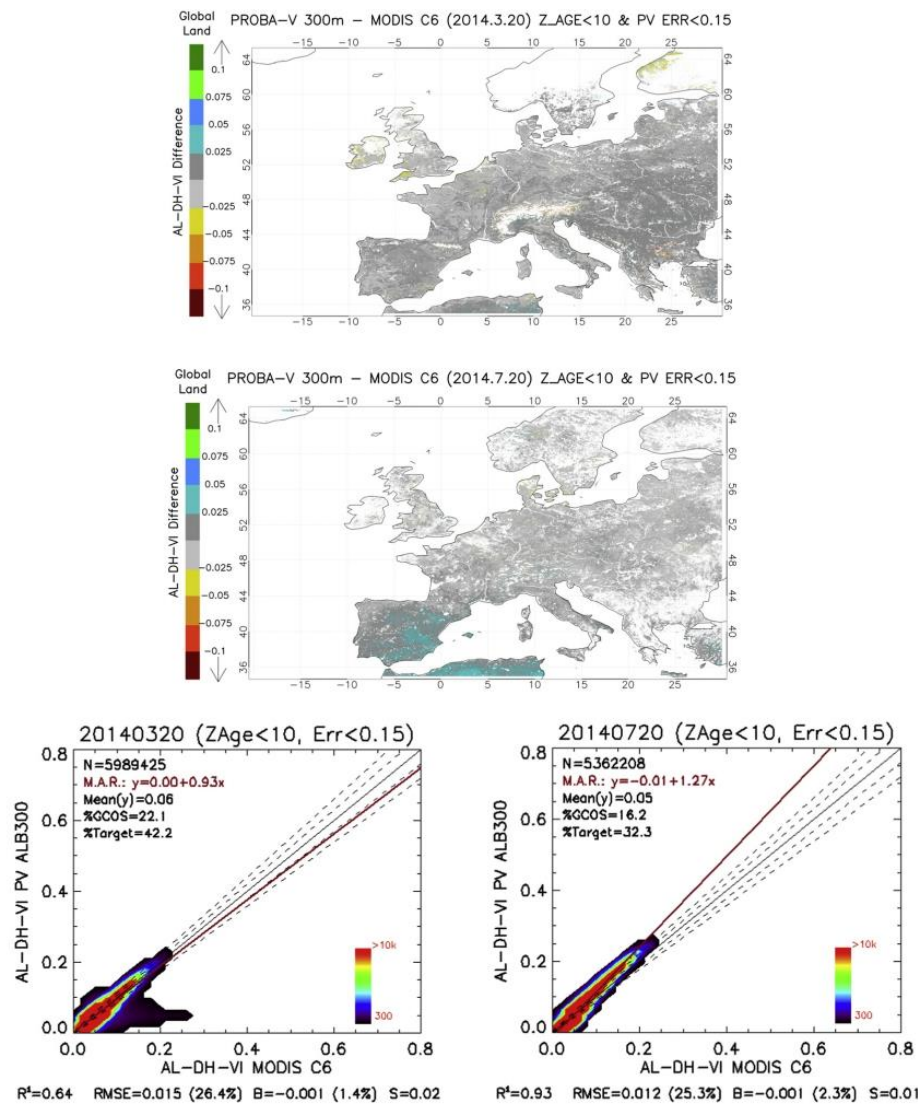


Fig. 7. AL-DH-VI difference maps (left side) and associated scatter plots (right side) between PROBA-V SA Collection 300 m and MODIS C6 products for the 20th March 2014 (Top) and 20th July 2014 (Bottom). Pixels with error estimates > 0.15 and Z_Age values > 10 days in cases of PROBA-V product were not considered for the analysis.

finally prevails with stations from the European Fluxes Database Cluster (EFDC) (<http://gaia.agraria.unitus.it/home/log-in/>). These latter are coping with the mandatory criteria aforementioned. Land cover characteristics were obtained at the spatial resolution of 500 m based on Google Earth™ for sites matching first the requirement of homogeneity around the tower flux (Román et al., 2009). Both daily and noon measurements were harnessed. Different strategies have been applied to the ground measurements in order to fairly match with satellite data, which depends on the instrument. In case of PROBA-V, the value of the composite period is assigned to the true date. In case of MODIS C6, the composite period is 16 days and the date corresponds to the center of the 16-day composite period (9th day). A composite value is therefore built only if 70% at least of daily ground measurements are available. Table 6 displays the list of 10 homogeneous sites used in this study. Most of the EFDC stations measure the diffuse down-welling shortwave

radiation information. If not then estimate of diffuse radiation was performed in using the aerosol optical depth from the nearest AERONET station and the MODTRAN code. In addition, the ground information from 7 EFDC (Table 7) was only used to appraise the temporal shape as the diffuse fraction was not available.

5. Results of quality assessment

5.1. Product content

Spatially consistency of pattern distribution of surface albedo and associated error estimates are conspicuous from Fig. 5. The completeness of the mapping is a benefit from the recursive temporal scheme. Consistent values of Z_Age were found for the whole region during the year 2014, with values typically ranging between 5 and 15 (see Fig. 6).

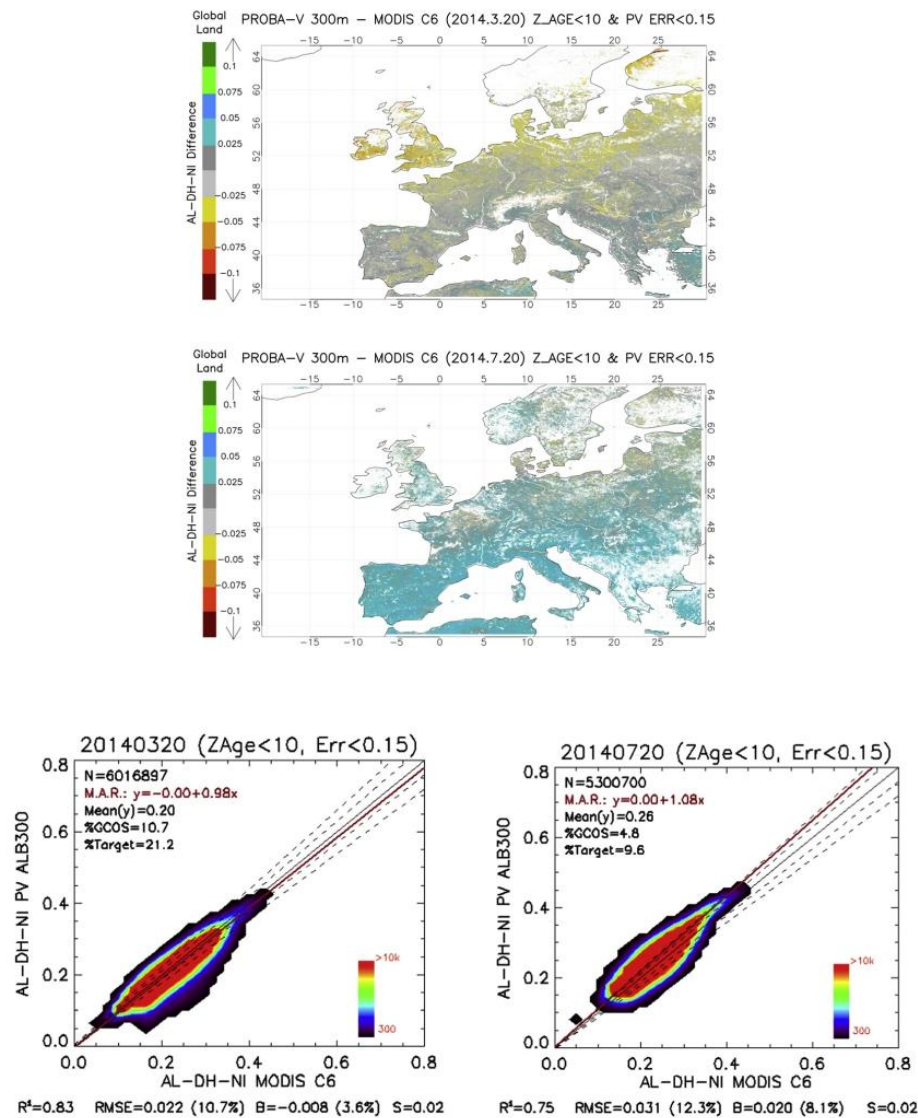


Fig. 8. Idem Fig. 7 for AL-DH-NI.

As expected, higher ZAge values were encountered for scenarios suffering from persistent cloud coverage (wintertime period and Northern latitudes).

5.2. Spatial consistency analysis

The set of Figs. 7–9 shows deviations in geographic distribution and scatter plots between PROBA-V Collection 300 m and MODIS C6 black-sky albedo products at mid-March and mid-July 2014. Snow flagged pixels were discarded from the analysis due to differences of strategy between the two sensors. For PROBA-V, rare pixels with error field > 0.15 were removed from the analysis as it is known possible residual cloud contamination with this first PROBA-V collection. Salient feature is the good spatial consistency that exists in visible domain (Fig. 7), with only differences of ± 0.025 in reflectance units. Also, dependable correlations (R^2 between 0.64 and 0.93) and mean bias close to zero are

evidenced. A slight tendency noticed with PROBA-V is lower values obtained for a low albedo (< 0.1), and higher values for a high albedo (> 0.1). This is a general trend observed if one excerpts the months of January and December 2014. As for NIR domain (Fig. 8), a good consistency is also reached with almost all differences within ± 0.05 . The tendency is rather a random bias between PROBA-V SA Collection 300 m and MODIS C6, with opposite signs of the bias at some places for different periods. A good statistical rendering is obtained (R^2 around 0.8, RMSE between 0.02 and 0.03). Finally, the upshots of analysis for shortwave products (Fig. 9) closely follow the ones for NIR with nevertheless higher values compared to MODIS C6 products for all dates and regions again with the exception of northern latitudes and winter time situations.

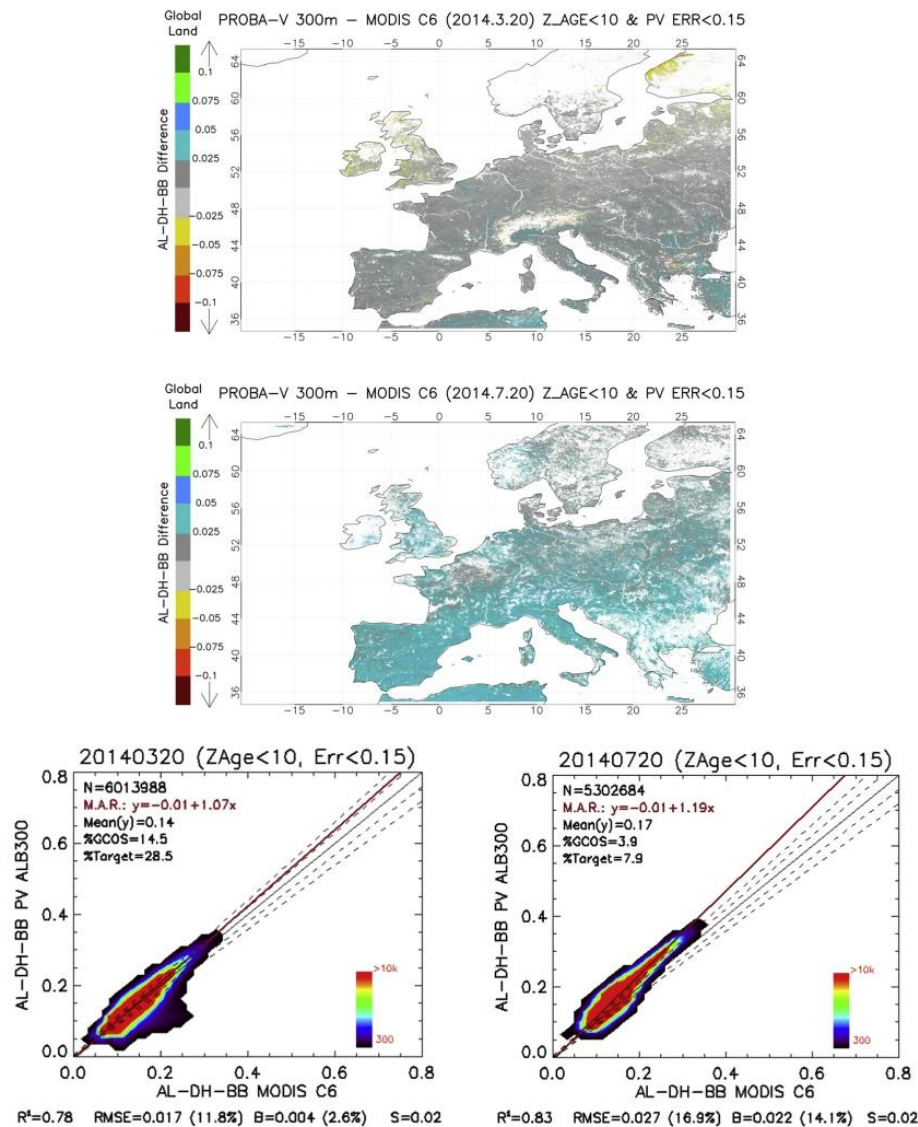


Fig. 9. Idem Fig. 7 for AL-DH-BB.

5.3. Temporal consistency analysis

Temporal profiles of PROBA-V and MODIS C6 of black-sky and white-sky albedo products were analyzed for the 109 EUVAL sites and over 17 ground stations where ground measurements were available. Results are displayed for the three spectral ranges and the nominal spatial resolution of the product (333 m for PROBA V, 500 m for MODIS) (Fig. 10).

Vertical bars of PROBA-V Collection 300 m correspond to the uncertainty assessment in the generation of the associated albedo product. Blue-sky albedos are shown whenever daily ground observations are available. Main lesson learned is that for Broadleaf Forests, PROBA-V well captures the rapid seasonality of albedo from dense to low vegetation coverage, providing reliable and smooth trajectories. Only over some sparse situations (a ratio of 25%), unexpected instabilities not observed in reference products were observed in case of Broadleaf

Forests (see *Asturias* site during August–September). Although it is prevalent in NIR, the shape also affects the shortwave band by spectral construction. Over Needle-leaf Forests, unexpected variations (as compared with reference products) in around 40% of cases were found for some period (see *B2.1#244* during July and *Cazorla NP* during August–September). As for Cropland sites, close patterns are noticed between sensors. To be outlined that PROBA-V well mimics the dynamic of surface albedo in link to phenological status. Such findings were deemed consistent with MODIS C6 temporal variations and with daily ground observations whenever available (see *El SalerSueca*, *Castel d'Asso2*). Smoother transitions are conspicuous in the case of PROBA-V due to the beneficial effect of a priori information that precludes dodgy scenarios. Over Herbaceous and Shrublands, compliant temporal trajectories are noticeable between sensor products and also ground daily observations (e.g. *Anklam* site and *Semi-arid Almeria* site). Error estimates were found generally concurring in magnitude with albedo

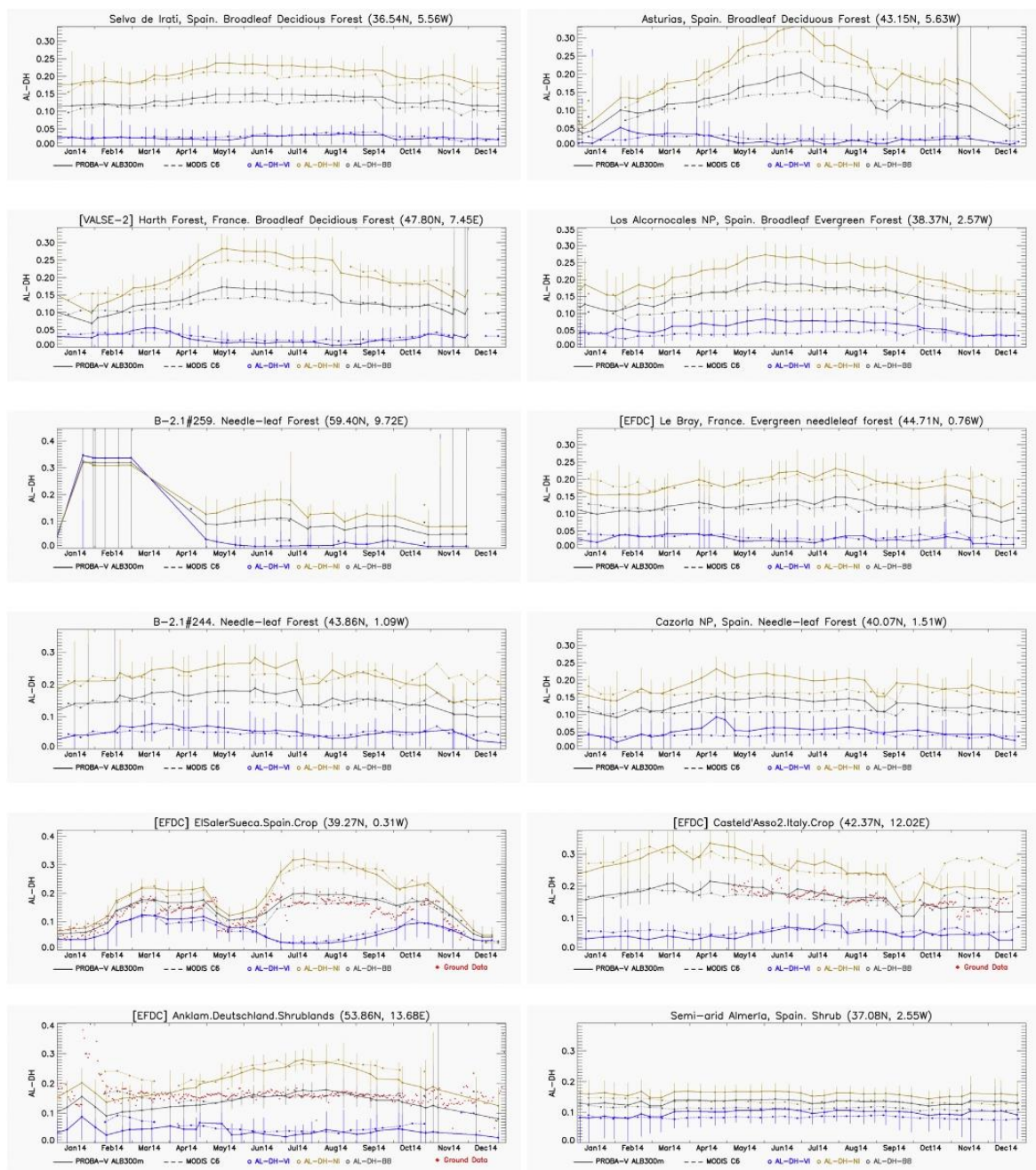


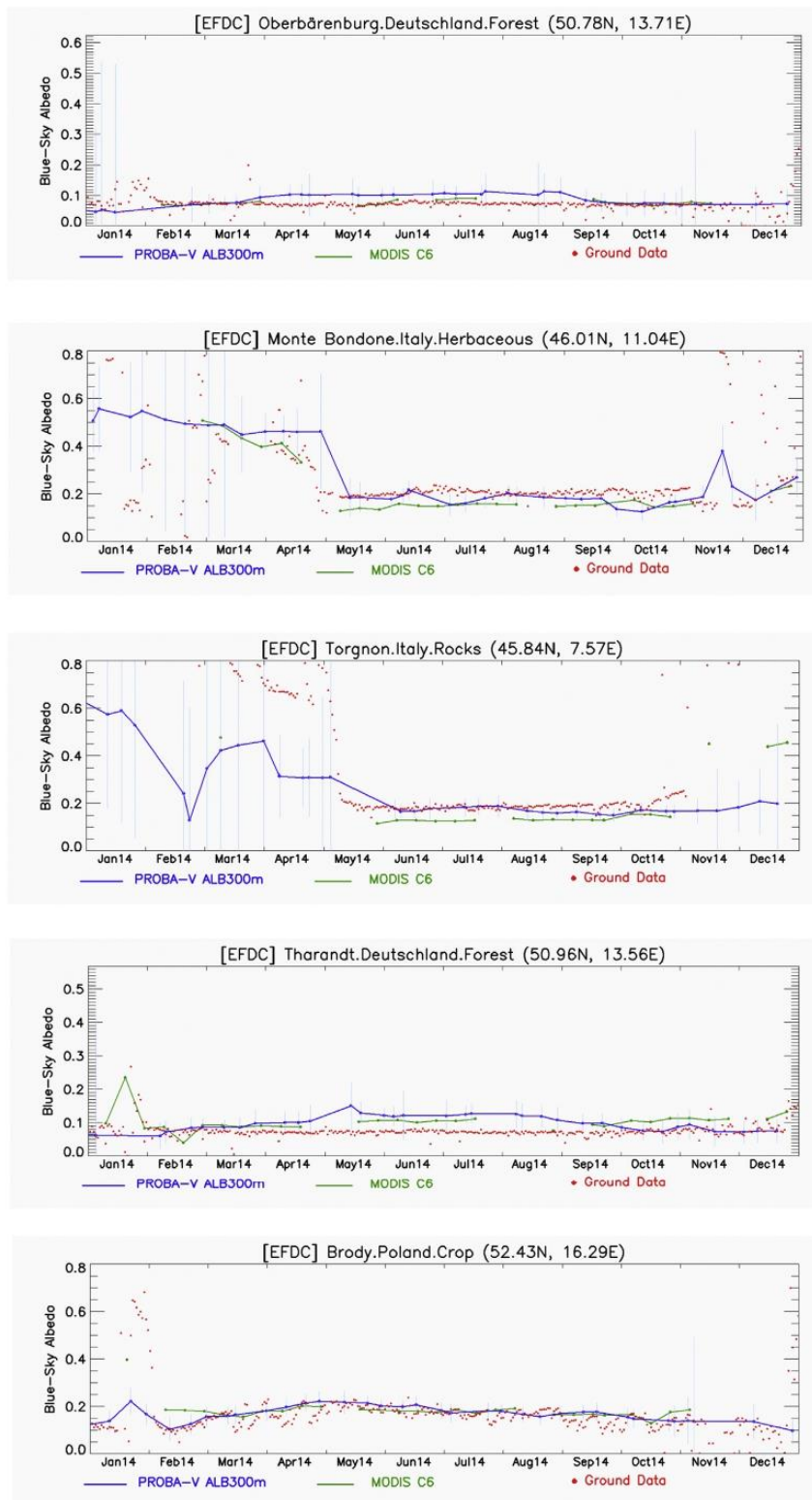
Fig. 10. Temporal profile of PROBA-V SA Collection 300 m (continuous line), and MODIS C6 (dashed line) AL-DH-BB (grey) and AL-DH-NI (yellow) and AL-DH-VI (blue) albedos over several selected sites. Vertical bars correspond to the associated error of PROBA-V SA Collection 300 m products. (For interpretation of the references to colour in this figure legend, the reader is referred to the web version of this article.)

retrievals, excepted during the wintertime periods due to the occurrence of snow and grazing solar angles. MODIS C6 shows major gaps, which limits the comparison with PROBA-V. The snow episodes were correctly reported by PROBA-V in 70% of cases as compared to MODIS or ground daily observations (e.g. B2.1#259). Unreported snow events may explain by the choice of the majority rule to segregate snow or

snow-free pixels over the spanning composite window.

5.4. Blue-sky albedo

Blue-sky albedo is a genuine product from the point of view of in situ measurement, although not yet included in the Copernicus GLS.



(caption on next page)

Fig. 11. Temporal profiles of PROBA-V SA Collection 300 m (blue), MODIS C6 (green) and ground measurements (red points) Blue-Sky albedos. Vertical bars correspond to the PROBA-V errors. (For interpretation of the references to colour in this figure legend, the reader is referred to the web version of this article.)

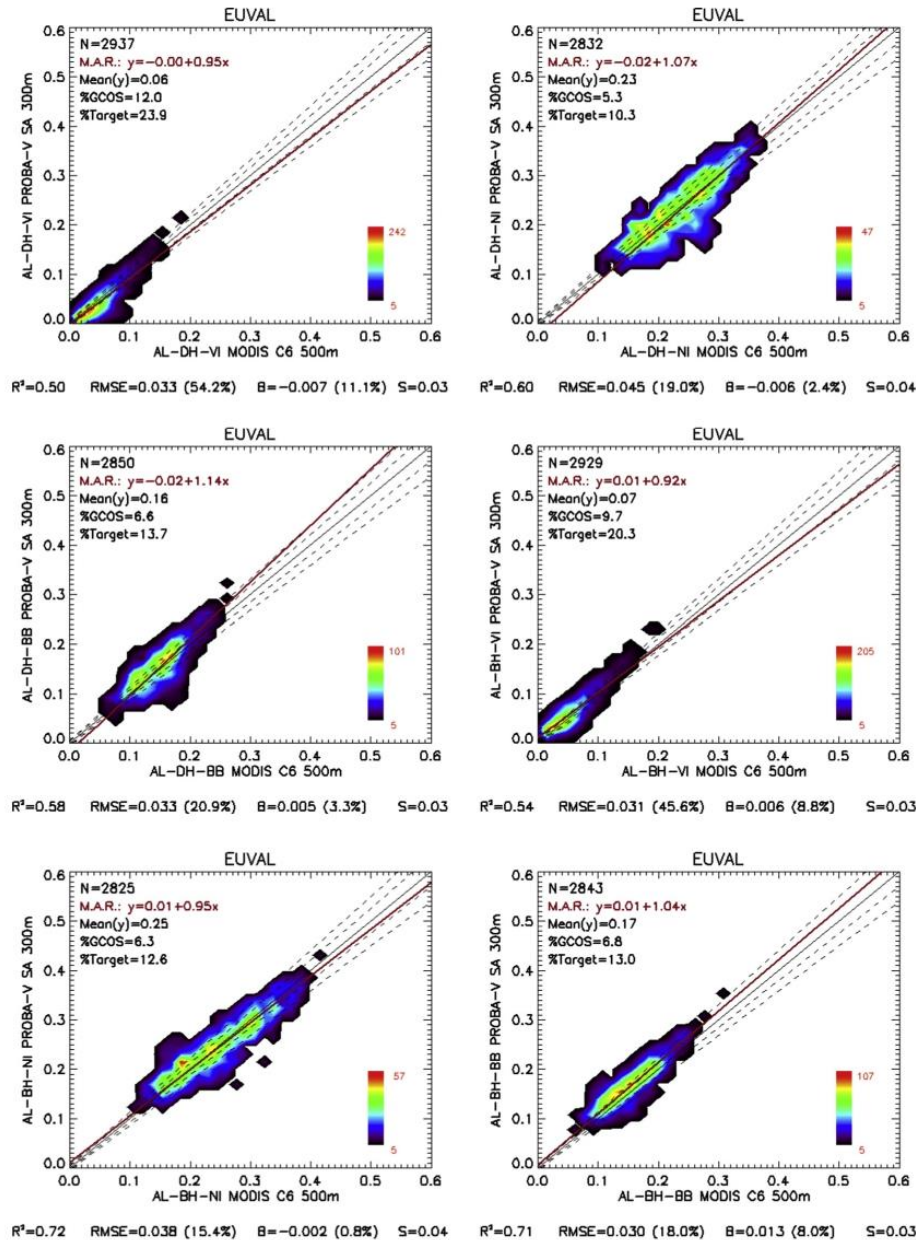


Fig. 12. Black-sky (Top) and White-Sky (Bottom) PROBA-V SA Collection 300 m versus MODIS C6 albedo products scatter-plots over all EUVAL sites during the 2014 year for PAR (left), NIR (center) and shortwave (right) domains. The terms B and S represent the mean and the standard deviation of the difference. Continuous black line corresponds to 1:1 line and dashed lines to GCOS uncertainty levels. Red line corresponds to the Major Axis Regression (MAR). (For interpretation of the references to colour in this figure legend, the reader is referred to the web version of this article.)

Over stationary targets like forests (e.g. *Billy Kriz Forest*, *Tharandt*), PROBA V products seems efficient for the reproduction, ditto MODIS C6 (Fig. 11). PROBA-V albedo shows however a slight seasonality in the bias, with larger values during the summer season. Over sites marked by topography (*Monte Bondone*, *Torgnon*), PROBA-V better agrees with

ground data. The surges in albedo values due to snow events in *Monte Bondone* and *Torgnon* were well captured by PROBA-V SA product. The case of *Brody* sites with crops also reveals the performance of PROBA-V product (Fig. 11).

Table 8

Relevant statistics between PROBA-V SA Collection 300 m versus MODIS C6 Albedos products over EUVAL sites for the 2014 year. *p*-value corresponds to the test on whether the slope is significantly different to 1.

PROBA-V SA Collection 300 m vs MODIS C6						
	AL-DH-VI	AL-DH-NI	AL-DH-BB	AL-BH-VI	AL-BH-NI	AL-BH-BB
Correlation (R ²)	0.5	0.6	0.58	0.54	0.72	0.71
Bias	-0.007	-0.006	0.005	0.006	-0.002	0.013
RMSE	0.033	0.045	0.033	0.031	0.038	0.03
Offset (MAR)	0	-0.0	-0.02	0.01	0.001	0.01
Slope (MAR)	0.95	1.07	1.14	0.92	0.95	1.04
<i>p</i> -Value	< 0.001	< 0.001	< 0.001	< 0.001	< 0.001	< 0.001
%optimal (GCOS)	12	5.3	6.6	9.7	6.3	6.8

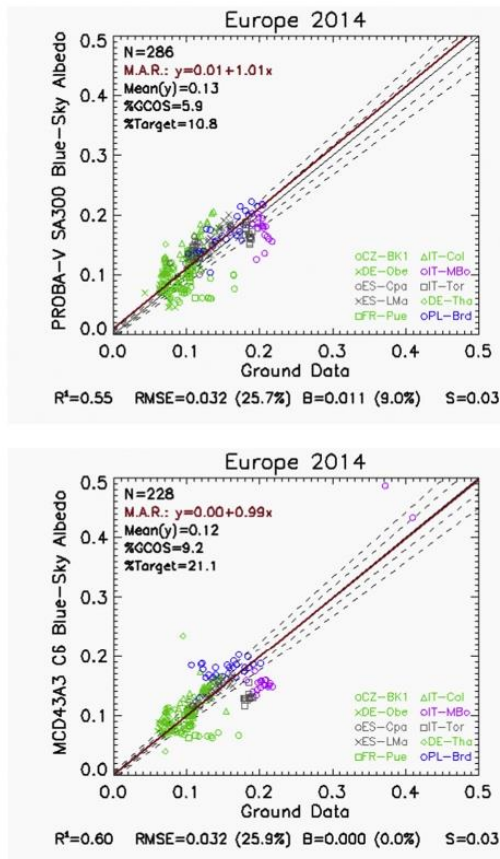


Fig. 13. Accuracy Assessment of PROBA-V SA Collection 300m (left) and MODIS MCD43A3 C6 (right) blue-sky albedo satellite products versus ground values coming from European stations during the 2014 year for Snow Free conditions. The terms B and S represent the mean and the standard deviation of the difference. Continuous black line corresponds to 1:1 line and dashed lines to GCOS uncertainty levels. Red line corresponds to the Major Axis Regression (MAR). (For interpretation of the references to colour in this figure legend, the reader is referred to the web version of this article.)

5.5. Overall statistical consistency and accuracy assessment

The overall consistency of the PROBA-V SA Collection 300m with reference MODIS C6 is resumed here with EUVAL sites for year 2014 (Fig. 12, Table 8).

For visible range, good overall consistency between PROBA-V and

MODIS C6 was found, with RMSE values around 0.03. It means PROBA-V is less than MODIS for low albedo values, mainly black-sky albedo. Slight negative bias (-0.007, 11%) was found for black-sky albedo, whereas the opposite trend (positive bias of 0.006, 9%) was observed for white-sky albedo. For the NIR, very good consistency was found, with RMSE values around 0.04 and very low negative mean bias (2.4% for AL-DH and 0.8% for AL-BH). Similar good results were found for Broad Band, showing low RMSE values of around 0.03 and low positive mean bias (< 8%). Different slopes were observed. This is reliant to the spectral albedo: slope < 1 for PAR, slope > 1 for Broad Band, with different trend in the slope for NIR. Opposite trends were observed depending on the albedo type (slope > 1 for AL-DH and slope < 1 for AL-BH). In all cases, slopes significantly differed to 1 with statistical significance (*p*-value < 0.05). To go further in the investigation of the appropriateness of the satellite albedo products (diagnosing “blue-sky” albedo), scatter plots versus field measurements were produced for the whole 2014 year over 10 EFDC sites of different vegetation types (Fig. 13, Table 9). Note that the number of samples (N = 286 in case of PROBA-V against N = 228 in case of MODIS C6) indicates the better completeness of PROBA-V, as already observed on the temporal profiles (Fig. 11), on which PROBA-V provides large number of retrievals. Overall accuracy of RMSE = 0.032 was found for PROBA-V SA Collection 300 m products, showing the same result in terms of RMSE as MODIS C6. Slight positive mean bias of 0.01 (9%) of PROBA-V SA Collection 300 m was found, showing improved results in case of MODIS C6, with no bias and relationship very close to the 1:1 line. In spite of positive results, the low percentage of pixels within GCOS requirements (5.9% in case of PROBA-V and 9.2% in case of MODIS C6) outlines the difficulty to achieve the requirements.

5.6. TOC-R product

Alongside developments on surface albedo, the normalized reflectance TOC-R appears as a surrogate for any application not necessarily reliant on the radiation transfer and energy budget. Such product targets a broad category of users eager to consider PROBA-V radiometry to catch up the phenology. A product like TOC-R is difficult to validate because it relies to a specific geometry serving for reference that should be obtained from ground using narrow field of view. In the case of PROBA-V, the TOC-R product required by users corresponds to a reflectance that would be measured at 10 AM local time. In practice, such virtual reflectance is obtained by using the adjusted BRDF coefficients to simulate it. In the case of MODIS, the strategy is different since the distributed normalized reflectance is a nadir BRDF-Adjusted Reflectance (NBAR). Furthermore, PROBA-V and MODIS spectra are not matching. Therefore, the option herein was to rather cross-compare NDVI products elaborated from TOC-R (PROBA-V) or NBAR (MODIS). To be noticed that the spatial resolution of PROBA-V is 300 m against 500 m for MODIS. Fig. 14 shows for the whole year 2014 the NDVI temporal profiles for varied land units belonging to different locations (France, Spain, Italy, UK, Tunisia).

J.-L. Roujean et al.

Remote Sensing of Environment 215 (2018) 57–73

Table 9

Relevant statistics of the Accuracy Assessment of PROBA-V SA Collection 300 m (left) and MODIS MCD43A3 C6 (right) blue-sky albedo satellite products versus ground values coming from European stations during the 2014 year for Snow Free conditions. *p*-value corresponds to the test on whether the slope is significantly different to 1.

	EFDC SITES (2014)	
	PROBA-V SA Collection 300 m	MCD43A3 C6
Correlation (R ²)	0.55	0.60
Bias	0.011	0.000
RMSE	0.032	0.032
Offset (MAR)	0.01	0.00
Slope (MAR)	1.01	0.99
<i>p</i> -value	0.784	0.919
%optimal (GCOS)	5.9	9.2

Twofold PROBA-V NDVI profiles are shown whenever considering the end of the composite period given in file name or accounting for Z_Age information. Significant shift in time is noticed. The cross-comparison with MODIS remains qualitative as long it is not the same spatial resolution. The cultivated site of Barrax (Spain) mirrors the same seasonal patterns for all plotted NDVI, with closest profile to MODIS C6 using PROBA-V Z_Age. Missing data are conspicuous for MODIS due to discarding data based on Quality Assurance. The NDVI of Chimbolton (UK) is garbled by cloudiness. But despite two sensors (TERRA and AQUA) against one sensor for PROBA-V, MODIS displays less and more erratic NDVI products. The site of Merguellil (Tunisia) with crops reveals a good correlation between MODIS and PROBA-V (using Z_Age) except at the onset where a bias is noticed. MODIS NDVI is above PROBA-V during winter months. Same conclusion applies for the deciduous forest of Harth (France) and the rice crop of Albufera (Spain). This remains valid for the cropped area of Castellaro (Italy) where PROBA-V NDVI shows at the onset a first vegetation peak not clearly depicted by MODIS C6. It follows shared features for a plateau and the decay.

6. Summary and future prospects

An initiative was undertaken to provide operational global estimates of the surface albedo (SA) and TOC-R 300 m and 1 km fields in the framework of the Global Land Service (GLS) of Copernicus. It is represented by the PROBA-V Collection 1. From the outcomes of the present study, it clearly offers a great potential in agricultural area for instance. It is glimpsed that product would improve owing to a better cloud detection, particularly ice cloud removal - at the contrary of MODIS no thermal band exists for PROBA V - and aerosol signal correction. The occurrence to have ice cloud flagged as snow was noticed and can at least be solved by a temporal filter. Besides, the analysis was performed for snow free conditions because of the different strategy of temporal sampling between the two sensor systems. Therefore, the cross-comparison was limited to data sets ingestion beyond a value of 0.5 typically. The narrow to broadband conversion process also represents a possible source of future improvement for PROBA-V.

Time and space good consistency are noticed between the two sensors, with overall discrepancies (RMSE) of 0.03 for PAR and short-wave domains, and around 0.04 for NIR. PROBA-V Collection 300 m displayed reliable temporal trajectories, matching with temporal trend from MODIS C6 and daily ground observations. Smooth transitions may prevail as well as surges in albedo values, to be reasonably reproduced. The accuracy assessment performed over 10 EFDC homogeneous targets shows overall uncertainty (RMSE) of 0.032 with a mean bias of 0.01, which is about the same order as MODIS C6. Although this new production presents some spurious variability on short time scales, the comparison against MODIS C6 is deemed quite promising at this stage. It will even offer enhanced perspectives with next PROBA-V

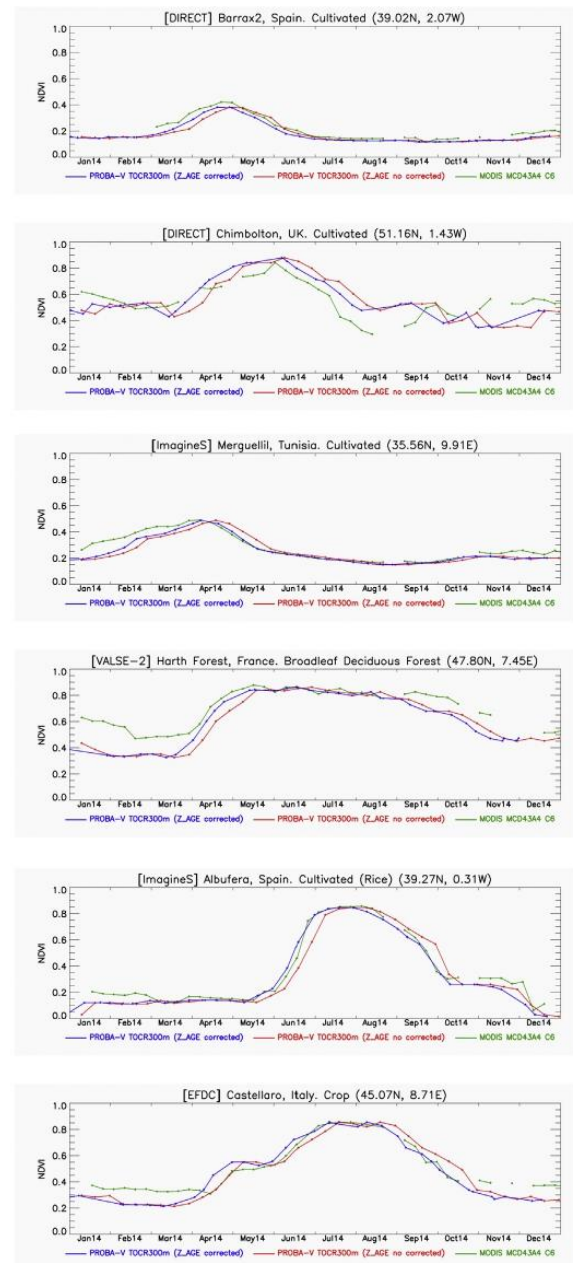


Fig. 14. Temporal profiles of PROBA-V TOC-R Collection 300 m using the date of the end of the composite period given in file name (blue) and the date corrected from Z_age (red). The Nadir BRDF-Adjusted Reflectance MODIS C6 (MCD43A4) is reported (green). (For interpretation of the references to colour in this figure legend, the reader is referred to the web version of this article.)

Collections, owing to users feedbacks. The TOC-R product was analyzed through NDVI for cross-comparing with MODIS. The Z_Age field improves the matching between the two sensors. Less number of outliers is noticed for PROBA-V due to the recurrent strategy applied. The existing bias with MODIS for the wintertime quiescent period is due to the use of a slant path as reference in the case of PROBA-V, which seems

J.-L. Roujean et al.

Remote Sensing of Environment 215 (2018) 57–73

to offer more dynamic on the phenology.

Acknowledgements

“This work was initiated under the FP7 Imagines project and thereafter continued and delivered through the land service of Copernicus, the Earth Observation program of the European Commission. The research leading to the current version of the product has received funding from various European Commission Research and Technical Development programs. The product is based on PROBA-V 300m data ((c) ESA and distributed by VITO).”

References

- Baret, F., Hagolle, O., Geiger, B., Bicheron, P., Miras, B., Huc, M., Berthelot, B., Weiss, M., Samain, O., Roujean, J.-L., Leroy, M., 2007. LAI, fAPAR and fCover CYCLOPES global products derived from VEGETATION. Part 1: principles of the algorithm. *Remote Sens. Environ.* 110, 275–286.
- Barnsley, M.J., Strahler, A.H., Morris, K.P., Muller, J.P., 1994. Sampling the surface bidirectional reflectance distribution function (BRDF): evaluation of current and future satellite sensors. *Remote Sens. Rev.* 8, 271–311.
- Cescatti, A., Marcolla, B., Vannan, S.K.S., Pan, J.Y., Roman, M.O., Yang, X., Ciaï, P., Cook, R.B., Law, B.E., Matteucci, G., Migliavacca, M., Moors, E., Richardson, A.D., Seufert, G., Schaaf, C.B., 2012. Intercomparison of MODIS albedo retrievals and in situ measurements across the global FLUXNET network. *Remote Sens. Environ.* 121, 323–334.
- Dierckx, W., Sterckx, S., Benhadj, I., Livens, S., Duhoux, G., Van Achteren, T., ... Saint, G., 2014. PROBA-V mission for global vegetation monitoring: standard products and image quality. *Int. J. Remote Sens.* 35 (7), 2589–2614.
- GCOS-154, 2016. Systematic Observation Requirements for Satellite-based Products for Climate Supplemental Details to the Satellite-based Component of the Implementation Plan for the Global Observing System for Climate in Support of the UNFCCC - 2016 Update. WMO, Geneva, Switzerland.
- Geiger, B., Carrer, D., Franchisteguy, L., Roujean, J.L., Meurey, C., 2008. Land surface albedo derived on a daily basis from Meteosat Second Generation observations. *IEEE Transactions on Geoscience and Remote Sensing* 46 (11), 3841–3856.
- Hagolle, O., Lobo, A., Maisongrande, P., Cabot, F., Duchemin, B., de Pereyra, A., 2004. Quality assessment and improvement of temporally composited products of remotely sensed imagery by combination of VEGETATION 1 & 2 images. *Remote Sens. Environ.* 94, 172–186.
- Hook, S.J., 1998. *ASTER Spectral Library*. <https://speclib.jpl.nasa.gov/>.
- Hu, B., Lucht, W., Li, X., Strahler, A.H., 1997. Validation of kernel-driven models for global modeling of bidirectional reflectance. *Remote Sens. Environ.* 62, 201–214.
- Jin, Y., Gao, F., Schaaf, C.B., Li, X., Strahler, A.H., Bruegge, C.J., Martonchik, J.V., 2002. Improving MODIS surface BRDF/albedo retrieval with MISR multiangle observations. *IEEE Trans. Geosci. Remote Sens.* 40, 1593–1604.
- Justice, C.O., et al., 1998. The moderate resolution imaging spectroradiometer (MODIS): land remote sensing for global change research. *IEEE Trans. Geosci. Remote Sens.* 36, 1228–1249.
- van Leeuwen, W., Roujean, J.-L., 2002. Land surface albedo from the synergistic use of polar (EPS) and geo-stationary (MSG) observing systems. An assessment of physical uncertainties. *Remote Sensing of Environment* 81, 273–289.
- Leroy, M., Deuzé, J.L., Bréon, F.M., Hauteceur, O., Herman, M., Buriez, J.C., Tanré, D., Bouffès, S., Chazette, P., Roujean, J.L., 1997. Retrieval of atmospheric properties and surface bidirectional reflectances over the land from POLDER/ADEOS. *J. Geophys. Res.* 102 (D14), 17023–17037.
- Li, X., Gao, F., Wang, J., Strahler, A., 2001. A priori knowledge accumulation and its application to linear BRDF model inversion. *J. Geophys. Res.* 106 (D11), 11925–11935.
- Liang, S., Strahler, A.H., Walthall, C., 1999. Retrieval of land surface albedo from satellite observations: a simulation study. *J. Appl. Meteorol.* 38, 712–725.
- Lucht, W., Lewis, P., 2000. Theoretical noise sensitivity of BRDF and albedo retrieval from the EOS-MODIS and MISR sensors with respect to angular sampling. *Int. J. Remote Sens.* 21 (1), 81–98.
- Lucht, W., Roujean, J.L., 2000. Considerations in the parametric modeling of BRDF and albedo from multiangular satellite sensor observations. *Remote Sens. Rev.* 18, 343–379.
- Muller, J.-P., et al., 2012. The ESA GlobAlbedo Project for Mapping the Earth's Land Surface Albedo for 15 Years From European Sensors. Paper Presented at IEEE Geoscience and Remote Sensing Symposium (IGARSS) 2012. IEEE, Munich, Germany (22-27.7.12).
- Pokrovsky, I.O., Pokrovsky, O.M., Roujean, J.-L., 2003. Development of an operational procedure to estimate surface albedo from the SEVIRI/MSG observing system in using POLDER BRDF measurements. *Remote Sens. Environ.* 87, 198–242.
- Press, W.H., Teukolsky, S.A., Vetterling, W.T., Flannery, B.P., 1995. *Numerical Recipes in Fortran*. Cambridge University Press.
- Rahman, H., Dedieu, G., 1994. SMAC: a simplified method for the atmospheric correction of satellite measurements in the solar spectrum. *Int. J. Remote Sens.* 15, 123–143.
- Román, M.O., Schaaf, C., Woodcock, C., et al., 2009. The MODIS (collection V005) BRDF/albedo product: assessment of spatial representativeness over forested landscapes. *Remote Sens. Environ.* 113 (11).
- Roujean, J.-L., Leroy, M., Deschamps, P.-Y., 1992. A bidirectional reflectance model of the Earth's surface for the correction of remote sensing data. *J. Geophys. Res.* 97 (D18), 20455–20468.
- Samain, O., Geiger, B., Roujean, J.-L., 2006. Spectral normalization and fusion of optical sensors for the retrieval of BRDF and albedo: application to VEGETATION, MODIS and MERIS data sets. *IEEE Trans. Geosci. Remote Sens.* 44 (11, Part 1), 3166–3179.
- Schaepman-Strub, G., Schaepman, M.E., Painter, T.H., Dangel, S., Martonchik, J.V., 2006. Reflectance quantities in optical remote sensing—definitions and case studies. *Remote sensing of environment* 103 (1), 27–42.
- Sterckx, S., Benhadj, I., Duhoux, G., Livens, S., Dierckx, W., Goor, E., ... Nackaerts, K., 2014. The PROBA-V mission: image processing and calibration. *International journal of remote sensing* 35 (7), 2565–2588.
- Strahler, A.H., 1994. *Vegetation Canopy Reflectance Modeling - Recent Developments and Remote Sensing Perspectives*. Proceedings of the 6th International Symposium on Physical Measurements and Signatures in Remote Sensing, 593–600.
- Strahler, A.H., Muller, J.P., et al., 1999. MODIS BRDF/Albedo Product: Algorithm Theoretical Basis Document, Version 5.0.
- Stroeve, J.C., Nolin, A.W., 2002. New methods to infer snow albedo from the MISR instrument with applications to the Greenland ice sheet. *IEEE Trans. Geosci. Remote Sens.* 40, 1616–1625.
- Sun, Q., Wang, Z., Li, Z., Erb, A., Schaaf, C.B., 2017. Evaluation of the global MODIS 30 arc-second spatially and temporally complete snow-free land surface albedo and reflectance anisotropy dataset. *Int. J. Appl. Earth Obs. Geoinf.* 58, 36–49.
- Verhoef, W., 1984. Light scattering by leaf layers with application to canopy reflectance modeling, the SAIL model. *Remote Sens. Environ.* 16, 125–141.
- Wang et al., 2018. Capturing rapid land surface dynamics with collection V006 MODIS BRDF/NBAR/albedo (MCD43) products. *Remote Sens. Environ.* 207, 50–64.
- Wanner, W., Li, X., Strahler, A.H., 1995. On the derivation of kernels for kernel-driven models of bidirectional reflectance. *J. Geophys. Res.* 100 (D10), 21077–21090.
- Wanner, W., Strahler, A., Hu, B., Lewis, P., Muller, J.-P., Li, X., Barker-Schaaf, C., Barnsley, M., 1997. Global retrieval of BRDF and albedo over land from EOS MODIS and MISR data: theory and algorithm. *J. Geophys. Res.* 102 (D14), 17143–17161.
- Wolters, E., Dierckx, W., Iordache, M.-D., Swinnen, E., February 2017. PROBA-V products user manual, version 2.1. http://habitat.vgt.vito.be/sites/default/files/PROBAV-Products_User_Manual_v2.1.pdf.



Anexo III – Copia de publicación 2



remote sensing



Article

Quality Assessment of PROBA-V Surface Albedo V1 for the Continuity of the Copernicus Climate Change Service**Jorge Sánchez-Zapero**^{1,*}, **Fernando Camacho**¹, **Enrique Martínez-Sánchez**¹, **Roselyne Lacaze**², **Dominique Carrer**³, **Florian Pinault**³, **Iskander Benhadj**⁴ and **Joaquín Muñoz-Sabater**⁵

¹ Earth Observation Laboratory (EOLAB), Parc Científic Universitat de València, C/Catedrático Augustín Escardino 9, 46980 Paterna (Valencia), Spain; fernando.camacho@eolab.es (F.C.); enrique.martinez@eolab.es (E.M.-S.)

² HYGEOs, Euratechnologies, 165 Avenue de Bretagne, 59000 Lille, France; rl@hygeos.com

³ Centre National de Recherches Météorologiques (CNRM), Université de Toulouse, Météo France, CNRS 42, Avenue Gaspard Coriolis, 31057 Toulouse, France; dominique.carrer@meteo.fr (D.C.); florian.pinault@meteo.fr (F.P.)

⁴ Flemish Institute for Technological Research (VITO), Remote Sensing Unit, Boeretang 200, B-2400 Mol, Belgium; iskander.benhadj@vito.be

⁵ European Centre for Medium-Range Weather Forecasts (ECMWF), Shinfield Road, Reading RG2 8JD, UK; joaquin.Munoz@ecmwf.int

* Correspondence: jorge.sanchez@eolab.es; Tel.: +34-963-769-448

Received: 15 July 2020; Accepted: 10 August 2020; Published: 12 August 2020



Abstract: The Copernicus Climate Change Service (C3S) includes estimates of Essential Climate Variables (ECVs) as a series of Climate Data Records (CDRs) derived from satellite data. The C3S Surface Albedo (SA) v1.0 CDR is composed of observations from National Oceanic and Atmospheric Administration (NOAA) Very High Resolution Radiometers (AVHRR) (1981–2005), and VEGETATION sensors onboard Satellites for the Observation of the Earth (SPOT/VGT) (1998–2014) and Project for Onboard Autonomy satellite (PROBA-V) (2014–2020), and will continue with Sentinel-3 (from 2020 onwards). The goal of this study is to assess the uncertainties associated with the C3S PROBA-V SA v1.0 product, with a focus on the transition from SPOT/VGT to PROBA-V. The methodology followed the good practices recommended by the Land Product Validation sub-group (LPV) of the Working Group on Calibration and Validation (WGCV) of the Committee on Earth Observing Satellites (CEOS) for the validation of satellite-derived global albedo products. Several performance criteria were evaluated, including an intercomparison with National Aeronautics and Space Agency (NASA) MCD43A3 C6 products. C3S PROBA-V SA v1.0 and MCD43A3 C6 showed similar completeness but had higher fractions of missing data than C3S SPOT/VGT SA v1.0. C3S PROBA-V SA v1.0 showed similar precision (~1%) to MCD43A3 C6, improving the results of SPOT/VGT SA v1.0 (2–3%), but C3S PROBA-V SA v1.0 provided residual noise in the near-infrared (NIR). Good spatio-temporal continuity between C3S PROBA-V and SPOT/VGT SA v1.0 products was found with a mean bias between $\pm 2\%$. The comparison with MCD43A3 C6 showed positive mean biases (5%, 8%, and 12% for visible, NIR and total shortwave, respectively). The accuracy assessment with ground measurements showed a median error of 18.4% with systematic overestimation (positive bias of 11.5%). The percentage of PROBA-V retrievals complying with the C3S target requirements was 28.6%.

Keywords: surface albedo; validation; PROBA-V; C3S; CEOS LPV; SPOT/VGT; MCD43

1. Introduction

The land surface albedo, which is defined as the ratio of the radiant flux reflected from the Earth's land surface to the incident flux, is a key forcing parameter controlling the planetary radiative energy budget and the partitioning of the radiative energy between the atmosphere and surface. The surface albedo varies in space and time as a result of both natural processes (e.g., solar illumination, snowfall, and vegetation growth) and human activities (e.g., the clearing and replanting of forests, the sowing and harvesting of crops, and the burning and grazing of rangelands) and is a sensitive indicator of environmental vulnerability [1]. Consequently, a long-term record of the surface albedo for the global landmass is required by climate, biogeochemical, hydrological, and weather forecast, models at a range of spatial (from a few meters to 30 km) and temporal (from daily to monthly) scales, and it is therefore, mandatory to quantitatively, and efficiently assess the uncertainties in SA measurement using these products.

The European's Union funded C3S [2] provides key indicators on climate change drivers by means of combining the observations of the climate system with the latest science to develop authoritative, quality-assured information about the past, current and future states of the climate. The C3S portfolio includes consistent estimates of multiple Essential Climate Variables (ECVs), including the surface albedo, which is primarily based on satellite data and provided as a series of gridded CDRs. In the frame of C3S, SA products have been derived from the data collected by NOAA/AVHRR (1981–2005) and SPOT/VGT (1998–2014). The Project for Onboard Autonomy satellite (PROBA-V) satellite [3], which was launched on May 2013 for seven years, was designed to bridge the gap in space-borne vegetation observation between SPOT/VGT (March 1998–May 2014) and the Sentinel-3 satellites. PROBA-V is comparable to the VGT sensors on SPOT platforms. In C3S, the PROBA-V SA v1.0 products are generated with the aim to extend the CDRs based on AVHRR and VGT observations over time. The algorithms for these C3S SA products were designed by Meteo-France based on previous research conducted within the Satellite Application Facility for Land Surface Analysis (LSA SAF) program of EUMETSAT [4,5]. Meteo-France developed the SA algorithms, Refs. [6–9] based on MSG/SEVIRI and MetOp/AVHRR within the EUMETSAT LSA SAF program, and were later adapted to these other sensors in C3S and Copernicus Global Land Service (CGLS) [10]. These products are generated by the processing line infrastructure implemented by VITO and openly distributed through the C3S Climate Data Store (CDS) [11].

Within the C3S CDS, a framework for the Evaluation and Quality Control (EQC) of climate data products derived from satellite and in situ observations to be catalogued was developed [12]. Validation, or quality assessment, is one of the main components defined in this EQC framework, and it is defined as the process of independently assessing the quality of the data products derived from the system outputs [13]. In terms of satellite-derived land products, validation is the procedure to assess their accuracy and quantify their uncertainties via analytical comparisons with reference data. Validation also constitutes the means of guaranteeing the compliance of products with user requirements, and helps end-users understand to what extent the product is suitable for their specific applications [14]. Based on previous validation works, mainly based on NASA products [15–19], but also on EUMETSAT [7], the CEOS WGCV LPV sub-group [20] has defined the global albedo product validation good practices [21]. Two main validation approaches have been defined: (i) The quantitative and qualitative product-to-product validation approach, which is referred to as satellite product intercomparison (i.e., indirect validation); and (ii) the direct point-to-pixel validation, which involves comparisons of satellite products with the albedo measured from in situ tower-based instruments (i.e., direct validation).

Indirect validation is helpful because most validation metrics cannot be computed using ground data, due to the limitations of ground measurements in terms of global conditions. Indirect validation approach mainly consists of comparing satellite-derived albedo products, particularly new products, with heritage albedo products [7,22–28]. In general, product intercomparison offers a means of assessing the discrepancies (systematic or random) between products. This method is particularly

valuable for finding spatial disagreements between products over large areas and for a wide range of cover types. However, this approach does not yield absolute validation results, and satellite product intercomparisons alone are insufficient to validate a new product. Then, direct validation enables the assessment of uncertainties, and it may be argued that only such methods can be seen as actual validation in the field of remote sensing [29]. Direct validation consists of comparing satellite retrievals with in-situ albedo measurements [30]. It is, therefore, mandatory to evaluate the spatial representativeness of ground albedo measurements, which depends on the land surface heterogeneity [31–34].

As the PROBA-V mission is arriving at the end of its lifetime, the aim of this paper is to perform the full quality assessment of PROBA-V based C3S SA v1.0 products. To achieve that, the main objectives are the following:

1. To evaluate the product completeness and spatio-temporal consistency of C3S PROBA-V SA v1.0 products over global conditions compared to SPOT/VGT SA v1.0 (and MCD43A3 C6 for benchmarking) to verify the continuity of the C3S time series;
2. To assess the precision of C3S PROBA-V SA v1.0 and to intercompare it with reference satellite products (C3S SPOT/VGT SA v1.0 and MCD43A3 C6);
3. To assess the accuracy and the associated uncertainties of the products via direct validation with ground measurements; and
4. To assess the compliance of the product with regards to climate user requirements.

The remainder of this paper is structured as follows: Sections 2 and 3 describe the datasets used in the study, which are for satellite-based products and ground data, respectively; Section 4 presents the validation methodology; Sections 5 and 6 gather and discuss the intercomparison and validation results, respectively; and the conclusions are summarized in Section 7.

2. Remote Sensing Surface Albedo Products

The main features of the three SA products investigated in this work (C3S PROBA-V SA v1.0, C3S SPOT/VGT SA v1.0 and MCD43A3 C6) are summarized in Table 1. The information of the spectral characteristics of the four optical bands of the VEGETATION sensors onboard the PROBA and SPOT satellites, and its equivalent Moderate resolution Imaging Spectroradiometer (MODIS) bands, is provided in Table 2.

Table 1. Characteristics of the global remote sensing SA products under study. GSD stands for Ground Sampling Distance.

Product	Satellite /Sensor	BRDF Model: Volumetric /Geometrical Kernels	Frequency /Composite Period	GSD /Projection	Reference
C3S PROBA-V SA v1.0	PROBA /VEGETATION	Ross_Thick /Roujean	10 days /30 days	1 km /Plate Carrée	[35]
C3S SPOT/VGT SA v1.0	SPOT /VEGETATION	Ross_Thick /Li_Sparse_Reciprocal	10 days /20 days	1 km /Plate Carrée	[36]
NASA MCD43A3 C6	TERRA+AQUA /MODIS	Ross_Thick /Li_Sparse_Reciprocal	Daily /16 days	500 m /Sinusoidal	[37]

Table 2. Spectral characteristics of PROBA-V, and its equivalent channels in the VGT-2 and MODIS sensors.

	PROBA-V			VGT-2			MODIS		
	Acronym	Center (nm)	Width (nm)	Acronym	Center (nm)	Width (nm)	Acronym	Center (nm)	Width (nm)
Blue	B0	463	46	B0	458	37	Band3	489	20
Red	B2	655	79	B2	653	74	Band1	645	50
NIR	B3	845	144	B3	838	109	Band2	858.5	35
SWIR	MIR	1600	73	MIR	1635	101	Band6	1639	24

The quality flag information of each product was used to filter low-quality pixels (Table 3). For the C3S PROBA-V SA v1.0 products, the land pixels showing an input status “out of range” or “invalid” or “saturated” in the B2 and B0 channels were discarded. The SPOT/VGT SA v1.0 pixels where the algorithm failed were not considered in the validation exercise. Additionally, two ancillary variables were also taken into account: The uncertainty (ERR) and the mean age (AGE, in number of days) of the observations that are used to produce the SA. The SPOT/VGT SA v1.0 pixels with associated uncertainty greater than 0.2 and an AGE greater than 20 were discarded. For MODIS C6, the quality flags are given in the MCD43A2 product, and those pixels with fewer than seven valid observations were discarded.

Table 3. Quality flag (QFLAG) information used to filter pixels flagged as ‘low-quality’.

Product	Quality Control Used to Discard Pixels
C3S PROBA-V SA v1.0	Sea (bit 1) Input status out of range or invalid (bit 6) B2 saturated (bit 10) B0 saturated (bit 11)
C3S SPOT/VGT SA v1.0	Sea and continental water (bits 0-1 of QFLAG) Algorithm Failed (bit 6 of QFLAG) ERR > 0.2 AGE > 20
MCD43A2 C6	BRDF_Albedo_Band_Quality_Band1-7: Magnitude inversion (number of observations lower than 7)

2.1. Evaluated Dataset: C3S SA v1.0 Based on PROBA-V Data

PROBA-V has operated since May 2013 at an altitude of 820 km in a sun-synchronous orbit with a local overpass time at launch of 10:45 a.m. However, because the satellite has no onboard propellant, this local overpass time gradually differs from the at-launch value [3]. The payload consists of three identical cameras, which are equipped with a very compact Three Mirror Anastigmat telescope. Each camera has two focal planes, one for the short-wave infrared (SWIR) and one for the visible and near-infrared (VNIR) bands, with a slightly different off-nadir along track viewing direction. PROBA-V observes four spectral bands: Blue (called B0: centered at 0.463 μm), Red (B1: 0.655 μm), NIR (B2: 0.845 μm), and SWIR (MIR: 1.600 μm). The target on the ground is imaged at different times and with different viewing angles. This specific technical concept makes the angular configurations of the observations in the VNIR and SWIR bands different, and hence, different angular information is provided. Observations are taken at resolutions from 100 to 180 m at nadir and up to 350 m and 660 m at the swath extremes for the VNIR and SWIR channels, respectively [38]. The final PROBA-V data [39], disseminated by the PROBA-V Ground Segment at 100 m, 300 m and 1 km resolutions, have been available on [40] since the end of 2013.

The C3S PROBA-V SA v1.0 products (example in Figure 1) are freely available in the C3S CDS [11]. They also provide Directional-Hemispherical albedos (AL-DH)—also called Black-Sky Albedo (BSA)—and the Bi-Hemispherical albedos (AL-BH)—also called White-Sky Albedo (WSA)—in three broadband spectral domains (visible [VI: 0.4–0.7 μm], NIR [NI: 0.7–4 μm] and total shortwave [BB: 0.3–4 μm]). These broadband albedos are taken from the CGLS [10]. In addition, the spectral AL-DH and AL-BH albedos in the four spectral channels (see Table 2) are made available in the C3S. These products have been produced every 10 days from the end of 2013 onwards, with the production dates on the 3rd, 13th, and 23rd of each month and delivered with a 12 day lag in near real-time. The spatial resolution of the grid is $1/112^\circ$, resulting in a pixel size of approximately 1 km at the equator. Apart from the layers corresponding to albedo retrievals, the ancillary layers corresponding to their respective errors (ERRs), the associated quality flag (QFLAG) and the number of valid observations during the synthesis period (NMOD) are provided. The information of each layer is described in the Product User Guide and Specification (PUGS) document [41].

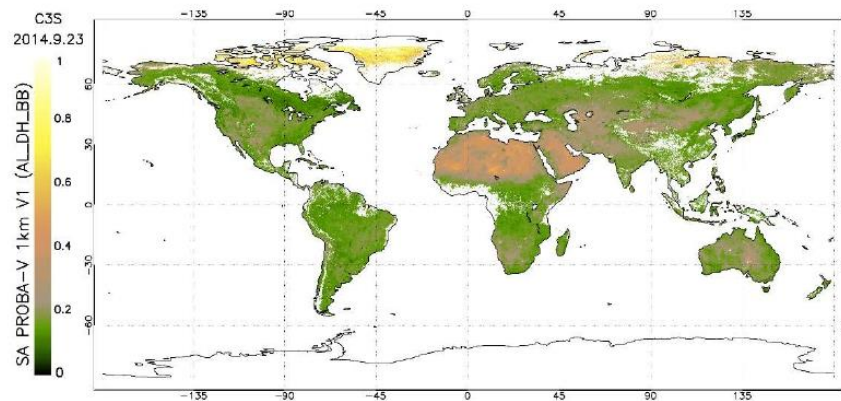


Figure 1. Global distribution of PROBA-V SA v1.0 black-sky albedo values in the total shortwave (AL-DH-BB) on 23 September 2014.

The methodology, which is described in the Algorithm Theoretical Basis Document (ATBD) [35], follows the approach of separating the atmospheric correction, directional reflectance normalization, and albedo determination. First, the top-of-atmosphere (TOA) data are processed to obtain the cloud-free top-of-canopy (TOC) reflectances. Then, the spectral TOC reflectances acquired under different solar-viewing configurations during the synthesis period are normalized by inverting a linear kernel-driven model [42]. The synthesis period is 30 day and a semi-Gaussian weighting function with the maximum weight on the last observation of the period was selected for near real-time production. Then, the spectral albedos are computed using the angular integration of the kernel functions with the retrieved parameters for each pixel. Finally, the broadband albedo is defined as a linear combination of the spectral albedo values in the available spectral channels. The narrow to broadband conversion coefficients are applied both for the black-sky and for the white-sky albedos.

2.2. C3S SA v1.0 Based on SPOT/VGT Data

C3S SPOT/VGT SA v1.0, which is available from C3S CDS [11], provides a CDR of the global black-sky and white-sky albedo estimates for the period from 1999 to 2014 at a ground sampling distance of $1/112^\circ$ and a temporal frequency of 10 days using a compositing window of 20 days. The dates of production are the 10th, 20th and 30th of each month. As for PROBA-V, the albedo quantities are provided for the three broadband domains (visible [0.4–0.7 μm], NIR [0.7–4 μm] and total shortwave [0.3–4 μm]) and in the four spectral channels (see Table 2) of the VEGETATION sensors.

The albedo products are based on the data acquired by the VEGETATION-1 and VEGETATION-2 sensors aboard the SPOT-4 and SPOT-5 satellites, respectively.

The retrieval algorithm [6,7,9] was developed based on the previous developments of the SA products [6–9] based on MSG/SEVIRI and Metop/AVHRR in the framework of the EUMETSAT LSA SAF project [4], and it was later adapted here to these other sensors in CGLS and C3S [43]. The input data were Collection 3 of SPOT/VGT, which corrects the bug previously detected regarding the incorrect calculation of the Sun-Earth distance of Collection 2, includes improved cloud and snow/ice detection, and revises the absolute radiometric calibration for the entire archive [44]. The main differences with the C3S PROBA-V SA v1.0 algorithm are related to the use of a different Bidirectional Reflectance Distribution Function (BRDF) model and temporal composite scheme. PROBA-V SA v1.0 implemented the Ross_Thick kernel for volumetric scattering and the Roujean kernel for geometric scattering [42], whereas SPOT/VGT SA v1.0 implemented the Ross_Thick kernel [42] for volumetric scattering and the Li_Sparse_Reciprocal kernel for geometrical scattering [45]. The synthesis period of PROBA-V SA v1.0 is 30 days using a semi-Gaussian weighting function. The SPOT/VGT SA v1.0 retrieval methodology uses a 20-day temporal composite, meaning that each surface albedo product is built from the valid SPOT/VGT observations corresponding to the 20-day period preceding the calculation date. At the BRDF inversion step, the previous inversion result is used as a priori information. Hence, a recursive temporal composition of the information over a longer time period (approximately three times longer than the production period) can be achieved to guarantee the coherence and spatial completeness of the product. The “age” (AGE parameter in the output product) of the clear-sky observations exploited in the recursive inversion scheme is an important piece of information for potential applications, and is therefore, also made available to users. This age corresponds to the mean age with respect to the date of the calculation of the clear observations considered for the albedo calculation. More details are given in the ATBD [36].

Sánchez-Zapero et al. [46] showed that the C3S SPOT/VGT SA v1.0 products were good quality based on most of the criteria evaluated, reaching validated stage 1 in the CEOS LPV hierarchy. However, two main limitations were found: (i) Some temporal noise existed at the short-time scale; and (ii) the product was not able to capture some snow events, showing large uncertainties (>0.2) in those cases. Comparisons with ground measurements (461 samples, 2000–2005 period) from 15 FLUXNET stations showed similar overall uncertainty (RMSD = 0.05) as other satellite products (MCD43A3 C6, GlobAlbedo, and GLASS), but a positive bias (14%) was found.

2.3. NASA MCD43 C6 Based on MODIS Data

The MODIS BRDF/Albedo (MCD43A3) Collection 6 (C6) dataset, which is available from [47], provides both directional albedo at local solar noon and bi-hemispherical albedo for MODIS bands 1–7 and for three broadbands (visible [0.3–0.7 μm], NIR [0.7–5.0 μm], and total shortwave [0.3–5.0 μm]). The MCD43A3 albedo quantities are delivered at a resolution of 500 m in a sinusoidal projection. They have been produced every day since 2000 with a synthesis period of 16 days. Data from both Terra and Aqua satellites are used in the generation of this product.

The MODIS albedo algorithm uses atmospherically corrected reflectance data (MOD09 product) to establish the best fit to a linear kernel-driven BRDF model, with the exception of the observations flagged as “cloud”, “cirrus high” or “aerosol high”. Like for C3S SPOT/VGT SA v1.0, the parametric BRDF model uses the Ross_Thick kernel for volumetric scattering and the Li_Sparse_Reciprocal kernel for geometrical scattering [45,48]. A full retrieval of the model is attempted if there are seven or more high-quality observations well distributed over the viewing hemisphere during the 16 day synthesis period. When the number of observations is strictly less than seven and strictly greater than two, or if observations are not well sampled or do not well fit the BRDF model, a back-up algorithm with prior information is used. Then, a fill value is stored if the number of observations is strictly less than three, and the separated snow-free gap-filled products are also accessible [49]. Then, the BRDF model parameters are used for estimating spectral albedos from angular integration. The broadband albedos

are computed using the spectral to broadband conversion approach [50]. The MCD43 C6 products use an improved back-up database, which is pixel-based updated from the latest full inversion as opposed to the land cover-based database used in the previous Collection 5.

MCD43A3 SA products have reached CEOS LPV validation stage 3 [51]. Sánchez-Zapero et al. [46] reported an overall uncertainty (RMSD) of 0.053 and a low negative bias (−11.9%) of MCD43A3 C6 compared with the ground data from 15 FLUXNET homogeneous sites for the 2000–2005 period (653 samples), and a slight overall uncertainty (RMSD = 0.032) was reported compared with European FLUXNET measurements over snow-free conditions [52]. Existing studies of the previous collection 5 indicate that the accuracy of the MODIS shortwave broadband albedo meets the requirements (<5%) for both snow-free and snow-covered surfaces [31–34].

3. Ground Dataset

3.1. Ground-Based Observations for Validation (GBOV) Database

The CGLS GBOV [53] initiative aims at facilitating the use of observations from operational ground-based monitoring networks and their comparison to Earth Observation (EO) products. In the case of the SA, GBOV provides the Reference Measurements (RMs) and upscaled Land Products (LPs) based on the RM data [54,55] from over 24 sites coming from different networks, such as BSRN, FLUXNET, or SURFRAD. Currently, the GBOV database is made available for the 2012–2018 period [53]. The RM GBOV data corresponds to blue-sky albedo, which is defined as the fraction between the downward and the upward shortwave radiative flux. The diffuse fraction is also included in the RM dataset.

The innovative approach for the generation of GBOV LPs could be very useful for the validation of satellite SA products since it can be applied to both homogeneous and heterogeneous land surfaces. However, we can expect large discrepancies over heterogeneous sites compared to homogeneous sites [54,56]. The CEOS LPV albedo validation protocol [21] recommends the use of ground values measured at the flux tower (i.e., the RM) for the direct validation of EO products. For those reasons, GBOV RMs are used in this study for the accuracy assessment. Note that RMs are provided daily in the GBOV database with a typical temporal step of 30 or 1 min depending on the station. The estimation of the uncertainty associated with a solar radiation measurement by a commercial pyranometer is around 5% (at a 95% confidence level) for daily values under ideal conditions [57]. Since satellite products are defined to provide SA retrievals at solar local noon, the RMs used in this study have been taken at the same time. For this study, the concomitant period to PROBA-V was used (i.e., 2014–2018). The main characteristics of the 20 GBOV sites providing the RMs at solar local noon for the period under study are summarized in Table 4.

3.2. Analysis of the Spatial Representativeness of Tower Measurements

The reference albedo measured from towers covers a circular footprint that varies with the tower height. It is unlikely that the footprint of the ground measurements exactly matches the satellite pixel sizes. Then, the spatial representativeness of the tower-based measurements should be evaluated to minimize the issues associated with spatial representativeness in the point-to-pixel comparison [31,32].

The semivariogram [58,59] is one of the most efficient tools for describing spatial representativeness. Semivariograms were computed for the stations under evaluation using Sentinel-2 surface reflectances at a spatial resolution of 10 m near-nadir. Two different periods (leaf-off and leaf-on) periods during the year were considered to evaluate the spatial representativeness of the region around the ground tower. The spatial attributes (e.g., the range, sill and nugget) were computed by fitting the variogram estimator to an isotropic spherical model [60], and they can reveal the spatial variability of land surfaces and the scaling effects associated with remotely sensed data [31–34,61–63]. The methodology adopted in this study for the estimation of the geostatistical indexes is based on the comparison of the variogram model parameters retrieved at different spatial resolutions (i.e., from 1.0 km² to 1.5 km²

squared subsets). Four different geostatistical attributes were used [16,32]: The relative coefficient of variation (R_{CV}), the scale requirement index (R_{SE}), the relative strength of the spatial correlation (R_{ST}) and the relative proportion of the structural variation (R_{SV}).

Table 4. Characteristics of the 20 GBOV sites providing data during the 2014–2018 period.

#	Site ID	Name	Country	Network	Land Cover	Lat (deg)	Lon (deg)
1	USA_BND	Bondville	USA	SURFRAD	Croplands	40.052	−88.373
2	USA_BAO	Boulder	USA	BSRN	Croplands	40.050	−105.004
3	BEL_BRA	Brasschaat	Belgium	FLUXNET	Mixed Forest	51.309	4.521
4	NET_CAB	Cabauw	Netherlands	BSRN	Grasslands	51.971	4.927
5	AUS_CLP	Calperum	Australia	FLUXNET	Shrublands	−34.003	140.588
6	USA_DRA	Desert Rock	USA	SURFRAD	Bare Soil	36.624	−116.019
7	USA_FPK	Fort Peck	USA	SURFRAD	Grasslands	48.308	−105.102
8	GER_GEB	Gebesee	Germany	FLUXNET	Croplands	51.100	10.914
9	NAM_GOB	Gobabeb	Namibia	BRSN	Bare Soil	−23.561	15.042
10	USA_GCM	Goodwin Creek	USA	SURFRAD	Deciduous Broadleaf	34.255	−89.873
11	FRA_GRI	Grignon	France	FLUXNET	Croplands	48.844	1.952
12	FRA_GUY	Guyflux	French Guyana	FLUXNET	Evergreen Broadleaf	5.279	−52.925
13	GER_HAI	Hainich	Germany	FLUXNET	Mixed Forest	51.070	10.450
14	USA_NRF	Niwot Ridge	USA	FLUXNET	Evergreen Needleleaf	40.033	−105.546
15	ITA_REN	Renon	Italy	FLUXNET	Evergreen Needleleaf	46.587	11.434
16	USA_PSU	Rock Springs	USA	SURFRAD	Deciduous Broadleaf	40.720	−77.931
17	USA_SFS	Sioux Falls	USA	SURFRAD	Croplands	43.730	−96.620
18	USA_SGP	Southern Great Plains	USA	FLUXNET	Croplands	36.606	−97.489
19	USA_TBL	Table Mountain	USA	SURFRAD	Bare soil and Rocks	40.125	−105.237
20	AUS_TMB	Tumbarumba	Australia	FLUXNET	Evergreen Broadleaf	−35.657	148.152

The four geostatistical attributes can be combined in a compact metric (ST_{score} [31,32], see Equation (1)), which represents a spatial representativeness score using R_{SE} as the primary marker and the others like secondary weights. When the spherical variogram model does not provide a good fit to the variogram estimator, another indicator (RAW_{score} [31,32], see Equation (2)) could be used to provide a spatial representativeness score, which is only based on the R_{CV} .

$$ST_{score} = \left(\frac{|R_{CV}| + |R_{ST}| + |R_{SV}|}{3} + R_{SE} \right)^{-1} \quad (1)$$

$$RAW_{score} = |2 R_{CV}|^{-1} \quad (2)$$

Both scores are directly proportional to the site representativeness. We consider that sites are heterogeneous or not spatially representative when both scores are lower than 2.0 (see Table 5) because large differences, due to spatial heterogeneity, are expected for scores below this threshold [16]. Based on it, the ground measurements coming from *Boulder* (USA_BAO), *Renon* (ITA_REN), *Rock Springs* (USA_PSU) and *Table Mountain* (USA_TBL) sites are not used for the accuracy assessment during the leaf-off seasonal period. In addition, the *Cabauw* (NET_CAB), *Goodwin Creek* (USA_GCM) and *Gobabeb* (NAM_GOB) sites were discarded during leaf-on seasonal period. Figure 2 shows two examples of sites of stations spatially representative (top side), and two examples of not spatially representative (bottom side).

Table 5. Geospatial statistics of the 20 selected GBOV sites for the accuracy assessment.

#	Site ID	Footprint (m)	Seasonal Period	R _{CV} (%)	R _{SE} (%)	R _{ST} (%)	R _{SV} (%)	ST _{score}	RAW _{score}
1	USA_BND	126	Leaf-off	5.24	42.63	-5.17	59.16	1.52	9.54
			Leaf-on	-4.56	48.50	2.84	37.10	1.58	10.9
2	USA_BAO	3788	Leaf-off	175.37	0.00	-3.30	-15.64	1.54	0.29
			Leaf-on	19.43	0.00	2.77	-44.65	4.49	2.57
3	BEL_BRA	505	Leaf-off	11.24	0.01	0.15	-4.37	19.02	4.45
			Leaf-on	12.74	0.06	-0.39	-14.61	10.74	3.93
4	NET_CAB	213	Leaf-off	11.31	0.00	-2.61	7.13	14.25	4.42
			Leaf-on	32.62	0.00	0.74	11.70	1.66	1.53
5	AUS_CLP	253	Leaf-off	-5.83	31.92	4.15	-4.62	2.72	8.58
			Leaf-on	-11.07	29.70	2.53	-3.13	2.83	4.52
6	USA_DRA	126	Single season	18.88	23.5	6.0	83.9	1.67	2.65
7	USA_FPK	126	Leaf-off	7.01	19.5	-2.03	-1.25	4.37	7.13
			Leaf-on	42.27	23.5	3.36	69.44	1.62	1.18
8	GER_GEB	76	Leaf-off	10.35	81.49	-1.70	41.86	1.01	4.83
			Leaf-on	-24.49	73.04	5.35	-13.41	1.14	2.04
9	NAM_GOB	10	Leaf-off	11.67	51.27	2.37	40.41	1.44	4.29
			Leaf-on	26.47	58.17	0.92	47.89	1.20	1.89
10	USA_GCM	126	Leaf-off	-17.17	75.3	2.94	10.00	1.17	2.91
			Leaf-on	30.21	75.2	-5.02	45.76	0.98	1.65
11	FRA_GRI	67	Leaf-off	5.30	68.84	-4.99	29.89	1.22	9.44
			Leaf-on	10.62	61.83	4.17	0.42	1.49	4.71
12	FRA_GUY	253	Single season	-0.72	7.85	2.47	-1.98	10.45	69.33
13	GER_HAI	530	Leaf-off	7.66	0.00	5.94	22.01	8.43	6.53
			Leaf-on	-6.37	0.00	1.94	7.40	19.11	7.85
14	USA_NRF	322	Leaf-off	-19.95	7.43	-12.98	-10.77	4.55	2.51
			Leaf-on	6.71	6.61	-7.07	3.28	8.13	7.45
15	ITA_REN	12	Leaf-off	59.74	15.75	7.80	84.41	1.51	0.84
			Leaf-on	21.44	32.85	-2.00	10.26	2.27	2.33
16	USA_PSU	126	Leaf-off	66.21	24.94	12.73	61.96	1.39	0.76
			Leaf-on	5.06	22.86	3.16	-14.45	3.29	9.89
17	USA_SFS	32	Leaf-off	7.33	75.5	1.56	-6.74	1.24	6.82
			Leaf-on	21.08	49.5	7.29	104.41	1.07	2.37
18	USA_SGP	152	Leaf-off	-14.76	37.13	-13.21	23.66	1.84	3.39
			Leaf-on	10.02	35.26	-10.84	104.30	1.30	4.99
19	USA_TBL	126	Leaf-off	26.68	69.72	-4.78	79.70	0.94	1.87
			Leaf-on	-17.46	64.91	6.59	-2.34	1.36	2.86
20	AUS_TMB	884	Single season	18.41	0.00	0.06	7.27	11.65	2.72

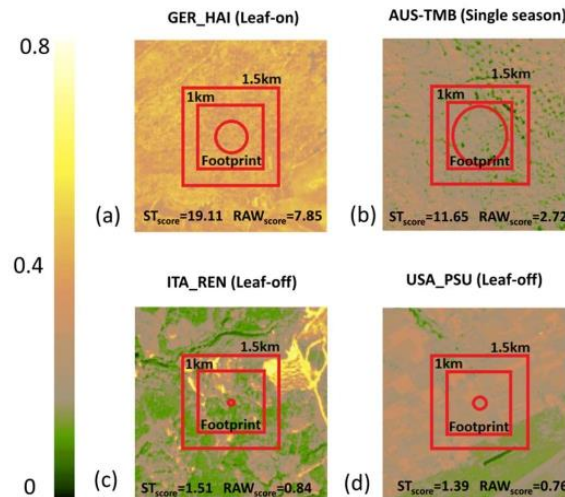


Figure 2. Sentinel-2 surface reflectance (Band 8A) images (3 km × 3 km) at a spatial resolution of 10 m centered over a selection of 4 GBOV sites (a) GER_HAI, (b) AUS_TMB, (c) ITA_REN, (d) USA_PSU. ST_{score} and RAW_{score} , indicators of the spatial representativeness, are displayed in the plots.

4. Quality Assessment Methodology

4.1. Uncertainty Requirements

The accuracy assessment results were analyzed against predefined uncertainty levels based on a review of the existing user requirements from the Global Climate Observing System (GCOS), the World Meteorological Organization (WMO) and the key performance indicators of C3S.

In the last update of the GCOS requirements [64], there is a distinction between the products targeted for “adaptation” and “modelling” applications that results in different needs for the horizontal resolution. Modelling requirements (i.e., uncertainty Max [5%; 0.0025], see Table 6) are the focus of this study since modelling is the main application targeted. Other requirements come from the WMO [65], which aids in the setting of the priorities to be agreed upon by WMO members and their space agencies for enhancing the space-based GCOS system. The WMO specifies the requirements for the SA for climatologic applications at three quality levels (Table 6): Threshold (minimum requirement), breakthrough (significant improvement) and goal (optimum, no further improvement required). The stated “goal” WMO uncertainty requirement of 5% is, thus, equivalent to the GCOS requirement in relative terms. Apart from the GCOS and WMO, the Key Performance Indicator (KPI) of the maximum accuracy being between 10% and 0.01 was defined in the C3S program [66].

Table 6. GCOS, WMO and C3S SA uncertainty requirements.

	GCOS	WMO	C3S KPI
Surface Albedo requirements	Max (5%; 0.0025)	Goal: 5% Breakthrough: 10% Threshold: 20%	Max (10%; 0.01)

Based on the existing requirements, three different levels (i.e., optimal, target and threshold) are predefined in this study (Table 7) with the aim to verify whether the results fit the purpose (Table 6). The optimal level (Max [5%, 0.0025]) was selected according to the GCOS uncertainty requirement and is equivalent to the WMO goal. The target level (Max [10%, 0.01]) is equivalent to the C3S KPI and partly equivalent to the WMO breakthrough level. Finally, the threshold level (Max [20%, 0.02]) was

adopted from the WMO. Poor performances of the product correspond to values above the threshold level (minimum requirement). Figure 3 displays the selected uncertainty levels as a function of the product values.

Table 7. Predefined uncertainty requirement levels used for SA validation.

	Optimal	Target	Threshold
Surface Albedo Uncertainty Requirements	Max [5%, 0.0025]	Max [10%, 0.01]	Max [20%, 0.02]

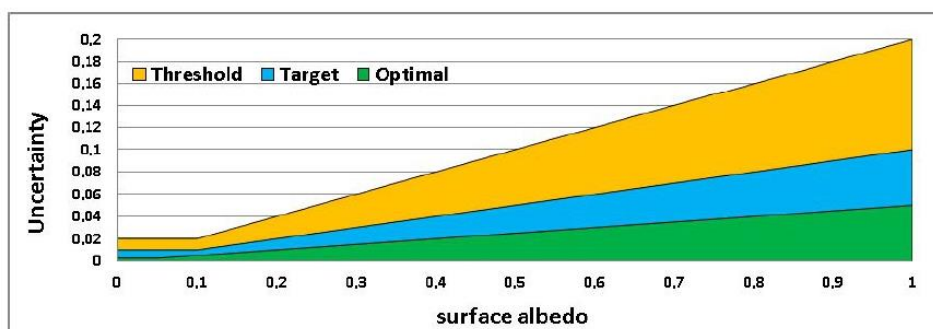


Figure 3. Uncertainty levels as a function of SA values.

4.2. Validation Methods

The validation methodology follows the CEOS LPV good practice protocol for the validation of satellite-derived albedo products [21], and the validation metrics are presented in Section 4.2.1. The different strategies for product intercomparison and direct validation are described in Sections 4.2.2 and 4.2.3, respectively.

Figure 4 shows the global distribution of the sampling used in this study. The product intercomparison is evaluated over a 725-site land validation network (LANDVAL) of sites [67], which is designed to globally represent the variability of land surface types, and was used as the spatial sampling to evaluate these criteria. This network also includes 20 well-known desert calibration sites [26] for the precision evaluation, due to their high temporal stability. For the direct validation, the 20 selected GBOV homogeneous stations with available ground data (see Table 5) were used.

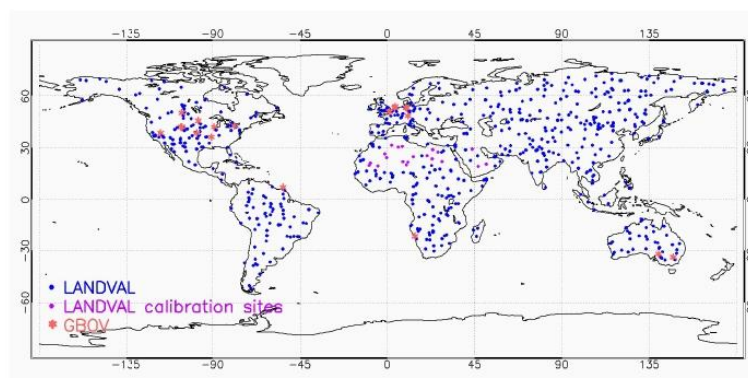


Figure 4. Global distribution of the 725 LANDVAL (including 20 desert calibration sites) and 20 GBOV sites.

4.2.1. Validation Metrics

The definitions of the completeness, precision, uncertainty and accuracy (Table 8), which are applicable to SA validation, are drawn from the experimental recommendations of the Joint Committee for Guides in Metrology (JCGM) regarding the expression of uncertainty in measurement [68] and from the GCOS [64].

Table 8. Validation metrics for product validation.

Quantity	Validation Metric
Completeness	Gap size distribution (spatial and temporal) Gap length
Precision	Median 3-point difference (intra-annual precision) Median absolute deviation (inter-annual precision)
Accuracy	Median Error Box-plots of the bias per albedo range
Uncertainty	Root mean square deviation (RMSD) Scatter-plots of match-ups (MAR Linear models and correlation)

Completeness is the proportion of valid retrievals over an observation domain at any given time. It is, therefore, mandatory to document the completeness of the product (i.e., the distribution in space and time of missing data).

Two aspects of the precision, which is also called the repeatability, are evaluated: The intra-annual and inter-annual precision. The intra-annual precision (smoothness or δ function) corresponds to the temporal noise assumed to have no serial correlation within a season. The δ function is computed for each triplet of consecutive observations [69,70] as the absolute value of the difference between the center and the corresponding linear interpolation between the two extremes, and the median of the δ values is provided as an indicator of the intra-annual precision of satellite albedo products [21]. The inter-annual precision (i.e., the dispersion of the albedo values from year to year) was assessed over the 20 desert calibration sites between two consecutive years, and the median absolute deviation is provided as an indicator of the inter-annual precision [21].

Accuracy is the degree of “closeness of the agreement between the result of a measurement and a true value of the measurand” [68]. Commonly, accuracy is used to describe systematic errors and measure statistical bias, but the best practice is to provide the median error as an indicator of accuracy [21].

Uncertainty is a “parameter, associated with the result of a measurement, that characterizes the dispersion of the values that could reasonably be attributed to the measurand” [68]. Uncertainty includes the bias and precision errors and can be estimated by the Root Mean Square Deviation (RMSD). Additionally, the linear model fits are used to quantify the goodness of fit. For this purpose, Major Axis Regressions (MARs) were computed instead of Ordinary Least Squares (OLS) because it is specifically formulated to handle errors in both the x and y variables [71]. Other metrics are used, such as the number of samples (N), which is indicative of the power of the validation; or the correlation coefficient (R , estimated as the Pearson coefficient), which indicates the descriptive power of the linear accuracy test. The percentage of pixels within the predefined uncertainty levels (Table 7, Figure 3) is also quantified.

4.2.2. Satellite Product Intercomparison

The intercomparison of satellite products must account for the differences in the spatial and temporal characteristics of the different datasets. Consequently, a spatial support area and temporal support period were defined consistent with the C3S SA characteristics (Table 1). Thus, the MCD43A4 C6 products were re-sampled to Plate Carrée using a 1 km spatial sampling grid. Satellite products

were compared using the closest date of their different temporal composites, using the 10 day temporal frequency of C3S SA products.

The completeness and precision of the different products were evaluated and compared, as well as the temporal consistency among the several products, which was qualitatively assessed per biome type. The uncertainty estimates from the intercomparisons provided an overall figure of the spatio-temporal consistency between products. Scatter-plots and the associated metrics between pairs of products were analyzed and complemented with box-plots of the bias per bin albedo value. Our analysis focuses on the consistency during the 6-month overlap period between PROBA-V SA v1.0 and SPOT/VGT SA v1.0, whereas the intercomparison with MCD43A3 C6 was conducted using one year (2014) of data.

4.2.3. Ground-Based Validation

The main steps in the accuracy assessment of albedo products include the generation of blue-sky albedo [30] for a direct comparison with in-situ measurements and the test of the spatial representativeness of the in situ albedometer footprints for the satellite pixel resolution of interest according to in situ measurements standards [31,32]. Consequently, a careful selection of ground points and the characterization of their spatial representativeness are crucial for a meaningful point-to-pixel comparison, as presented in Section 3.2. For the first step, the blue-sky albedo from a satellite is estimated from the retrieved AL-DH-BB and AL-BH-BB satellite EO product under study, and weighted by the fraction of diffuse down-welling shortwave radiation from the ground station [30]. The next step is the careful selection of the homogeneous sites, which are similar to the footprints of the satellite pixel resolution of interest. The accuracy assessment of the SA satellite products was performed against the measurements coming from the 20 selected GBOV homogeneous stations presented in Section 3.

The study here was extended to the period from 2014 to 2018 to have the maximum concomitant samples from the GBOV dataset to PROBA-V observations. The accuracy assessment of MCD43A3 C6 for the same period and sampling was performed for benchmarking. This exercise was carried out at a resolution of 1 km, which is equivalent to one pixel in the case of PROBA-V SA v1.0, and averages of 2×2 pixels in the case of MCD43A3 C6. The 10 day frequency of C3S products was used as temporal sampling, and the average values of the daily ground data were computed to compare with satellite estimations during the corresponding temporal composite window of each product (see Table 1). This analysis was performed over the best quality pixels of C3S PROBA-V SA v1.0 and MCD43A3 C6, according to QFLAGS (Table 3).

5. Results

5.1. Satellite Product Intercomparison

5.1.1. Product Completeness

The global map of the percentage of gaps (i.e., values with missing data) during one whole year of data (2014) for the PROBA-V SA v1.0 products (Figure 5) shows poor spatio-temporal continuity over latitudes higher than 45° north and over the equatorial belt, with a percentage of missing values up to 100% in some pixels over these areas. Note that the information from the quality flags was not considered here in the computation of the gaps (i.e., a gap or missing value corresponds to a fill value in the product). C3S products are not provided over areas out of the region from latitudes of 60°S to 75°N .

The temporal evolution of missing values (Figure 6a) shows the highest percentage of missing PROBA-V SA v1.0 values during wintertime in the northern hemisphere. The percentage of missing values ranges, on average, from approximately 12% (July and August 2014) to 32% (January and December 2014). PROBA-V SA v1.0 shows a similar temporal trend of missing data to MCD43A3 C6. Better completeness was found for SPOT/VGT SA v1.0 with almost no missing data during the months from March to May and a percentage up to 10% in wintertime in the northern hemisphere.

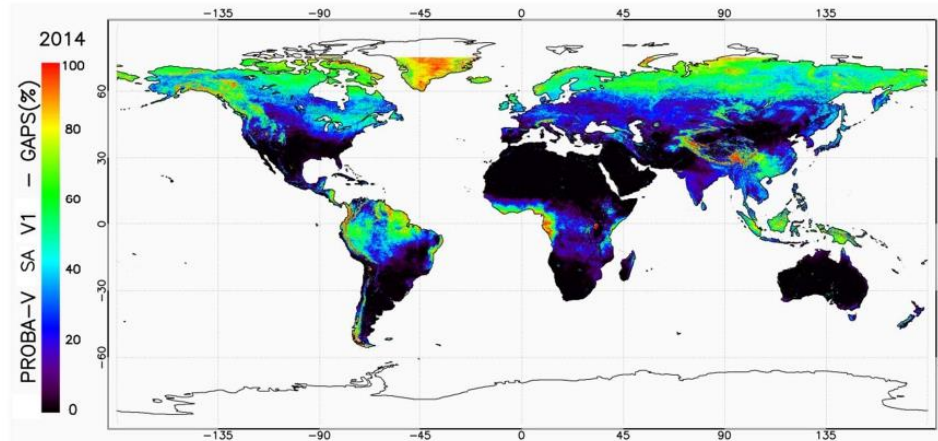


Figure 5. Percentage of gaps (%) during the year 2014 for the C3S PROBA-V SA v1.0 product considering all land pixels.

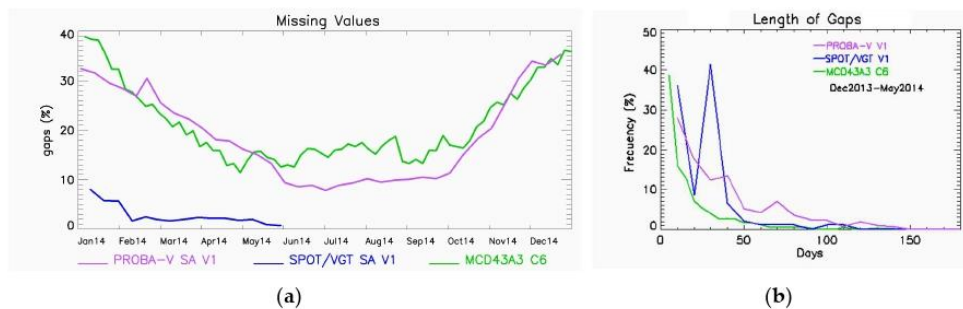


Figure 6. Temporal variations of missing values for the year 2014 (a), and distribution of the temporal length of the missing values from December 2013 to May 2014 (b). Computation over LANDVAL sites for C3S PROBA-V SA v1.0 (purple), SPOT/VGT SA v1.0 (blue) and MCD43A3 C6 (green).

The distribution of the temporal length of the missing values (Figure 6b) allows one to better understand the impact of the gaps for monitoring the temporal variations. PROBA-V SA v1.0 shows that approximately 65% of the gaps are shorter than 30 days and approximately 35% are shorter than 10 days (time resolution of the product). Similarly, typically, approximately 35–40% of the SPOT/VGT SA v1.0 gaps are shorter than 10 days, and approximately 75% of gaps are shorter than 30 days during the overlap period between SPOT/VGT and PROBA-V. MCD43A3 C6 has a shorter length of gaps, with approximately 40% of the gaps corresponding to 5 days.

5.1.2. Temporal Consistency

The temporal profiles of the different SA products (PROBA-V SA v1.0, SPOT/VGT SA v1.0 and MCD43A3 C6) in the three broadband domains (visible, NIR, and total shortwave) were analyzed over the 725 LANDVAL sites for each main biome type (Figure 7). The analytical focus of the transition between SPOT/VGT and PROBA-V and the 2013–2014 period was represented. All the satellite products are displayed at the center of their temporal composite windows (30 days in the case of PROBA-V SA v1.0, 20 days in the case of SPOT/VGT SA v1.0 and 16 days in the case of MCD43A3 C6). Note that the information of the PROBA-V SA v1.0 QFLAG was also displayed in these graphs: Filled dots correspond to pixels flagged as good quality, and unfilled dots correspond to pixels flagged as low-quality (land pixels with bit 6, 10 or 11 to 1) according to Table 3.

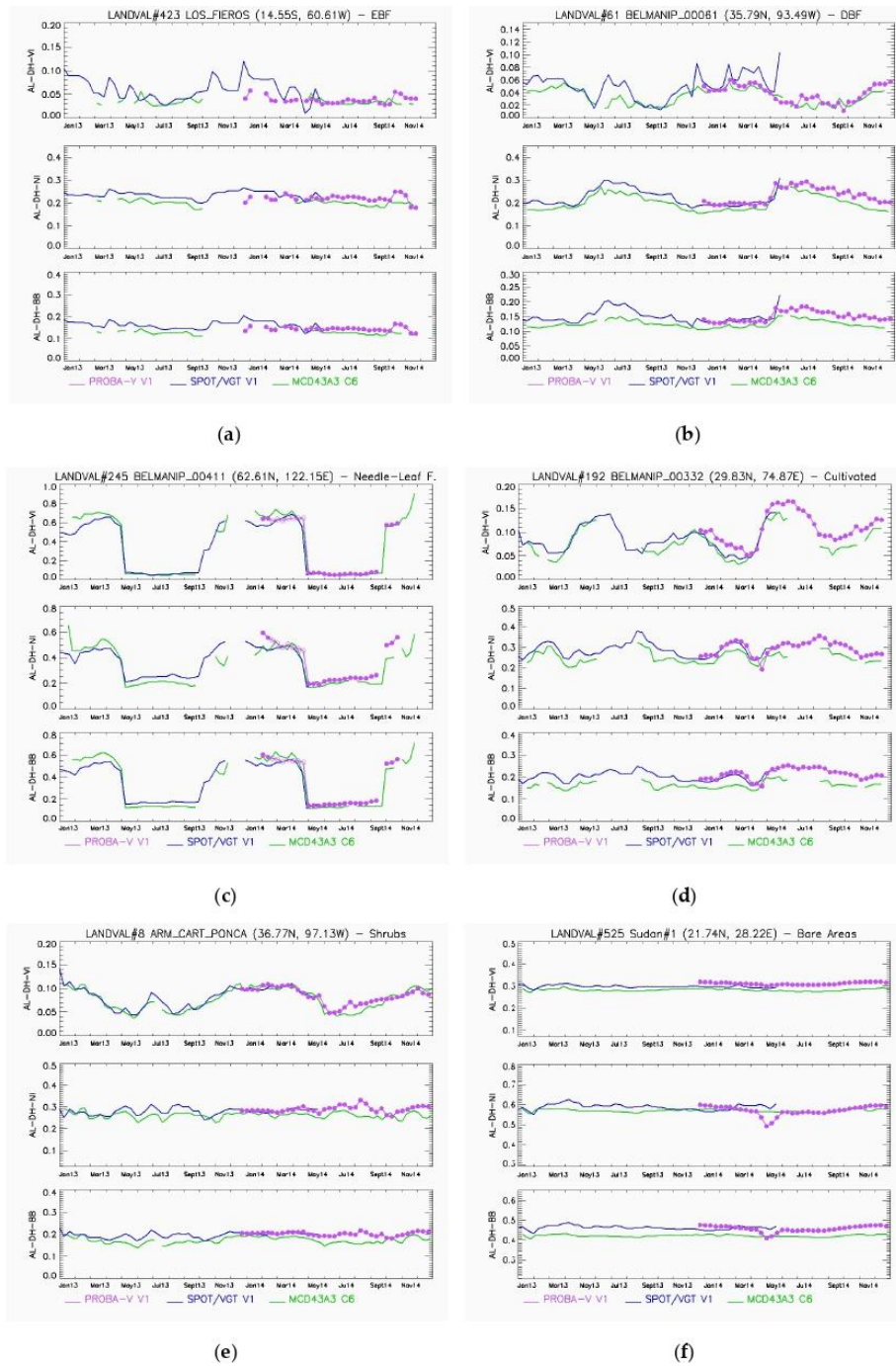


Figure 7. SA time series of the C3S PROBA-V SA v1.0, C3S SPOT/VGT SA v1.0 and MCD43A3 C6 broadband black-sky albedos for selected LANDVAL sites (a) Evergreen Broadleaf Forest, (b) Broadleaved Deciduous Forest, (c) Needle-leaf Forest, (d) cultivate, (e) shrublands/herbaceous/sparse vegetation, and (f) bare areas during the 2013–2014 period. Information on the sites is shown at the top of the corresponding figures. In the case of PROBA-V, filled dots correspond to ‘good quality’ pixels, and unfilled dots correspond to pixels flagged as ‘low-quality’ according to QFLAG (Table 3).

For evergreen broadleaved forests, some temporal noise was observed in all satellite products. However, PROBA-V SA v1.0 and MCD43A3 C6 seem to provide less noise (i.e., flatter temporal trajectories) than SPOT/VGT SA v1.0, which seems to be more realistic for this biome type. For the rest of the biomes, the PROBA-V SA v1.0 profiles follow the temporal trends of SPOT/VGT SA v1.0 and MCD43A3 C6. The presence of rapid changes due to snow events, the occurrence of stable profiles and the phenological changes were consistent among the three datasets. However, PROBA-V SA v1.0 displays slightly large variability compared to other satellite products in the NIR domain (also affecting the total spectrum). Note that the use of the C3S PROBA-V SA v1.0 Quality Flag in northern latitudes removes valid snow observations in most cases.

A seasonality effect was observed with the sign of the bias between C3S PROBA-V SA v1.0 and SPOT/VGT SA v1.0 during the short overlap period over desert areas for the NIR and total spectrum. PROBA-V SA v1.0 tends to provide slightly higher values than SPOT/VGT SA v1.0 from December 2013 to February 2014, and the opposite trend was found from March 2014 to May 2014. Additionally, the SPOT/VGT SA v1.0 temporal trajectories show some temporal noise over desert sites, which is not observed for the other satellite products (PROBA-V SA v1.0 and MCD43A3 C6).

5.1.3. Spatio-Temporal Consistency

The overall spatio-temporal consistency between PROBA-V SA v1.0 and the reference products is assessed over the LANDVAL network sites considering all good quality observations according to the quality flags (see Table 3).

- PROBA-V SA v1.0 versus SPOT/VGT SA v1.0 (overlap period)

For the visible domain (Figure 8a–d and Table 9), PROBA-V SA v1.0 tends to provide slightly lower values than SPOT/VGT SA v1.0, with small negative mean biases of −2.2% and −2.8% for black-sky and white sky albedos, respectively. Optimal lineal regression relationships from the MAR were found (offset ~0 and slope close to 1). Worse results were found in terms of the RMSD (uncertainty), with values of approximately 0.05 (~35%).

Table 9. Main performance statistics of C3S PROBA-V SA v1.0 versus SPOT/VGT SA v1.0 broadband albedo products over all LANDVAL sites during December 2103 to May 2014 period. The computation was performed over good quality pixels according to PROBA-V and SPOT/VGT QFLAGS.

PROBA-V SA v1.0 vs. SPOT/VGT SA v1.0 (Dec 2013–May 2014)						
	AL-DH-VI	AL-DH-NI	AL-DH-BB	AL-BH-VI	AL-DH-NI	AL-BH-BB
Median_Err (Median_Err %)	0.01 (8%)	0.014 (5%)	0.01 (4.7%)	0.013 (10%)	0.02 (6.3%)	0.014 (5.9%)
Bias (Bias %)	−0.003 (2.2%)	0.007 (2.3%)	0.002 (0.9%)	−0.024 (2.8%)	0.007 (2.4%)	0.002 (1.0%)
RMSD (RMSD %)	0.044 (35.3%)	0.031 (10.5%)	0.032 (14.5%)	0.047 (36.1%)	0.037 (11.7%)	0.036 (15.2%)

For the near-infrared (Figure 8b–e and Table 9), positive biases (PROBA-V SA v1.0 > SPOT/VGT SA v1.0) of 2.3–2.4% were found, with an RMSD of approximately 10% and high correlations (>0.94). PROBA-V SA v1.0 tends to provide higher values than SPOT/VGT SA v1.0 for albedo values lower than 0.5 and the opposite trend for albedo values higher than 0.5 (typically snow cases). In all cases, a median bias close to zero was found, which was within the optimal level of consistency.

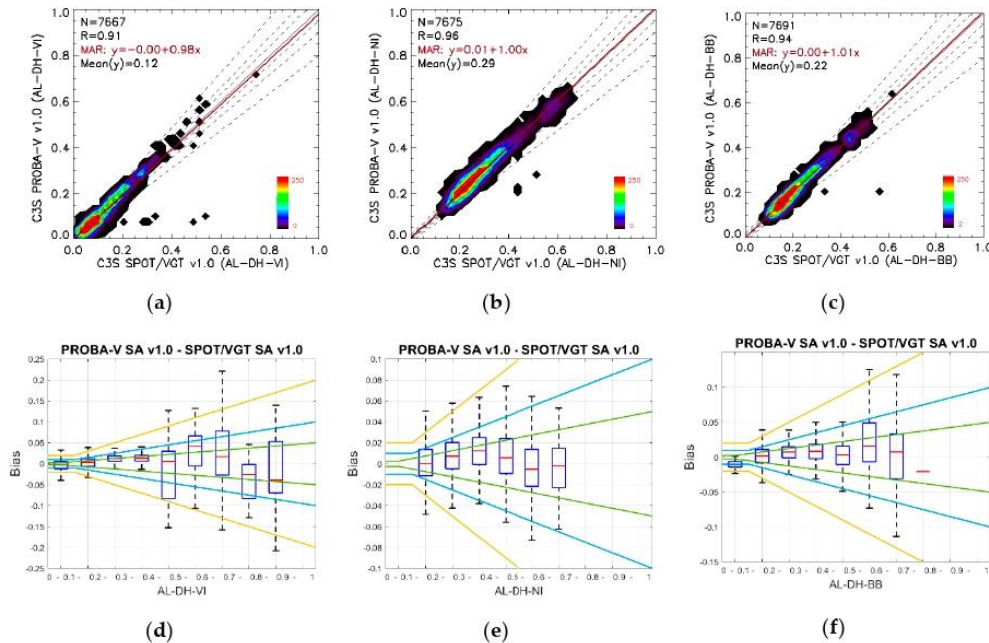


Figure 8. Top: C3S PROBA-V SA v1.0 versus C3S SPOT/VGT SA v1.0 products' scatter-plots, where the dashed lines correspond to the optimal, target and predefined threshold uncertainty levels around the 1:1 relation (continuous line). Bottom: Box-plots of the bias per bin albedo range, where red bars indicate the median values, blue boxes stretch from the 25th percentile to the 75th percentile of the data and whiskers include 99.3% of the coverage data ($\pm 2.7 \sigma$). Outliers are not displayed. The green, blue and orange lines correspond to optimal, target and threshold uncertainty levels, respectively. Computation over all LANDVAL sites for the December 2013–May 2014 period over good quality pixels according to the quality flags (Table 3) for AL-DH-VI (a,d), AL-DH-NII (b,e), and AL-DH-BB (c,f).

Remarkably low mean biases ($<1\%$) were found for the total shortwave (Figure 8c–f and Table 9), as well as high correlations (>0.93). Total uncertainties (RMSD) of 0.03 ($\sim 15\%$) were found. A systematic positive bias was found for almost all ranges, except for values lower than 0.1 and higher than 0.7, with the median bias typically within the optimal (GCOS) level of consistency (Table 6).

- PROBA-V SA v1.0 versus MCD43A3 C6 (2014 year)

Positive bias (PROBA-V SA v1.0 $>$ MCD43A3 C6) of $\sim 5\%$ was found for the visible domain (Figure 9a–d and Table 10) with uncertainties (RMSD) lower than 0.05. Box-plots show slight median positive bias for albedo ranges up to 0.4, which is the range where most of the samples are located in this spectral domain. Large discrepancies were found for the highest ranges, mainly affected by snow cases, with a tendency towards the negative sign of the bias.

PROBA-V SA v1.0 tends to provide higher values than MCD43A3 C6 ($\sim 8\text{--}9\%$) for the near-infrared (Figure 9b–e and Table 10), with overall RMSD of approximately 14–15%. PROBA-V SA v1.0 tends to provide higher values than MCD43A3 C6 for albedo values lower than 0.5, and the opposite trend for albedo values higher than 0.5.

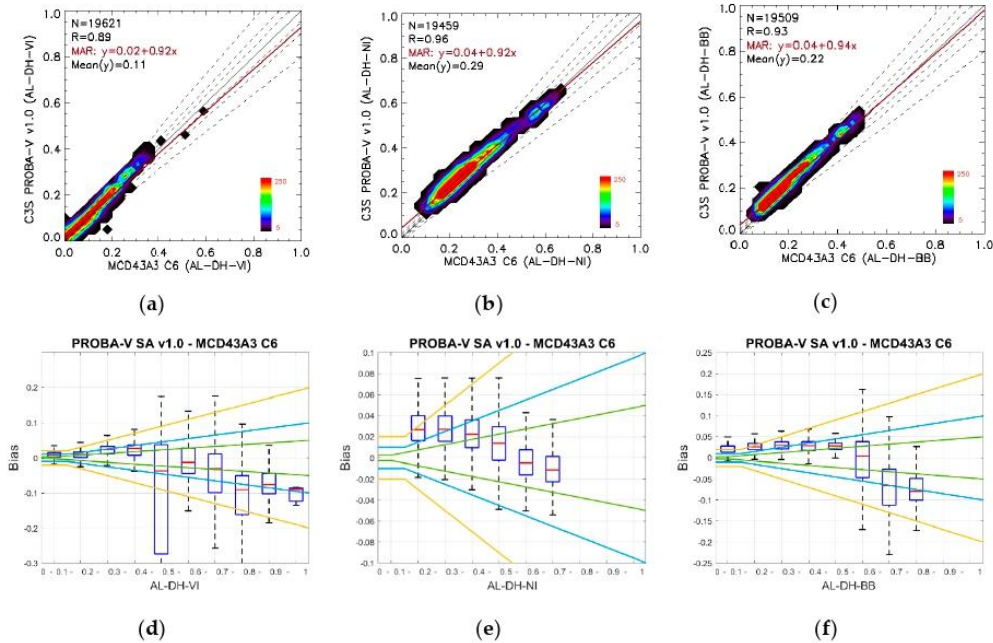


Figure 9. Top: C3S PROBA-V SA v1.0 versus MCD43A3 C6 products scatter-plots, where the dashed lines correspond to the optimal, target and predefined threshold uncertainty levels around the 1:1 relation (continuous line). Bottom: Box-plots of the bias per bin albedo range, where red bars indicate the median values, blue boxes stretch from the 25th percentile to the 75th percentile of the data and whiskers include 99.3% of the coverage data ($\pm 2.7 \sigma$). Outliers are not displayed. The green, blue and orange lines correspond to the optimal, target and threshold uncertainty levels, respectively. Computation over all LANDVAL sites during the year 2014 over good quality pixels according to the quality flags for AL-DH-VI (a,d), ALI-NI (b,e), and AL-DH-BB (c,f).

Table 10. Main performance statistics of C3S PROBA-V SA v1.0 versus MCD43A3 C6 broadband albedo products over all LANDVAL sites during the year 2014. The computation was performed over good quality pixels according to PROBA-V and MCD43A2 QFLAGS.

	PROBA-V SA v1.0 vs. MCD43A3 C6 (2014)					
	AL-DH-VI	AL-DH-NI	AL-DH-BB	AL-BH-VI	AL-BH-NI	AL-BH-BB
Median_Err	0.011	0.025	0.027	0.012	0.029	0.031
(Median_Err %)	(9.8%)	(9%)	(13.4%)	(10.1%)	(9.9%)	(14.5%)
Bias	0.006	0.024	0.024	0.006	0.029	0.029
(Bias %)	(5.3%)	(8.4%)	(11.9%)	(5.1%)	(9.6%)	(13.3%)
RMSD	0.048	0.039	0.044	0.048	0.045	0.048
(RMSD %)	(43.3%)	(14%)	(21.5%)	(41.4%)	(15.1%)	(22.2%)

The worse performance in the comparison PROBA-V SA v1.0 versus MCD43A3 C6 was found for the total spectrum (Figure 9c–f and Table 10), with a large positive bias of ~12–13%. As observed for the NIR, PROBA-V tends to provide higher values than MODIS C6 for albedo values lower than 0.5 and the opposite trend for albedo values higher than 0.5 (i.e., snow cases).

- Compliance with user requirements

The compliance matrix of C3S PROBA-V SA v1.0 versus the reference products (SPOT/VGT SA v1.0 and MCD43A3) with predefined uncertainty levels based on different user requirements is presented in Table 11.

Table 11. Compliance matrix (percentage of pixels filing the predefined uncertainty levels) of C3S PROBA-V SA v1.0 versus SPOT/VGT SA v1.0 (December 2103 to May 2014 period) and MCD43A3 C6 (2014 year) broadband albedo products. Computation over LANDVAL sites for good quality pixels according to QFLAGS (Table 3).

PROBA-V SA v1.0 vs. SPOT/VGT SA v1.0 (December 2013–May 2014)						
	AL-DH-VI	AL-DH-NI	AL-DH-BB	AL-BH-VI	AL-BH-NI	AL-BH-BB
% optimal (GCOS)	28.9	48.6	50.2	23.9	39.9	41.8
% target (C3S KPI)	62.9	76.8	78.5	51.3	68.5	69.9
% threshold	83.1	92.6	88.1	72.8	90.2	82.6
PROBA-V SA v1.0 vs. MCD43A3 C6 (2014 year)						
	AL-DH-VI	AL-DH-NI	AL-DH-BB	AL-BH-VI	AL-BH-NI	AL-BH-BB
% optimal (GCOS)	20.4	24.5	6.5	20.9	22.9	6.7
% target (C3S KPI)	55.5	50.4	24.8	52.7	46.4	23
% threshold	83.5	78.7	50.7	80.5	77.4	49.8

5.1.4. Intra-Annual Precision

The Probability Density Functions (PDFs) of the intra-annual precision (the so-called smoothness) are analyzed (Figure 10). The computation was performed over LANDVAL sites during the overlap period between SPOT/VGT, PROBA-V and MODIS products (i.e., December 2013–May 2014 period).

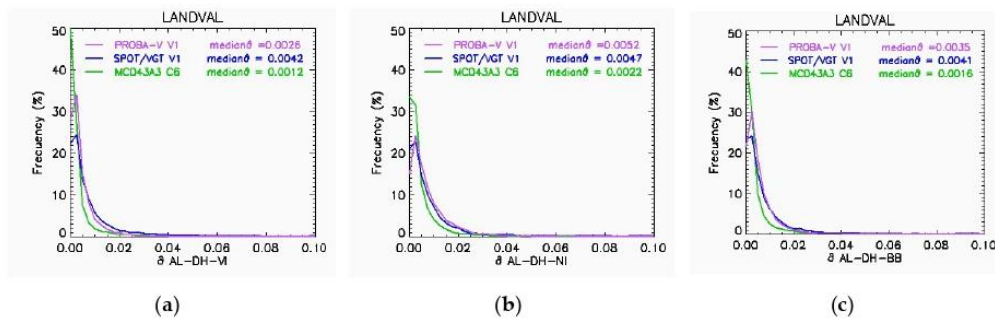


Figure 10. Histograms of the δ function (smoothness) for black-sky C3S PROBA-V SA v1.0, C3S SPOT/VGT SA v1.0 and MCD43A3 C6 for visible (a), NIR (b) and total shortwave (c). Computation over LANDVAL sites during the overlap period (December 2013–May 2014 period). The median δ values are presented for each product.

The three products present similar distributions of the smoothness (δ). Most of the delta values are below 0.01, which demonstrates the high stability over a short time scale for the albedo products. In all satellite products, worse intra-annual precision (i.e., higher δ values) was found for white-sky albedos compared with equivalent black-sky albedos. The median δ values (Table 12), which are indicative of the intra-annual precision, show improved results (i.e., lower δ values) of PROBA-V SA v1.0 compared to SPOT/VGT SA v1.0 for visible and total shortwave and worse performance for NIR. Both C3S products provide much worse intra-annual precision than MODIS C6.

Table 12. Intra-annual precision indicator (Median of the 3-point difference) of the C3S PROBA-V SA v1.0, C3S SPOT/VGT SA v1.0 and MCD43A3 C6 products. Computation over LANDVAL sites during the overlap period (December 2013–May 2014 period).

	Median of 3-Point Difference (i.e., Median δ Values)					
	AL-DH-VI	AL-DH-NI	AL-DH-BB	AL-BH-VI	AL-BH-NI	AL-BH-BB
PROBA-V SA v1.0	0.0026	0.0052	0.0035	0.0039	0.0074	0.0050
SPOT/VGT SA v1.0	0.0042	0.0047	0.0041	0.0057	0.0063	0.0055
MCD43A3 C6	0.0012	0.0022	0.0016	0.0018	0.0032	0.0023

5.1.5. Inter-Annual Precision

PROBA-V SA v1.0 black-sky albedo shows an inter-annual precision of approximately 1%, showing improved results compared to SPOT/VGT SA v1.0 (2–3%). MCD43A3 C6 provides better inter-annual precision, with median absolute deviations lower than 1%. As observed for the intra-annual precision, all products provided worse results for white-sky albedos compared to black-sky albedos (Table 13).

Table 13. The median absolute deviation between two consecutive years of the PROBA-V SA v1.0, SPOT/VGT SA v1.0 and MCD43A3 C6 products. Computation over desert calibration sites.

	Inter-Annual Precision (Median Absolute Deviation)					
	AL-DH-VI	AL-DH-NI	AL-DH-BB	AL-BH-VI	AL-BH-NI	AL-BH-BB
PROBA-V SA v1.0	0.004 (1.2%)	0.006 (1.1%)	0.004 (0.9%)	0.004 (1.3%)	0.008 (1.3%)	0.006 (1.2%)
SPOT/VGT SA v1.0	0.008 (2.6%)	0.012 (2%)	0.009 (2%)	0.011 (3.7%)	0.02 (3.3%)	0.014 (3%)
MCD43A3 C6	0.003 (0.9%)	0.005 (0.8%)	0.004 (0.8%)	0.003 (1.2%)	0.006 (1.1%)	0.005 (1.1%)

5.2. Ground-Based Direct Validation

To investigate the accuracy of C3S PROBA-V SA v1.0 and MCD43A3 C6 satellite albedo products, scatter plots versus field measurements (GBOV RM) were produced for the 2014–2018 period over 20 homogeneous sites (see Section 3) with different vegetation types. Figure 11 and Table 14 show the scatter-plots, and relevant statistics from the direct validation exercise, whilst Table 15 summarizes the compliance of both satellite products with user requirements (predefined in Section 4.1). The relevant statistics per biome type are presented in Tables 16 and 17 for PROBA-V SA v1.0 and MCD43A3 C6, and the scatter-plots per biome type can be found in Appendix A. The temporal trajectories of both PROBA-V SA v1.0 and MCD43A3 C6 compared to the daily GBOV RMs are presented in Appendix B.

C3S PROBA-V SA v1.0 shows an overall accuracy (median error) of 18.2%, with a tendency to overestimate ground values (positive bias of 11.5%). This positive bias was mainly observed for low albedo values (up to 0.2, forest sites) showing an offset of 0.07 and a slope of 0.7 in the MAR relationship. MCD43A3 C6 provides a lower median error of 11.2% with a negative mean bias of −5.9%. C3S PROBA-V SA v1.0 products provide similar results in terms of uncertainty (RMSD of 22.4%) than MCD43A3 C6 (RMSD of 24.8%).

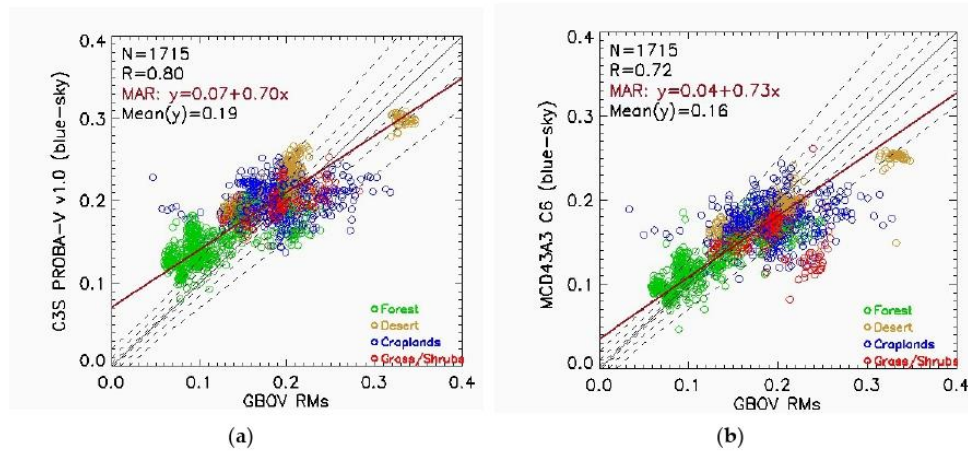


Figure 11. Direct validation of the best quality pixels of the C3S PROBA-V SA v1.0 (a) and MODIS MCD43A3 C6 (b) blue-sky albedo satellite products versus the ground measurements (RMs) at 20 GBOV stations during the 2014–2018 period. The continuous black lines correspond to the 1:1 lines and the dashed lines correspond to the optimal (GCOS uncertainty requirement), target (C3S KPI) and predefined threshold levels. The red lines correspond to the Major Axis Regression (MAR).

Table 14. Relevant statistics of the direct validation of the best quality pixels (Table 3) of the C3S PROBA-V SA v1.0 and MODIS MCD43A3 C6 blue-sky albedo satellite products versus the GBOV ground values coming from 20 GBOV stations during the 2014–2018 period.

	PROBA-V SA v1.0	MCD43A3 C6
Median Error (Median Error %)	0.032 (18.2%)	0.018 (11.2%)
Bias (Bias %)	0.020 (11.5%)	−0.010 (5.9%)
RMSD (RMSD %)	0.04 (22.4%)	0.04 (24.8%)

Note that 15.5% of the 1715 PROBA-V SA v1.0 samples achieved the optimal predefined level (i.e., GCOS requirements) and 28.6% of the target level (i.e., C3S KPI), as shown in Table 15. Slightly improved results were found for MCD43A3 C6 (23.7% and 45.5% of the optimal and target levels, respectively).

Per biome type, PROBA-V SA v1.0 provides a large positive bias for forest (22.4%) and desert (10.4%) sites compared to crop (7.4%) and grassland/shrubland (4.2%) sites. MCD43A3 C6 systematically provides a large negative bias for most biome cases (croplands, grassland/shrublands and desert) except for forests, where a low positive bias was found (2.8%).

Table 15. Compliance matrix of the direct validation of the C3S PROBA-V SA v1.0 and MODIS MCD43A3 C6 blue-sky albedo satellite retrievals (best quality pixels, Table 3) versus ground values (N = 643) from 20 GBOV stations during the 2014–2018 period. N stands for the number of samples.

	PROBA-V SA v1.0	MCD43A3 C6
% optimal (GCOS)	15.5	23.7
% target (C3S KPI)	28.6	45.5
% threshold	44.2	58.0

Table 16. Relevant statistics per main biome type and the compliance matrix of the direct validation of the C3S PROBA-V SA v1.0 blue-sky albedo satellite retrievals (best quality pixels, Table 3) versus the ground values (RMs) from 20 GBOV stations during the 2014–2018 period.

PROBA-V SA v1.0 vs. GBOV RM				
	Forest	Crops	Grass/Shrubs	Desert
Number of Samples (stations)	608 (8)	488 (6)	316 (3)	303 (3)
Median Error (Median Error %)	0.037 (27.0%)	0.036 (18.3%)	0.015 (7.8%)	0.037 (16.7%)
Bias (Bias %)	0.030 (22.4%)	0.014 (7.4%)	0.008 (4.2%)	0.023 (10.4%)
RMSD (RMSD %)	0.044 (32.6%)	0.044 (22.4%)	0.024 (12.2%)	0.038 (17.2%)
% optimal (GCOS)	6.1	12.4	38.9	15.5
% target (C3S KPI)	13.8	25.8	59.5	30.4
% threshold	22.9	38.7	75.3	63.4

Table 17. Relevant statistics per main biome type and the compliance matrix of the direct validation of the MCD43A3 C6 blue-sky albedo satellite retrievals (best quality pixels, Table 3) versus the ground values (RMs) from 20 GBOV stations during the 2014–2018 period. N stands for the number of samples.

MCD43A3 C6 vs. GBOV RM				
	Forest	Crops	Grass/Shrubs	Desert
Number of Samples (stations)	608 (8)	488 (6)	316 (3)	303 (3)
Median Error (Median Error %)	0.015 (12.1%)	0.021 (11.3%)	0.020 (11.5%)	0.017 (8.4%)
Bias (Bias %)	0.003 (2.8%)	−0.012 (6.7%)	−0.027 (15.3%)	−0.013 (6.5%)
RMSD (RMSD %)	0.031 (25.2%)	0.051 (28.0%)	0.042 (24.1%)	0.036 (17.8%)
% optimal (GCOS)	21.5	25.4	18.4	30.7
% target (C3S KPI)	41.1	44.5	43.4	58.1
% threshold	58.9	53.5	52.8	68.6

6. Discussion

C3S SA v1.0 based on PROBA-V provides continuity to the CDRs of global albedo products in the C3S from December 2013 onwards. Previously, SA products were derived from SPOT/VGT (1998–2014) and NOAA/AVHRR (1981–2005) data. Good spatio-temporal consistency in the transition from SPOT/VGT to PROBA-V for both black-sky and white-sky albedos, with mean biases below $\pm 3\%$ for the overlap period, was found. However, the comparison of C3S PROBA-V SA v1.0 with MCD43A3 C6 SA showed lower spatio-temporal consistency between satellite products with mean biases up to 13%. C3S PROBA-V SA v1.0 (and MCD43A3 C6) displayed more gaps (typically between 10% and 20%) than C3S SPOT/VGT v1.0.

Different aspects of the retrieval methodology play important roles in the existing discrepancies between the satellite products under study (C3S PROBA-V SA v1.0, C3 SPOT/VGT SA v1.0 and MCD43A3 C6) starting from the different input data and different atmospheric correction methods; including the BRDF parameterization, temporal compositing and angular integration; and finalizing with the narrow to broadband conversion.

Regarding the input data, each sensor works in different spectral channels (see Table 2). The SPOT/VGT and PROBA-V channels provide very similar spectral characteristics in the Blue, Red and NIR bands, whereas significant differences are found for the SWIR channel. The central wavelengths of the MODIS spectral bands are comparable to the corresponding bands for PROBA-V and VGT, albeit the MODIS spectral bands are narrower. These differences could translate into reflectance discrepancies in regions with high absorption features like in the visible domain, where large uncertainty values were found between pairs of products.

Each satellite processing chain uses its own method for cloud/shadow screening and atmospheric correction according to the spatial, spectral and directional capabilities of each instrument. Cloud or snow contamination is the main reason for missing data in the EO products derived from optical onboard satellite sensors. The conservative PROBA-V cloud detection algorithm [72] is one of the

reasons for the higher fraction of missing data of PROBA-V SA v1.0 products compared to SPOT/VGT SA v1.0.

Discrepancies between different albedo estimates can also be attributed to the different BRDF models used [7]. Moreover, the performance of the BRDF model for good clear-sky observations also depends on the number of available looks during the synthesis period and the angular distribution of the sampling. Large BRDF uncertainties are associated with snow targets (as observed for the highest albedo ranges) for which none of these parametric BRDF models were well suited [73]. PROBA-V, SPOT/VGT and MODIS are wide-FOV sensors on polar-orbiting platforms, and a low impact of discrepancies is expected, due to different sun-view configurations. However, the different compositing periods (see Table 1) could play an important role in the differences between satellite products, mainly in rapid SA variations, such as snow events. Different techniques for temporal composite approaches also affect the completeness of EO satellite products. SPOT/VGT SA v1.0 uses a recursive temporal composition approach [9], which is the main reason for the improved completeness compared to the other satellite products (C3S PROBA-V SA v1.0 and MCD43A3 C6) that are computed using classical composite schemes based on predefined temporal windows.

In the last step, the broadband albedos are defined using slightly different spectral regions. The same broadband spectral regions are defined in both C3S PROBA-V SA v1.0 and SPOT/VGT SA v1.0 products, which contribute to a better agreement, whereas the MCD43A3 C6 broadband albedos are slightly differently defined.

In addition, the temporal noise (i.e., large temporal variability) observed for C3S PROBA-V SA v1.0 in the NIR domain through the qualitative inspection of the temporal variations (see Section 5.1.2) has a strong relationship with the precision, since low intra-annual precision was found compared to both reference EO products in this spectral range. In terms of the inter-annual precision, improved results were found for C3S PROBA-V SA v1.0 (~1%) compared to C3S SA v1.0 based on SPOT/VGT SA data (2%).

Regarding the accuracy with the ground measurements, PROBA-V SA v1.0 provided a similar accuracy (bias of 11.5%) to that found for C3S SPOT/VGT SA v1.0 during the validation exercise [44], where a positive bias (14%) was also reported for a different sampling (i.e., different stations and dates). PROBA-V SA v1.0 also provided a slightly worse accuracy (median error of 18.2%) than MCD43A3 C6 (median error of 11.2%). PROBA-V SA v1.0 tends to overestimate the ground values, whereas MCD43A3 C6 showed the opposite sign of the mean bias. The positive bias of PROBA-V SA v1.0 was mainly observed for forest sites ($SA < 0.2$) explained in the fact that the Roujean kernel [42] for geometrical scattering may not fit some cover types well, especially dense forest canopies, where it showed a weak hotspot effect [74–76]. The negative bias of MCD43A3 C6 is mainly influenced by some outliers detected in *Gobabeb* (bare soil) and *Cabaw* (grassland). For the *Cabaw* case, the lower MCD43A3 C6 values are explained by the persistent cloudiness at the MODIS overpass times [56]. It is important to note that only the satellite retrievals classified as the best quality, according to QFLAGs (Table 3), were used in the direct validation. As observed in the temporal consistency, the use of QFLAGs removes most of the valid snow retrievals in the case of PROBA-V. Then, this exercise is almost equivalent to snow-free conditions, which is more convenient for assessing the uncertainty of satellite EO products, since it is expected that the spatial representativeness of the pixels dropped during the fall and winter months as a consequence of the increased sub-pixel heterogeneity, due to processes, such as non-uniform patterns of snowmelt [77]. The positive bias of C3S PROBA-V SA v1.0 is consistent with previous studies performed on the CGLS, where a positive bias of approximately 22% was found compared to ground measurements over 17 stations [27], and a positive bias of approximately 14% was found compared to National Ecological Observatory Network (NEON) ground data [78]. The accuracy assessment of MCD43A3 C6 was also consistent with that previously reported when comparing the combined TERRA+AQUA albedo product with eight field stations during the spring and summer months of 2003 and 2004 (i.e., equivalent to snow-free conditions), where an accuracy of 0.013 was reported in terms of the absolute bias [79]. It should be noted that the estimation of the

uncertainty of ground reference data is around 5% under ideal conditions [58]. Thus, fiducial reference measurements must be characterized with highly calibrated instrumentation at dedicated cal/val sites to better estimate the satellite product uncertainty budget.

The compliance of satellite EO products versus ground data with user requirements showed a low percentage of pixels within GCOS (only <25%) and C3S (<50%) requirements, which indicates the difficulties of achieving these requirements using current products. To further improve the compliance with requirements, it is recommended that EO programs provide the uncertainties associated with the processing chain, mainly related to the sensor calibration and atmospheric correction. In that way, the steps providing higher error can be improved. However, the comparison between satellite C3S SA v1.0 products showed an overall good spatio-temporal consistency in the comparison of SPOT/VGT versus PROBA-V during the 6-month overlapping period (December 2013–May 2014), with typically more than 60% of the samples within the C3S target requirements for the visible domain, and more than 75% of the samples within the requirements for the NIR and total shortwave.

7. Conclusions

This paper presents the quality assessment results of C3S PROBA-V SA v1.0 products (broadband albedos) through intercomparison with reference satellite products (C3S SPOT/VGT SA v1.0 and MCD43 C6) at the global scale and the direct validation with a representative amount of ground data (1715 samples) across different biomes types (eight stations over forests, six over crops, three over grassland/shrubs, and three over desert). This validation exercise is a novelty in the literature, since very few global and temporally representative SA validation exercises have been published [21], and they are mainly based on MODIS observations [15–17]. The validation methodology adopted the guidelines, protocols and metrics defined by the CEOS LPV best practices for the validation of global albedo satellite products [21]. Additional results, such as the comparison of the spectral albedos or the presentation of the satellite products intercomparison per biome type, are not shown in this manuscript for the sake of brevity; however, they can be found in the product quality assessment report [66].

The main conclusions are the following.

- The good spatio-temporal consistency of C3S PROBA-V and SPOT/VGT SA v1.0 products assures the continuity of the CDRs in terms of the uncertainty between products. However, C3S PROBA-V SA v1.0 (and MCD32A3 C6) provides low numbers of valid retrievals compared to C3S SPOT/VGT SA v1.0.
- C3S PROBA-V SA v1.0 shows similar inter-annual precision (~1%) to MCD43A3 C6, improving the results of SPOT/VGT SA v1.0 (2–3%), since they provide some temporal instability over desert calibration targets. Both C3S products provide lower intra-annual precision than MCD43A3 C6, mainly in the NIR domain where some temporal noise was found.
- The accuracy of the C3S PROBA-V SA v1.0 best quality retrievals with respect to the ground data over a five-year period (2014–2018) showed systematic positive overestimation, which was mainly observed for the lowest albedo ranges (SA < 0.2) over forest sites. Similar uncertainty (RMSD~ 0.4) was found for MCD43A3 C6 products using the same sampling, showing the opposite sign for the mean bias.
- Few current satellite EO albedo products comply with the GCOS, C3S and WMO uncertainty requirements.

Additionally, it is important to remark that the use of PROBA-V QFLAGS (bit 6, input status; and bits 10–11, B2–B0 saturation status) removes most of the valid snow retrievals. Therefore, masking out data by means of the QFLAGS is not recommended for snow applications (users should ignore the information of QFLAGS over snow targets for specific applications).

Based on these results, C3S PROBA-V SA v1.0 has reached validation stage 3 in the validation hierarchy of the CEOS LPV [20]. The continuity of the C3S SA CDR time series will be ensured using Sentinel-3 OLCI and SLSTR data, and the algorithm and design of the processing chain are currently being developed. C3S is also developing multi-sensor albedo products combining NOAA/AVHRR, SPOT/VGT and PROBA-V input data. The long-term CDRs, provided by the Copernicus Climate Change Service from 1981 to the present (with the aim of extending to the future), are an added extra compared with the existing EO programs, providing the longest and state-of-the-art albedo products.

Author Contributions: J.S.-Z. and F.C. conceived and conceptualized the work. J.S.-Z., F.C. and R.L. defined the methodology. J.S.-Z. and E.M.-S. developed the validation software for generating the results. J.S.-Z. wrote the first version of the manuscript. All authors contributed to the analysis, writing, review and editing of the manuscript. The C3S_Lot5 consortium is structured as follows: validation team (J.S.-Z., F.C. and E.M.-S.), algorithm development (D.C. and F.P.), project management (I.B.), and technical officer (J.M.-S.). All authors have read and agreed to publish the manuscript.

Funding: This work was funded by the European Centre for Medium-Range Weather Forecasts in the framework of the Copernicus Climate Change Service (Official reference number service contract: 2018/C3S_312b_Lot5_VITO/SC1), led by VITO as the prime contractor. Previously, the development of the algorithm and the methodology were defined in the framework of the Copernicus Global Land Service (European Commission/Joint Research Centre under Framework Service Contract N°199494).

Acknowledgments: This study has been undertaken using data from GBOV “Ground Based Observation for Validation” (<https://land.copernicus.eu/global/gbov>) founded by the European Commission Joint Research Centre FWC932059 as part of the Global Component of the European Union’s Copernicus Land Monitoring Service.

Conflicts of Interest: The authors declare no conflict of interest.

Abbreviations

The following abbreviations are used in this manuscript:

AL-DH	Directional-Hemispherical ALbedos
AL-BH	Bi-Hemispherical Albedos
ATBD	Algorithm Theoretical Basis Document
AVHRR	Advanced Very High Resolution Radiometer
BB	total shortwave
BRDF	Bidirectional Reflectance Distribution Function
BSA	Black-Sky Albedo
BSRN	Baseline Surface Radiation Network
CDR	Climate Data Records
CDS	Climate Data Store of C3S
CEOS	Committee on Earth Observing Satellites
CGLS	Copernicus Global Land Service
C3S	Copernicus Climate Change Service
C6	Collection 6 of MODIS products
ECV	Essential Climate Variables
EO	Earth Observation
EQC	Evaluation and Quality Control
EUMETSAT	European Organization for the Exploitation of Meteorological Satellites
FLUXNET	FLUXes NETWORK (network of regional networks)

GBOV	Ground-Based Observations for Validation
CGOS	Global Climate Observing System
GLASS	Global Land Surface Satellite
GSD	Ground Sampling Distance
JCGM	Joint Committee for Guides in Metrology
KPI	Key Performance Indicator
LANDVAL	LAND VALidation network
LSA SAF	Satellite Application Facility for Land Surface Analysis
LPV	Land Product Validation sub-group
MAR	Major Axis Regression
MCD43	TERRA+AQUA MODIS BRDF/Albedo/NBAR Product
MetOp	Polar-orbiting Meteorological satellites
MIR	Mid InfraRed
MODIS	MODerate resolution Imaging Spectroradiometer
MSG	Meteosat Second Generation
N	Number of samples
NASA	National Aeronautics and Space Agency
NEON	National Ecological Observatory Network
NIR (or NI)	Near-Infrared
NOAA	National Oceanic and Atmospheric Administration
OLCI	Ocean and Land Colour Instrument
OLS	Ordinary Least Squares
LP	Land Products
PROBA-V	Project for Onboard Autonomy satellite, the V standing for vegetation
PUGS	Product User Guide and Specification document
QFLAG	Quality FLAG
R	Correlation coefficient
RM	Reference Measurements
RMSD	Root Mean Square Deviation
RTLSR	Ross Thick kernel and Li Sparse-Reciprocal kernels
SA	Surface Albedo
SEVIRI	Spinning Enhanced Visible and Infrared Imager
SLSTR	Sea and Land Surface Temperature Radiometer
SPOT	Satellites for the Observation of the Earth
SURFRAD	Surface Radiation budget
SWIR	Short-Wave InfraRed
TOA	Top-Of-Atmosphere
TOC	Top-Of-Canopy
VGI	VeGeTation sensor
VI	Visible domain
VNIR	Visible and Near-InfRared
WGCV	Working Group on Calibration and Validation
WMO	World Meteorological Organization
WSA	White-Sky Albedo

Appendix A. Ground-Based Direct Validation per Biome Type

- C3S PROBA-V SA v1.0

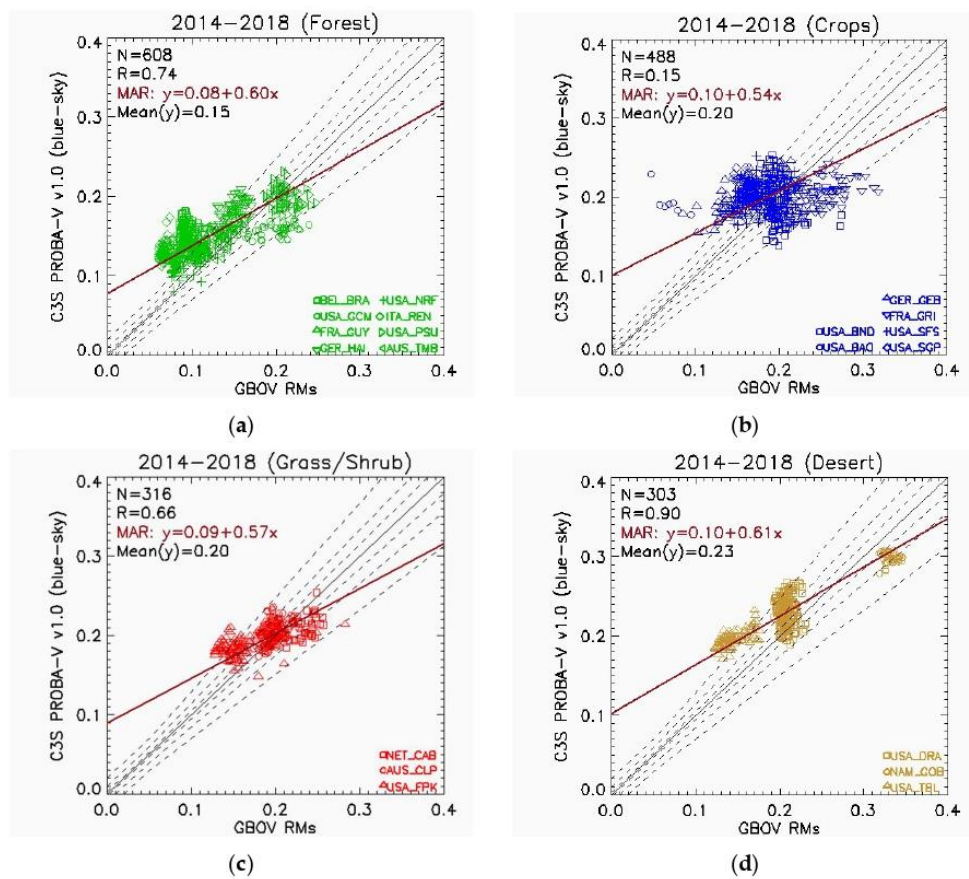


Figure A1. Direct validation per biome type (a) Forest, (b) Crops, (c) grass/shrublands, and (d) desert of the C3S PROBA-V SA v1.0 blue-sky albedo best quality pixels versus the ground measurements (RMs) at 20 GBOV stations during the 2014–2018 period. The continuous black lines correspond to the 1:1 lines and the dashed lines correspond to the optimal (GCOS uncertainty requirement), target (C3S KPI) and predefined threshold levels. The red lines correspond to the Major Axis Regression (MAR).

- MCD43A3 C6

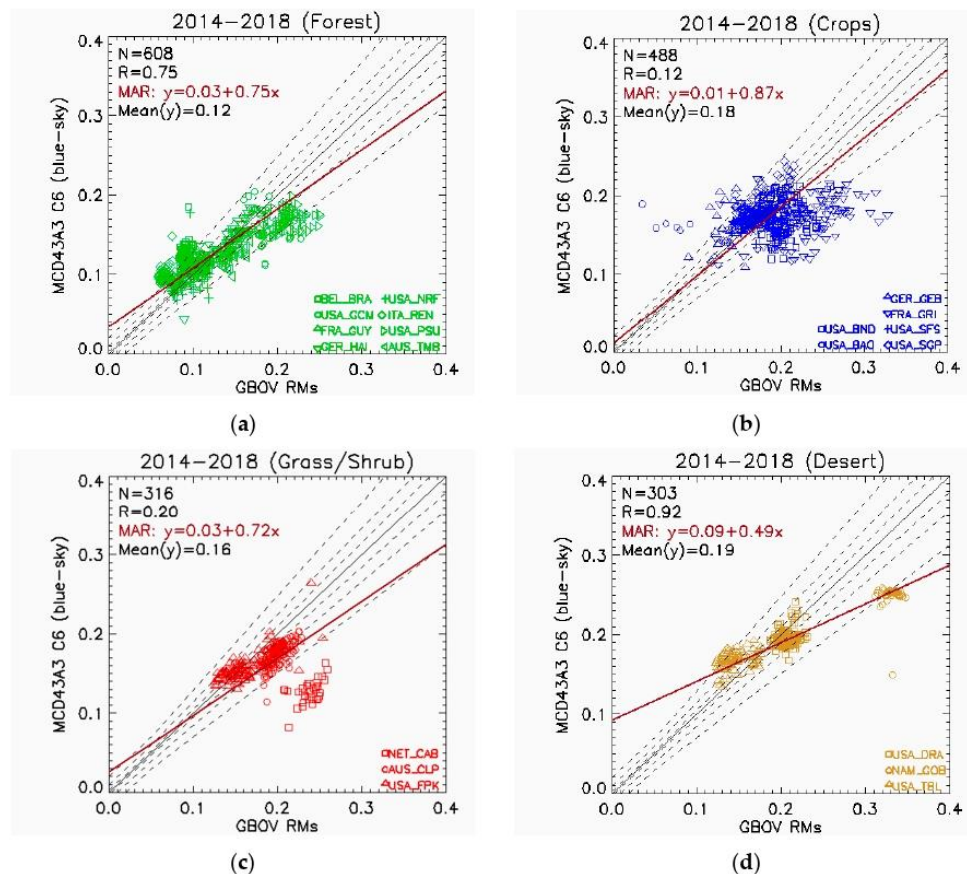


Figure A2. Direct validation per biome type (a) Forest, (b) Crops, (c) grass/shrublands, and (d) desert of the MCD43A3 C6 blue-sky albedo best quality pixels versus the ground measurements (RMs) at 20 GBOV stations during the 2014–2018 period. The continuous black lines correspond to the 1:1 lines and the dashed lines correspond to the optimal (GCOS uncertainty requirement), target (C3S KPI) and predefined threshold levels. The red lines correspond to the Major Axis Regression (MAR).

Appendix B. Temporal Realism of Blue-Sky Albedos over Gbov Sites

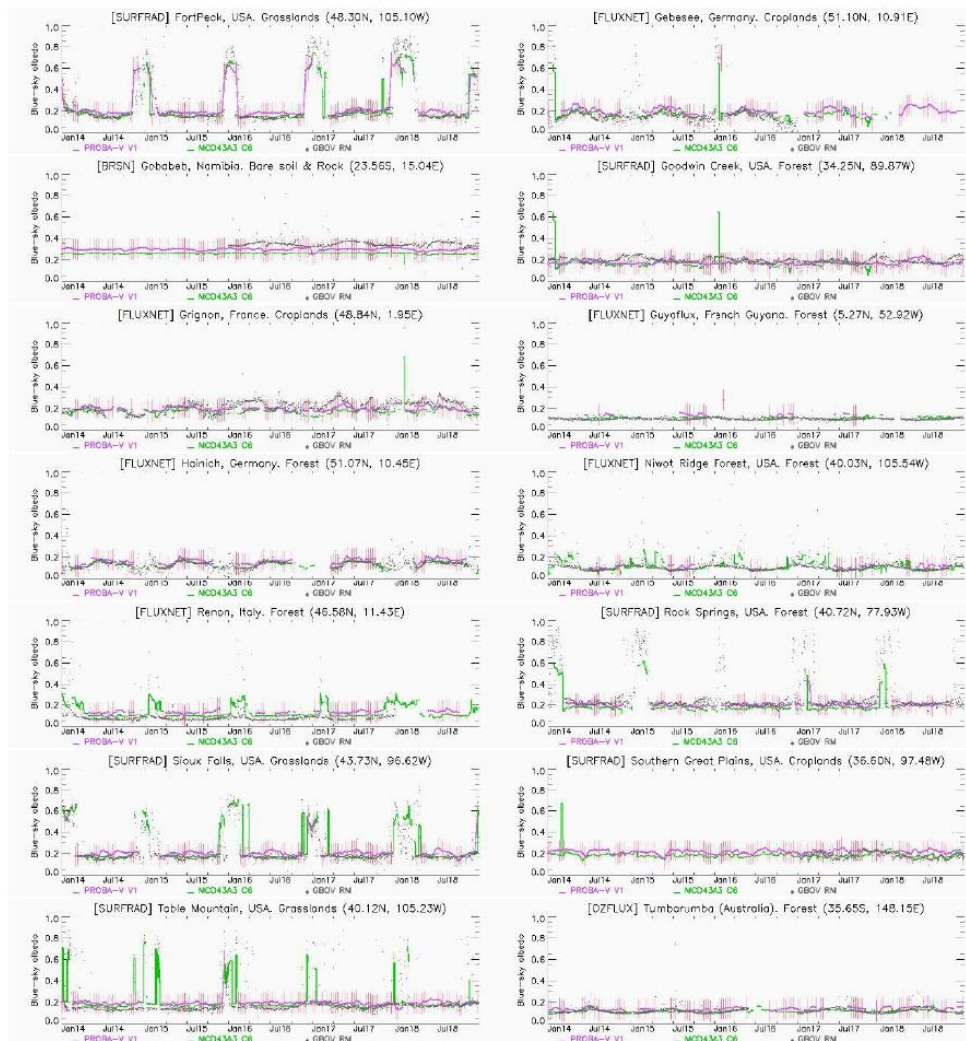


Figure A3. Time series of the blue-sky C3S PROBA-V SA v1.0 and MCD43A3 C6 satellite albedos and GBOV RMs for the selected sites during the 2014–2018 period. In the case of PROBA-V, the filled dots correspond to ‘good quality’ pixels, and the unfilled dots correspond to pixels flagged as ‘low-quality’ according to the QFLAGS (Table 3).

References

1. Implementation Plan for the Global Observing System for Climate in Support of the United Nations Framework Convention on Climate Change (UNFCCC). GCOS-N^o 92. 2004. Available online: https://library.wmo.int/index.php?lvl=notice_display&id=6678#.Xowv2-ozat5t (accessed on 7 April 2020).
2. Copernicus Climate Change Service (C3S). Available online: <https://climate.copernicus.eu/> (accessed on 7 April 2020).

Remote Sens. 2020, 12, 2596

30 of 34

3. Wolters, E.; Dierckx, W.; Iordache, M.-D.; Swinnen, E. PROBA-V Products User Manual Document v3.01. Available online: http://proba-v.vgt.vito.be/sites/proba-v.vgt.vito.be/files/products_user_manual.pdf (accessed on 7 April 2020).
4. Trigo, I.F.; Dacamara, C.C.; Viterbo, P.; Roujean, J.-L.; Olesen, F.; Barroso, C.; Camacho-de-Coca, F.; Carrer, D.; Freitas, S.C.; García-Haro, J.; et al. The Satellite Application Facility for Land Surface Analysis. *Int. J. Remote Sens.* **2011**, *32*, 2725–2744. [CrossRef]
5. Land Surface Analysis (LSA-SAF) of EUMETSAT. Available online: <https://landsaf.ipma.pt/en/> (accessed on 8 April 2020).
6. Geiger, B.; Carrer, D.; Franchistéguy, L.; Roujean, J.L.; Meurey, C. Land surface albedo derived on a daily basis from meteosat second generation observations. *IEEE Trans. Geosci. Remote Sens.* **2008**, *46*, 3841–3856. [CrossRef]
7. Carrer, D.; Roujean, J.L.; Meurey, C. Comparing operational MSG/SEVIRI Land Surface albedo products from Land SAF with ground measurements and MODIS. *IEEE Trans. Geosci. Remote Sens.* **2010**, *48*, 1714–1728. [CrossRef]
8. Carrer, D.; Roujean, J.-L.; Hautecoeur, O.; Elias, T. Daily estimates of aerosol optical thickness over land surface based on a directional and temporal analysis of SEVIRI MSG visible observations. *J. Geophys. Res.* **2010**, *115*, D10208. [CrossRef]
9. Carrer, D.; Moparthy, S.; Lellouch, G.; Ceamanos, X.; Pinault, F.; Freitas, S.C.; Trigo, I.F. Land surface albedo derived on a ten daily basis from Meteosat Second Generation Observations: The NRT and climate data record collections from the EUMETSAT LSA SAF. *Remote Sens.* **2018**, *10*, 1262. [CrossRef]
10. Copernicus Global Land Service (CGLS) Portal. Available online: <https://land.copernicus.eu/global/index.html> (accessed on 8 April 2020).
11. Climate Data Store of Copernicus Climate Change Service. Available online: <https://cds.climate.copernicus.eu/#!/home> (accessed on 10 May 2020).
12. Nightingale, J.; Mittaz, J.P.D.; Douglas, S.; Dee, D.; Ryder, J.; Taylor, M.; Old, C.; Dieval, C.; Fouron, C.; Duveau, G.; et al. Ten Priority Science Gaps in Assessing Climate Data Record Quality. *Remote Sens.* **2019**, *11*, 986. [CrossRef]
13. Justice, C.; Belward, A.; Morisette, J.; Lewis, P.; Privette, J.; Baret, F. Developments in the validation of satellite sensor products for the study of the land surface. *Int. J. Remote Sens.* **2000**, *21*, 3383–3390. [CrossRef]
14. Zeng, Y.; Su, Z.; Calvet, J.C.; Manninen, T.; Swinnen, E.; Schulz, J.; Roebeling, R.; Poli, P.; Tan, D.; Riihelä, A.; et al. Analysis of current validation practices in Europe for space-based climate data records of essential climate variables. *Int. J. Appl. Earth Obs. Geoinf.* **2015**, *42*, 150–161. [CrossRef]
15. Liang, S.; Fang, H.; Chen, M.; Shuey, C.J.; Walthall, C.; Daughtry, C.; Morisette, J.; Schaaf, C.; Strahler, A. Validating MODIS land surface reflectance and albedo products: Methods and preliminary results. *Remote Sens. Environ.* **2002**, *83*, 149–162. [CrossRef]
16. Cescatti, A.; Marcolla, B.; Santhana Vannan, S.K.; Pan, J.Y.; Román, M.O.; Yang, X.; Ciais, P.; Cook, R.B.; Law, B.E.; Matteucci, G.; et al. Intercomparison of MODIS albedo retrievals and in situ measurements across the global FLUXNET network. *Remote Sens. Environ.* **2012**, *121*, 323–334. [CrossRef]
17. Liu, Q.; Wang, L.; Qu, Y.; Liu, N.; Liu, S.; Tang, H.; Liang, S. Preliminary evaluation of the long-term GLASS albedo product. *Int. J. Digit. Earth* **2013**, *6*, 69–95. [CrossRef]
18. Liu, Y.; Wang, Z.; Sun, Q.; Erb, A.M.; Li, Z.; Schaaf, C.B.; Zhang, X.; Román, M.O.; Scott, R.L.; Zhang, Q.; et al. Evaluation of the VIIRS BRDF, Albedo and NBAR products suite and an assessment of continuity with the long term MODIS record. *Remote Sens. Environ.* **2017**, *201*, 256–274. [CrossRef]
19. Shuai, Y.; Schaaf, C.B.; Strahler, A.H.; Liu, J.; Jiao, Z. Quality assessment of BRDF/albedo retrievals in MODIS operational system. *Geophys. Res. Lett.* **2008**, *35*, 1–5. [CrossRef]
20. LPV (Land Product Validation). Subgroup CEOS Validation Hierarchy 2019. Available online: <https://lpvs.gsfc.nasa.gov/> (accessed on 12 April 2020).
21. Wang, Z.; Schaaf, C.; Lattanzio, A.; Carrer, D.; Grant, I.; Roman, M.; Camacho, F.; Yang, Y.; Sánchez-Zapero, J. Global Surface Albedo Product Validation Best Practices Protocol. Version 1.0. In *Best Practice for Satellite Derived Land Product Validation* (p. 45): Land Product Validation Subgroup (WGCV/CEOS); Wang, Z., Nickeson, J., Román, M., Eds.; Available online: https://lpvs.gsfc.nasa.gov/PDF/CEOS_ALBEDO_Protocol_20190307_v1.pdf (accessed on 1 April 2020). [CrossRef]

22. Taberner, M.; Pinty, B.; Govaerts, Y.; Liang, S.; Verstraete, M.M.; Gobron, N.; Widlowski, J.L. Comparison of MISR and MODIS land surface albedos: Methodology. *J. Geophys. Res. Atmos.* **2010**, *115*, 1–13. [CrossRef]
23. Qu, Y.; Liu, Q.; Liang, S.; Wang, L.; Liu, N.; Liu, S. Direct-estimation algorithm for mapping daily land-surface broadband albedo from modis data. *IEEE Trans. Geosci. Remote Sens.* **2014**, *52*, 907–919. [CrossRef]
24. Sütterlin, M.; Schaaf, C.B.; Stöckli, R.; Sun, Q.; Hüsler, F.; Neuhaus, C.; Wunderle, S. Albedo and reflectance anisotropy retrieval from AVHRR operated onboard NOAA and MetOp satellites: Algorithm performance and accuracy assessment for Europe. *Remote Sens. Environ.* **2015**, *168*, 163–176. [CrossRef]
25. Fell, F.; Bennartz, R.; Loew, A. Validation of the EUMETSAT Geostationary Surface Albedo Climate Data Record -2- (ALBEDOVAL-2). Available online: <https://www.eumetsat.int/website/home/Data/TechnicalDocuments/index.html> (accessed on 12 April 2020).
26. Camacho, F.; Sánchez-Zapero, J. Quality Assessment Report SPOT/VGT Surface Albedo V1 (I1.10). Gio Global Land Component - Lot I "Operation of the Global Land Component" Framework Service Contract N° 388533 (JRC). Available online: https://land.copernicus.eu/global/sites/cgls.vito.be/files/products/GIOGL1_VR_SAV1_I1.10.pdf (accessed on 25 March 2020).
27. Sánchez-Zapero, J.; de la Madrid, L.; Camacho, F. Validation Report of Surface Albedo (SA) from PROBA-V Collection 1km Version 1.5 (I2.21). Copernicus Global Land Operations CGLOPS-1 (Framework Service Contract N° 199494 - JRC). Available online: https://land.copernicus.eu/global/sites/cgls.vito.be/files/products/CGLOPS1_VR_SA1km-PROBAV-V1.5_I2.21.pdf (accessed on 9 April 2020).
28. Sánchez-Zapero, J.; de la Madrid, L.; Camacho, F. Quality Assessment Report Normalized TOC-r from PROBA-V Collection 1 km Version 1.5 (I2.21). Copernicus Global Land Operations "Vegetation and Energy" "CGLOPS-1" Framework Service Contract N° 199494 (JRC). Available online: https://land.copernicus.eu/global/sites/cgls.vito.be/files/products/CGLOPS1_QAR_TOCR1km-PROBAV-V1.5_I2.21.pdf (accessed on 11 August 2020).
29. Mayr, S.; Kuenzer, C.; Gessner, U.; Klein, I.; Rutzinger, M. Validation of Earth Observation Time-Series: A Review for Large-Area and Temporally Dense Land Surface Products. *Remote Sens.* **2019**, *11*, 2616. [CrossRef]
30. Lewis, P.; Barnsley, M. Influence of the sky radiance distribution on various formulations of the earth surface albedo. In Proceedings of the 6th International Symposium on Physical Measurements and Signatures in Remote Sensing (ISPRS), Val d'Isere, France, 17–21 January 1994; pp. 707–715.
31. Román, M.O.; Schaaf, C.B.; Woodcock, C.E.; Strahler, A.H.; Yang, X.; Braswell, R.H.; Curtis, P.S.; Davis, K.J.; Dragoni, D.; Goulden, M.L.; et al. The MODIS (Collection V005) BRDF/albedo product: Assessment of spatial representativeness over forested landscapes. *Remote Sens. Environ.* **2009**, *113*, 2476–2498. [CrossRef]
32. Román, M.O.; Schaaf, C.B.; Lewis, P.; Gao, F.; Anderson, G.P.; Privette, J.L.; Strahler, A.H.; Woodcock, C.E.; Barnsley, M. Assessing the coupling between surface albedo derived from MODIS and the fraction of diffuse skylight over spatially-characterized landscapes. *Remote Sens. Environ.* **2010**, *114*, 738–760. [CrossRef]
33. Wang, Z.; Schaaf, C.B.; Chopping, M.J.; Strahler, A.H.; Wang, J.; Román, M.O.; Rocha, A.V.; Woodcock, C.E.; Shuai, Y. Evaluation of Moderate-resolution Imaging Spectroradiometer (MODIS) snow albedo product (MCD43A) over tundra. *Remote Sens. Environ.* **2012**, *117*, 264–280. [CrossRef]
34. Wang, Z.; Schaaf, C.B.; Strahler, A.H.; Chopping, M.J.; Román, M.O.; Shuai, Y.; Woodcock, C.E.; Hollinger, D.Y.; Fitzjarrald, D.R. Evaluation of MODIS albedo product (MCD43A) over grassland, agriculture and forest surface types during dormant and snow-covered periods. *Remote Sens. Environ.* **2014**, *140*, 60–77. [CrossRef]
35. Carrer, D.; Ceamanos, X.; Pinault, F.; Benhadj, I.; Toté, C. Algorithm Theoretical Basis Document (ATBD) of PROBA-V CDR and ICDR Surface Albedo v1.0 (Official Reference Number Service Contract: 2018/C3S_312b_Lot5_VITO/SC1). Available online: <https://cds.climate.copernicus.eu/cdsapp#!/dataset/satellite-albedo?tab=doc> (accessed on 9 April 2020).
36. Carrer, D.; Pinault, F.; Ramon, D.; Benhadj, I.; Swinnen, E. Algorithm Theoretical Basis Document (ATBD) of CDR SPOT/VGT Surface Albedo v1.0 (Official Reference Number Service Contract: 2018/C3S_312b_Lot5_VITO/SC1). Available online: <https://cds.climate.copernicus.eu/cdsapp#!/dataset/satellite-albedo?tab=doc> (accessed on 9 April 2020).
37. Schaaf, C.B.; Gao, F.; Strahler, A.H.; Lucht, W.; Li, X.; Tsang, T.; Strugnell, N.C.; Zhang, X.; Jin, Y.; Muller, J.P.; et al. First operational BRDF, albedo nadir reflectance products from MODIS. *Remote Sens. Environ.* **2002**, *83*, 135–148. [CrossRef]
38. Francois, M.; Santandrea, S.; Mellab, K.; Vrancken, D.; Versluys, J. The PROBA-V mission: The space segment. *Int. J. Remote Sens.* **2014**, *35*, 2548–2564. [CrossRef]

39. Dierckx, W.; Sterckx, S.; Benhadj, I.; Livens, S.; Duhoux, G.; Van Achteren, T.; Francois, M.; Mellab, K.; Saint, G. PROBA-V mission for global vegetation monitoring: Standard products and image quality. *Int. J. Remote Sens.* **2014**, *35*, 2589–2614. [CrossRef]
40. PROBA-V Products Data Access. Available online: <http://proba-v.vgt.vito.be/en/product-types> (accessed on 8 April 2020).
41. Carrer, D.; Benhadj, I. Product User Guide and Specification (PUGS) of PROBA-V CDR and ICDR Surface Albedo v1.0 (Official Reference Number Service Contract: 2018/C3S_312b_Lot5_VITO/SC1). Available online: <https://cds.climate.copernicus.eu/cdsapp#!/dataset/satellite-albedo?tab=doc> (accessed on 9 April 2020).
42. Roujean, J.-L.; Leroy, M.; Deschamps, P.-Y. A bidirectional reflectance model of the Earth's surface for the correction of remote sensing data. *J. Geophys. Res.* **1992**, *97*, 20455–20468. [CrossRef]
43. Carrer, D.; Smets, B.; Ceamanos, X.; Roujean, J.-L. SPOT/VEGETATION and PROBA-V Surface Albedo Products—1 Km Version 1; Algorithm Theoretical Basis Document (ATBD), Issue 2.11. Copernicus Global Land Operations CGLOPS-1 (Framework Service Contract N° 199494-JRC). Available online: https://land.copernicus.eu/global/sites/cgls.vito.be/files/products/CGLOPS1_ATBD_SA1km-V1_I2.11.pdf (accessed on 10 May 2020).
44. Toté, C.; Swinnen, E.; Sterckx, S.; Clarijs, D.; Quang, C.; Maes, R. Evaluation of the SPOT/VEGETATION Collection 3 reprocessed dataset: Surface reflectances and NDVI. *Remote Sens. Environ.* **2017**, *201*, 219–233. [CrossRef]
45. Lucht, W.; Schaaf, C.B.; Strahler, A.H. An algorithm for the retrieval of albedo from space using semiempirical BRDF models. *IEEE Trans. Geosci. Remote Sens.* **2000**, *38*, 977–998. [CrossRef]
46. Sanchez-Zapero, J. Product Quality Assessment Report (PQAR) of CDR SPOT/VGT-Based Surface Albedo v1.0 (Official Reference Number Service Contract: 2018/C3S_312b_Lot5_VITO/SC1). Available online: <https://cds.climate.copernicus.eu/cdsapp#!/dataset/satellite-albedo?tab=doc> (accessed on 9 April 2020).
47. Schaaf, C.; Wang, Z. MCD43A3 MODIS/Terra+Aqua BRDF/Albedo Daily L3 Global-500m V006 [Data set]. NASA EOSDIS Land Processes DAAC. 2015. Available online: <https://doi.org/10.5067/MODIS/MCD43A3.006> (accessed on 10 April 2020).
48. Lucht, W.; Lewis, P. Theoretical noise sensitivity of BRDF and albedo retrieval from the EOS-MODIS and MISR sensors with respect to angular sampling. *Int. J. Remote Sens.* **2000**, *21*, 81–98. [CrossRef]
49. Sun, Q.; Wang, Z.; Li, Z.; Erb, A.; Schaaf, C.B. Evaluation of the global MODIS 30 arc-second spatially and temporally complete snow-free land surface albedo and reflectance anisotropy dataset. *Int. J. Appl. Earth Obs. Geoinf.* **2017**, *58*, 36–49. [CrossRef]
50. Liang, S.; Strahler, A.H.; Walthall, C. Retrieval of Land Surface Albedo from Satellite Observations: A Simulation Study. *J. Appl. Meteorol.* **1999**, *38*, 712–725. [CrossRef]
51. Wang, Z.; Schaaf, C.B.; Sun, Q.; Shuai, Y.; Román, M.O. Capturing rapid land surface dynamics with Collection V006 MODIS BRDF/NBAR/Albedo (MCD43) products. *Remote Sens. Environ.* **2018**, *207*, 50–64. [CrossRef]
52. Roujean, J.L.; Leon-Tavares, J.; Smets, B.; Claes, P.; Camacho De Coca, F.; Sanchez-Zapero, J. Surface albedo and toc-r 300 m products from PROBA-V instrument in the framework of Copernicus Global Land Service. *Remote Sens. Environ.* **2018**, *215*, 57–73. [CrossRef]
53. Ground-Based Observations for Validation (GBOV) of Copernicus Global Land Products Site. Available online: <https://land.copernicus.eu/global/gbov> (accessed on 1 April 2020).
54. Song, R.; Muller, J.-P.; Kharbouche, S.; Woodgate, W. Intercomparison of Surface Albedo Retrievals from MISR, MODIS, CGLS Using Tower and Upscaled Tower Measurements. *Remote Sens.* **2019**, *11*, 644. [CrossRef]
55. Kharbouche, S.; Song, R.; Muller, J.-P. Algorithm Theoretical Basis Document of Energy products: RM1 (short wave radiation), LP1 (Top Of Canopy Reflectance), LP2 (Albedo). Ground-Based Observations for Validation (GBOV) of CGLS Products (Framework Contract reference: 932059-JRC). Available online: https://gbov.acri.fr/public/docs/products/2019-11/GBOV-ATBD-RM1-LP1-LP2_v1.3-Energy.pdf (accessed on 10 April 2020).
56. Song, R.; Muller, J.P.; Kharbouche, S.; Yin, F.; Woodgate, W.; Kitchen, M.; Roland, M.; Arriga, N.; Meyer, W.; Koerber, G.; et al. Validation of space-based albedo products from upscaled tower-based measurements over heterogeneous and homogeneous landscapes. *Remote Sens.* **2020**, *12*, 833. [CrossRef]

57. Reda, I. Method to calculate uncertainties in measuring shortwave solar irradiance using thermopile and semiconductor solar radiometers, Tech. Rep. NREL/TP-3B10-52194, 20 pp., Natl. Renewable Energy Lab., Golden, Colo. 2011. Available online: <http://www.osti.gov/servlets/purl/1021250/> (accessed on 5 August 2020). [CrossRef]
58. Hohn, M.E. An Introduction to Applied Geostatistics: By Edward H. Isaaks and R. Mohan Srivastava, 1989, Oxford University Press, New York, 561 p., ISBN 0-19-505012-6, ISBN 0-19-505013-4. *Comput. Geosci.* **1991**, *17*, 471–473. [CrossRef]
59. Carroll, S.S.; Cressie, N. A COMPARISON OF GEOSTATISTICAL METHODOLOGIES USED TO ESTIMATE SNOW WATER EQUIVALENT. *J. Am. Water Resour. Assoc.* **1996**, *32*, 267–278. [CrossRef]
60. Matheron, G. Principles of geostatistics. *Econ. Geol.* **1963**, *58*, 1246–1266. [CrossRef]
61. Woodcock, C.E.; Strahler, A.H.; Jupp, D.L.B. The use of variograms in remote sensing: I. Scene models and simulated images. *Remote Sens. Environ.* **1988**, *25*, 323–348. [CrossRef]
62. Woodcock, C.E.; Strahler, A.H.; Jupp, D.L.B. The use of variograms in remote sensing: II. Real digital images. *Remote Sens. Environ.* **1988**, *25*, 349–379. [CrossRef]
63. Wang, Z.; Schaaf, C.B.; Sun, Q.; Kim, J.H.; Erb, A.M.; Gao, F.; Román, M.O.; Yang, Y.; Petroy, S.; Taylor, J.R.; et al. Monitoring land surface albedo and vegetation dynamics using high spatial and temporal resolution synthetic time series from Landsat and the MODIS BRDF/NBAR/albedo product. *Int. J. Appl. Earth Obs. Geoinf.* **2017**, *59*, 104–117. [CrossRef]
64. Systematic Observation Requirements for Satellite-Based Data Products for Climate. Supplemental Details to the Satellite-Based Component of the “Implementation Plan for the GCOS in Support of the UNFCCC”. [GCOS-154, 2011 Update]. Available online: https://library.wmo.int/doc_num.php?explnum_id=3710 (accessed on 10 April 2020).
65. World Meteorological Organization (WMO) Requirements for Earth Surface Albedo. Available online: <https://www.wmo-sat.info/oscar/variables/view/54> (accessed on 10 April 2020).
66. Sánchez-Zapero, J.; Camacho, F. Product Quality Assessment Report (PQAR) of CDR and ICDR Surface Albedo v1.0 Based on PROBA-V (Official Reference Number Service Contract: 2018/C3S_312b_Lot5_VITO/SC1). Available online: <https://cds.climate.copernicus.eu/cdsapp#!/dataset/satellite-albedo?tab=doc> (accessed on 9 April 2020).
67. Fuster, B.; Sánchez-Zapero, J.; Camacho, F.; García-Santos, V.; Verger, A.; Lacaze, R.; Weiss, M.; Baret, F.; Smets, B. Quality Assessment of PROBA-V LAI, fAPAR and fCOVER Collection 300 m Products of Copernicus Global Land Service. *Remote Sens.* **2020**, *12*, 1017. [CrossRef]
68. Joint Committee for Guides in Metrology (JCGM)-Guides to the Expression of Uncertainty in Measurement (GUM). [ISO/IEC Guide 98-Part 3, 2008]. Available online: <https://www.iso.org/sites/JCGM/GUM-introduction.htm> (accessed on 10 April 2020).
69. Weiss, M.; Baret, F.; Garrigues, S.; Lacaze, R. LAI and fAPAR CYCLOPES global products derived from VEGETATION. Part 2: Validation and comparison with MODIS collection 4 products. *Remote Sens. Environ.* **2007**, *110*, 317–331. [CrossRef]
70. Sánchez, J.; Camacho, F.; Lacaze, R.; Smets, B. Early validation of PROBA-V GEOV1 LAI, FAPAR and FCOVER products for the continuity of the copernicus global land service. *Int. Arch. Photogramm. Remote Sens. Spat. Inf. Sci.-ISPRS Arch.* **2015**, *40*, 93–100. [CrossRef]
71. Harper, W.V. Reduced Major Axis regression: Teaching alternatives to Least Squares. In Proceedings of the 9th International Conference on Teaching Statistics (ICOTS-9), Flagstaff, AZ, USA, 13–18 July 2014; pp. 1–4. Available online: https://digitalcommons.otterbein.edu/math_fac/24 (accessed on 11 August 2020).
72. Iannone, R.Q.; Niro, F.; Goryl, P.; Dransfeld, S.; Hoersch, B.; Stelzer, K.; Kirches, G.; Paperin, M.; Brockmann, C.; Gomez-Chova, L.; et al. Proba-V cloud detection Round Robin: Validation results and recommendations. In Proceedings of the 2017 9th International Workshop on the Analysis of Multitemporal Remote Sensing Images, MultiTemp 2017, Brugge, Belgium, 27–29 June 2017; pp. 1–8. Available online: <https://ieeexplore.ieee.org/document/8035219> (accessed on 11 August 2020). [CrossRef]
73. Maignan, F.; Bréon, F.M.; Lacaze, R. Bidirectional reflectance of Earth targets: Evaluation of analytical models using a large set of spaceborne measurements with emphasis on the Hot Spot. *Remote Sens. Environ.* **2004**, *90*, 210–220. [CrossRef]
74. Liu, S.; Liu, Q.; Liu, Q.; Wen, J.; Li, X. The Angular and Spectral Kernel Model for BRDF and Albedo Retrieval. *IEEE J. Sel. Top. Appl. Earth Obs. Remote Sens.* **2010**, *3*, 241–256. [CrossRef]

75. Chen, J.M.; Cihlar, J. A hotspot function in a simple bidirectional reflectance model for satellite applications. *J. Geophys. Res. Atmos.* **1997**, *102*, 25907–25913. [[CrossRef](#)]
76. Wu, A.; Li, Z.; Cihlar, J. Effects of land cover type and greenness on advanced very high resolution radiometer bidirectional reflectances: Analysis and removal. *J. Geophys. Res.* **1995**, *100*, 9179–9192. [[CrossRef](#)]
77. Jin, Y.; Schaaf, C.B.; Woodcock, C.E.; Gao, F.; Li, X.; Strahler, A.H.; Lucht, W.; Liang, S. Consistency of MODIS surface bidirectional reflectance distribution function and albedo retrievals: 1. Validation. *J. Geophys. Res. D Atmos.* **2003**, *108*, 1–15. [[CrossRef](#)]
78. Sanchez-Zapero, J. Scientific Quality Evaluation (SQE) of PROBA-V Surface Albedo (SA) Collection 1 km Version 1.5 (I2.00). Copernicus Global Land Operations CGLOPS-1 (Framework Service Contract N° 199494-JRC). Available online: https://land.copernicus.eu/global/sites/cgls.vito.be/files/products/CGLOPS1_SQE2017_SA1km-V1_I1.00.pdf (accessed on 9 April 2020).
79. Salomon, J.G.; Schaaf, C.B.; Strahler, A.H.; Gao, F.; Jin, Y. Validation of the MODIS Bidirectional Reflectance Distribution Function and albedo retrievals using combined observations from the Aqua and Terra platforms. *IEEE Trans. Geosci. Remote Sens.* **2006**, *44*, 1555–1564. [[CrossRef](#)]



© 2020 by the authors. Licensee MDPI, Basel, Switzerland. This article is an open access article distributed under the terms and conditions of the Creative Commons Attribution (CC BY) license (<http://creativecommons.org/licenses/by/4.0/>).

Anexo IV – Copia de publicación 3



remote sensing



Article

Surface ALbedo VALidation (SALVAL) Platform: Towards CEOS LPV Validation Stage 4—Application to Three Global Albedo Climate Data RecordsJorge Sánchez-Zapero ^{1,*}, Enrique Martínez-Sánchez ¹, Fernando Camacho ¹, Zhuosen Wang ^{2,3}, Dominique Carrer ⁴, Crystal Schaaf ⁵, Francisco Javier García-Haro ⁶, Jaime Nickeson ^{7,8} and Michael Cosh ⁹

- ¹ Earth Observation Laboratory (EOLAB), C/ Savina 8–A4, 46980 Paterna, València, Spain
 - ² Earth System Science Interdisciplinary Center, University of Maryland College Park, College Park, MD 20742, USA
 - ³ Terrestrial Information Systems Laboratory, NASA Goddard Space Flight Center, Greenbelt, MD 20771, USA
 - ⁴ CNRM—Centre National de Recherches Météorologiques (CNRM), Université de Toulouse, Météo France, CNRS, 42 Avenue Gaspard Coriolis, 31057 Toulouse, France
 - ⁵ School for the Environment, University of Massachusetts Boston, Boston, MA 02125, USA
 - ⁶ Earth Physics and Thermodynamics Department, Faculty of Physics, Universitat de València, Dr. Moliner, 46100 Burjassot, València, Spain
 - ⁷ Science Systems and Applications, Inc., 10210 Greenbelt Rd., Lanham, MD 20706, USA
 - ⁸ NASA Goddard Space Flight Center (GSFC), Biospheric Sciences Laboratory, 8800 Greenbelt Rd., Greenbelt, MD 20771, USA
 - ⁹ USDA Agricultural Research Service, Hydrology and Remote Sensing Laboratory, 10300 Baltimore Ave., Beltsville, MD 20705, USA
- * Correspondence: jorge.sanchez@eolab.es



Citation: Sánchez-Zapero, J.; Martínez-Sánchez, E.; Camacho, F.; Wang, Z.; Carrer, D.; Schaaf, C.; García-Haro, F.J.; Nickeson, J.; Cosh, M. Surface ALbedo VALidation (SALVAL) Platform: Towards CEOS LPV Validation Stage 4—Application to Three Global Albedo Climate Data Records. *Remote Sens.* **2023**, *15*, 1081. <https://doi.org/10.3390/rs15041081>

Academic Editor: Yi Luo

Received: 11 January 2023

Revised: 9 February 2023

Accepted: 11 February 2023

Published: 16 February 2023



Copyright: © 2023 by the authors. Licensee MDPI, Basel, Switzerland. This article is an open access article distributed under the terms and conditions of the Creative Commons Attribution (CC BY) license (<https://creativecommons.org/licenses/by/4.0/>).

Abstract: The Surface ALbedo VALidation (SALVAL) online platform is designed to allow producers of satellite-based albedo products to move to operational validation systems. The SALVAL tool integrates long-term satellite products, global in situ datasets, and community-agreed-upon validation protocols into an online and interactive platform. The SALVAL tool, available on the ESA Cal/Val portal, was developed by EOLAB under the framework outlined by the Committee on Earth Observation Satellites (CEOS) Working Group on Calibration and Validation (WGCV) Land Product Validation (LPV) subgroup, and provides transparency, consistency, and traceability to the validation process. In this demonstration, three satellite-based albedo climate data records from different operational services were validated and intercompared using the SALVAL platform: (1) the Climate Change Service (C3S) multi-sensor product, (2) the NASA MODIS MCD43A3 product (C6.1) and (3) Beijing Normal University's Global Land Surface Satellites (GLASS) version 4 products. This work demonstrates that the three satellite albedo datasets enable long-term reliable and consistent retrievals at the global scale, with some discrepancies between them associated with the retrieval processing chain. The three satellite albedo products show similar uncertainties (RMSD = 0.03) when comparing the best quality retrievals with ground measurements. The SALVAL platform has proven to be a useful tool to validate and intercompare albedo datasets, allowing them to reach stage 4 of the CEOS LPV validation hierarchy.

Keywords: surface albedo; validation; MODIS; MCD43; C3S; SPOT/VGT; PROBA-V; GLASS; CEOS LPV

1. Introduction

Land Surface Albedo (SA), defined as the ratio of the radiant flux reflected from the Earth's land surface to the incident flux on it, is a parameter of critical importance in understanding both climate and vegetation dynamics [1], and plays a significant role in quantifying the surface energy balance and parameterizing global and regional climate models [2]. SA, established as an Essential Climate Variable (ECV) by the Global Climate

Observing System (GCOS) [3], connects the land surface and climate system through the regulation of the shortwave energy exchange [4–6].

Many SA products derived from satellites have been developed and made available to the user community over the last 40 years [7,8] thanks to the availability of well-characterized and calibrated satellite data, and pressing demands from the user community to have access to consistent and ready to use products. The current state-of-the-art method for the computation of surface albedo is to use a Bidirectional Reflectance Distribution Function (BRDF) kernel-based approach for the development of hemispherical albedo products from a number of multi-angular space-borne sensors. This approach is a pragmatic and cost-effective solution to the surface brightness inversion problem of operational programs that are constrained by the need to process extensive amounts of satellite data in near real time. Such an approach was adopted for near real time retrieval of albedo from ADEOS/POLDER [9], Terra + Aqua/MODIS [10,11], MSG/SEVIRI, and MetOp/AVHRR [12–16] in the framework of the Land Surface Analysis Satellite Application Facility (LSA SAF) [17,18], from SPOT/VGT and PROBA-V in Copernicus Global Land Service (CGLS) [19] and Copernicus Climate Change Service (C3S) [14,20], and recently adopted for Sentinel-3 data [21] in the C3S.

Due to the multitude of albedo products available, users face a complex situation because of the spatial and temporal discrepancies among them [13,22–24]. Therefore, product quality needs to be assessed, the product's compliance with requirements must be known, and the user should know to what extent a product is suitable for their specific application [25]. Thus, the availability of reliable in situ data for direct validation of remote sensing ECV products is a key scientific requisite for users to make effective decisions [26] about the utility of a given ECV.

The Land Product Validation (LPV) subgroup [27] of the Committee for Earth Observation Satellites (CEOS) Working Group on Calibration and Validation (WGCV) (the so-called CEOS LPV) coordinates the quantitative validation of satellite-derived land products, focusing on standardized intercomparisons and evaluation across products from different satellites, algorithms, and agency sources. Validation is defined as the process of independently assessing and evaluating the quality of the data products from the system outputs [28]. In terms of satellite-based land products, validation refers to the assessment and quantification of their accuracy and uncertainties via analytical comparisons with reference datasets. In 2019, the CEOS LPV subgroup compiled a global surface albedo product validation best practices protocol [29], a community-agreed-upon document on validation best practices for satellite-based albedo products. The validation protocol is mainly based on two strategies: comparison of satellite products versus in situ data (direct validation) and intercomparison of satellite products (indirect validation).

A hierarchical approach that identifies four land product validation stages (Table 1) was adopted by CEOS LPV, following CEOS validation principles [30]. Stage 3 implies that uncertainties are evaluated over a significant set of locations (>30), using community consensus protocols, where spatial and temporal consistency is evaluated over globally representative locations. Stage 4 includes systematic and regular update of stage 3 validation results when new product versions are released, or as the time series expands. Stage 4 implies an operational validation that ensures time series are systematically validated.

A current review of the literature revealed only a few long-term global SA validation exercises [31]. Among them, global albedo products from MODIS observations [22,32,33], PROBA-V [24], SPOT/VGT, and EPS/AVHRR [15] were validated to the CEOS LPV stage 3 hierarchy level. However, in most cases, the existing validation results are not directly comparable, as validation practices are rather diverse in terms of methods, reference data and locations, lack of traceability and transparency, spatiotemporal coverage, scaling, metrics and target accuracies, resulting in a considerable lack of consistency in validation outputs [8]. These inconsistencies support the movement of the future validation activities into an operational validation workflow that would align all the various aspects, thus

allowing for consistent and traceable validation of the existing satellite-based albedo products.

Table 1. The CEOS LPV validation stages [27].

Stage	Description
0	No validation. Product accuracy has not been assessed. Product considered beta.
1	Product accuracy is assessed from a small (typically < 30) set of locations and time periods by comparison with in situ or other suitable reference data.
2	Product accuracy is estimated over a significant (typically > 30) set of locations and time periods by comparison with reference in situ or other suitable reference data. Spatial and temporal consistency of the product, and its consistency with similar products, has been evaluated over globally representative locations and time periods. Results are published in the peer-reviewed literature.
3	Uncertainties in the product and its associated structure are well quantified over a significant (typically > 30) set of locations and time periods representing global conditions by comparison with reference in situ or other suitable reference data. Validation procedures follow community-agreed-upon good practices. Spatial and temporal consistency of the product, and its consistency with similar products, has been evaluated over globally representative locations and time periods. Results are published in the peer-reviewed literature.
4	Validation results for stage 3 are systematically updated when new product versions are released or as the inter-annual time series expands. When appropriate for the product, uncertainties in the product are quantified using fiducial reference measurements over a global network of sites and time periods (if available).

An operational validation workflow to validate remote sensing global terrestrial ECV products should consider, at least, four key components [8]: (1) the long-term Climate Data Records (CDRs) of satellite-based ECVs; (2) a set of representative, reliable, and globally distributed in situ measurements; (3) a suitable standard assessment framework based on community-agreed-upon validation best practice protocols; and (4) an online validation platform that provides open-access tools to generate standardized validation reports.

In this context, the Surface ALbedo VALidation (SALVAL) web tool [34] has been developed, integrating these four key components, in order to facilitate the evaluation of global albedo products derived from satellite data in accordance with the CEOS LPV validation good practice [29]. The main objectives of the SALVAL tool are: (i) to provide transparency and traceability (i.e., reproducibility) to the validation process; (ii) to integrate the protocols and metrics from the CEOS LPV albedo product validation best practices document [29] into a tool within which the user can analyze the different validation criteria; (iii) to provide a platform where new versions or new products can be consistently evaluated; and (iv) to facilitate the update of validation results and to achieve CEOS LPV validation stage 4. The SALVAL tool currently includes existing CDRs and a representative network of ground observations, and, additionally, it also allows for user-friendly result updates for new products or periods.

The objective of this paper is two-fold: (1) to introduce the SALVAL tool and functionalities; and (2) to show an application of validation and intercomparison of three existing surface albedo CDRs: the NASA's MCD43A3 Collection 6.1 (C6.1), C3S SPOT/VGT and PROBA-V V2, and Beijing Normal University's (BNU) GLASS albedo products. The remainder of this paper is structured as follows: Section 2 describes the functionalities of the SALVAL tool; Section 3 presents the specifications and validation results from an intercomparison and validation exercise including these three remote sensing SA products; and Sections 4 and 5 discuss the results and provide the conclusions, respectively.

2. Methods and Datasets: The SALVAL Tool

2.1. Validation Methodology

The validation methodology follows the CEOS LPV best practices protocol for the validation of satellite-derived albedo products [29]. The methods are divided into four categories: product intercomparison, direct validation, precision, and stability. Each category has several sub-criteria, including completeness, spatial consistency, temporal consistency, accuracy, precision, and stability. Table 2 describes the validation methods associated with each criterion. The definitions of the completeness, precision, uncertainty, and accuracy are drawn from the experimental recommendations of the Joint Committee for Guides in Metrology (JCGM) regarding the expression of uncertainty in measurement [35] and from the GCOS [36]. The summary of accuracy, precision, and uncertainty (APU) validation metrics is provided in Table 3. The SALVAL tool allows users the possibility of directly visualizing the results by category and criteria, or they can generate a validation report document of the results.

Table 2. Summary of SALVAL validation methods.

Category	Criteria	Methods
Product inter-comparison	Completeness	Gap size distribution (spatial and temporal) and gap length.
	Spatial consistency	Mean residual and mean difference maps, percentage of cases within requirements
	Temporal consistency	Temporal profiles and histograms of cross-correlation
	Overall analysis	Product histograms, difference histograms, scatterplots (APU validation metrics) and box plots of bias and Root Mean Square Deviation (RMSD) per bin
Direct validation	Temporal realism	Temporal evolution of the satellite-derived products vs ground data
	Overall analysis	Scatterplots (APU validation metrics)
Precision	Intra-annual precision	Median 3-point difference (smoothness)
	Inter-annual precision	Median absolute deviation over desert calibration sites
Stability	Stability	Slope of the 10-year linear regression over desert calibration sites

The validation exercise is based on two main approaches: indirect validation (i.e., satellite product intercomparison) and direct validation. The indirect validation offers a means of assessing the discrepancies (systematic or random) between products and allows the evaluation of the metrics at a global scale due to the limited availability of ground measurements. For satellite-derived albedo, direct validation involves comparison of satellite products with the albedo measured from in situ tower-based instruments. Direct validation enables the assessment of uncertainties, and it may be argued that only such methods can be considered actual validation in the field of remote sensing [23]. SALVAL uses two different sampling strategies for product intercomparison and direct validation, as described below. The list of sites is available at the CEOS Cal/Val portal [37].

The quantitative and qualitative product-to-product intercomparisons are performed over the 720-site land validation (LANDVAL) network [17,28] (shown in Figure 1), which was designed to globally represent the variability of land surface types. This network also includes 19 well-known desert calibration sites [29] for the precision and stability evaluation. Product intercomparison of different satellite products needs a common spatial and temporal sampling. The comparison is performed at 3 km × 3 km spatial support area with the aim of reducing the co-registration errors between products and differences in their sensor point spread function which determines the actual footprint of the data [38,39].

The temporal frequency used corresponds to that of the products under evaluation, which are compared with the closest date of the reference satellite products.

Table 3. APU validation metrics.

Statistics	Comment
N	Number of samples. Indicative of the strength of the validation.
B	Mean Bias. Difference between average values of x and y. Indicative of accuracy and offset. Bias (%) is the relative mean bias between the average of x and y.
MD	Median (i.e., 50th percentile) deviation between x and y. MD is the CEOS LPV good practice reporting of the accuracy. MD (%) is the relative MD between the average of x and y.
STD	Standard deviation of the pair differences. Indicates precision. STD (%) is the relative STD between the average of x and y.
MAD	Median (i.e., 50th percentile) absolute deviation between x and y. MAD is the CEOS LPV good practice indicator of precision. MAD (%) is the relative MAD between the average of x and y.
RMSD	Root Mean Square Deviation. RMSD is the square root of the average of squared errors between x and y. The RMSD is the CEOS LPV good practice reporting of uncertainty. RMSD (%) is the relative RMSD between the average of x and y.
R	Correlation coefficient. Indicates descriptive power of the linear accuracy test. Pearson coefficient is used.
MAR	Slope and offset of the Major Axis Regression (MAR) linear fit. Indicates possible bias.

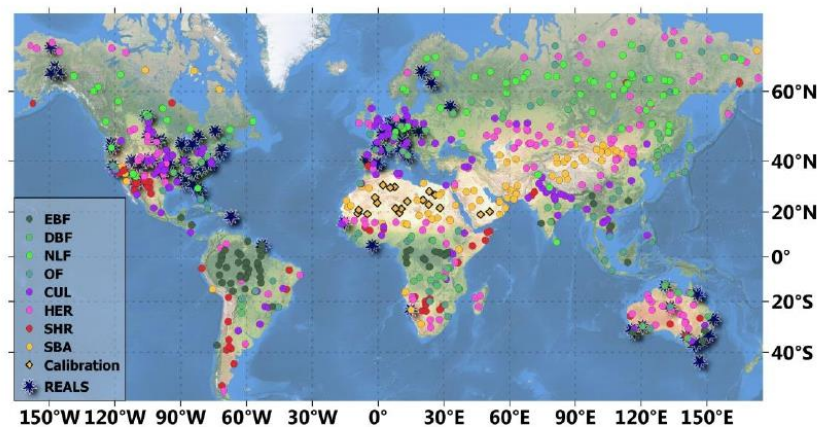


Figure 1. Global distribution of 99 REALS and 720 LANDVAL (including 19 desert calibration) sites used for product intercomparison and direct validation, respectively. LANDVAL are displayed as per biome type: EBF stands for evergreen broadleaved forest, DBF for deciduous broadleaved forest, NLF for needle-leaf forests, OF for other forests, CUL for cultivated, HER for herbaceous, SHR for shrublands, and SBA for sparse and bare areas.

The 99 sites of the Representativeness-Evaluated ALbedo Stations (REALS) dataset (also depicted in Figure 1) are used for the direct point-to-pixel validation (see Section 2.3). In order to compare tower in situ measurements to satellite-based albedo products, the generation of clear blue-sky satellite albedo [40] is performed as the weighted average of black-sky and white-sky retrieved albedos by the fraction of diffuse downwelling shortwave radiation from the ground station at a particular illumination and atmospheric condition. The test of spatial representativeness of the in situ albedometer footprints was performed for

the satellite pixel resolution of interest according to in situ measurement standards [41,42]. This exercise is usually performed at a resolution of 1 km considering only sites that are homogeneous over a footprint area of at least a 1 km² around the albedo in situ station. More details about the test of the spatial representativeness can be found below in Section 2.3. Temporal averages of daily ground data are computed to allow comparison with satellite products generated in composited time intervals.

It is important to highlight the fact that the sampling of LANDVAL and REALS sites allows the validation exercise to reach CEOS LPV stage 3, as uncertainties can be quantified over a significant set of in situ stations (99 REALS) and the spatial and temporal consistency with similar satellite datasets can be evaluated over globally representative locations (LANDVAL).

2.2. Satellite Datasets

Currently, the SALVAL platform incorporates satellite-based albedo datasets from existing programs, such as NASA MODIS [43], Copernicus C3S [20], BNU GLASS [44], or GlobAlbedo [45]. Additionally, the tool also allows for importing either a new product dataset or expanding the temporal coverage of existing products.

In this work, we selected three satellite-based CDRs with around 20 years of data from existing operational programs: NASA MCD43A3 C6.1, C3S multi-sensor V2, and BNU GLASS. These products include the total shortwave domain [0.3 μm , 4 μm], which is the most relevant albedo quantity in terms of energy budget. The total shortwave domain also includes visible [0.4 μm , 0.7 μm] and near-infrared [0.7 μm , 4 μm]. Additionally, different definitions of satellite albedo products exist according to the domain of directional integration [46]: the directional-hemispherical reflectance (DHR) or black-sky albedo (BSA or AL-DH), and the bi-hemispherical reflectance (BHR) or white-sky albedo (WSA or AL-BH). BSA is defined as the ratio of the radiant flux for light reflected by a unit surface area into the view hemisphere to the illumination radiant flux, when the surface is illuminated with a parallel beam of light from a single direction [47]. WSA is the ratio of the radiant flux reflected from a unit surface area into the whole hemisphere to the incident radiant flux of hemispherical angular extent [48]. The combination of both BSA and WSA in relation to the proportion of sky irradiance provides the actual albedo value, also called blue-sky albedo [40].

The three satellite albedo products provide both BSA at local solar noon and WSA for three broadband ranges (visible, NIR, and total shortwave).

2.2.1. NASA MCD43A3 C6.1

The MODIS BRDF/Albedo MCD43A3 C6.1 dataset, available from the LPDAAC [49], produces albedo quantities at a resolution of 500 m in a sinusoidal projection. These quantities have been produced daily since 2000 with a synthesis period of 16 days, using data from both the Terra and Aqua satellites. The MODIS albedo algorithm uses atmospherically corrected cloud-free reflectance data (the MOD/MYD09 product) to establish the best fit to a linear kernel-driven BRDF model. Observations flagged as “cloud”, “cirrus high” or “aerosol high”, or “very high solar zenith angles” are not utilized. The parametric BRDF model uses the Ross_Thick kernel for volumetric scattering and the Li_Sparse_Reciprocal kernel for geometrical scattering [47,50]. A full retrieval of the model is attempted if there are at least seven or more high-quality observations that are well-distributed over the viewing hemisphere during the 16-day synthesis period. When the number of observations is strictly less than 7 and strictly greater than 2, or if observations are not well sampled or do not fit the BRDF model well, though the number of observations is larger than 7, a backup algorithm (magnitude inversion) with prior information is used and the values are designated with a lower quality flag. A fill value is stored if the number of observations is strictly less than 3. Snow and snow-free albedos are processed separately depending on the ground condition of the day of interest. In addition, products at 30 arc second and 0.05 degree resolutions on a geographic lat/lon projection are also available for ease of use

by modelers. Separate 30 arc second snow-free gap-filled products (MCD43GF) are also accessible [51]. The BRDF model parameters are then used for estimating spectral albedos from angular integration. The broadband albedos are then computed using the spectral to broadband conversion approach [52]. The MCD43 C6.1 products use an improved backup database [53], which is pixel-based, updated from the latest high quality full inversion, as opposed to the land cover-based BRDF database used in the previous Collection 5. In this work, the updated C6.1 version is being used, which incorporates the latest improved calibration coefficients and surface reflectance values.

MCD43A3 C6.1 SA products have reached CEOS LPV validation stage 3 [53]. Existing studies of the previous MCD43 Collections 5 and 6 indicate that the accuracy of the MODIS shortwave broadband albedo met the GCOS accuracy requirements (Max [5%, 0.0025]) for both snow-free and snow-covered surfaces [41,42,54,55].

2.2.2. C3S Multi-Sensor V2

The C3S V2 products, which are available in the C3S Climate Data Store (CDS, [56]), provide a CDR of global albedo estimates in a nearly 40-year record of satellite observations from 1981 to 2020, using multiple input datasets: NOAA/AVHRR from 1981 to 2005 (around 4 km pixel size), SPOT/VGT from 1998 to 2014 (1 km pixel size), and PROBA-V from 2014 to 2020 (1 km pixel size). The temporal frequency of the products is 10 days, built with a compositing window of 20 days. The dates of production are the 10th, 20th, and final days of each month.

C3S V2 version builds on V1 [57] and adds a multi-sensor aspect to the albedo products delivered so far. The retrieval algorithm [14,58] uses Top-of-Canopy (TOC) reflectance resulting from both the harmonized pixel classification approach (cloud, snow, and shadow pixels) and the Simplified Method for Atmospheric Correction (SMAC) algorithm [59], to improve satellite cross-consistency. Additionally, a spectral harmonization is performed, by creating TOC reflectance values as if they had been acquired with SPOT/VGT. The harmonized TOC reflectance values are processed to determine the coefficients of a semi-empirical kernel-based reflectance model, which accounts for the complete angular dependence of the bi-directional reflectance factor. This inversion step is performed using prior information and a climatology of surface BRDF. To estimate albedo using a multi-sensor time series, a second harmonization was conducted, using BRDF climatology data from SPOT/VGT. The algorithm [14] relies on a similar method to that of previous versions (Kalman filters and BRDF model fit) but with the addition of a reference BRDF (climatology derived from VGT BRDF) to (i) reduce the gaps in the time series, and (ii) introduce multi-sensor information in each albedo estimation to increase homogeneity among the datasets derived from each sensor. In the final steps, the spectral albedo values are determined from the angular integrals of the model functions using the retrieved parameter, and the narrow-to-broadband conversion is performed with a linear regression formula. A different set of narrow-to-broadband conversion coefficients is applied for snow-free pixels and for pixels flagged as “snow/ice” in the input data status map.

An independent scientific quality assessment of the C3S multi-sensor V2 products was performed [60], considering the whole CDR (1981–2020), achieving CEOS LPV validation stage 2. The V2 time series was demonstrated to be more consistent compared with V1 when changing input data in the transitions from AVHRR to SPOT/VGT and from SPOT/VGT to PROBA-V. Direct validation results of SPOT/VGT SA V2 showed positive bias (12.5%) and overall uncertainty (RMSD) of 0.048 in the comparison with albedo measurements from 15 homogeneous FLUXNET stations (2000–2005 period). The comparison of C3S PROBA-V SA V2 with field data for 20 homogeneous sites from the Copernicus Ground-Based Observations for Validation (GBOV) program (2014–2018 period) also showed positive bias (9.1%) and RMSD of 0.039

2.2.3. BNU GLASS V4

The Global LAnd Surface Satellites [61] (GLASS) product suite provides albedo products from 1981 to 2019 with a temporal resolution of 8 days, and is available from BNU [44]. Products from 1981 to 1999 are derived from AVHRR data, with a spatial resolution of 0.05° in the global Climate Modelling Grid (CMG) projection. The GLASS albedo products from 2000 to 2019 are derived from MODIS data, with a spatial resolution of 1 km in a tile-based sinusoidal projection.

The GLASS albedo products are generated in two steps. First, the albedo is directly retrieved from remote sensing data by employing the second simulation of a satellite signal in the solar spectrum (6S) atmospheric radiative transfer model (RTM) to simulate the TOA directional reflectance, calculating the broadband albedos based on the POLDER BRDF dataset, and then establishing a relationship between the TOA reflectance and surface broadband albedo using an angular bin regression method [62]. Intermediate products from this first step are merged to generate a unique and gap-filled final product based on the Statistics-based Temporal Filtering (STF) algorithm [63]. Additionally, the current version 4 data have been improved with respect to previous versions: the snow/ice BRDF model has been updated [64] and a water surface BRDF model has been adopted for the ocean surface as well as for mixed pixels of water/sea ice [65].

The preliminary evaluation of the GLASS albedo product [22] showed that it is a gapless, long-term, continuous and self-consistent dataset with an accuracy similar to that of the MODIS MCD43 C5 product. Recent validation efforts for version 4 [61] showed that products are consistent with MODIS MCD43A3 C6 over snow-free pixels, and overall uncertainty (RMSD) of 0.052 was found in comparison with tower-based observations from 53 spatially homogeneous global sites. The RMSD was reduced to 0.037 for snow-free pixels.

2.2.4. Summary and Quality Flags

Table 4 summarizes the main features of the three SA products used in this study. Both MCD43A3 and C3S are based on a BRDF model resulting from the combination of two of the same models for defining the volumetric (Ross_Thick) and geometric (Li_Sparse_Reciprocal) kernels [47]. Unlike the MCD43A3 and C3S albedo products, which are based on inversions of BRDF model parameters, the GLASS albedo products are based on the direct-estimation method and represent surface albedo under general clear-sky atmospheric conditions.

Table 4. Characteristics of the global remote sensing SA products under study. GSD stands for the Ground Sampling Distance.

Product	Satellite /Sensor	Methodology	Broadband Definition	Frequency /Period	GSD /Projection	Reference
NASA MCD43A3 C6.1	TERRA + AQUA /MODIS	BRDF model inversion and angular/spectral integration	visible [0.3–0.7 μm] NIR [0.7–5.0 μm] total SW [0.3–5.0 μm]	Daily (*) /16 days	500 m /Sinusoidal	[10]
C3S V2	SPOT /VGT PROBA /VGT	BRDF model inversion and angular/spectral integration	visible [0.4–0.7 μm] NIR [0.7–4 μm] total SW [0.3–4.0 μm]	10 days /20 days using prior climatology BRDF	1 km /Plate Carrée	[14,58]
GLASS V4	TERRA + AQUA /MODIS	RTM + gap-filling	visible [0.3–0.7 μm] NIR [0.7–5.0 μm] total SW [0.3–5.0 μm]	8 days /16 days	1 km /Sinusoidal	[61]

(*) MCD43A3 C6.1 products are produced daily but are ingested into the SALVAL tool at a temporal frequency of 5 days.

The production frequency of C3S V2 and GLASS V4 is 10 and 8 days, respectively. MCD43A3 C6.1 products are originally produced daily, but are ingested into the SALVAL

platform at a temporal frequency of 5 days, due to the limitations in memory storage and processing capabilities of the server.

The quality flag information for each product was used to filter low quality pixels (Table 5), and the SALVAL tool provides the results for both cases of “best quality” retrievals, and all retrieved valid pixels (quality flag not considered).

Table 5. Quality flag information used to filter pixels flagged as “low quality”.

Product	Quality Control Used as “Best Quality”	Quality Control Used to Discard Pixels
MCD43A2 C6.1	Full BRDF inversion	Magnitude inversion
C3S V2	Land (bits 0–1 QFLAG) Normally processed (bit 7 QFLAG) ERR \leq 0.2 AGE \leq 20	Sea and continental water (bits 0–1 QFLAG) Algorithm Failed (bit 7 QFLAG) ERR $>$ 0.2 AGE $>$ 20
GLASS V4	Overall uncertainty ‘best quality’	Overall uncertainty ‘acceptable’, ‘with uncertainty’ or ‘fill value’

For MCD43A3 only “best quality” full BRDF inversions were considered, and magnitude BRDF inversions were discarded. Higher confidence is expected for a “full inversion” retrieval that is performed under good sampling of the viewing and illumination geometry for a grid location. The “magnitude inversion” is a backup algorithm, which performs generally well, but relies on prior estimates of the BRDF when insufficient observations are available to fully sample the viewing and illumination geometry. On the other hand, the C3S V2 pixels where the algorithm failed were not considered in this validation exercise. Additionally, two ancillary variables were also considered: the uncertainty (ERR) and the mean age (AGE, in number of days) of the observations used to produce the SA. The C3S V2 pixels with associated uncertainty of greater than 0.2 and an AGE greater than 20 were discarded, indicating excessive use of prior information [60]. Finally, in the case of GLASS V4, only pixels classified as “good overall uncertainty” were considered as “best quality”, while pixels flagged as “acceptable”, “with uncertainty” or “fill value” resulting from gap-filling methods were not considered.

2.3. Representativeness-Evaluated ALbedo Stations (REALS) Dataset

REALS is a database of sites with the objective to generate an extensive in situ dataset for direct validation purposes. The database has been defined as a combination of 99 sites with availability of ground data in the 2000–2020 period from existing networks and initiatives, such as Ground-Based Observations for Validation (GBOV) [66], Flux Network (FLUXNET) [67], the National Science Foundation’s National Ecological Observatory Network (NEON) [68], European Fluxes Database Cluster (EFDC) [69], Integrated Carbon Observation System (ICOS) [70], and Australia’s Land Ecosystem Observatory or Terrestrial Ecosystem (TERN) [71]. Some GBOV, FLUXNET, and EFDC sites incorporate measurements from the Baseline Surface Radiation Network (BSRN) [72] and its U.S. component known as the Surface Radiation Budget (SURFRAD) Network [73]. BSRN is considered the gold standard of albedo measurements according to the GCOS [36] and CEOS LPV albedo best practices protocol [29]. It is worth noting that 23 of these REALS sites are considered “Super Sites” endorsed by the CEOS LPV subgroup, meaning that they are well-characterized (canopy structure and biogeophysical variables) following well-established protocols, and are active in long-term operation, supported by appropriate funding and infrastructural capacity.

The albedo measured from a tower covers a circular footprint (dependent upon the tower height) that should be ideally equivalent to the pixel size of satellite estimation. However, satellite footprints are often much larger than the tower footprints. For that reason, the representativeness of the measurement, both within the tower footprint and in the surrounding landscape, is evaluated through geostatistical indices based on a semi-

variogram model [74,75], following current state-of-the-art protocols [33,41,42] and CEOS LPV recommendations. Four different geostatistical attributes have been used for this evaluation: relative coefficient of variation (R_{CV}), scale requirement index (R_{SE}), relative strength of the spatial correlation (R_{ST}), and relative proportion of structural variation (R_{SV}). They are combined in a condensed indicator of spatial representativeness: the standard score (ST, see Equation (1)). For those situations where the semivariogram estimator does not provide a good fit with a semi-spherical variogram, the first order score (RAW, see Equation (2)) can be adopted to evaluate the spatial representativeness [41]. Both scores are directly proportional to the representativeness or relative homogeneity of a site, so a higher score means that a ground site (point) is more suitable to be comparable to satellite-based measurements (pixel). Note that the cover does not have to be uniform, and can be a heterogeneous landscape, as long as that heterogeneous landscape is similar both within the tower footprint and the surrounding landscape.

$$ST = \left(\frac{|R_{CV}| + |R_{ST}| + |R_{SV}|}{3} + R_{SE} \right)^{-1} \quad (1)$$

$$RAW = |2 R_{CV}|^{-1} \quad (2)$$

The methodology adopted for the evaluation of the representativeness of the sites is based on the estimation of the spherical semivariogram for different spatial resolutions (1, 1.5, and 3 km²). When the semivariogram has been estimated, geostatistical indices are calculated in order to quantify the level of representativeness of a site.

The spatial representativeness is estimated for each site of the REALS sites in different temporal conditions (leaf-off season and leaf-on season) using high-resolution Sentinel-2 imagery [76] for the B8 band, which is the most spectrally representative of the total shortwave [77]. Figure 2 shows an example of variogram fitting and ST estimation over two different sites of the REALS database, Desert Rock (DRAK) and Talladega National Forest (TALL). These results show more homogeneity or spatial representativeness in the case of TALL (ST = 8) in the leaf-on period than in DRAK (no seasonality) (ST = 0.96). Appendix A describes the ST summary of the REALS sites.

In order to choose a ST threshold for filtering non-representative or differing heterogeneous sites, an analysis of the variation in RMSD (uncertainty) of number of sites and samples between the NASA MCD43A3 C6.1 product and REALS sites was performed for the available period (2000–2020). Figure 3 shows the evolution of number of sites, number of samples, and RMSD as function of the ST score for the comparison between the MCD43A3 C6.1 satellite-derived product and REALS in situ measurements for the 2000–2020 period. According to the results, the RMSD tends to decrease when the ST threshold increases, but the numbers of sites and samples decrease. For this reason, a threshold of 1.5 for ST was selected as the filter in the REALS database because the RMSD tends to be stable at this score and the number of sites and samples discarded is reasonable. This threshold is similar to that used in previous works [24,33].

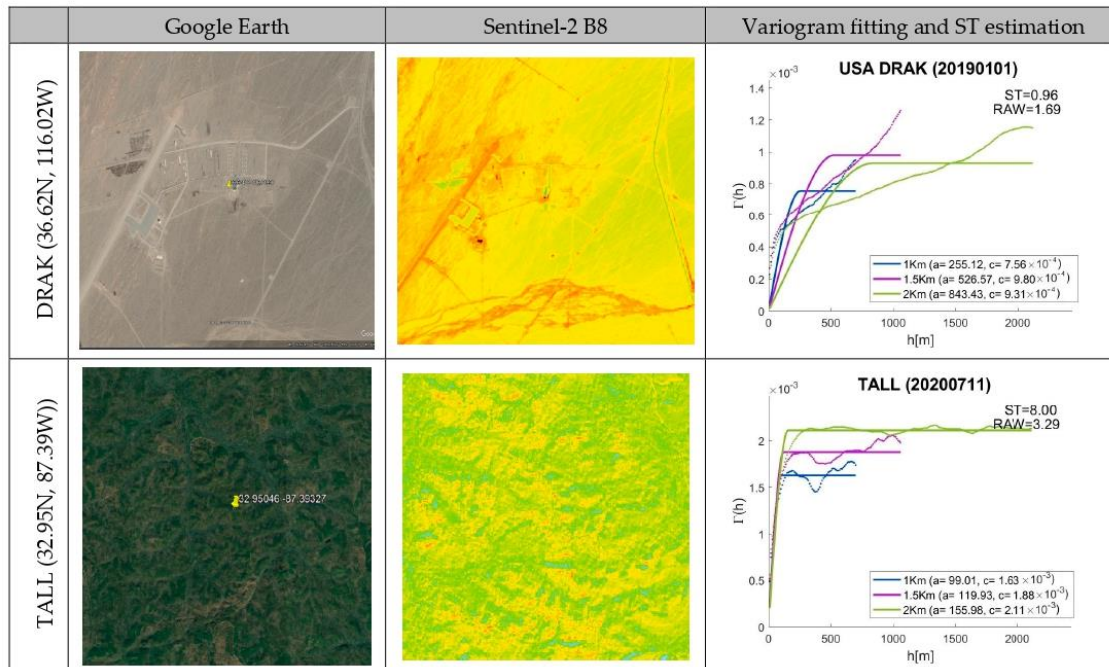


Figure 2. Example of variogram fitting and ST estimation over two different sites, Desert Rock (DRAK) and Talladega National Forest (TALL).

The main characteristics of REALS sites and ST scores for each site are summarized in Appendix A.

2.4. SALVAL Functionalities and Configuration

The SALVAL tool has three main functionalities: (i) to select both the product to be evaluated and the reference products based on existing datasets or importing a new test candidate product; (ii) to configure the validation exercise by selecting a set of user requirements, spectral region, spatial domain, and temporal domain of the study; and (iii) to run the validation exercise according to the previously set configuration, based on the protocols and metrics implemented from the CEOS LPV albedo protocol [29]. More information about the use of the tool can be found in the SALVAL user guide [34] or in Appendix B.

After the selection of the products to be evaluated, SALVAL requires the configuration of the validation exercise. Different sets of configurations should be introduced by the user, such as the period, the albedo type (black-sky or white-sky albedo) for product intercomparison, the user requirements for the evaluation of stability and accuracy, and the spatial region of the study (global or continental region).

The stability and accuracy results were evaluated against three predefined requirement levels (optimal, target, and threshold), which are used for both BSA and WSA products in all spectral broadband domains. We used default values within the SALVAL tool (Table 6), which are based on a review of the existing user requirements for measuring global climate change [78], and from the Global Climate Observing System (GCOS) [36] and the World Meteorological Organization (WMO) [79]. The optimal accuracy level (Max [5%, 0.0025]) was selected according to the GCOS uncertainty threshold and is equivalent to the WMO goal. The target level is equivalent to the WMO breakthrough level, which is an intermediate level between “goal” and “threshold” (i.e., if achieved, would result in

a significant improvement for the targeted application). The breakthrough level may be considered as an optimum, from a cost–benefit point of view, when planning or designing observing systems. Poor performances of the product correspond to values above the threshold levels (WMO minimum requirement). Figure 4 displays the selected uncertainty levels as a function of the product values.

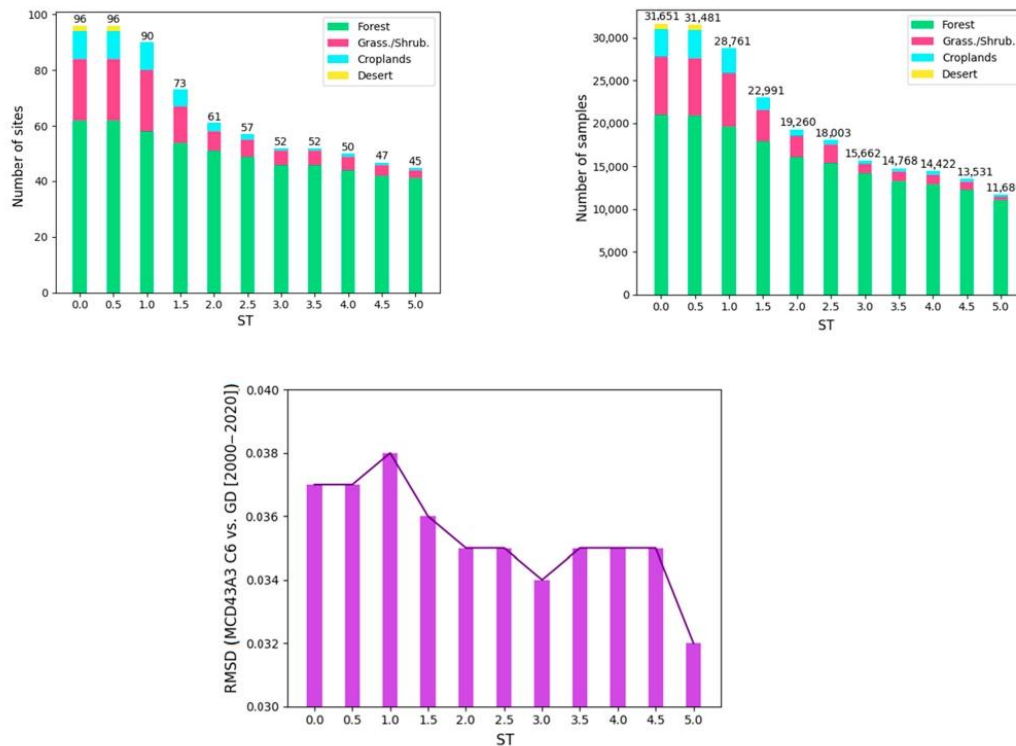


Figure 3. Evolution of Number of sites (top left), Number of samples (top right), and RMSD (bottom) of the comparison of MCD43A3 C6.1 versus REALS sites as a function of the ST score in the 2000–2020 period.

In the recent update of GCOS requirements [80], a new goal uncertainty level of 3% was defined. The SALVAL platform allows modifying the predefined requirements as a function of the user needs.

Table 6. Predefined accuracy and stability requirement levels used for SA validation.

	Optimal	Target	Threshold
Accuracy requirement	Max [5%, 0.0025]	Max [10%, 0.01]	Max [15%, 0.015]
Stability requirement	Max [1%, 0.001]	Max [2%, 0.002]	Max [3%, 0.003]

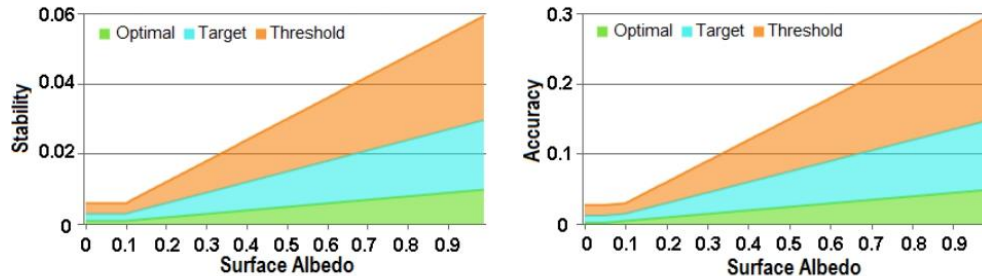


Figure 4. Stability (left) and Accuracy (right) requirement levels as a function of SA values.

The defined temporal domain is the 20-year period from 2000 to 2019. For this period, NASA MCD43A3 C6.1 and GLASS are based on MODIS data whereas C3S multi-sensor V2 products are based on input data from two different platforms (SPOT/VGT for 2000 to May 2014, and PROBA-V from May 2014 to 2019). The whole period is used for direct validation with ground data, and 10 years (2001–2010) is used for the stability evaluation. Product intercomparison and completeness are based on five years (2001–2005) of data, as the SALVAL platform is restricted for those exercises due to computational constraints. The spatial domain covers the whole globe and retrievals from all LANDVAL and REALS sites are included in the analysis.

Results are displayed for total shortwave black-sky albedo (AL-DH-BB) for product intercomparison. For the direct evaluation with in situ measurements, the SALVAL platform computes satellite blue-sky albedos as the weighted average of total shortwave black-sky and white-sky albedos by the fraction of diffuse downwelling shortwave radiation from the ground station.

3. Results

3.1. Product Completeness

The three products (C3S V2, GLASS V4, and MCD43A3 C6.1) show a similar spatial distribution of missing data when all pixels are considered (left side in Figure 5), with gaps mainly located at northern regions. However, when quality flags (see Table 5) are used (right side in Figure 5), MCD43A3 C6.1 is more restrictive, if only pixels based on high-quality full BRDF inversions are considered, compared to C3S V3 and GLASS V4.

The temporal evolution of missing values (Figure 6) is displayed at the different temporal resolutions being used in this effort (i.e., 10, 8, and 5 days for C3S, GLASS, and MCD43A3, respectively) showing similar trends, with the highest percentage of missing data during wintertime in the northern hemisphere (December and January). Products based on MODIS (MCD43A3 C6.1 and GLASS V4) and VGT (C3S V2) show maximum percentages of LANDVAL missing data, typically around 20% and 10%, respectively. When only best quality observations are considered according to quality flags, the most (around 80%) missing values are found for MCD43A3 C6.1, and around 30% missing values are found for the other products (C3S V2 and GLASS V4) that incorporate gap-filling techniques in their algorithms.

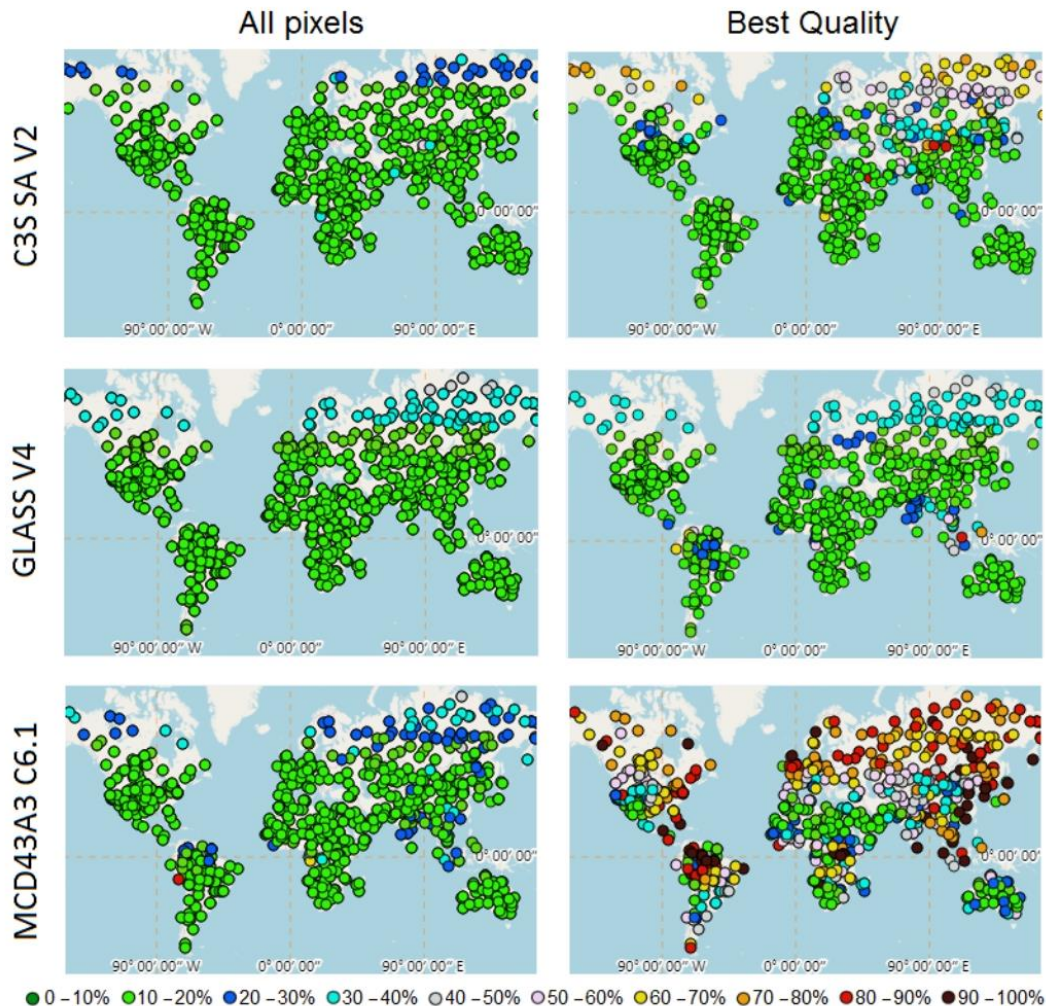


Figure 5. Global maps of the percentage of missing values for C3S V2 (top), GLASS V4 (center), and MCD43A3 C6.1 (bottom) for all pixels (left), and only best quality pixels (right) in the 2003 year, evaluated over the 720 LANDVAL sites.

3.2. Spatial Consistency

The spatial consistency is quantitatively assessed through the global distribution of residuals between pair of products. The residual represents the remaining discrepancies regarding the general trend between products, which means that systematic differences are not considered, depicting more clearly the patterns associated with the spatial distribution of retrievals [81]. Two products are considered spatially consistent when the residual lies within predefined uncertainty requirements. Figure 7 shows the spatial distribution of residuals (average value for 2001–2005 period) between pairs of evaluated products (C3S V2, GLASS V4 and MCD43A3 C6.1). The percentages of residuals within the predefined requirements are summarized in Table 7.

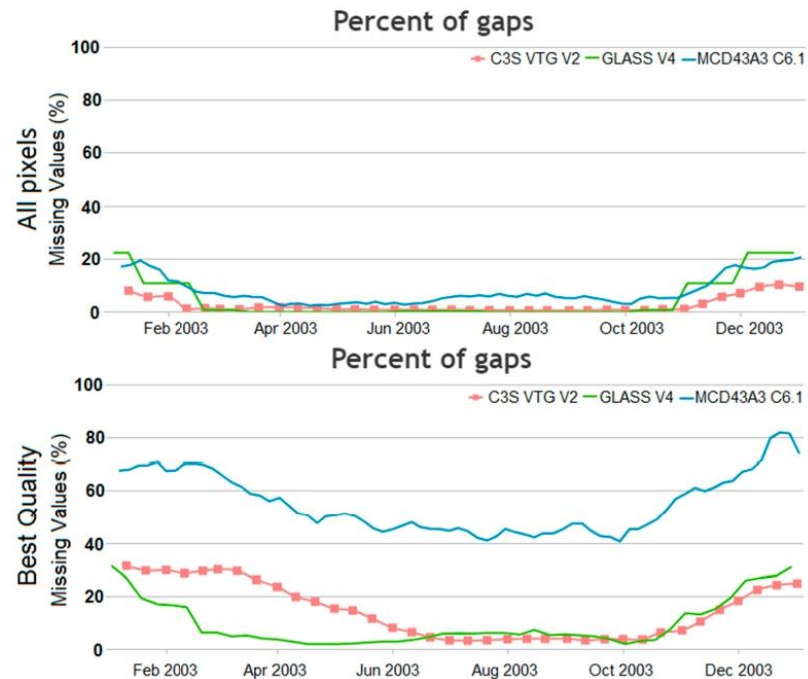


Figure 6. Temporal evolution of the percentage of LANDVAL missing data in the 2003 for C3S V2 (red), GLASS V4 (green), and MCD43A3 C6.1 (blue) considering all pixels (**top**), and only best quality pixels (**bottom**) according to quality flags.

Table 7. Percentage of mean residuals between pair of products (C3S V2, GLASS V4 and MCD43A3 C6.1) within each level of uncertainty requirements. Evaluation in the 2001–2005 period over LANDVAL sites using best quality total shortwave black-sky albedo (AL-DH-BB) retrievals.

Residual	Optimal	Target	Threshold	Non-Compliance
C3S V2 vs. GLASS V4	83.5%	98.1%	99.7%	0.3%
C3S V2 vs. MCD43A3 C61	72.8%	91.8%	95.4%	4.6%
GLASS V4 vs. MCD43A3 C61	89.6%	94.5%	94.9%	5.1%

Most residuals between pairs of products are within ± 0.015 , demonstrating overall good spatial consistency among them. The comparison between GLASS and MCD43A3 shows the higher percentage (around 90%) of evaluated samples within optimal requirements. The comparison of C3S and GLASS seems to display the better spatial consistency, with 98% of cases within target level and almost no non-compliant cases (0.3%). The results show that, in all comparisons, more than 90% of residuals are within target requirements, and typically less than 5% of cases are non-compliant.

3.3. Temporal Consistency

To assess the realism of the seasonal and inter-annual temporal variations, examples of temporal profiles of C3S V2, GLASS V4, and MCD43A3 C6.1 satellite products are qualitatively compared with ground data over REALS sites. It should be noted that two different time periods are displayed due to the different input data used to retrieve C3S V2 products: 2001–2005 (Figure 8, SPOT/VGT) and 2014–2019 (Figure 9, PROBA-V).

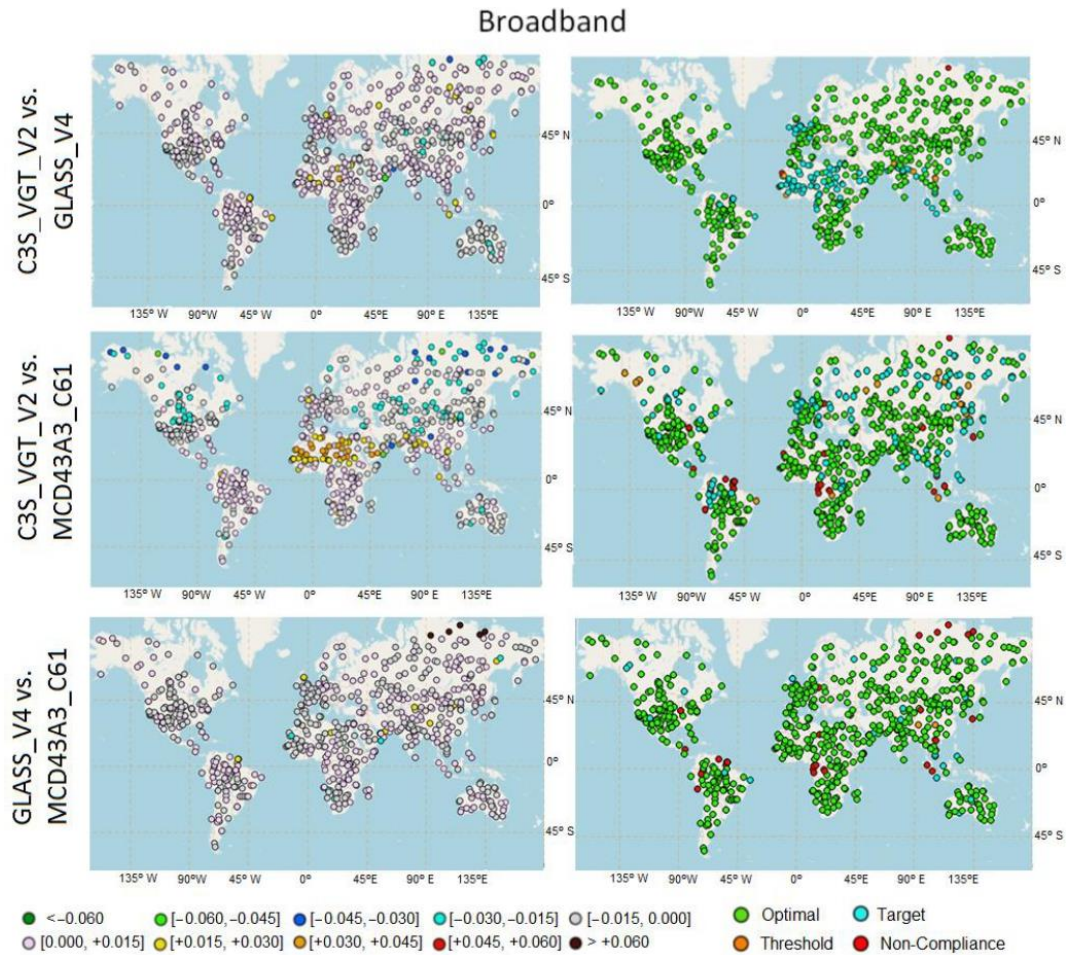


Figure 7. Global spatial distribution of average residuals (**left**) and number of residuals that reach the requirements (**right**) for C3S V2 vs. GLASS V4 (**top**), C3SV2 vs. MCD43A3 C6.1 (**middle**), and GLASS V4 vs. MCD43A3 C6.1 (**bottom**). Evaluation in the 2001–2005 period with a 10-day temporal frequency over LANDVAL sites using best quality total shortwave black-sky albedo (AL-DH-BB) retrievals.

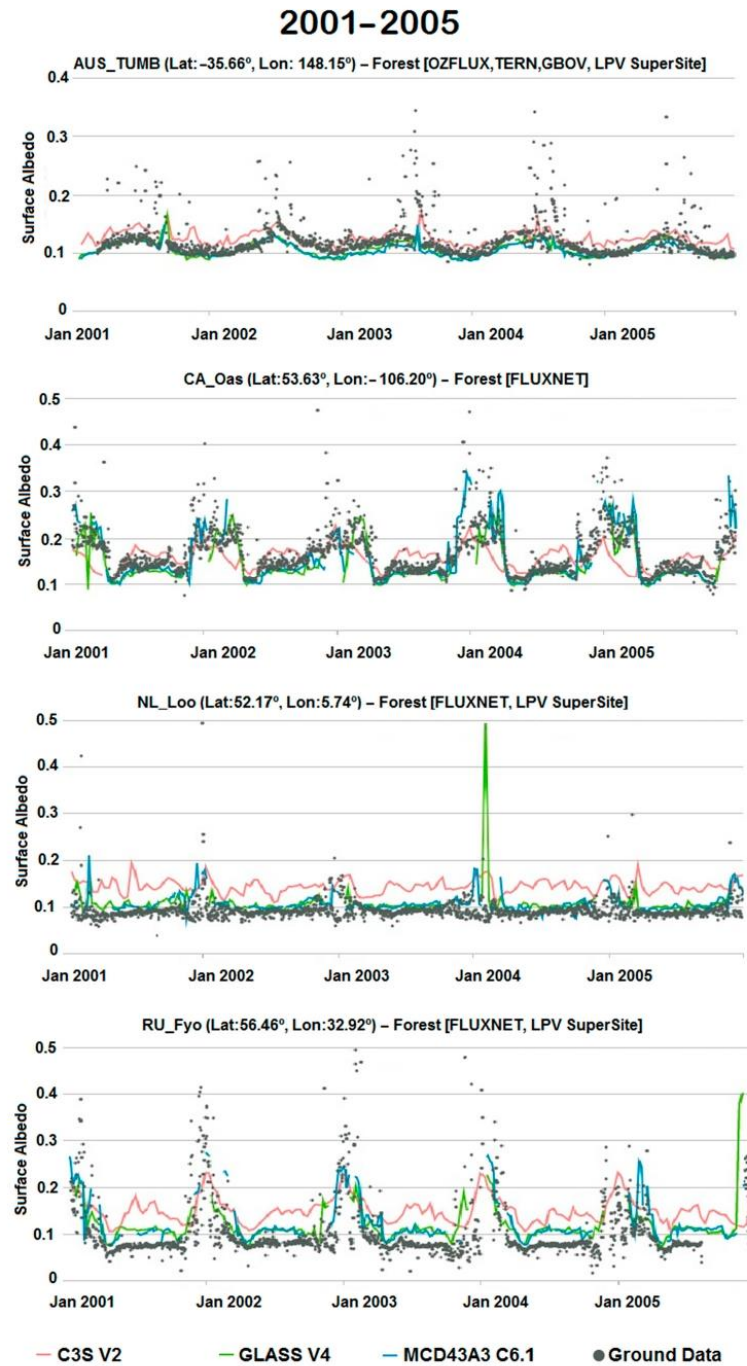


Figure 8. Examples of albedo temporal variations in C3S V2 (red), GLASS V4 (green), and MCD43A3 C6.1 (blue) satellite products (all quality pixels not just high quality) and ground data (black dots) from 4 REALS sites during the 2001–2005 period.

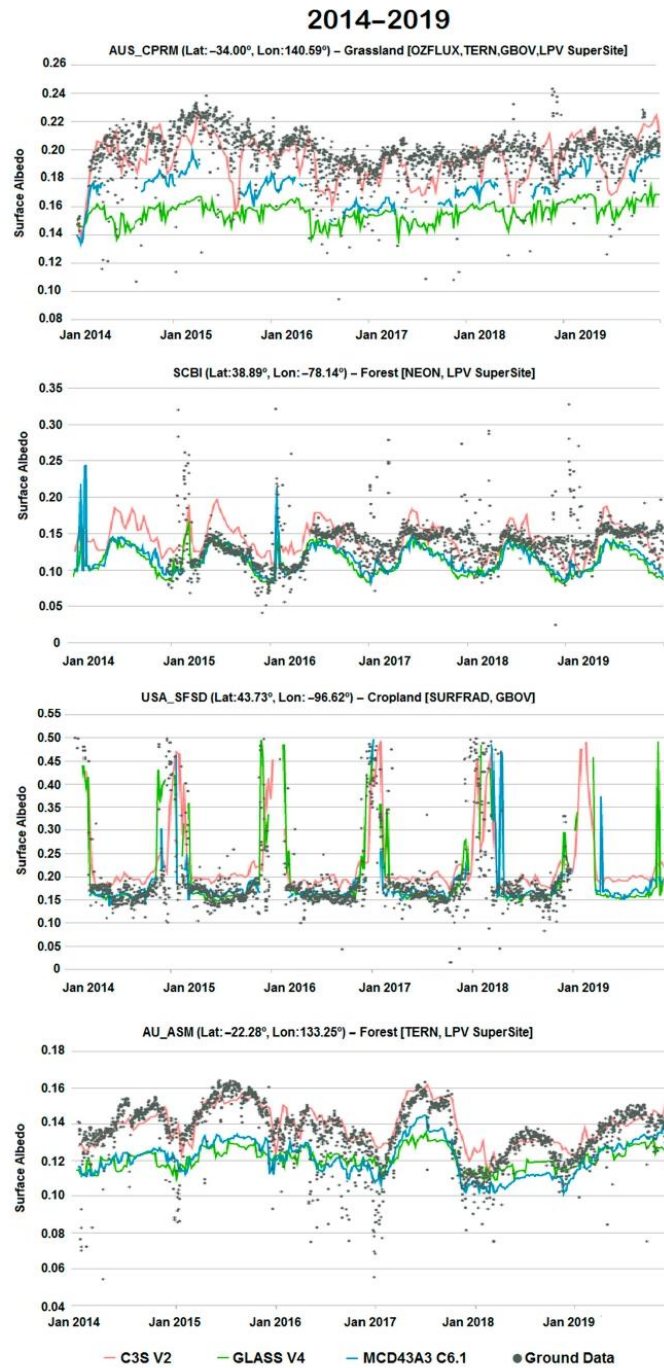


Figure 9. Examples of albedo temporal variations in C3S V2 (red), GLASS V4 (green), and MCD43A3 C6.1 (blue) satellite products (all quality pixels not just high quality) and ground data (black dots) from 4 REALS sites during the 2014–2019 period.

Good temporal agreement is found between satellite products and ground data over forest sites in the 2001–2005 period, properly reproducing the different situations: rapid changes due to snow events (CA_Oas, RU_Fyo), stable values over long periods (NL_Loo, RU_Fyo), and variation due to phenological changes (AUS_TUMB). C3S V2 products based on SPOT/VGT typically tend to provide higher values than ground data (and other satellite products) for most snow-free cases. GLASS V4 shows, on the other hand, some unexpected peaks (e.g., NL_Loo in January 2004) which are not captured by the other satellite products and ground data.

Good temporal agreement is also found between satellite retrievals and in situ data in the 2014–2019 period for different biome types, following similar temporal trajectories. C3S V2 (based on PROBA-V for this period) shows an overestimation compared with ground truth and the other satellite products for USA_SFSD (cropland) and SCBI (forest) sites, but better accordance with ground data over AUS_CPRM (grassland) and AU_ASM (forest) than GLASS V4 and MCD43A3 C6.

The snow episodes were correctly reported by the three satellite products in most cases but MCD43A3 C6.1 reaches typically higher values, which are more consistent with daily ground observations. Some spurious events (e.g., February 2015 and 2016 in SCBI) were not captured by C3S V2, which could be attributed to its larger temporal composite and lower production frequency, and to the more conservative approach of the PROBA-V cloud-masking algorithm [24,82].

3.4. Intra-Annual Precision

Intra-annual precision (so-called smoothness) corresponds to temporal noise assumed to have no serial correlation within a season and is quantitatively assessed as the anomaly between the product value for one date and the linear estimate based on its neighbors [83]. Figure 10 shows the Probability Density Function (PDF) of the intra-annual precision for C3S V2, GLASS V4, and MCD43A3 C6.1 products. The median values (indicative of intra-annual precision) of each product are summarized in Table 8.

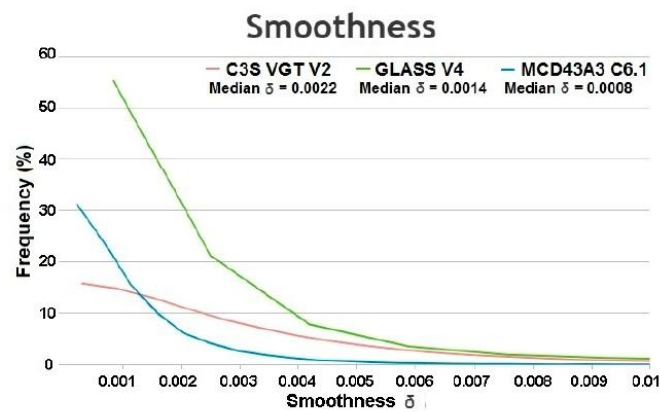


Figure 10. Histogram of the smoothness (δ) for C3S V2 (red), GLASS V4 (green), and MCD43A3 C6.1 (blue) total shortwave black-sky albedo products. Evaluation in the 2001–2005 period over LANDVAL sites considering all pixels.

Table 8. Summary of median δ for C3S V2, GLASS V4, and MCD43A3 C6.1 total shortwave black-sky albedo products. Evaluation in the 2001–2005 period over LANDVAL sites considering all pixels.

Satellite Product	Median δ
C3S V2	0.0022
GLASS V4	0.0014
MCD43A3 C6.1	0.0008

Smoothness histograms reveal that most values are below 0.005, which demonstrates that the three satellite products show high precision. The temporal resolution of each product directly impacts their smoothness, as MCD43A3 C6.1 (smoothness calculated at 5 days temporal step rather than the actual daily temporal resolution) shows better intra-annual precision than GLASS V4 (8 days) and C3S V2 (10 days).

3.5. Inter-Annual Precision

Inter-annual precision (Figure 11, Table 9) for each satellite product under study is assessed by comparison of retrievals for consecutive years over 19 desert calibration sites [84] during 5 years of data (2001–2005). The best inter-annual precision (i.e., MAD, CEOS LPV best practice) is observed for GLASS V4 (MAD = 0.002, 0.55%), while the C3S VGT V2 product provides the worst results (MAD = 0.007, 1.64%), with median absolute deviations of 1.64%. MCD43A3 C6.1 shows intra-annual precision better than 1% (MAD = 0.004, 0.84%).

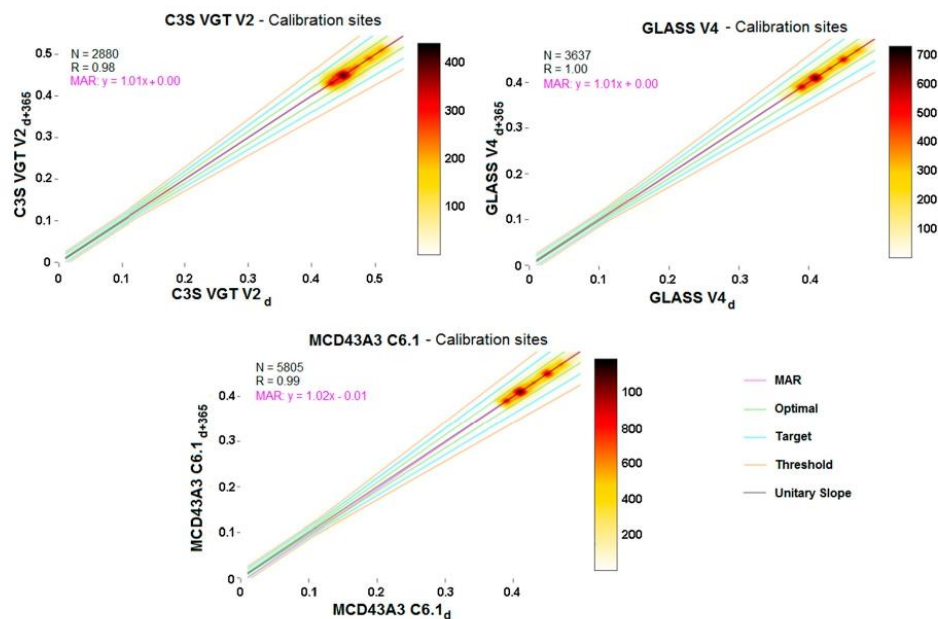


Figure 11. Scatterplots (X-Axis: retrieval for a given date, Y-axis: retrieval for equivalent date of the following year) of the inter-annual precision of C3S V2 (top left), GLASS V4 (top right), and MCD43A3 C6.1 (bottom) products. Evaluation for total shortwave black-sky retrievals over LANDVAL sites in the 2001–2005 period considering all pixels.

Table 9. Inter-annual precision indicator (median absolute deviation between two consecutive years) of C3S V2, GLASS V4, and MCD43A3 C6.1 products. Evaluation for total shortwave black-sky albedo retrievals over LANDVAL sites in the 2001–2005 period considering all pixels.

	C3S V2	GLASS V4	MCD43A3 C6.1
Inter-annual precision: median absolute deviation	0.007 (1.64%)	0.002 (0.55%)	0.004 (0.84%)

3.6. Overall Spatio-Temporal Consistency

The overall consistency between a pair of satellite products is evaluated by reporting several metrics indicative of the goodness of the fit, such as accuracy (mean bias, B, and median deviation, MD), precision (standard deviation, STD, and median absolute deviation, MAD) and uncertainty (RMSD). Scatterplots (Figure 12) and validation metrics between products are computed over LANDVAL sites for the period of 2001–2005 and two different postulates: taking into account all pixels (Table 10) and only considering best quality pixels (Table 11).

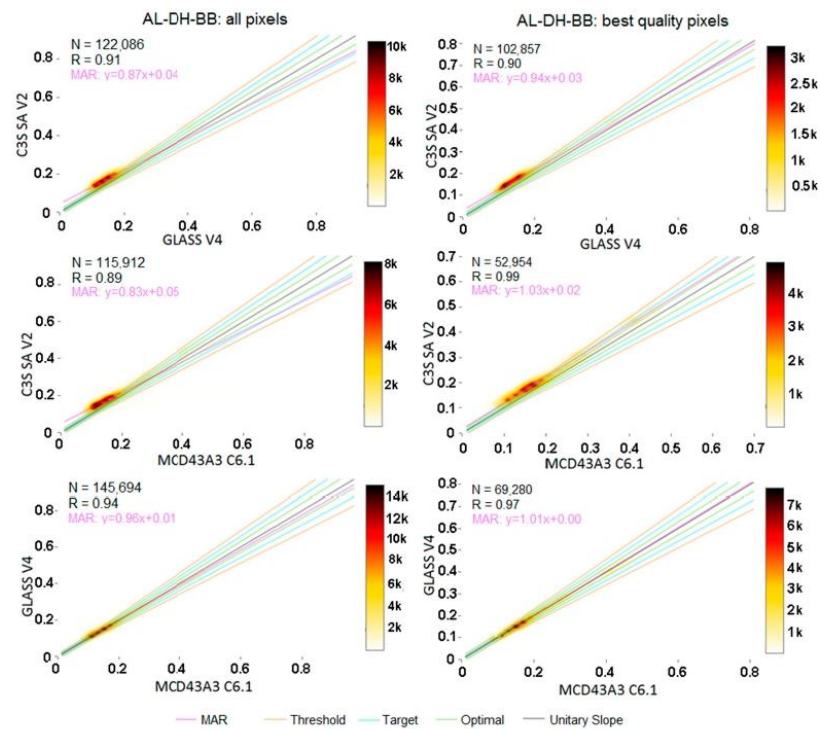


Figure 12. Scatterplots of C3S V2 vs. GLASS V4 (top), C3S V2 vs. MCD43A3 C6.1 (middle), and GLASS V4 vs. MCD43A3 C6.1 (bottom) for all pixels (left) and best quality pixels (right) for black-sky total shortwave retrievals in the 2001–2005 period over LANDVAL sites.

Table 10. Summary of the main statistics for scatterplots between C3S V2 vs. GLASS V4, C3S V2 vs. MCD43A3 C6.1, and GLASS V4 vs. MCD43A3 C6.1 for black-sky total shortwave retrievals in the 2001–2005 period over LANDVAL sites. All quality pixels are taken into account.

	C3S V2 vs. GLASS V4	C3S V2 vs. MCD43A3 C6.1	GLASS V4 vs. MCD43A3 C6.1
N	122086	115912	145694
R	0.91	0.89	0.94
MAR	$y = 0.87x + 0.04$	$y = 0.83x + 0.05$	$y = 0.96x + 0.01$
B	0.017 (8.1%)	0.015 (7.1%)	−0.001 (−0.3%)
MD	0.024 (11.4%)	0.024 (11.2%)	<0.001 (0.2%)
STD	0.052 (24.8%)	0.062 (28.7%)	0.043 (21.0%)
MAD	0.027 (12.7%)	0.027 (12.8%)	0.006 (3.0%)
RMSD	0.055 (26.1%)	0.064 (29.6%)	0.043 (21.0%)
%Optimal	10.2	9.6	61.8
%Target	28.4	29.4	83.7
%Threshold	49.4	49.7	90.9

Table 11. Summary of the main statistics for scatterplots between C3S V2 vs. GLASS V4, C3S V2 vs. MCD43A3 C6.1, and GLASS V4 vs. MCD43A3 C6.1 for black-sky total shortwave retrievals in the 2001–2005 period over LANDVAL sites. Only best quality pixels are taken into account.

	C3S V2 vs. GLASS V4	C3S V2 vs. MCD43A3 C6.1	GLASS V4 vs. MCD43A3 C6.1
N	102857	52954	69280
R	0.90	0.99	0.97
MAR	$y = 0.94x + 0.03$	$y = 1.03x + 0.02$	$y = 1.01x + 0.00$
B	0.021 (11.0%)	0.022 (10.6%)	>−0.001 (−0.0%)
MD	0.025 (13.0%)	0.022 (10.3%)	−0.001 (−0.5%)
STD	0.037 (19.5%)	0.013 (6.2%)	0.026 (12.4%)
MAD	0.026 (13.5%)	0.022 (10.3%)	0.005 (2.3%)
RMSD	0.042 (22.4%)	0.026 (12.3%)	0.026 (12.4%)
%Optimal	9.8	12.4	77.5
%Target	28.7	43.1	95.8
%Threshold	50.6	70.4	98.7

The best agreement in terms of accuracy and uncertainty is found between MCD43A3 C6.1 and GLASS V4, with almost no bias and RMSD of 0.043 (21%). Improved results are found when considering best quality retrievals (RMSD of 0.026 (12.4%)). The C3S V2 product tends to provide systematically higher values compared to MODIS-based products (MCD43A3 C6.1 and GLASS V4), with mean bias of 7–8% (0.015–0.017) and MD of 11% (0.024) when all pixels are considered. The uncertainty between C3S V2 and the MODIS-based products significantly improves when only best quality retrievals are considered (mainly in the comparison with MCD43A3 C6.1) but a large bias is found, indicating systematic positive differences.

3.7. Stability

Stability is the extent to which a product remains constant over a long period, typically a decade or more [36]. Temporal stability can be also defined as the change in bias over a

predefined time period [85], and stability can be estimated as the slope of a linear regression for the bias over time [86]. In SALVAL implementation, pseudo-invariant desert calibration sites [84] are used for stability evaluation, and the slope of albedo values per decade is provided as an indicator of stability. As desert sites are supposed to experience very little temporal variation, variation in albedo time series can be considered to be equivalent to evaluation of the bias over time.

Figure 13 displays some examples of C3S V2, GLASS V4, and MCD43A3 C6.1 temporal profiles in the 2001–2010 period for some selected desert calibration sites. The box plots of the decadal slopes over all calibration sites are displayed in Figure 14. The three products show some seasonality that could be attributed to changes in illumination, but no deviations at the long-term scale. Furthermore, C3S V2 shows more noise in the signal compared with GLASS V4 and MCD43A3 C6.1, as previously revealed in its worst intra-annual (see Section 3.4) and inter-annual (see Section 3.5) precision. This noise could be partly attributed to the BRDF climatology data used as prior information in the C3S V2 algorithm, which presents the same behavior. Median slopes in all calibration sites revealed no deviation for C3S V2 and GLASS V4 and a very slight positive slope (i.e., 0.003, which is equivalent to 0.6%) for MCD43A3 C6.1, largely fulfilling the GCOS requirements in terms of stability (1%).

3.8. Direct Validation

Direct validation involves the comparison of satellite retrievals with albedo measured from tower-based instruments (REALS dataset). Figure 15 shows the scatterplots between blue-sky satellite albedo quantities and REALS during the 2000–2019 period, taking into account all quality pixels (left side), and only best quality pixels (right side), where most of the outliers are removed. The main statistics resulting from the direct validation are summarized in Table 12 (all pixels) and Table 13 (best quality pixels).

The overall accuracy (median error) of C3S V2 is 15%, with a systematic tendency to provide higher values than ground measurements (mean bias of 12.2%). GLASS V4 and MCD43A3 C6.1 show better results, and an opposite sign of differences (mean bias of −2.5%). In terms of overall uncertainty, the three satellite products provide similar results in the comparison with in situ data, with RMSD of around 0.04 when all pixels are considered in the comparison, and RMSD around 0.03 when only best quality retrievals are contemplated. However, C3S V2 shows a lower percentage of cases within the predefined accuracy levels than GLASS V4 and MCD43A3 C6.1.

The MAR relationship of the best quality pixels indicates a tendency of all satellite products to overestimate ground data for the lowest albedo values (mainly dominated by forests) and the opposite trend for higher albedo values (sparse vegetation), with slopes lower than 0.7 in the line comparing results to other validation studies over a significant set of locations [15,24,33].

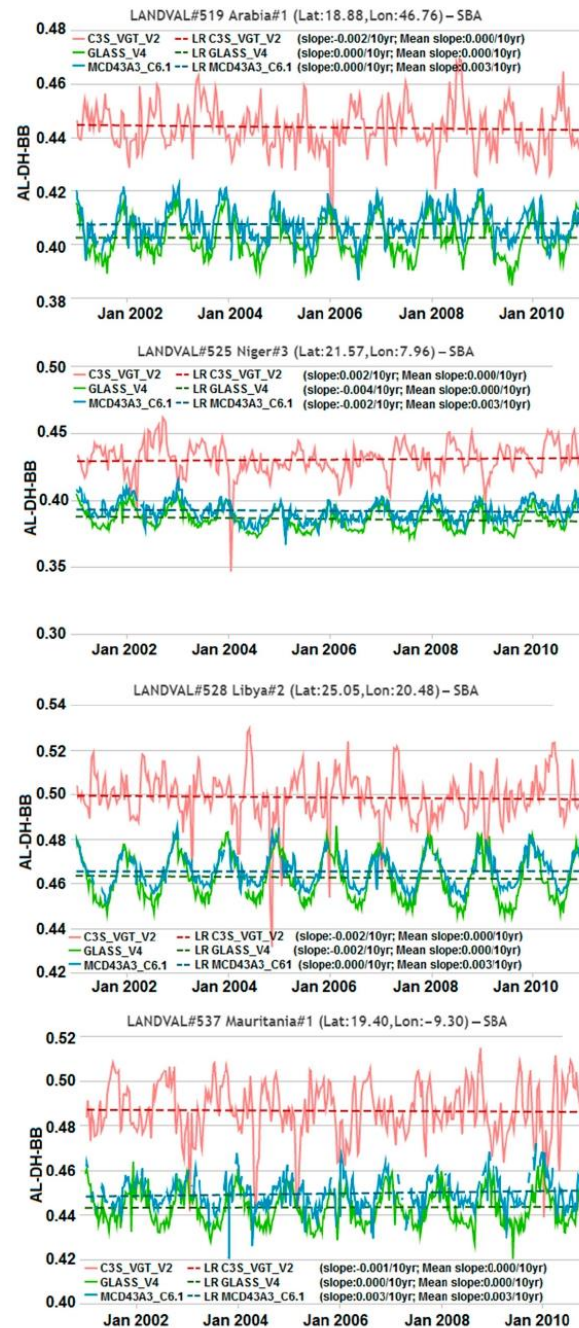


Figure 13. Examples of temporal profiles of C3S V2 (red), GLASS V4 (green), and MCD43A3 C6.1 (blue) for black-sky total shortwave albedos over calibration sites of LANDVAL in the 2001–2010 period for best quality pixels. Dashed lines represent the linear regression of each product trend. Mean slope value corresponds to the mean slope considering all calibration sites.

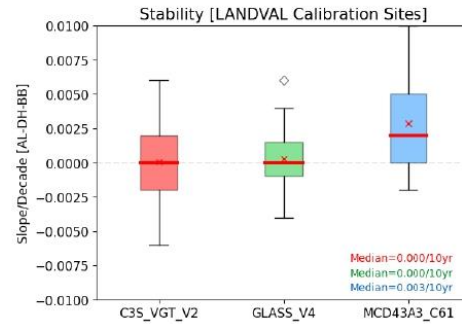


Figure 14. Box plots of the slope per decade (2001–2010) for C3S V2 (red), GLASS V4 (green) and MCD43A3 C6.1 (blue) for black-sky albedos where each box stretches from the 25th percentile to the 75th percentile of the data and whiskers include 99.3% of the coverage data ($\pm 2.7 \sigma$). Outliers are represented by rhombus. Red lines/crosses represent median/mean values. Computation over desert calibration sites.

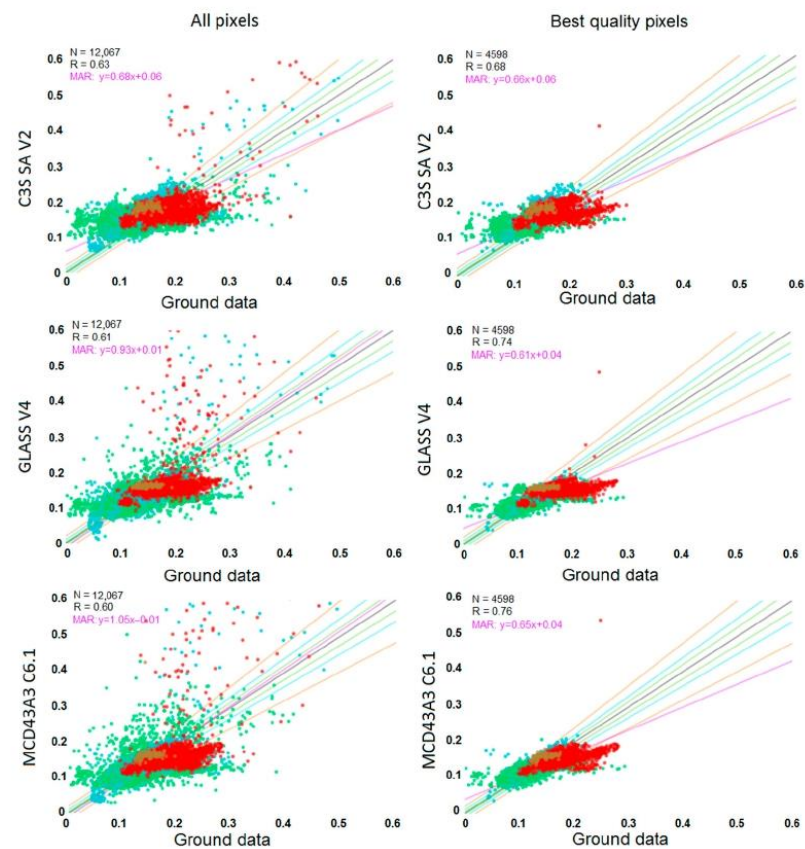


Figure 15. Direct validation of C3S V2 (top), GLASS V4 (middle), and MCD43A3 C6.1 (bottom) blue-sky albedo satellite products vs. REALS ground values during the 2000–2019 period for all pixels (left) and only best quality pixels (right). Green, blue, red, and orange points represent forest, crop, shrublands/herbaceous, and desert biome types, respectively.

Table 12. Summary of the main statistics for the direct validation of C3S V2, GLASS V4, and MCD43A3 C6.1 satellite blue-sky albedo products vs. blue-sky albedo ground values from the REALS dataset in the 2000–2019 period. All pixels were taken into account.

	C3S V2	GLASS V4	MCD43A3 C6.1
N	12067	12067	12067
R	0.63	0.61	0.60
MAR	$y = 0.68x + 0.06$	$y = 0.93x + 0.01$	$y = 1.05x - 0.01$
B	0.017 (12.2%)	−0.003 (−2.5%)	−0.003 (−2.5%)
MD	0.021 (14.9%)	<0.001 (−0.1%)	−0.002 (−1.2%)
STD	0.040 (27.8%)	0.043 (32.7%)	0.047 (35.2%)
MAD	0.029 (20.4%)	0.017 (13.2%)	0.017 (13.2%)
RMSD	0.043 (30.4%)	0.043 (32.8%)	0.047 (35.3%)
%Optimal	12.6	20.6	18.1
%Target	24.5	38.3	37.0
%Threshold	46.8	63.1	64.7

Table 13. Summary of the main statistics for the direct validation of C3S V2, GLASS V4, and MCD43A3 C6.1 satellite blue-sky albedo products vs. blue-sky albedo ground values from the REALS dataset in the 2000–2019 period. Only best quality pixels were taken into account.

	C3S V2	GLASS V4	MCD43A3 C6.1
N	4598	4598	4598
R	0.68	0.74	0.76
MAR	$y = 0.66x + 0.06$	$y = 0.61x + 0.04$	$y = 0.65x + 0.04$
B	0.014 (9.7%)	−0.008 (−6.2%)	−0.008 (−5.7%)
MD	0.017 (11.7%)	−0.004 (−2.9%)	−0.005 (−3.8%)
STD	0.032 (22.2%)	0.030 (22.3%)	0.029 (21.6%)
MAD	0.024 (16.7%)	0.013 (10.1%)	0.015 (11.3%)
RMSD	0.035 (24.2%)	0.031 (23.2%)	0.030 (22.4%)
%Optimal	16.8	27.5	20.9
%Target	32.2	48.1	43.3
%Threshold	56.8	72.0	73.4

4. Discussion

The three products under study (MCD43A3 C6.1, C3S V2, and CLASS V4) show remarkably good completeness, with missing data mainly located over northern regions and wintertime, typically affected by persistent clouds. The three products introduce different techniques to improve the spatiotemporal continuity: a poorer quality back-up algorithm is used in the case of MCD43A3 C6.1, a prior climatology of BRDF data is used in the case of C3S V2, and gap-filling techniques are used in the case of GLASS. When considering best quality pixels, MCD43A3 C6.1 is the most restrictive product, as only full retrievals of the model are provided when at least 50% of high-quality observations are well-distributed over the viewing hemisphere during the 16-day synthesis period.

In terms of spatial consistency (i.e., residuals), all combinations between pairs of products largely meet uncertainty requirements, with more than 70% of global cases achieving optimal level of consistency (residuals typically lower than 0.015). As expected, the best spatial consistency between pairs of products was found between MCD43A3 C6.1 and GLASS, as they are based on data from the same MODIS instruments on board Terra

and Aqua, whereas C3S products are retrieved using SPOT/VGT or PROBA-V depending on the temporal range. Different spectral response functions among the instruments show dissimilarities in band location, band width, and response percentage of input signal over similar spectral channels [87]. The main discrepancies are typically located over equatorial areas and northern regions, which can be explained by cloud contamination and differences in the pre-processing chain. The underestimation of C3S products over snow targets [60] is another reason for the discrepancies over northern areas.

The three satellite products provide good temporal agreement among them and in comparison with in situ data. The better temporal resolution of MCD43A3 C6.1 allows us to capture smoother temporal variations than is possible from C3S V2 and GLASS V4, despite the incorporation of gap-filling techniques in the C3S and GLASS algorithms, and the inclusion of a temporal smoothing method in GLASS V4.

The evaluation of the APU metrics from the indirect evaluation also indicated that the best agreement is found between GLASS V4 and MCD43A3 C6.1. More than 77.5% of best quality observations lie within the optimal uncertainty level (Max [5%, 0.0025]) when the same sensor is used (i.e., GLASS V4 versus MCD43A3 C6.1). C3S V2 provides larger differences from both MODIS-based products, but satisfactory results, with systematically higher values of around 10%.

As a corollary, we can conclude that the use of a different sensor is the most important factor contributing to discrepancies among products. Nevertheless, the inversion algorithm is another contributing factor to differences between products. C3S V2 and MCD43A3 C6.1 make use of semi-empirical linear kernel-driven models to first retrieve BRDF coefficients and then compute surface albedo by angular and spectral integration. By comparison, GLASS adopts the angular bin and STF algorithm, and incorporates improvements in the inversion of snow and ice using an asymptotic radiative transfer model [88]. Additionally, the different spectral integration approach also contributes to differences between products. MODIS and GLASS adopt the same broadband albedo range and narrow-to-broadband conversion algorithm [89]. C3S products are computed over slightly different broadband albedo intervals and a different conversion algorithm [14].

The direct validation showed systematic positive bias of around 10% for C3S (SPOT/VGT and PROBA-V) V2 products for the period under study (2000–2019), in line with that found for previous C3S V1 versions [15,24], where positive bias of 11.5% was also reported. GLASS V4 and MCD43A3 C6.1 showed the opposite sign of differences, but improved results (with mean bias of around 6% and median deviation of 3%).

The comparison of satellite-based surface albedo estimates versus ground measurements indicates the difficulty in complying with existing user uncertainty requirements. Typically, less than 20% of satellite-based best quality retrievals actually achieve the GCOS target (Max [5%, 0.0025]) and the WMO goal requirements in terms of accuracy. By comparison, the three satellite products investigated largely accomplished stability optimal requirements (Max [1%, 0.001]).

5. Conclusions

This paper demonstrates the functionality of the SALVAL online platform to validate currently available operational albedo products. A validation and intercomparison exercise was conducted on three long-term global products generated by C3S, MODIS, and GLASS. Completeness, spatiotemporal consistency, precision, and accuracy were evaluated. Results from the SALVAL tool indicate that the three datasets under evaluation provide long-term reliable and highly consistent retrievals at a global scale. Discrepancies between products are primarily associated with differences in the retrieval processing chain: different input data sensors, pre-processing and atmospheric corrections, and inversion algorithms.

The CEOS LPV validation stage assigned to these global satellite albedo products is currently stage 3, which means that direct validation with in situ data or other reference datasets is performed over a significant set of locations and time periods representing global conditions. Thanks to the availability of the SALVAL online platform, the four

main components [8] for an operational validation system of satellite-based surface albedo products have been integrated: long term satellite products, a global in situ dataset, the CEOS LPV validation best practices protocol, and an online validation platform. The SALVAL tool provides the potential functionality to achieve CEOS LPV validation stage 4 as it is also designed to accommodate regular updates of the validation results, providing albedo ECVs the readiness level for ongoing operational validation.

SALVAL provides transparency, consistency, and traceability to the validation process. The tool is available within the CEOS Cal/Val Portal [90], and offers a way to contribute to and collaborate with the greater the scientific community, thus allowing new products or ground reference datasets to be incorporated into the tool.

Author Contributions: J.S.-Z. is the main author and wrote the majority of the manuscript. J.S.-Z. and F.C. conceived and conceptualized the work and contributed to all phases of the investigation. J.S.-Z. initially developed the software and E.M.-S. developed the final software tool and generated the REALS database. Z.W. extracted the satellite dataset of MODIS MCD43A3 C6.1. All authors contributed to the discussion of results. All authors have read and agreed to the published version of the manuscript.

Funding: This research received no external funding.

Data Availability Statement: SALVAL tool is available online at www.salval.eolab.es.

Acknowledgments: The authors would like to thank the different site networks and services dedicated to providing all the ground measurements that are integrated in the REALS dataset (GBOV, FLUXNET, NEON, EFDC, ICOS, TERN, BSRN, SURFRAD). Thanks are due to ESA for publishing the SALVAL tool through the CEOS WGCV Cal/Val Portal. Thanks to the CEOS WGCV LPV subgroup for its contribution to validation practices implemented in SALVAL. This research was supported in part by the U.S. Department of Agriculture, Agricultural Research Service. USDA is an equal opportunity provider and employer.

Conflicts of Interest: The authors declare no conflict of interest.

Abbreviations

The following abbreviations are used in this manuscript:

ADEOS	ADvanced Earth Observing Satellite
AL-BH	Bi-Hemispherical ALbedos
AL-DH	Directional-Hemispherical Albedos
APU	Accuracy, Precision and Uncertainty
AVHRR	Advanced Very High Resolution Radiometer
B	Mean Bias
BHR	Bi-Hemispherical Reflectance
BNU	Beijing Normal University's
BRDF	Bidirectional Reflectance Distribution Function
BSA	Black-Sky Albedo
BSRN	Baseline Surface Radiation Network
C3S	Copernicus Climate Change Service
Cal/Val	Calibration/Validation
CDR	Climate Data Record
CDS	Climate Data Store
CEOS	Committee on Earth Observation Satellites
CGLS	Copernicus Global Land Service
CMG	Climate Modelling Grid
CUL	CULTivated
DBF	Deciduous Broadleaved Forest
DHR	Directional-Hemispherical Reflectance
EBF	Evergreen Broadleaved Forest
ECV	Essential Climate Variable
EFDC	European Fluxes Database Cluster
EOLAB	Earth Observation LABoratory

EPS	EUMETSAT Polar System
ESA	European Space Agency
FLUXNET	FLUXes NETwork
GBOV	Ground-Based Observations for Validation
GCOS	Global Climate Observing System
GLASS	Global LAnd Surface Satellites
GSD	Ground Sampling Distance
HER	HERbaceous
ICOS	Integrated Carbon Observation System
JCGM	Joint Committee for Guides in Metrology
LANDVAL	LAND VALidation network
LPDAAC	Land Processes Distributed Active Archive Center
LPV	Land Product Validation subgroup
MAD	Median Absolute Deviation
MAR	Major Axis Regression
MCD43	TERRA + AQUA MODIS BRDF/Albedo/NBAR Product
MD	Median Deviation
MetOp	Polar-orbiting Meteorological satellites
MODIS	MODERate resolution Imaging Spectroradiometer
MSG	Meteosat Second Generation
N	Number of samples
NASA	National Aeronautics and Space Agency
NEON	National Science Foundation's National Ecological Observatory Network
NIR	Near-Infrared
NLF	Needle-Leaf Forest
NOAA	National Oceanic and Atmospheric Administration
OF	Other Forests
PDF	Probability Density Function
POLDER	POLarization and Directionality of the Earth's Reflectances
PROBA-V	Project for Onboard Autonomy satellite, the V standing for vegetation
R	Correlation coefficient
R _{CV}	Relative Coefficient of Variation
REALS	Representativeness-Evaluated ALbedo Stations
RMSD	Root Mean Square Deviation
R _{SE}	Scale REquirement index
R _{ST}	Relative STrength of the spatial correlation
R _{SV}	Relative proportion of Structural Variation
RTM	Radiative Transfer Model
SA	Surface Albedo
SALVAL	Surface ALbedo VALidation tool
RAW	First order score
SBA	Sparse and Bare Areas
SEVIRI	Spinning Enhanced Visible and Infrared Imager
SHR	SHRublands
SMAC	Simplified Method for Atmospheric Correction
SPOT	Satellites for the Observation of the Earth
ST	STandard score
STD	Standard deviation
STF	Statistics-based Temporal Filtering
SURFRAD	SURFace RADiation budget network
SW	ShortWave
TERN	Australia's Land Ecosystem Observatory or Terrestrial Ecosystem
TOA	Top-Of-Atmosphere
TOC	Top-Of-Canopy
VGT	VeGeTation sensor
WGCV	Working Group on Calibration and Validation
WMO	World Meteorological Organization
WSA	White-Sky Albedo

Appendix A. REALS Sites' Characteristics and ST Scores

Table A1. Characteristics and ST scores of REALS sites.

ID	Code	Latitude	Longitude	Name	Network	Class	ST Leaf-Off	ST Leaf-On
1	USA_BOND	40.05192	−88.37309	Bondville	SURFRAD, GBOV	Croplands	1.52	1.58
2	USA_BAOR	40.05005	−105.00387	Boulder	BSRN, GBOV	Croplands	1.29	2.98
3	BEL_BRAS	51.30761	4.51984	Brasschaat	FLUXNET, GBOV(LPV SuperSite)	Forest	19.36	10.42
4	NET_CABA	51.97100	4.92700	Cabauw	BSRN, GBOV	Grass/shrub	13.86	6.65
5	AUS_CPRM	−34.00270	140.58771	Calperum	OZFLUX, TERN, GBOV(LPV SuperSite)	Grass/shrub	2.72	2.83
6	USA_DRAK	36.62418	−116.01990	Desert Rock	SURFRAD, GBOV	Desert	0.96	0.96
7	USA_FPEK	48.30783	−105.10170	Fort Peck	SURFRAD, GBOV	Grass/shrub	1.85	1.60
8	GER_GEBE	51.10010	10.91430	Gebesee	FLUXNET, GBOV	Croplands	1.08	1.22
9	NAM_GOBA	−23.56184	15.04131	Gobabeb	BSRN, GBOV(LPV SuperSite)	Desert	0.95	0.87
10	USA_GCMK	34.25505	−89.87360	Goodwin Creek	SURFRAD, GBOV	Forest	2.92	1.96
11	FRA_GRIG	48.84420	1.95191	Grignon	FLUXNET, GBOV	Croplands	1.04	1.05
12	FRA_GUYA	5.27877	−52.92486	Guyafux	FLUXNET, GBOV(LPV SuperSite)	Forest	5.47	5.47
13	GER_HAIN	51.07920	10.45220	Hainich	FLUXNET, GBOV(LPV SuperSite)	Forest	6.84	18.17
14	USA_NRFT	40.03287	−105.54690	Niwot Ridge Forest	FLUXNET, GBOV	Forest	4.06	n/a
15	ITA_RENO	46.58690	11.43370	Renon	FLUXNET, GBOV	Forest	1.45	1.79
16	USA_PSUS	40.72012	−77.93085	Rock Springs	SURFRAD, GBOV	Forest	1.04	2.96
17	USA_SFSD	43.73403	−96.62331	Sioux Falls SurfRad	SURFRAD, GBOV	Croplands	1.85	2.11
18	USA_SGP	36.60575	−97.48876	Southern Great Plains	SURFRAD, GBOV	Croplands	1.02	0.80
19	USA_TBLN	40.12498	−105.23680	Table Mountain	SURFRAD, GBOV	Desert	2.24 (*)	2.24 (*)
20	AUS_TUMB	−35.65652	148.15163	Tumbarumba	OZFLUX, TERN, GBOV (LPV SuperSite)	Forest	11.65	11.65
21	LENO	31.85388	−88.16122	Lenoir Landing	NEON	Forest	2.33	4.96
22	TALL	32.95046	−87.39327	Talladega National Forest	NEON(LPV SuperSite)	Forest	103.65	8.00
23	BONA	65.15401	−147.50258	Caribou-Poker	NEON	Forest	n/a	2.78
24	DEJU	63.88112	−145.75136	Delta Junction	NEON	Forest	n/a	3.77
25	HEAL	63.87569	−149.21334	Healy	NEON	Grass/shrub	n/a	1.42
26	TOOL	68.66109	−149.37047	Toolik	NEON	Grass/shrub	n/a	1.28
27	SRER	31.91068	−110.83549	Santa Rita Experimental Range	NEON	Grass/shrub.	5.92	4.29
28	SOAP	37.03337	−119.26219	Soaproot Saddle	NEON	Forest	19.48	10.58
29	TEAK	37.00583	−119.00602	Lower Teakettle	NEON	Forest	25.17	8.46
30	CPER	40.81550	−104.7456	Central Plains Experimental Range	NEON (LPV SuperSite)	Grass/shrub	1.12	0.98
31	NIWO	40.05425	−105.58237	Niwot Ridge Mountain Research Station	NEON	Forest	0.71	0.88
32	STER	40.46190	−103.02930	Sterling	NEON	Croplands	1.05	0.92
33	DSNY	28.12504	−81.43620	Disney Wilderness Preserve	NEON	Croplands	1.34	1.51
34	OSBS	29.68927	−81.99343	Ordway-Swisher Biological Station	NEON(LPV SuperSite)	Forest	0.65	0.61
35	JERC	31.19484	−84.46861	Jones Ecological Research Center	NEON	Forest	12.99	4.83
36	KONA	39.11044	−96.61295	Konza Prairie Biological Station–Relocatable	NEON	Grass/shrub	1.60	1.26

Table A1. Cont.

ID	Code	Latitude	Longitude	Name	Network	Class	ST Leaf-Off	ST Leaf-On
37	KONZ	39.10077	−96.56309	Konza Prairie Biological Station	NEON	Grass/shrub	4.37	1.26
38	UKFS	39.04043	−95.19215	The University of Kansas Field Station	NEON	Forest	0.55	10.60
39	SERC	38.89008	−76.56001	Smithsonian Environmental Research Center	NEON	Forest	2.64	4.13
40	HARV	42.53690	−72.17266	Harvard Forest	NEON(LPV SuperSite)	Forest	40.01	6.32
41	UNDE	46.23388	−89.53725	UNDERC	NEON	Forest	2.29	2.08
42	BART	44.06388	−71.28731	Bartlett Experimental Forest	NEON(LPV SuperSite)	Forest	6.50	3.04
43	JORN	32.59068	−106.84254	Jornada LTER	NEON	Grass/shrub	0.83	1.04
44	DCPS	47.16165	−99.10656	Dakota Coteau Field School	NEON	Grass/shrub	0.87	1.18
45	NOGP	46.76972	−100.91535	Northern Great Plains Research Laboratory	NEON	Grass/shrub	1.74	1.43
46	OAES	35.41059	−99.05879	Klemme Range Research Station	NEON	Grass/shrub	1.04	1.41
47	GUAN	17.96955	−66.86870	Guanica Forest	NEON(LPV SuperSite)	Forest	9.75	9.75
48	LAJA	18.02125	−67.07690	Lajas Experimental Station	NEON	Grass/shrub	1.35	1.23
49	GRSM	35.68896	−83.50195	Great Smoky Mountains National Park	NEON	Forest	7.39	4.27
50	ORNL	35.96412	−84.28260	Oak Ridge	NEON(LPV SuperSite)	Forest	13.12	1.46
51	MOAB	38.24833	−109.38827	Moab	NEON(LPV SuperSite)	Grass/shrub	0.43	1.19
52	ONAQ	40.17759	−112.45244	Onaqui	NEON	Grass/shrub	1.30	1.59
53	MLBS	37.37828	−80.52484	Mountain Lake Biological Station	NEON(LPV SuperSite)	Forest	7.41	1.55
54	SCBI	38.89292	−78.1395	Smithsonian Conservation Biology Institute	NEON (LPV SuperSite)	Forest	2.51	13.86
55	ABBY	45.76243	−121.24700	Abby Road	NEON	Forest	2.42	7.30
56	WREF	45.82049	−121.95191	Wind River Experimental Forest	NEON	Forest	6.17	5.76
57	STEI	45.50894	−89.58637	Steigerwaldt Land Services	NEON(LPV SuperSite)	Forest	6.44	1.84
58	TREE	45.49369	−89.58571	Treehaven	NEON	Forest	8.10	6.44
59	AT-Neu	47.11667	11.3175	Neustift	FLUXNET	Grass/shrub	1.14	1.86
60	CA-Gro	48.2167	−82.1556	Ontario–Groundhog River, Boreal Mixedwood Forest	FLUXNET	Forest	6.32	4.91
61	CA-Oas	53.62889	−106.19779	Saskatchewan–Western Boreal, Mature Aspen	FLUXNET	Forest	27.82	9.18
62	CA-Obs	53.98717	−105.11779	Saskatchewan–Western Boreal, Mature Black Spruce	FLUXNET	Forest	7.98	3.23
63	CA-Qfo	49.6925	−74.34206	Quebec–Eastern Boreal, Mature Black Spruce	FLUXNET	Forest	1.40	1.47
64	CZ-BK1	49.50208	18.53688	Bily Kriz forest	FLUXNET(LPV SuperSite)	Forest	4.63	7.44
65	DE-Lnf	51.32822	10.3678	Leinefelde	FLUXNET	Forest	13.88	3.06
66	DE-Tha	50.96256	13.56515	Tharandt	FLUXNET(LPV SuperSite)	Forest	5.51	2.86
67	FR-Gri	48.84422	1.95191	Grignon	FLUXNET	Croplands	n/a	n/a
68	FR-LBr	44.71711	−0.7693	Le Bray	FLUXNET	Forest	10.82	1.59

Table A1. Cont.

ID	Code	Latitude	Longitude	Name	Network	Class	ST Leaf-Off	ST Leaf-On
69	FR-Pue	43.7413	3.5957	Puechabon	FLUXNET(LPV SuperSite)	Forest	1.22	1.22
70	GH-Ank	5.26854	-2.69421	Ankasa	FLUXNET	Forest	17.71	17.71
71	IT-Col	41.84936	13.58814	Collelongo	FLUXNET(LPV SuperSite)	Forest	1.63	1.44
72	IT-MBo	46.01468	11.04583	Monte Bondone	FLUXNET	Grass/shrub	2.03	1.26
73	IT-SR2	43.73202	10.29091	San Rossore 2	FLUXNET	Forest	13.04	12.66
74	NL-Hor	52.24035	5.0713	Horstermeer	FLUXNET	Grass/shrub	0.60	0.60
75	NL-Loo	52.16658	5.74356	Loobos	FLUXNET(LPV SuperSite)	Forest	29.14	1.55
76	RU-Fyo	56.46153	32.92208	Fyodorovskoye	FLUXNET(LPV SuperSite)	Forest	17.98	119.73
77	SN-Dhr	15.40278	-15.43222	Dahra	FLUXNET(LPV SuperSite)	Grass/shrub	1.03	0.83
78	US-Me2	44.4523	-121.5574	Metolius mature ponderosa pine	FLUXNET	Forest	0.79	2.18
79	US-UMd	45.5625	-84.6975	UMBS Disturbance	FLUXNET	Forest	0.69	0.80
80	US-Var	38.4133	-120.9507	Vaira Ranch- Ione	FLUXNET	Grass/shrub	4.84	2.58
81	ES-Cpa	39.22417	-0.90305	Cortes de Pallas	EFDC	Grass/shrub	6.88	4.70
82	ES-ES2	39.27556	-0.31528	El Saler-Sueca	EFDC	Croplands	5.36	4.68
83	ES-LMa	39.9415	-5.77336	Las Majadas del Tietar	EFDC	Grass/Shrub	1.66	1.24
84	DE-HoH	52.08656	11.22235	Hohes Holz	ICOS (LPV SuperSite)	Forest	6.95	5.28
85	SE-Svb	64.25611	19.7745	Svartberget	ICOS (LPV SuperSite)	Forest	1.11	1.11
86	FI-Hyy	61.84741	24.29477	Hyytiala	FLUXNET (LPV SuperSite)	Forest	1.37	1.37
87	DE-RuS	50.86591	6.44714	Selhausen Juelich	FLUXNET, ICOS (LPV SuperSite)	Croplands	1.82	1.40
88	AU_ASM	-22.2828	133.2493	Alice Springs Meller	TERN (LPV SuperSite)	Forest	8.88	6.78
89	AU_Boy	-32.477093	116.93856	Boyaginj Wandoo Woodland	TERN (SuperSite)	Forest	0.72	0.33
90	AU_Cum	-33.61528	150.72361	Cumberland Plain	TERN (LPV SuperSite)	Forest	6.18	1.04
91	AU_DRF	-16.23819	145.42715	Daintree Rainforest	TERN (SuperSite)	Forest	13.17	4.53
92	AU_Gin	-31.37635	115.71377	Gingin Banksia Woodland	TERN (SuperSite)	Forest	1.74	0.97
93	AU_GWW	-30.1914	120.65416	Great Western Woodlands	TERN (LPV SuperSite)	Forest	23.87	1.79
94	AU_LiS	-13.17904	130.79455	Litchfield Savanna	TERN (LPV SuperSite)	Forest	34.74	7.66
95	AU_RCR	-17.11747	145.63014	Robson Creek Rainforest	TERN (LPV SuperSite)	Forest	17.90	28.67
96	AU_SPU	-27.38806	152.87778	Samford Peri-Urban	TERN (SuperSite)	Forest	14.49	4.71
97	AU_Wrr	-43.09502	146.65452	Warra Tall Eucalypt	TERN (LPV SuperSite)	Forest	3.76	3.30
98	AU_WSE	-37.4222	144.0944	Wombat Stringybark Eucalypt	TERN (LPV SuperSite)	Forest	8.34	13.02
99	AU_WDE	-36.6732	145.0294	Whroo Dry Eucalypt	TERN (SuperSite)	Forest	4.15	91.64

(*) For those cases, RAW score (see Equation (2)) was adopted due to the semivariogram estimator does not provide a good fit with a semi-spherical variogram (i.e., ST score cannot be computed).

Appendix B. Using the SALVAL Tool

Follow these steps to start using SALVAL. More technical details about tool functionalities, satellite reference products, in situ datasets, etc., can be found in the SALVAL user guide [34].

- (1) Sign up to start using the SALVAL Tool.

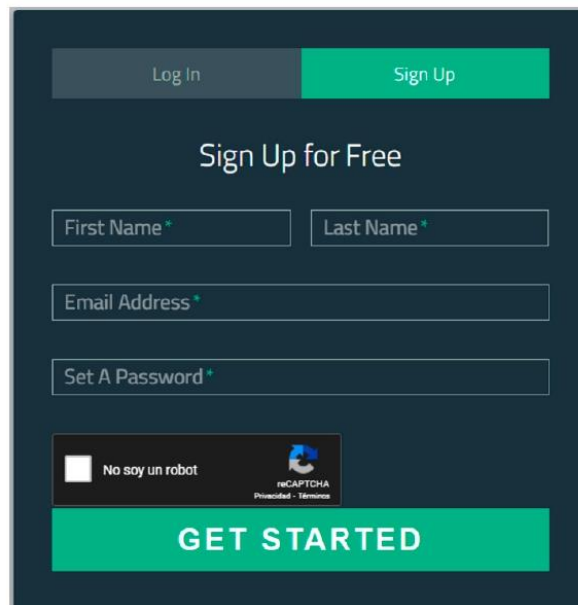


Figure A1. Snapshot of SALVAL configuration step 1. "*" stands for mandatory fields.

- (2) Specify the product being validated and the reference products. Select from the existing database of products or import new products.

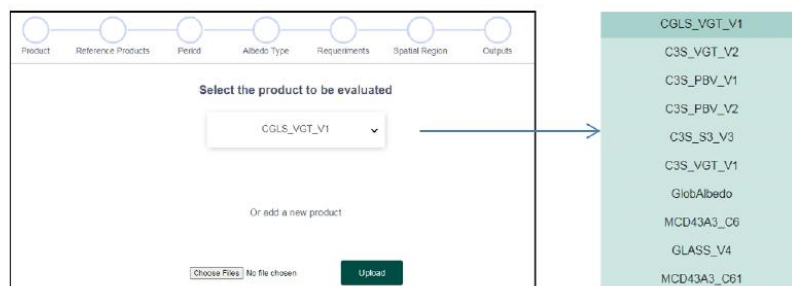


Figure A2. Snapshot of SALVAL configuration step 2.

- (3) Define the input product: time period, albedo type, requirements, and spatial coverage.

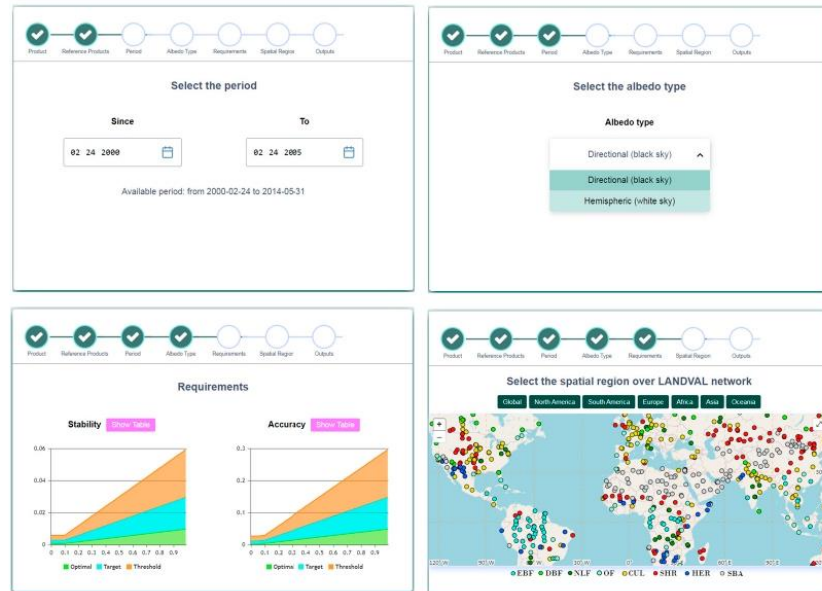


Figure A3. Snapshot of SALVAL configuration step 3.

- (4) Visualize the validation results for different criteria, or generate a standardized validation report in PDF.

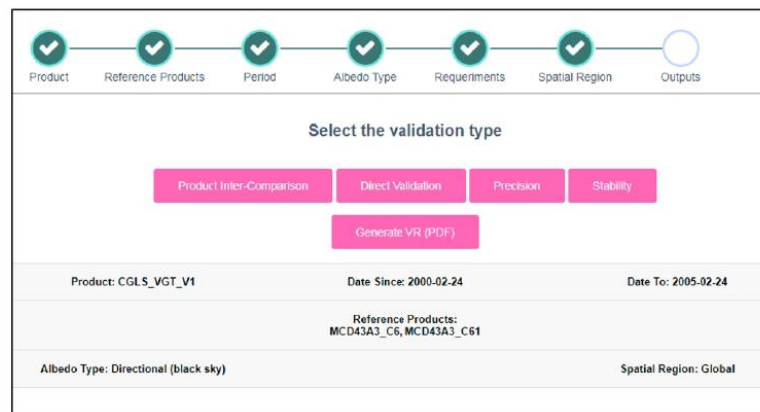


Figure A4. Snapshot of SALVAL configuration step 4.

- (5) Enjoy the interactive validation process (see below Direct Validation type results).

References

1. Dickinson, R.E. Land processes in climate models. *Remote Sens. Environ.* **1995**, *51*, 27–38. [CrossRef]
2. Liang, S. A direct algorithm for estimating land surface broadband albedos from MODIS imagery. *IEEE Trans. Geosci. Remote Sens.* **2003**, *41*, 136–145. [CrossRef]
3. WMO; United Nations Educational, Scientific and Cultural Organization; Intergovernmental Oceanographic Commission; United Nations Environment Programme; International Science Council. The 2022 GCOS Implementation Plan (GCOS-244). Available online: <https://gcos.wmo.int/en/publications/gcos-implementation-plan2022> (accessed on 10 November 2022).

4. Zhou, Y.; Wang, D.; Liang, S.; Yu, Y.; He, T. Assessment of the Suomi NPP VIIRS Land Surface Albedo Data Using Station Measurements and High-Resolution Albedo Maps. *Remote Sens.* **2016**, *8*, 137. [CrossRef]
5. Wang, D.; Liang, S.; Zhou, Y.; He, T.; Yu, Y. A New Method for Retrieving Daily Land Surface Albedo from VIIRS Data. *IEEE Trans. Geosci. Remote Sens.* **2017**, *55*, 1765–1775. [CrossRef]
6. Wang, D.; Liang, S.; He, T.; Yu, Y. Direct estimation of land surface albedo from VIIRS data: Algorithm improvement and preliminary validation. *J. Geophys. Res. Atmos.* **2013**, *118*, 12577–12586. [CrossRef]
7. Balsamo, G.; Agusti-Panareda, A.; Albergel, C.; Arduini, G.; Bejaars, A.; Bidlot, J.; Bousserez, N.; Boussetta, S.; Brown, A.; Buizza, R.; et al. Satellite and In Situ Observations for Advancing Global Earth Surface Modelling: A Review. *Remote Sens.* **2018**, *10*, 2038. [CrossRef]
8. Bayat, B.; Camacho, F.; Nickeson, J.; Cosh, M.; Bolten, J.; Vereecken, H.; Montzka, C. Toward operational validation systems for global satellite-based terrestrial essential climate variables. *Int. J. Appl. Earth Obs. Geoinf.* **2021**, *95*, 102240. [CrossRef]
9. Leroy, M.; Deuzé, J.L.; Bréon, F.M.; Hautecoeur, O.; Herman, M.; Buriez, J.C.; Tanré, D.; Bouffiès, S.; Chazette, P.; Roujean, J.L. Retrieval of atmospheric properties and surface bidirectional reflectances over land from POLDER/ADEOS. *J. Geophys. Res. Atmos.* **1997**, *102*, 17023–17037. [CrossRef]
10. Schaaf, C.B.; Gao, F.; Strahler, A.H.; Lucht, W.; Li, X.; Tsang, T.; Strugnell, N.C.; Zhang, X.; Jin, Y.; Muller, J.P.; et al. First operational BRDF, albedo nadir reflectance products from MODIS. *Remote Sens. Environ.* **2002**, *83*, 135–148. [CrossRef]
11. Strahler, A.H.; Muller, J.-P.; MODIS Science Team Members. MODIS BRDF/Albedo Product: Algorithm Theoretical Basis Document Version 5.0. Available online: https://modis.gsfc.nasa.gov/data/atbd/atbd_mod09.pdf (accessed on 15 February 2023).
12. Geiger, B.; Carrer, D.; Franchistéguy, L.; Roujean, J.L.; Meurey, C. Land surface albedo derived on a daily basis from meteosat second generation observations. *IEEE Trans. Geosci. Remote Sens.* **2008**, *46*, 3841–3856. [CrossRef]
13. Carrer, D.; Roujean, J.L.; Meurey, C. Comparing operational MSG/SEVIRI Land Surface albedo products from Land SAF with ground measurements and MODIS. *IEEE Trans. Geosci. Remote Sens.* **2010**, *48*, 1714–1728. [CrossRef]
14. Carrer, D.; Pinault, F.; Lellouch, G.; Trigo, I.F.; Benhadj, I.; Camacho, F.; Ceamanos, X.; Moparthy, S.; Muñoz-Sabater, J.; Schüller, L.; et al. Surface Albedo Retrieval from 40-Years of Earth Observations through the EUMETSAT/LSA SAF and EU/C3S Programmes: The Versatile Algorithm of PYALUS. *Remote Sens.* **2021**, *13*, 372. [CrossRef]
15. Lellouch, G.; Carrer, D.; Vincent, C.; Pardé, M.; Frietas, S.C.; Trigo, I.F. Evaluation of Two Global Land Surface Albedo Datasets Distributed by the Copernicus Climate Change Service and the EUMETSAT LSA-SAF. *Remote Sens.* **2020**, *12*, 1888. [CrossRef]
16. Carrer, D.; Moparthy, S.; Lellouch, G.; Ceamanos, X.; Pinault, F.; Freitas, S.C.; Trigo, I.F. Land surface albedo derived on a ten daily basis from Meteosat Second Generation Observations: The NRT and climate data record collections from the EUMETSAT LSA SAF. *Remote Sens.* **2018**, *10*, 1262. [CrossRef]
17. Trigo, I.F.; Dacamara, C.C.; Viterbo, P.; Roujean, J.-L.; Olesen, F.; Barroso, C.; Camacho-de-Coca, F.; Carrer, D.; Freitas, S.C.; García-Haro, J.; et al. The Satellite Application Facility for Land Surface Analysis. *Int. J. Remote Sens.* **2011**, *32*, 2725–2744. [CrossRef]
18. Land Surface Analysis (LSA-SAF) of EUMETSAT. Available online: <https://landsaf.ipma.pt/en/> (accessed on 10 November 2022).
19. Copernicus Global Land Service (CGLS) portal. Available online: <https://land.copernicus.eu/global/index.html> (accessed on 10 November 2022).
20. Copernicus Climate Change Service (C3S). Available online: <https://climate.copernicus.eu/> (accessed on 10 November 2022).
21. Sanchez-Zapero, J.; Camacho, F.; Leon-Tavares, J.; Martinez-Sanchez, E.; Gorrone, J.; Benhadj, I.; Tote, C.; Swinnen, E.; Muñoz-Sabater, J. Prototype for Surface Albedo Retrieval Based on Sentinel-3 OLCI and SLSTR Data in the Framework of Copernicus Climate Change. In Proceedings of the 2021 IEEE International Geoscience and Remote Sensing Symposium IGARSS, Brussels, Belgium, 11–16 July 2021; pp. 2377–2380.
22. Liu, Q.; Wang, L.; Qu, Y.; Liu, N.; Liu, S.; Tang, H.; Liang, S. Preliminary evaluation of the long-term GLASS albedo product. *Int. J. Digit. Earth* **2013**, *6*, 69–95. [CrossRef]
23. Liu, Y.; Wang, Z.; Sun, Q.; Erb, A.M.; Li, Z.; Schaaf, C.B.; Zhang, X.; Román, M.O.; Scott, R.L.; Zhang, Q.; et al. Evaluation of the VIIRS BRDF, Albedo and NBAR products suite and an assessment of continuity with the long term MODIS record. *Remote Sens. Environ.* **2017**, *201*, 256–274. [CrossRef]
24. Sánchez-Zapero, J.; Camacho, F.; Martínez-Sánchez, E.; Lacaze, R.; Carrer, D.; Pinault, F.; Benhadj, I.; Muñoz-Sabater, J. Quality Assessment of PROBA-V Surface Albedo V1 for the Continuity of the Copernicus Climate Change Service. *Remote Sens.* **2020**, *12*, 2596. [CrossRef]
25. Zeng, Y.; Su, Z.; Calvet, J.C.; Manninen, T.; Swinnen, E.; Schulz, J.; Roebeling, R.; Poli, P.; Tan, D.; Riihelä, A.; et al. Analysis of current validation practices in Europe for space-based climate data records of essential climate variables. *Int. J. Appl. Earth Obs. Geoinf.* **2015**, *42*, 150–161. [CrossRef]
26. Nightingale, J.; Mittaz, J.P.D.; Douglas, S.; Dee, D.; Ryder, J.; Taylor, M.; Old, C.; Dieval, C.; Fouron, C.; Dubeau, G.; et al. Ten Priority Science Gaps in Assessing Climate Data Record Quality. *Remote Sens.* **2019**, *11*, 986. [CrossRef]
27. LPV (Land Product Validation). Subgroup CEOS Validation Hierarchy 2019. Available online: <https://lpvs.gsfc.nasa.gov/> (accessed on 2 March 2022).

28. Justice, C.; Belward, A.; Morisette, J.; Lewis, P.; Privette, J.; Baret, F. Developments in the ‘validation’ of satellite sensor products for the study of the land surface. *Int. J. Remote Sens.* **2000**, *21*, 3383–3390. [CrossRef]
29. Wang, Z.; Schaaf, C.; Lattanzio, A.; Carrer, D.; Grant, I.; Roman, M.; Camacho, F.; Yang, Y.; Sánchez-Zapero, J. Global Surface Albedo Product Validation Best Practices Protocol. Version 1.0. In *Good Practices for Satellite-Derived Land Product Validation* (p. 45); *Land Product Validation Subgroup (WGCV/CEOS)*; Wang, Z., Nickeson, J., Román, M., Eds.; Available online: https://lpvs.gsfc.nasa.gov/PDF/CEOS_ALBEDO_Protocol_20190307_v1.pdf (accessed on 1 March 2022).
30. Nightingale, J.; Schaepman-Strub, G.; Nickeson, J.; Baret, F.; Herold, M. Assessing Satellite-Derived Land Product Quality for Earth System Science Applications: Overview of the CEOS LPV Sub-Group. In *Proceedings of the 34th International Symposium on Remote Sensing of Environment, Sydney, NSW, Australia, 10–15 April 2011*.
31. Mayr, S.; Kuenzer, C.; Gessner, U.; Klein, I.; Rutzinger, M. Validation of Earth Observation Time-Series: A Review for Large-Area and Temporally Dense Land Surface Products. *Remote Sens.* **2019**, *11*, 2616. [CrossRef]
32. Liang, S.; Fang, H.; Chen, M.; Shuey, C.J.; Walthall, C.; Daughtry, C.; Morisette, J.; Schaaf, C.; Strahler, A. Validating MODIS land surface reflectance and albedo products: Methods and preliminary results. *Remote Sens. Environ.* **2002**, *83*, 149–162. [CrossRef]
33. Cescatti, A.; Marcolla, B.; Santhana Vannan, S.K.; Pan, J.Y.; Román, M.O.; Yang, X.; Ciais, P.; Cook, R.B.; Law, B.E.; Matteucci, G.; et al. Intercomparison of MODIS albedo retrievals and in situ measurements across the global FLUXNET network. *Remote Sens. Environ.* **2012**, *121*, 323–334. [CrossRef]
34. EOLAB. Surface ALbedo VALidation (SALVAL) Tool. Available online: <https://salval.eolab.es/> (accessed on 10 November 2022).
35. JCGM-GUM Joint Committee for Guides in Metrology (JCGM)—Guides to the Expression of Uncertainty in Measurement (GUM). [ISO/IEC Guide 98—Part 3, 2008]. Available online: <https://www.iso.org/sites/JCGM/GUM-introduction.htm> (accessed on 10 November 2022).
36. GCOS-154 Systematic Observation Requirements for Satellite-Based Data Products for Climate. *Supplemental Details to the Satellite-Based Component of the “Implementation Plan for the GCOS in Support of the UNFCCC”*. Available online: https://library.wmo.int/doc_num.php?explnum_id=3710 (accessed on 10 April 2022).
37. SALVAL Sampling—CalValPortal. Available online: <https://calvalportal.ceos.org/sampling> (accessed on 19 December 2022).
38. Camacho, F.; Cernicharo, J.; Lacaze, R.; Baret, F.; Weiss, M. GEOVI: LAI, FAPAR essential climate variables and FCOVER global time series capitalizing over existing products. Part 2: Validation and intercomparison with reference products. *Remote Sens. Environ.* **2013**, *137*, 310–329. [CrossRef]
39. Sánchez, J.; Camacho, F.; Lacaze, R.; Smets, B. Early validation of PROBA-V GEOVI LAI, FAPAR and FCOVER products for the continuity of the copernicus global land service. *Int. Arch. Photogramm. Remote Sens. Spat. Inf. Sci.—ISPRS Arch.* **2015**, *40*, 93–100. [CrossRef]
40. Lewis, P.; Barnsley, M. Influence of the sky radiance distribution on various formulations of the earth surface albedo. In *Proceedings of the 6th International Symposium on Physical Measurements and Signatures in Remote Sensing, ISPRS, Val d’Isère, France, 17–22 January 1994*; pp. 707–715.
41. Román, M.O.; Schaaf, C.B.; Woodcock, C.E.; Strahler, A.H.; Yang, X.; Braswell, R.H.; Curtis, P.S.; Davis, K.J.; Dragoni, D.; Goulden, M.L.; et al. The MODIS (Collection V005) BRDF/albedo product: Assessment of spatial representativeness over forested landscapes. *Remote Sens. Environ.* **2009**, *113*, 2476–2498. [CrossRef]
42. Román, M.O.; Schaaf, C.B.; Lewis, P.; Gao, F.; Anderson, G.P.; Privette, J.L.; Strahler, A.H.; Woodcock, C.E.; Barnsley, M. Assessing the coupling between surface albedo derived from MODIS and the fraction of diffuse skylight over spatially-characterized landscapes. *Remote Sens. Environ.* **2010**, *114*, 738–760. [CrossRef]
43. MODIS Data Products. Available online: <https://modis.gsfc.nasa.gov/data/dataproduct/> (accessed on 10 November 2022).
44. Global Land Surface Satellite (GLASS). Available online: <http://www.glass.umd.edu/> (accessed on 1 April 2022).
45. Globalbedo Portal. Available online: <http://www.globalbedo.org/> (accessed on 10 November 2022).
46. Schaepman-Strub, G.; Schaepman, M.E.; Painter, T.H.; Dangel, S.; Martonchik, J.V. Reflectance quantities in optical remote sensing—definitions and case studies. *Remote Sens. Environ.* **2006**, *103*, 27–42. [CrossRef]
47. Lucht, W.; Schaaf, C.B.; Strahler, A.H. An algorithm for the retrieval of albedo from space using semiempirical BRDF models. *IEEE Trans. Geosci. Remote Sens.* **2000**, *38*, 977–998. [CrossRef]
48. Shuai, Y.; Tuerhanjiang, L.; Shao, C.; Gao, F.; Zhou, Y.; Xie, D.; Liu, T.; Liang, J.; Chu, N. Re-understanding of land surface albedo and related terms in satellite-based retrievals. *Big Earth Data* **2020**, *4*, 45–67. [CrossRef]
49. Schaaf, C.; Wang, Z. MODIS/Terra+Aqua BRDF/Albedo Daily L3 Global—500m V061 [Data set]. NASA EOSDIS Land Processes DAAC. Available online: <https://lpdaac.usgs.gov/products/mcd43a3v061/> (accessed on 20 December 2022).
50. Lucht, W.; Lewis, P. Theoretical noise sensitivity of BRDF and albedo retrieval from the EOS-MODIS and MISR sensors with respect to angular sampling. *Int. J. Remote Sens.* **2000**, *21*, 81–98. [CrossRef]
51. Sun, Q.; Wang, Z.; Li, Z.; Erb, A.; Schaaf, C.B. Evaluation of the global MODIS 30 arc-second spatially and temporally complete snow-free land surface albedo and reflectance anisotropy dataset. *Int. J. Appl. Earth Obs. Geoinf.* **2017**, *58*, 36–49. [CrossRef]
52. Liang, S.A.H.S.C.W. Retrieval of Land Surface Albedo from Satellite Observations: A Simulation Study. *J. Appl. Meteorol.* **1999**, *38*, 712–725. [CrossRef]
53. Wang, Z.; Schaaf, C.B.; Sun, Q.; Shuai, Y.; Román, M.O. Capturing rapid land surface dynamics with Collection V006 MODIS BRDF/NBAR/Albedo (MCD43) products. *Remote Sens. Environ.* **2018**, *207*, 50–64. [CrossRef]

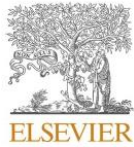
54. Wang, Z.; Schaaf, C.B.; Chopping, M.J.; Strahler, A.H.; Wang, J.; Román, M.O.; Rocha, A.V.; Woodcock, C.E.; Shuai, Y. Evaluation of Moderate-resolution Imaging Spectroradiometer (MODIS) snow albedo product (MCD43A) over tundra. *Remote Sens. Environ.* **2012**, *117*, 264–280. [CrossRef]
55. Wang, Z.; Schaaf, C.B.; Strahler, A.H.; Chopping, M.J.; Román, M.O.; Shuai, Y.; Woodcock, C.E.; Hollinger, D.Y.; Fitzjarrald, D.R. Evaluation of MODIS albedo product (MCD43A) over grassland, agriculture and forest surface types during dormant and snow-covered periods. *Remote Sens. Environ.* **2014**, *140*, 60–77. [CrossRef]
56. Climate Data Store of Copernicus Climate Change Service. Available online: <https://cds.climate.copernicus.eu/#!/home> (accessed on 10 May 2020).
57. Carrer, D.; Pinault, F.; Ramon, D.; Benhadj, I.; Swinnen, E. Algorithm Theoretical Basis Document (ATBD) of CDR SPOT/VGT Surface Albedo v1.0 (Official Reference Number Service Contract: 2018/C3S_312b_Lot5_VITO/SC1). Available online: https://datastore.copernicus-climate.eu/documents/satellite-albedo/D1.3.3-v1.0_ATBD_CDR-ICDR_SA_PROBAV_v1.0_PRODUCTS_v1.0.2.pdf (accessed on 1 November 2022).
58. Carrer, D.; Pinault, F.; Bigeard, G.; Ramon, D.; Jolivet, D.; Kirches, G.; Brockmann, C.; Boettcher, M.; Benhadj, I. Algorithm Theoretical Basis Document Multi sensor CDR Surface Albedo v2.0 (Official Reference Number Service Contract: 2018/C3S_312b_Lot5_VITO/SC1). Available online: https://datastore.copernicus-climate.eu/documents/satellite-albedo/D1.3.4-v2.0_ATBD_CDR_SA_MULTISENSOR_v2.0_PRODUCTS_v1.1.pdf (accessed on 10 November 2022).
59. Rahman, H.; Dedieu, G. SMAC: A simplified method for the atmospheric correction of satellite measurements in the solar spectrum. *Int. J. Remote Sens.* **1994**, *15*, 123–143. [CrossRef]
60. Sánchez-Zapero, J.; Martínez-Sánchez, E.; Camacho, F.; León-Tavares, J. Product Quality Assessment Report Multi-sensor Surface Albedo v2.0 (Official Reference Number Service Contract: 2018/C3S_312b_Lot5_VITO/SC1). Available online: https://datastore.copernicus-climate.eu/documents/satellite-albedo/D2.3.4-v2.0_PQAR_CDR_SA_MULTISENSOR_v2.0_PRODUCTS_v1.1.pdf (accessed on 10 November 2022).
61. Liang, S.; Cheng, J.; Jia, K.; Jiang, B.; Liu, Q.; Xiao, Z.; Yao, Y.; Yuan, W.; Zhang, X.; Zhao, X.; et al. The Global Land Surface Satellite (GLASS) product suite. *Bull. Am. Meteorol. Soc.* **2020**, *102*, E323–E337. [CrossRef]
62. Qu, Y.; Liu, Q.; Liang, S.; Wang, L.; Liu, N.; Liu, S. Direct-estimation algorithm for mapping daily land-surface broadband albedo from modis data. *IEEE Trans. Geosci. Remote Sens.* **2014**, *52*, 907–919. [CrossRef]
63. Liu, N.F.; Liu, Q.; Wang, L.Z.; Liang, S.L.; Wen, J.G.; Qu, Y.; Liu, S.H. A statistics-based temporal filter algorithm to map spatiotemporally continuous shortwave albedo from MODIS data. *Hydrol. Earth Syst. Sci.* **2013**, *17*, 2121–2129. [CrossRef]
64. Qu, Y.; Liang, S.; Liu, Q.; Li, X.; Feng, Y.; Liu, S. Estimating Arctic sea-ice shortwave albedo from MODIS data. *Remote Sens. Environ.* **2016**, *186*, 32–46. [CrossRef]
65. Feng, Y.; Liu, Q.; Qu, Y.; Liang, S. Estimation of the Ocean Water Albedo From Remote Sensing and Meteorological Reanalysis Data. *IEEE Trans. Geosci. Remote Sens.* **2016**, *54*, 850–868. [CrossRef]
66. Ground-Based Observations for Validation (GBOV) of Copernicus Global Land Products Site. Available online: <https://land.copernicus.eu/global/gbov> (accessed on 3 November 2022).
67. FLUXNET. The Data Portal serving the FLUXNET Community. Available online: <https://fluxnet.org/> (accessed on 10 November 2022).
68. NSF NEON. Open Data to Understand our Ecosystems. Available online: <https://www.neonscience.org/> (accessed on 10 November 2022).
69. European Fluxes Database Cluster. Available online: <http://www.europe-fluxdata.eu/> (accessed on 10 November 2022).
70. ICOS—Integrated Carbon Observation System. Available online: <https://www.icos-cp.eu/> (accessed on 10 November 2022).
71. TERN—Australia’s Terrestrial Ecosystem Research Network. Available online: <https://www.tern.org.au/> (accessed on 10 November 2022).
72. Ohmura, A.; Dutton, E.G.; Forgan, B.; Fröhlich, C.; Gilgen, H.; Hegner, H.; Heimo, A.; König-Langlo, G.; McArthur, B.; Müller, G.; et al. Baseline Surface Radiation Network (BSRN/WCRP): New Precision Radiometry for Climate Research. *Bull. Am. Meteorol. Soc.* **1998**, *79*, 2115–2136. [CrossRef]
73. ESRL Global Monitoring Laboratory—Global Radiation and Aerosols. SURFRAD. Available online: <https://gml.noaa.gov/grad/surfrad/> (accessed on 20 December 2022).
74. Matheron, G. Principles of geostatistics. *Econ. Geol.* **1963**, *58*, 1246–1266. [CrossRef]
75. Hohn, M.E. An Introduction to Applied Geostatistics: By Edward H. Isaaks and R. Mohan Srivastava, 1989, Oxford University Press, New York, 561 p., ISBN 0-19-505012-6, ISBN 0-19-505013-4. *Comput. Geosci.* **1991**, *17*, 471–473. [CrossRef]
76. Copernicus Sentinel-2 Mission. Available online: <https://sentinel.esa.int/web/sentinel/missions/sentinel-2> (accessed on 20 December 2022).
77. Bonafoni, S.; Sekertekin, A. Albedo Retrieval from Sentinel-2 by New Narrow-to-Broadband Conversion Coefficients. *IEEE Geosci. Remote Sens. Lett.* **2020**, *17*, 1618–1622. [CrossRef]
78. Ohring, G.; Wielicki, B.; Spencer, R.; Emery, B.; Datta, R. Satellite Instrument Calibration for Measuring Global Climate Change: Report of a Workshop. *Bull. Am. Meteorol. Soc.* **2005**, *86*, 1303–1314. [CrossRef]
79. World Meteorological Organization (WMO) Requirements for Earth Surface Albedo. Available online: <https://www.wmo-sat.info/oscar/variables/view/54> (accessed on 10 April 2020).

80. The 2022 GCOS ECVs Requirements (GCOS 245). Available online: https://library.wmo.int/index.php?lvl=notice_display&id=22135#Y5eLMofMI2whhttps://library.wmo.int/doc_num.php?explnum_id=11318 (accessed on 20 December 2022).
81. Sánchez-Zapero, J.; Camacho, F. Product Quality Assessment Report (PQAR) of CDR and ICDR Surface Albedo v1.0 based on PROBA-V (Official Reference Number Service Contract: 2018/C35_312b_Lot5_VITO/SC1). Available online: <https://cds.climate.copernicus.eu/cdsapp#!/dataset/satellite-albedo?tab=doc> (accessed on 9 April 2022).
82. Iannone, R.Q.; Niro, F.; Goryl, P.; Dransfeld, S.; Hoersch, B.; Stelzer, K.; Kirches, G.; Paperin, M.; Brockmann, C.; Gomez-Chova, L.; et al. Proba-V cloud detection Round Robin: Validation results and recommendations. In Proceedings of the 2017 9th International Workshop on the Analysis of Multitemporal Remote Sensing Images, MultiTemp, Bruges, Belgium, 27–29 June 2017; pp. 1–8. [[CrossRef](#)]
83. Weiss, M.; Baret, F.; Block, T.; Koetz, B.; Burini, A.; Scholze, B.; Lecharpentier, P.; Brockmann, C.; Fernandes, R.; Plummer, S.; et al. On line validation exercise (OLIVE): A web based service for the validation of medium resolution land products. application to FAPAR products. *Remote Sens.* **2014**, *6*, 4190–4216. [[CrossRef](#)]
84. Lacherade, S.; Fougne, B.; Henry, P.; Gamet, P. Cross calibration over desert sites: Description, methodology, and operational implementation. *IEEE Trans. Geosci. Remote Sens.* **2013**, *51*, 1098–1113. [[CrossRef](#)]
85. Merchant, C.J. Thermal remote sensing of sea surface temperature. *Therm. Infrared Remote Sens. Sens. Methods Appl.* **2013**, *17*, 287–313.
86. Fell, F.; Bennartz, R.; Loew, A. Validation of the EUMETSAT Geostationary Surface Albedo Climate Data Record -2- (ALBEDOVAL-2). Available online: <https://www.eumetsat.int/website/home/Data/TechnicalDocuments/index.html> (accessed on 12 April 2020).
87. Gu, L.; Shuai, Y.; Shao, C.; Xie, D.; Zhang, Q.; Li, Y.; Yang, J.; Gu, L.; Shuai, Y.; Shao, C.; et al. Angle Effect on Typical Optical Remote Sensing Indices in Vegetation Monitoring. *Remote Sens.* **2021**, *13*, 1699. [[CrossRef](#)]
88. Kokhanovsky, A.A.; Breon, F.M. Validation of an analytical snow BRDF model using PARASOL multi-angular and multispectral observations. *IEEE Geosci. Remote Sens. Lett.* **2012**, *9*, 928–932. [[CrossRef](#)]
89. Liang, S. Narrowband to broadband conversions of land surface albedo I Algorithms. *Remote Sens. Environ.* **2001**, *76*, 213–238. [[CrossRef](#)]
90. CalVal Portal: SALVAL Tool. Available online: <https://calvalportal.ceos.org/salval> (accessed on 14 November 2022).

Disclaimer/Publisher’s Note: The statements, opinions and data contained in all publications are solely those of the individual author(s) and contributor(s) and not of MDPI and/or the editor(s). MDPI and/or the editor(s) disclaim responsibility for any injury to people or property resulting from any ideas, methods, instructions or products referred to in the content.

Anexo V – Copia de publicación 4

Remote Sensing of Environment 287 (2023) 113460



Contents lists available at ScienceDirect

Remote Sensing of Environment

journal homepage: www.elsevier.com/locate/rse

Global estimates of surface albedo from Sentinel-3 OLCI and SLSTR data for Copernicus Climate Change Service: Algorithm and preliminary validation

Jorge Sánchez-Zapero^{a,*}, Fernando Camacho^a, Enrique Martínez-Sánchez^a, Javier Gorroño^a, Jonathan León-Tavares^b, Iskander Benhadj^b, Carolien Toté^b, Else Swinnen^b, Joaquín Muñoz-Sabater^c

^a Earth Observation Laboratory (EOLAB), C/ Savina 8 – A4, 46980 Paterna, Valencia, Spain

^b Flemish Institute for Technological Research (VITO), Remote Sensing Unit, Boeretang 200, B-2400 Mol, Belgium

^c European Centre for Medium-Range Weather Forecasts (ECMWF), Shinfield Road, RG2 9AX Reading, UK

ARTICLE INFO

Edited by Jing M. Chen

Keywords:

Albedo
Algorithm
Sentinel-3
Validation

ABSTRACT

The aim of Copernicus Climate Change Service (C3S) is to supply reliable climate data in support of strategies to adaptation and mitigation to climate change. The C3S provides access to high-quality climate data through its Climate Data Records (CDRs) of atmospheric, marine and land Essential Climate Variables (ECVs). Global Earth Surface Albedo (SA) satellite-based products are included in the land (biosphere) portfolio. SA is a magnitude which quantifies the fraction of solar energy reflected by the surface of the Earth. This paper details the retrieval methodology and preliminary validation results for global estimates of surface albedo based on Sentinel-3 observations for the C3S ECVs data (C3S SA v3.0). The retrieval algorithm exploits the synergistic use of the Ocean and Land Colour Instrument (OLCI) and the Sea and Land Surface Temperature Radiometer (SLSTR) on-board Sentinel-3 A and B satellites. Firstly, the atmospherically corrected reflectances are generated in the Copernicus Global Land Service framework. After that, the Bidirectional Reflectance Distribution Function (BRDF) inversion module concludes the BRDF model parameters, which are transferred to the angular integration module in order to generate spectral albedo quantities for the selected OLCI (Oa03, Oa04, Oa07, Oa17 and Oa21) and SLSTR (S1, S2, S5 and S6) bands. At the end, the spectral integration module generates broadband albedo quantities in three different standard broadband spectral regions (visible [0.4 μ m – 0.7 μ m], near infrared [0.7 μ m – 4 μ m] and total shortwave [0.3 μ m – 4 μ m]). Preliminary validation results over 10-months demonstration period (July 2018–April 2019) show, in terms of spatial and temporal consistency, that C3S Sentinel-3 SA global estimates reached in general good agreement as compared to other satellite operational references derived from MODIS (MCD43A3 C6) and PROBA-V (C3S PROBA-V SA v1.0) acquisitions. The comparison with ground data shows similar results to the MCD43A3 C6 comparisons but opposite sign in differences (marginally positive in case of Sentinel-3), with accuracy of 0.005 (3.7%), precision of 0.016 (11.3%) and uncertainty of 0.032 (22.7%). Our results have demonstrated the feasibility to estimate global fields of SA from Sentinel-3 observations, with similar quality of existing operational products. These Sentinel-3 based SA datasets will give the continuity to the existing C3S SA CDR, introducing improvements in terms of spatial resolution (300 m) and spectral information (9 spectral albedos) in contrast to previous datasets based on Advanced Very High Resolution Radiometer (AVHRR; 4 km, 4 channels) and Vegetation instruments (VGT; 1 km, 4 channels).

1. Introduction

Surface albedo (SA), defined as the ratio of the radiant flux reflected from the Earth's land surface to the incident flux, is considered a terrestrial Essential Climate Variable (ECV) according to the Global

Climate Observing System (GCOS) to characterize the state of the global climate system and its evolution resulting from natural and anthropogenic forcing (GCOS-154, 2011; GCOS-200, 2016). SA is both a forcing variable controlling the surface energy budget and a sensitive indicator of environmental changes including land degradation (Dickinson,

* Corresponding author.

E-mail addresses: jorge.sanchez@eolab.es (J. Sánchez-Zapero), iskander.benhadj@vito.be (I. Benhadj), joaquin.munoz@ecmwf.int (J. Muñoz-Sabater).

<https://doi.org/10.1016/j.rse.2023.113460>

Received 8 June 2022; Received in revised form 21 December 2022; Accepted 14 January 2023

Available online 28 January 2023

0034-4257/© 2023 Elsevier Inc. All rights reserved.

J. Sánchez-Zapero et al.

Remote Sensing of Environment 287 (2023) 113460

1995). As a corollary, it also determines the fraction of solar energy absorbed by the surface and transformed into heat or latent energy. Land SA is therefore a key variable for characterizing the energy balance in the coupled surface-atmosphere system and constitutes an indispensable input quantity for soil-vegetation-atmosphere transfer models (Stephens et al., 2015). Also worth noting, climate sensitivity studies with Global Circulation Models have confirmed the unsteady nature of the energy balance with respect to small changes in Surface Albedo (Amut et al., 2007; Henderson-Sellers and Wilson, 1983; Ollinger et al., 2008; Sellers et al., 1995).

The albedo quantity most relevant in terms of energy budget comprises the shortwave domain (SW [0.3 μm , 4 μm]), where the solar downwelling radiation is more relevant (Gueymard et al., 2019). SW domain includes the visible (VI [0.4 μm , 0.7 μm]) and near-infrared (NIR [0.7 μm , 4 μm]). Actually, different definitions of satellite albedo products exist according to the domain of directional integration (Schaepman-Strub et al., 2006): the directional-hemispherical reflectance (DHR) or black-sky albedo (BSA or AL-DH), and the bi-hemispherical reflectance (BHR) or white-sky albedo (WSA or AL-BH). BSA is defined as the ratio of the radiant flux for light reflected by a unit surface area into the view hemisphere to the illumination radiant flux, when the surface is illuminated with a parallel beam of light from a single direction (Lucht et al., 2000). On the other hand, WSA is the ratio of the radiant flux reflected from a unit surface area into the whole hemisphere to the incident radiant flux of hemispherical angular extent (Shuai et al., 2020). Combining BSA and WSA in relation to the proportion of sky irradiance, the blue-sky albedo is obtained, which is the actual albedo value (Lewis and Bamsley, 1994).

The Climate Change Service (C3S, <https://climate.copernicus.eu/>) of Copernicus European Union's Earth Observation (EO) programme aims to provide key indicators on the drivers of climate change, combining climate observations with the most recent science to develop and deliver quality guaranteed information about the past, current and future climate conditions in Europe and in the whole worldwide. In response to GCOS, the C3S produces Climate Data Records (CDRs) of many ECVs, including land SA. In the C3S, three broadband quantities are provided (visible, NIR, total shortwave) in both angular integration domains (black-sky and white-sky albedos). The existing C3S SA CDR, available in the Climate Data Store (CDS, <https://cds.climate.copernicus.eu/#/!home>) is based on past EO satellites time series, retrieved from the National Oceanic and Atmospheric Administration / Advanced Very High Resolution (NOAA/AVHRR) (Apr 1981 - Dec 2005, at 4 km), Satellite Pour l'Observation de la Terre / Vegetation (SPOT/VGT) (Dec 1999 - May 2014, at 1 km) and Project for On-Board Autonomy Vegetation (PROBA-V) (Dec 2013 - Jun 2020, at 1 km). The primary objective of C3S is to continuously monitor the status of existing CDRs to support adaptation and mitigation policies of the European Union by providing consistent and authoritative information about climate change. SA is also mandatory for the continuity other C3S ECVs, as serves as input for the generation of Leaf Area Index (LAI) and Fraction of Absorbed Photosynthetically Active Radiation (FAPAR) products, which are based on Two-stream Inversion Package (TIP) algorithm (Pinty et al., 2006).

The continuity of the SA ECV service can be ensured thanks to the switch to measurements from Ocean and Land Colour Instrument (OLCI) and Sea and Land Surface Temperature Radiometer (SLSTR) on-board ESA Sentinel-3 A (S3A) and B (S3B) satellites (Mecklenburg et al., 2018). The synergistic use of both sensors allows the characterization of total solar spectrum, necessary for broadband albedo calculation, as they provide complementary information. OLCI provides spectral information in blue region, which is important for VI broadband albedo estimation. SLSTR has, however, spectral channels in SWIR domain, playing important role in NIR broadband albedo estimation. The spatial resolution of existing SA CDR (1 km) is also improved thanks to the exploitation of Sentinel-3 OLCI (~ 300 m) and SLSTR (~ 500 m) data, in response to GCOS (GCOS-200, 2016) implementation plan actions.

A rigorous approach for SA determination from EO top-of-

atmosphere (TOA) data consists in solving the radiative transfer problem in the coupled surface-atmosphere system simultaneously (Betts, 2009). Such method was adopted in both algorithms to retrieve SA from both MISR (Diner et al., 1998, 2008) and Meteosat (Govaerts et al., 2008; Pinty et al., 2000a, 2000b) instruments. Other methods are based on TOA reflectances direct conversion to broadband SA without performing atmospheric correction (Liang, 2003). A robust and pragmatic approach for surface albedo determination distinguishes different steps in the processing chain (i.e., cloud masking and atmospheric correction, BRDF inversion, spectral albedo calculation, and narrow-to-broadband albedo conversion), and treats them independently. The atmospherically corrected surface reflectance values serve as the input quantities for the inversion of a linear kernel-driven Bidirectional Reflectance Distribution Function (BRDF) model, which allows taking into account the angular dependence of the reflectance factor (Barnsley et al., 1994; Hu et al., 1997; Roujean et al., 1992; Wanner et al., 1995). This approach for retrieving surface albedo products was firstly included in the Polarization and Directionality of the Earth's Reflectances (POLDER) (Leroy et al., 1997) processing chain, then in Moderate Resolution Imaging Spectroradiometer (MODIS) MCD43 (Schaaf et al., 2002; Strahler et al., 1999), Spinning Enhanced Visible and InfraRed Imager (SEVIRI) (Carer et al., 2010; Geiger et al., 2008), AVHRR (Lellouch et al., 2020), and adapted to Vegetation sensors in C3S (Carer et al., 2021) afterwards. This robust approach was selected in the first albedo retrieval algorithm implementation using Sentinel-3 data in the framework of the C3S (named as C3S SA v3.0) as it gives a good compromise between simplicity of implementation, computation time and quality of the outputs. This explains why it is widely used in operational contexts, such as NASA MODIS (<https://modis.gsfc.nasa.gov/>), the Satellite Application Facility for Land Surface Analysis (LSA SAF, <https://landsaf.ipma.pt/en/>) program of EUMETSAT or the Copernicus Global Land Service (CGLS, <https://land.copernicus.eu/global/index.html>).

On the other hand, a framework for the Evaluation and Quality Control (EQC) of climate data products derived from satellite and in-situ observations was developed within the C3S CDR (Nightingale et al., 2019). Validation, or quality assessment, is one of the main components defined in this EQC framework, and it is defined as the process of independently assessing the quality of the data products derived from the system outputs (Justice et al., 2000). Scientific quality assessment is necessary to ensure the compliance of the products to user requirements, and C3S SA v3.0 demonstration products underwent a scientific evaluation before they are realised to the users.

The validation methodology follows the good practices recommended by the Land Product Validation sub-group (LPV, <https://lpvs.gsfc.nasa.gov/>) of the Working Group on Calibration and Validation (WGCV) of the Committee on Earth Observing Satellites (CEOS) for the validation of satellite-derived global albedo products (Wang et al., 2019). The validation strategy includes two different approaches, the direct and indirect validation. The direct point-to-pixel validation (i.e. direct validation) consists of satellite products comparisons with albedo measured from in-situ tower-based instruments (Lewis and Bamsley, 1994). Direct validation enables the assessment of uncertainties, and it may be argued that only such methods can be seen as actual validation in the field of remote sensing (Mayr et al., 2019). Product-to-product validation approach refers to the intercomparison of satellite products (i.e., indirect validation), which allows the evaluation of discrepancies (systematic or random) between products and relative uncertainties. Indirect validation is very helpful to compute metrics that cannot be obtained with ground measurements for the limitations in terms of representativeness and global conditions. However, indirect validation does not provide absolute validation results, since satellite products intercomparison alone are not enough to validate new products.

This paper describes the algorithm and preliminary validation results over a demonstration period of 10 months (July 2018–April 2019) of the SA retrieval algorithm based on Sentinel-3 OLCI and SLSTR data, developed in the framework of the C3S. The paper is structured as

J. Sánchez-Zapero et al.

Remote Sensing of Environment 287 (2023) 113460

follows: Sections 2 and 3 describe the input datasets and validation methodology respectively; section 4 presents the albedo retrieval algorithm, section 5 presents the quality assessment results while conclusions are summarized in section 6.

2. Data

2.1. Sentinel-3 input data

2.1.1. Characteristics of Sentinel-3 OLCI and SLSTR instruments

As part of the Copernicus programme, Sentinel-3 is the third of the Sentinel satellite series, originally dedicated to ocean and land applications including sea-ice, water quality monitoring in open-ocean, coastal and inland areas, surface temperature, sea height, and vegetation productivity. The mission provides continuity to the observations from Envisat space-borne missions. The first platform, Sentinel-3 A, has been flying since 16 February 2016. The second platform, Sentinel-3 B, was successfully launched on 25 April 2018. Sentinel-3 is a Low Earth Orbit (LEO), with a mean altitude of 815 km and sun-synchronous, and a local equatorial crossing time of 10:00 am.

OLCI (<https://sentinels.copernicus.eu/web/sentinel/user-guide/s/sentinel-3-olci>) is one of the four instruments present on the Sentinel-3 platform. As a continuity of the Envisat MEdium Resolution Imaging Spectrometer (MERIS), OLCI is a push-broom imaging spectrometer that measures solar radiation reflected by the Earth in 21 spectral bands encompassed in visible and NIR, with a high spatial resolution of 300 m at the nadir view, and a swath width of 1270 km. It includes five camera modules; the field of view (FOV) of each camera is arranged in a fan-shaped configuration in the vertical plane perpendicular to the platform velocity. Each camera has an individual FOV of 14.2° with a 0.6° overlap with its neighbours to cover a wide 68.5° across-track FOV.

SLSTR (<https://sentinels.copernicus.eu/web/sentinel/user-guide/s/sentinel-3-slstr>) is a conical scanning imaging radiometer employing the along-track scanning dual-view technique to measure the radiance at the top of the atmosphere in nine spectral channels: six solar channels from the visible (554 nm) to the Short Wave-Infrared (SWIR) (3.74 μm), and two in the thermal infrared (10.85 and 12.02 μm). Each scene is observed twice: in nadir and backwards views. SLSTR is an evolution of the Along Track Scanning Radiometer (ATSR) series and Advanced Along Track Scanning Radiometer (AATSR) with a wider swath (1420 km in nadir, 750 km in backwards view) and an increased spatial resolution (~500 m for solar reflectance bands).

2.1.2. Pre-processing of Sentinel-3 OLCI and SLSTR data

Atmospherically corrected reflectances derived from OLCI and SLSTR observation on-board of Sentinel-3 A and B satellites (PDGS, 2016) are the input for SA retrieval algorithm. These surface reflectances are brokered from CGLS Sentinel-3 pre-processing chain, which is common to all Sentinel-3 based CGLS biophysical variables. Surface reflectances are retrieved from Level 1B Sentinel-3 TOA radiometry following the next steps: i) collocation and reprojection of OLCI and SLSTR Level 1B input on the regular 300 m plate carrée grid using the nearest neighbour resampling and S3-MPC SYN_L1C tool (<https://github.com/bdev/11c-syn-tool>); ii) cloud, cloud shadow and snow classification based on the OLCI Identification of Pixel (IdePix) properties algorithm (S3_MPC, 2019) and the SLSTR summary cloud flag (S3_MPC, 2021a); and iii) Atmospheric Correction (Ramon et al., 2021) based on the Simplified Method for Atmospheric Correction (SMAC) (Rahman and Dedieu, 1994).

The Atmospheric Correction (AC) was evaluated in the CGLS (Jolivet, 2021) following the AC intercomparison exercise approach (Doxani et al., 2018). Sentinel-3 surface reflectances were compared to a reference product retrieved from Aerosol Robotic Network (AERONET) aerosols optical thickness in-situ data and the Second Simulation of the Satellite Signal in the Solar Spectrum (6S) correction method (Vermote et al.,

1997). The comparison of surface reflectances with reference products from 48 AERONET sites show accuracy variability, depending on the spectral channel, from 10^{-3} to $1.2 \cdot 10^{-2}$ and precision and uncertainty from 0.012 to 0.033. Reference product was retrieved using an accurate radiance transfer code and inversion of the in-situ Aerosol Robotic Network (AERONET) products for aerosols optical thickness and model.

The internal CGLS quality assessment of Sentinel-3 surface reflectances (Sánchez-Zapero et al., 2021b) demonstrated reliable performance at global scale and spatially accordance with Sentinel-2 at local study cases. OLCI and SLSTR equivalent channels showed good consistency and similar temporal trends. The comparison of OLCI and SLSTR equivalent channels surface retrievals over selected local cases of interest (representatives of different biome types) showed also good agreement (positive bias <5%). Observations over desert calibration sites (Lacherade et al., 2013) from different satellites (S3A versus S3B) were found also consistent: bias indicator typically <1% while uncertainty and precision around 10%. The comparison with Radiometric Calibration Network (RadCalNet) in-situ measurements over four different sites showed good temporal agreement and positive bias, with median deviation (accuracy) lower than 3% (typically) and large differences in the OLCI and SLSTR lower channels. However, large negative differences were found in the comparison of SLSTR S5 and S6 channels against RadCalNet, that could be reduced applying the vicarious calibration coefficients (from -11% to -1% in S5, from -18% to 4% in S6). In summary, the quality assessment demonstrated the reliability and suitability of Sentinel-3 surface reflectances to produce biophysical products. The main limitations come from the ancillary quality layers (cloud masking and error characterization) and the underestimation in the SWIR region (S5 and S6 SLSTR channels) (S3_MPC, 2021b).

A well-known limitation of the IdePix cloud/snow algorithm is the misidentification of snow and clouds (Toté, 2020), removing most of snow observations when all the IdePix cloud flags (i.e., "cloud", "cloud_ambiguous", "cloud_buffer", "cloud_shadow") are applied. Consequently, an alternative decision rule (see Fig. 1.) based on Normalized Difference Snow Index (NDSI) threshold in combination with less restrictive IdePix flags (i.e., "cloud", "cloud_ambiguous") has been implemented to identify pixels likely associated with snow. The NDSI was computed using the ground reflectance of green (S1) and SWIR (S5) SLSTR spectral bands. A threshold of 0.42 (<https://sentinels.copernicus.eu/web/sentinel/technical-guides/sentinel-2-msi/level-2a/algorithm>) was found useful to identify snow pixels from Sentinel-3. For snow-free pixels (NDSI < 0.42) the additional two cloud flags ("cloud_shadow", "cloud_buffer") were applied.

CGLS includes a total of 20 spectral bands of Sentinel-3 surface reflectances (15 from OLCI and 5 from SLSTR). The use of both sensors allows covering the total shortwave range for broadband albedo calculation, as OLCI provides spectral information in blue spectral region (i.e., Oa03 and Oa04 channels; Table 1) and SLSTR in SWIR domain (i.e., S5 and S6 channels; Table 1). In this version of the Sentinel-3 surface albedo retrieval algorithm, the bands that provide less information, predominate in highly sensitive areas or are spectrally redundant were discarded. As similar accuracy of surface reflectances was found for equivalent OLCI and SLSTR channels (Sánchez-Zapero et al., 2021b), the broader bands were selected for OLCI and SLSTR overlaps due to they are more representative of broadband albedo. Furthermore, as OLCI swath (1270 km) has 100% overlap with SLSTR swath (1420 km), SLSTR acquisitions out of OLCI swath were not used for sake of consistency. Table 1 summarizes the information of the 9 selected bands (central wavelength and width) used as the input in the Sentinel-3 SA algorithm.

2.2. Validation data

2.2.1. Ground measurements

A careful selection of best in-situ reference albedo measured from tower-based instrument is mandatory for the comparison with satellite albedo products. For a meaningful point-to-pixel comparison, it is

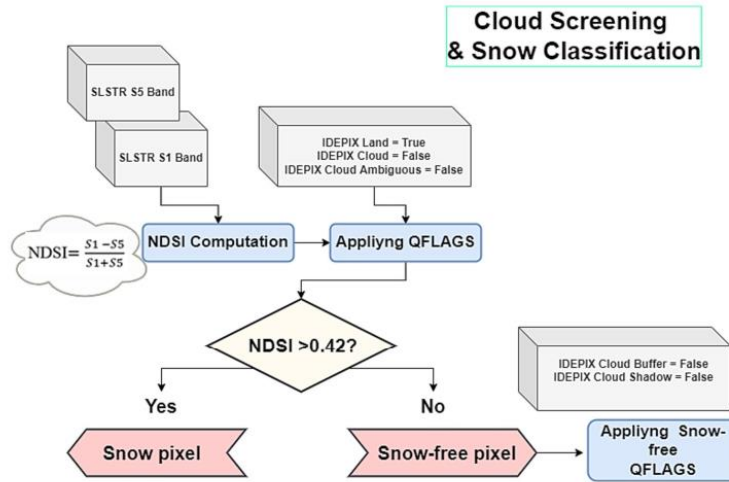


Fig. 1. Diagram for cloud screening and snow classification.

Table 1

Characteristics of Sentinel-3 OLCI (Oa03, Oa04, Oa07, Oa17, Oa21) and SLSTR (S1, S2, S5, S6) channels used as input of the surface albedo retrievals.

Spectral band	Oa03	Oa04	Oa07	Oa17	Oa21	S1	S2	S5	S6
λ centre (nm)	442.5	490	620	865	1020	554.27	659.47	1613.4	2255.7
Width (nm)	10	10	10	20	40	19.26	19.25	60.68	50.15

crucial the good characterization of the spatial representativeness around the ground-based measurements. Homogeneous sites were selected showing similar footprints than satellite pixel resolutions of interests. 58 stations (see details in Annex I) were taking into account in the evaluation of the spatial representativeness: 17 sites come from the CGLS Ground-Based Observations for Validation (GBOV, <https://gbov.acri.fr/>), which collects data from other existing networks such as ESRL GMD, SURFRAD, BSRN, FLUXNET and OZFLUX), 25 from the National Ecological Observatory Network (NEON, <https://www.neonscience.org/>), 4 from the Integrated Carbon Observation System (ICOS, <http://www.icos-cp.eu/>) and 12 from The Environmental Resources Network (TERN, <https://www.tern.org.au/>). Most of them (33 sites) are considered ‘Super Sites’ endorsed by the CEOS LPV, as they are deeply characterized in terms of bio-geophysical variables and canopy structure and have infrastructural capacity to keep active in long-term operations.

The stations provide measurements from the top of ground-based tower sites of downward shortwave radiation (SW_IN), upward shortwave radiation (SW_OUT) and downward diffuse shortwave radiative flux (SW_DIF). Measurements are available for each day with a temporal frequency acquisition typically lower than 30 min. SW_IN is the sum of the direct and diffuse downwelling (SW_DIF) components of the solar radiation and SW_OUT is the upwelling solar radiation reflected by the surface. The fraction of SW_OUT and SW_IN results in blue-sky albedo measurements. A broadband albedometer consists of two pyranometers (e.g., Kipp & Zonen CMP, CMA, CNR or SpectroSun SR-75), which measure SW_IN and SW_OUT, respectively. SW_DIF is measured by an independent shaded pyranometer (e.g., Eppley i-48) using a sun tracker to shield the sensor from direct sunlight. The uncertainty of albedo tower-based measurements depends on absolute accuracy of the pyranometers and the associated non-ideal cosine response (Cescatti et al., 2012). Most of the errors associated with the absolute accuracy of the instrument are similar for SW_IN and SW_OUT and therefore compensate. Overall the expected accuracy related to albedo measurements is in the order of 4–7% in clear sky and 1–4% in overcast condition (Pirazzini,

2004; Pirazzini et al., 2006).

The spatial representativeness was evaluated at 1 km, with aim to ensure that ground measurements are comparable with satellite retrievals from different sources and spatial resolutions (Sentinel-3 at 300 m, MODIS at 500 m and PROBA-V at 1 km). The methodology, adopted from CEOS LPV recommendations, is based on the estimation of geostatistical indexes (Román et al., 2009, 2010), comparing the variogram model parameters obtained at different spatial resolutions (1 km - 1.5 km). Four geostatistical attributes were procured from variogram model parameters (Cescatti et al., 2012; Román et al., 2010): relative strength of the spatial correlation (R_{ST}), relative coefficient of variation (R_{CV}), scale requirement index (R_{SE}), and relative proportion of structural variation (R_{SV}). Combining the four geostatistical attributes it is generated the standard score (ST_{SCORE} , a score of spatial representativeness which use R_{SE} as more weighted marker and the others like secondary markers (see Eq. 1). In cases when semi-spherical variogram model does not provide a good fit to the variogram estimator, the first order score (RAW_{SCORE}) could be used to provide a mark of the spatial representativeness (Eq. 2), less recommended due to are only based on the R_{CV} .

$$ST_{score} = \left(\frac{|R_{CV}| + |R_{ST}| + |R_{SV}| + R_{SE}}{3} \right)^{-1} \tag{1}$$

$$RAW_{score} = |2 R_{CV}|^{-1} \tag{2}$$

Both, ST and RAW scores are directly proportional to site spatial homogeneity or representativeness. It is proposed to use a score threshold of 2.0 in ST_{SCORE} to decide which one is a homogeneous or spatially representative site as large differences are expected for sites below to this threshold (Cescatti et al., 2012; Sánchez-Zapero et al., 2020). In case where ST_{SCORE} cannot be computed, same threshold of 2.0 in RAW_{SCORE} was used.

Finally, 32 sites (Fig. 2) were considered homogeneous or spatially

J. Sánchez-Zapero et al.

Remote Sensing of Environment 287 (2023) 113460

representative for the comparison of satellite products at 1 km resolution (see Annex II, where a summary of the main geostatistical attributes for each selected site used in accuracy assessment at 1 km resolution is presented). The ground stations are grouped according to the main biome types (26 forests, 4 grasslands, 1 croplands and 1 bare area). Note that *KONZ*, *ORNL*, *MLBS*, *STEI*, *AU_Cum* and *AU_GWW* are not considered representative at 1 km resolution during the leaf-on season and *USA_PSUS* and *USA_SFS* during the leaf-off season. Additionally, *USA_NRFT*, *BONA* and *DEJU* were not used in the leaf-off season period due to not clear images were found in the period to analyze the representativeness of the site due to persistent cloudy or snow events.

2.2.2. Satellite products

In this section, the main characteristics of SA products involved in the quality assessment are described (Table 2). MODIS BRDF/Albedo (MCD43A3) Collection 6 (C6) (Schaaf and Wang, 2015) and C3S PROBA-V SA v1.0 (Carrer et al., 2019) products are used as a reference. They have reached CEOS LPV validation stage level three (Wang et al., 2018), as products are evaluated over global conditions and validation procedures followed community-agreed good practices. C3S PROBA-V SA v1.0 validation results (Sánchez-Zapero and Camacho, 2019) showed systematic overestimation (11.5%) compared with 20 homogeneous GBOV sites (2014–2018 period), mainly over forest sites for lower albedo ranges ($SA < 0.2$) (Sánchez-Zapero et al., 2020). MCD43A3 C6 showed better accuracy and opposite sign of differences (negative bias of -5.9%). Both reference products showed similar uncertainty (RMSD ~ 0.04) in comparison with GBOV data over homogeneous sites.

Equivalent spatial and temporal support sampling must be defined for intercomparison of satellite products. The comparison was performed at 1 km spatial support area, which is the spatial resolution of PROBA-V SA products. For that, Sentinel-3 (300 m resolution) average values in a 3×3 pixels window and 2×2 pixels for MCD43A3 C6 (500 m resolution) were calculated. Previously, MCD43A3 C6 products were re-located in Plate Carrée projection. Furthermore, as C3S products temporal frequency is 10-days, it was selected as common temporal support period.

The Quality Flag information (Table 3) was applied to discard retrievals which have been flagged as low quality in case of reference products. For C3S SA v1.0 products, land pixels which show input status invalid or out of range and/or saturation in blue and red channels were discarded. In case of MODIS C6, pixels with best quality (i.e., magnitude inversion with number of valid observations of at least 7 days) and good quality (full inversion) were considered for the re-sampling over C3S spatial grid. Then, MODIS C6 inversions with < 7 days were discarded.

3. Validation methods

The methods for quality assessment follow the CEOS LPV good practice protocol for the validation of satellite-derived albedo products (Wang et al., 2019).

For direct validation purposes, the in-situ albedometer footprints were tested in terms of spatial representativeness at the satellite evaluated pixel resolution, in concordance with tower-based measurements standards (Román et al., 2009, 2010) (see section 2.2.1). The next step involves the computation of satellite blue-sky albedo (Lewis and Bamsley, 1994) to compare ground measurements (direct validation). For that, the proportion of direct and diffuse down-welling shortwave radiation measured at the station is used to weight the corresponding BSA and WSA satellite best quality retrievals (Table 3). Since satellite products provide BSA estimations at the Solar Local Noon (SLN), ground measurements have been chosen at SLN, too. Finally, the average of daily ground data values during the temporal composite window of satellite product (see Table 2) were computed for the comparison.

The product intercomparison approach is evaluated over LAND VALidation (LANDVAL) 720-site network. This selection of sites is representative of the global variability of land surface types (Fuster et al., 2020; Sánchez-Zapero et al., 2020). The product comparison is also performed per biome type, as well as for the specific case of snow targets.

The temporal consistency is evaluated through qualitative inspection of temporal trajectories. The error is quantitatively characterized assessing the Accuracy, Precision and Uncertainty (APU) metrics (see Table 4), reporting the goodness of fit between the evaluated dataset and

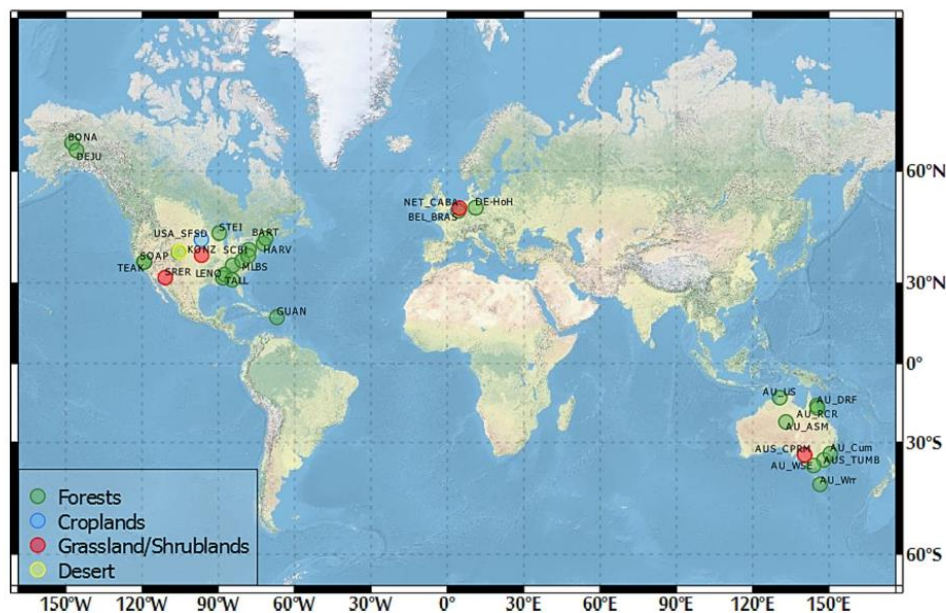


Fig. 2. Global distribution of spatially-representative tower sites selected for direct validation.

Table 2
Features of the global remote sensing SA products involved in the quality assessment.

Product	Satellite /Sensor	BRDF Model: Volumetric /Geometrical Kernels	Spatial resolution /Projection	Production frequency /Composite period	Period available	Reference
C3S SA v3.0	Sentinel-3 /OLCI & SLSTR	Ross_Thick /Li_Sparse_Reciprocal	1/336° (~300 m) /Plate Carrée	10 days /20 days (recursive using BRDF MODIS climatology).	July 2018 – April 2019	(Sánchez-Zapero et al., 2021a)
C3S SA v1.0	PROBA /VEGETATION	Ross_Thick /Roujean	1/112° (~1 km) /Plate Carrée	10 days /30 days	2014 – June 2020	(Carrer et al., 2019)
NASA MCD43A3 C6	TERRA+AQUA /MODIS	Ross_Thick /Li_Sparse_Reciprocal	500 m /Sinusoidal	Daily /16 days	2000 - present	(Schaaf and Wang, 2015),

Table 3
Summary of the quality flags used to discard invalid or low quality pixels.

Product	Quality Control Flag
C3S PROBA-V SA v1.0 QFLAG	Sea (bit 1) Input status out of range or invalid (bit 6) Saturation in Red (bit 10) and blue (bit 11) channels BRDF Albedo Band Quality Bands 1 to 7;
MCD43A2 C6	Magnitude inversion (number of observations lower than 7)

the corresponding reference. They are adopted from experimental recommendations of Joint Committee for Guides in Metrology (JCGM) to the expression of uncertainty in measurement (JCGM-GUM, 2008) and from GCOS (GCOS-154, 2011). In addition to APU metrics, other statistics including linear model fits or correlation between datasets are used to evaluate the goodness of fit. Major Axis Regression (MAR) was chosen as linear fit model instead of Ordinary Least Squares (OLS) due to MAR is particularly conceived to handle error in both variables (x- and y-axis) (Harper, 2014).

The quality assessment of the C3S Sentinel-3 SA v3.0 satellite products is performed for a global test dataset covering the period from June 2018 to April 2019.

For the conformity testing, a review of a user uncertainty requirements (Table 5) collection was done. C3S, GCOS (GCOS-154, 2011) and World Meteorological Organization (WMO, https://space.oscar.wmo.int/variables/view/earth_surface_albedo) requisites are considered.

Table 4
Validation metrics.

Statistics	Comment
N	Number of samples. Indicative of the power of the validation
B	Mean Bias. Difference between average values of x and y. Indicative of accuracy and offset. Bias (%) is the relative mean bias between the average of x and y. Median deviation between x and y. CEOS LPV good practice reporting the accuracy.
MD	MD (%) is the relative MD between the average of x and y.
STD	Standard deviation of the pair differences. Indicates precision. STD (%) is the relative STD between the average of x and y. Median absolute deviation between x and y. CEOS LPV good practice reporting precision.
MAD	MAD (%) is the relative MAD between the average of x and y.
RMSD	Root Mean Square Deviation. RMSD is the square root of the average of squared errors between x and y. CEOS LPV good practice reporting uncertainty. RMSD (%) is the relative RMSD between the average of x and y.
R	Correlation coefficient. Indicates descriptive power of the linear accuracy test. Pearson coefficient is used.
MAR	Slope and offset of the Major Axis Regression (MAR) linear fit. Indicates some possible bias
Conformity test	Percentage of pixels matching the user requirements (Table 6).

Table 5
Review of uncertainty requirements (GCOS, WMO and C3S SA).

GCOS	WMO	C3S
Max (5%; 0.0025)	Goal: 5% Breakthrough: 10% Threshold: 20%	Max (10%; 0.01)

Three different conformity levels (i.e., optimal, target and threshold) based on the existing requirements are predefined (Table 6), aiming at verifying whether the results are fit for validation purpose. The optimal level (Max [5%, 0.0025]) corresponds to the GCOS uncertainty requirement (which is partly equivalent to WMO goal level). The target level (Max [10%, 0.01]) is selected according to the C3S key performance indicator (KPI) (which is partly equivalent to the WMO breakthrough level). Lastly, the threshold level (Max [20%, 0.02]) is more similar to WMO threshold level. When products performances are above threshold level, it is considered as suboptimal quality.

4. Sentinel-3 albedo retrieval algorithm

4.1.1. Algorithm overview

The proposed Sentinel-3 SA retrieval approach flow diagram is described in Fig. 3. It starts from OLCI and SLSTR surface reflectances, which are generated in the CGLS service in a common 300 m spatial grid aiming to facilitate the integration of both data sources. The BRDF inversion and the albedo calculation (which involves angular and spectral integration) are constructed in the context of the C3S, and described in the following sections, being the outputs the spectral and broadband albedos (and associated uncertainties), delivered every 10 days (3 per month). Spectral albedos are provided for each OLCI or SLSTR channel described in Table 1 and they are finally combined in the last step, which is related to the narrow to broadband conversion.

4.1.2. BRDF descriptors retrieval

Land Surface reflectance values depend on the spectral wavelength, as well as on different conditions in terms of observation, illumination and geometry (sensor and Sun locations). The BRDF, which quantifies the anisotropy of the reflectance, can be approximated by numerical inversion of kernel-driven semi-empirical models (e.g. RossThick-

Table 6
Predefined levels for uncertainty requirements used in the SA validation.

	Optimal	Target	Threshold
Surface Albedo Uncertainty Requirements	Max [5%, 0.0025]	Max [10%, 0.01]	Max [20%, 0.02]

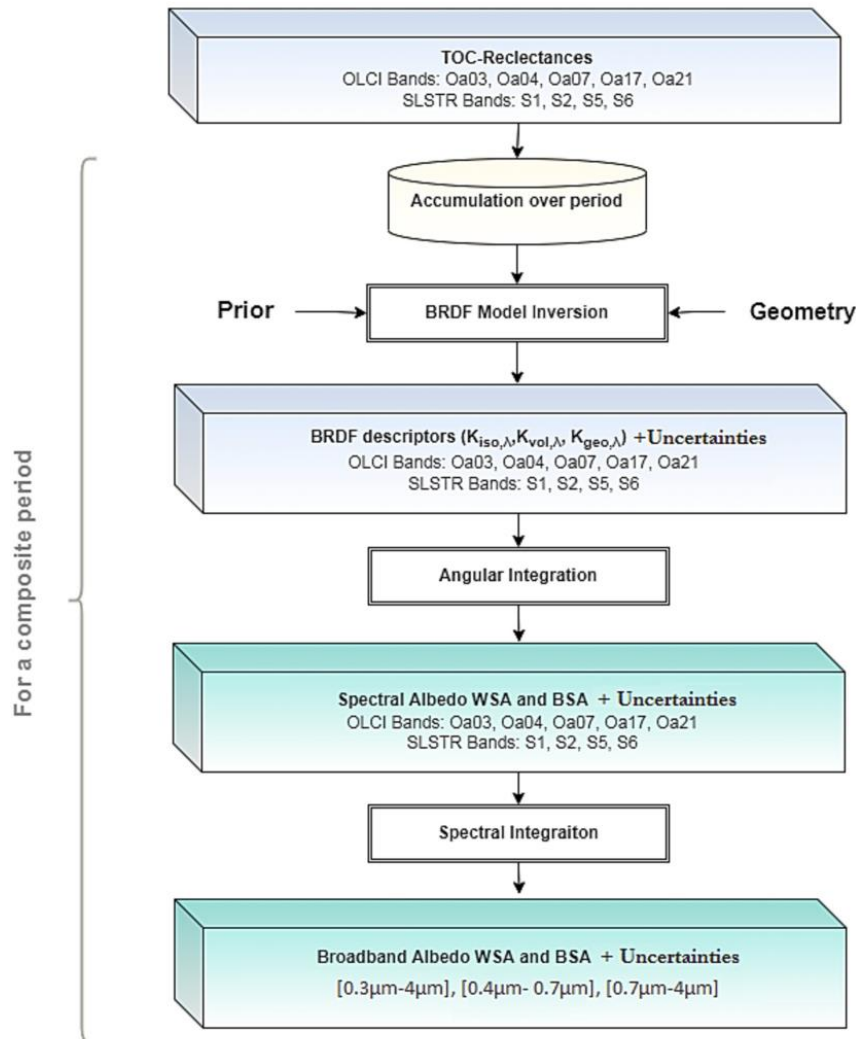


Fig. 3. Flow diagram of the SA retrieval algorithm.

LiSparseReciprocal) making use of three parameters called BRDF descriptors or parameters (Roujean, 2017). It is now widely accepted that kernel-driven semi-empirical BRDF models can adequately represent the directional signature of most natural targets (Breon and Maignan, 2017; Bréon and Vermote, 2012; Claverie et al., 2015; Franch et al., 2014; Los et al., 2005; Lucht et al., 2000; Roujean et al., 1992, 2018; Roy et al., 2016; Schaaf et al., 2002; Vermote et al., 2009; Wanner et al., 1995). In the framework of C3S, the Regularised BRDF inversion for land surface reflectance (ReBeLS) processor, initially developed within CGLS (Leon-Tavares, 2020), was used to retrieve the BRDF model from Sentinel-3 surface reflectance data for the required OLCI and SLSTR channels (see Table 1).

ReBeLS starts with the ingestion of surface reflectances, their associated geometries (solar viewing/azimuth, viewing and viewing azimuth angles), pixel quality flags and priors auxiliary data. The priors were built from climatology of MCD43 BRDF descriptors (Strahler et al.,

1999) products (MCD43A1 and MCD43A2) and are used as auxiliary information for the optimization of the BRDF inversion process (Muller et al., 2011). Layers are accumulated over a predefined period of time (for this version of the algorithm, 30 days and 365 days for near-real time (NRT) and back processing products, respectively).

The next step is the BRDF modeling, where kernels from a semi-empirical BRDF model are computed for each observation. ReBeLS uses the Roujean (Roujean et al., 1992) and RossThick-LiSparse (Wanner et al., 1995) models, which are the most popular kernel-driven semi-empirical models to approximate the BRDF of land surface, adopted in the operational data processing system of the MODIS MCD43 products and other operational chains (Baret et al., 2013; Geiger et al., 2008; Lucht et al., 2000; Roujean et al., 2018; Schaaf et al., 2002). Finally, the BRDF inversion is performed, and BRDF descriptors that best represent the ensemble of observations are found by solving an inverse problem (Geiger et al., 2008; Pokrovsky et al., 2003; Roujean et al., 2018) with

J. Sánchez-Zapero et al.

Remote Sensing of Environment 287 (2023) 113460

the addition of regularisation (prior) (Quaife and Lewis, 2010).

The outputs of the BRDF model inversion stage are the retrieved RossThickLiSparse BRDF descriptors (k_{iso} , k_{vol} , k_{geo}) and their respective variances ($\sigma^2_{k_{iso}}$, $\sigma^2_{k_{vol}}$, $\sigma^2_{k_{geo}}$). An output control is also performed, and a quality information layer is assembled to reflect availability of observations and whether (or not) the BRDF model inversion was successful (Leon-Tavares, 2020). The quality control of BRDF retrieval is propagated to final albedo products.

4.1.3. Angular integration (spectral albedo)

For albedo calculation, the BRDF angular integration over all viewing angles is needed. Then, the spectral albedo values can be estimated by computing an angular integral of the kernel functions (f_i), once the BRDF descriptors are known (k_i). The algorithm estimates the black-sky and white-sky albedos to each sensor channel (Table 1) separately. BSA is the albedo over only direct illumination component (any diffuse component) and is function of the solar zenith angle. The BSA is computed at local solar noon. WSA is the albedo only comprised of isotropic diffuse illumination (in absence of direct component). As BSA is not affected by atmospheric scattering, WSA is variable with the intrinsic coupling between the surface and the scattering atmosphere. Instead of directly calculating the integrals of BSA and WSA, the same pragmatic method of polynomial representation of the BSA and WSA integrals proposed in the MODIS albedo estimating procedure (Strahler et al., 1999) is used.

SLSTR SWIR radiometry channels are known to suffer high radiometry calibration inaccuracies, which are translated to Sentinel-3 surface reflectances brokered from CGLS. To correct adequately the measured radiance, vicarious calibration exercises have been performed and multiplicative corrections are strongly advised to be applied (S3.MPC, 2021b). Since ESA post launch vicarious calibration coefficients proposed by the Sentinel-3 Mission Performance Centre (correction factors in SWIR domain of 1/1.1 and 1/1.13 for S5 and S6 SLSTR channels) were not ingested in the CGLS pre-processing chain, they were directly applied in the computation of spectral albedos.

4.1.4. Spectral integration (broadband albedo)

The integral of spectral albedos over a defined wavelength interval domain weighted by the spectral irradiance results in broadband albedo quantities (Liang, 2001). Most studies calculate broadband albedos by linear combination of available spectral albedo values in each spectral channel (Geiger et al., 2008; Liang, 2001; Liang et al., 2003; Van Leeuwen and Roujean, 2002) due to the approximation of the integral as a weighted sum of the integrand at discrete values of the integration variable. Then, the broadband albedo estimates (a_r) for a certain spectral interval ($\gamma = [\lambda_1, \lambda_2]$) can be computed using a linear transformation of the spectral albedo values (a_i) following the expression:

$$a_r = c_{0r} + \sum_j (c_{jr} a_i) \quad (3)$$

where c_{0r} and c_{jr} refer to the linear combination coefficients.

For the C3S SA v3.0 products, a different assemblage of coefficients was produced for both snow scenes and snow-free targets in three different broadband spectral domains: visible (VI - [0.4 μ m - 0.7 μ m]), near infra-red (NI - [0.7 μ m - 4 μ m]) and total shortwave (SW or BB - [0.3 μ m - 4 μ m]).

The methodology to generate the combination coefficients applies a linear regression over a dataset of reference spectral albedo versus its respective broadband albedo. Both spectral and broadband albedo are acquired from a database of simulated/measured spectral albedo and radiative transfer simulations of downwelling irradiance.

For the generation of the linear combination coefficients, the linear regression is trained considering global representativeness of atmospheric and surface properties at global scale (i.e., a weighted linear regression). The global representativeness of the land surfaces has been

Table 7

Approximate percentage area of the Earth represented by the majority of 10 biome types.

Land Class	% Land area	Land Class	% Land area
Evergreen Broadleaved Forest	6.85	Grass	9.34
Deciduous Broadleaved Forest	7.05	Crop	15.85
Needle-Leaf Forest	15.22	Bare	13.08
Other	7.66	Snow	2.54
Shrub	22.20	Urban	0.20

achieved by extracting the data information from the global land cover classification GLC2000 (Bartholome and Belward, 2005). The aggregation per main biome was performed into 10 different classes, and the weights in the linear regression for the generation of narrow to broadband coefficients are proportional to the land surface area they represent at a global scale (see Table 7).

Canopy reflectances in the radiation spectrum (400–2500 nm) at 1 nm for forests are simulated using the PROSAIL (PROSPECT + SAIL) model, which combines the SAIL canopy level bidirectional (Scattering by Arbitrarily 82 Inclined Leaves; (Verhoef, 1984)) and the PROSPECT leaf spectral (Jacquemoud and Baret, 1990) models. Therefore, the albedo for deciduous broadleaf (DBF), needle-leaf (NLF) and evergreen broadleaf (EBF) forest biomes are generated using this method. PROSAIL parameters settings (Table 8) are based in similar studies (Bacour et al., 2002; le Maire et al., 2008). General parameters include the values of carotenoid content (C_{car})[μ g/cm²], brown pigment content (C_{bp}), equivalent water thickness (C_w)[cm] and dry matter content (C_m)[g/cm²] for leaf properties and the leaf angle distribution type (LIDF) (set to 2 which represent ellipsoidal distribution) for the canopy, the soil reflectance (p_{soil}) parameter (considering wet and dry soils) and, finally, the BRDF hot-spot parameter. Biome specific parameterization (Table 8) includes the chlorophyll a and b content (Cab)[μ g/cm²] and structure coefficient (N) for leaf properties, the leaf area index (LAI) and for mean leaf angle parameter (lifda) (0° for planophile, 90° for erectophile). In tropical forests the upper layers have a leaf angle around 35° with the lower layers having horizontal inclination angles. The boreal forests has vertical leaf inclination angles throughout the canopy (Huemmerich, 2013). Based on the results of latitude dependence of the different forest types, the value of lifda is set to 10° for EBF, 40° for DBF, and 80° for NLF. Finally, for the solar zenith angle (SZA) the mean value of an entire year at noontime and for the mean latitude of each biome was used.

The use of the PROSAIL radiative cannot be extended to describe any complex surface such as bare fields with mixed vegetation. In consequence, the spectral albedo characterization database for the other biomes was done using different strategy. For that, the United States

Table 8

Summary of PROSAIL parameters setting.

Parameter	Setting value
Carotenoid content (C_{car})[μ g/cm ²]	8
Brown pigment content (C_{bp})	0
Equivalent Water Thickness (C_w)[cm]	0.01
Dry matter content (C_m)[g/cm ²]	0.009
Soil reflectance (p_{soil})	0 (wet), 0.5 and 1 (dry)
Hot-spot parameter (s_1)	0.05, 0.25 and 0.5
Leaf angle distribution type (LIDF)	2
mean leaf angle (lifda)	EBF: 10° DBF: 40° NLF: 80°
Structure co-efficient (N)	EBF: 5 values from 1.5 to 2.5 DBF: 5 values from 0.8 to 2.5 NLF: 5 values from 0.8 to 2.5
Chlorophyll a and b content (C_{ab})[μ g/cm ²]	EBF: 5 values from 30 to 80 DBF: 5 values from 0 to 80 NLF: 5 values from 10 to 80
Leaf Area Index (LAI)[m ² /m ²]	EBF: 1, 2, 4, 6, 8, 10 DBF: 0.2, 0.5, 1, 2, 5, 10 NLF: 0.5, 1, 1.5, 2.5, 5, 7

J. Sánchez-Zapero et al.

Remote Sensing of Environment 287 (2023) 113460

Geological Survey (USGS) spectral library (USGSspeclib) (Kokaly et al., 2017) and the Ecosystem Spaceborne Thermal Radiometer Experiment on Space Station (ECOSTRESS) library (Meerdink et al., 2019) provides different reflectance signatures. These data represent a conical-conical reflectance obtained from different in-situ and airborne sources (Nicodemus et al., 1977; Schaepman-Strub et al., 2006). Although they do not represent either a directional-hemispherical or bi-hemispherical reflectances, they can be used as an approximation (Liang, 2001; Samain et al., 2006) when the surface is near-Lambertian (i.e., spectral albedo is equivalent to spectral reflectance) or the surface has no strong directionality and the spectral reflectance shape is not measured under critical areas such as hot-spot. The selection of reflectance curves in the database discarded those spectra that were not essentially representative of a Sentinel-3 pixel (e.g., rocks, mineral and meteorites), or spectral ranges not representative for Sentinel-3 configuration. The use of multi-source information including model simulations and hyperspectral libraries might include an impact in the generation of reference spectral albedo dataset. Since the main goal of this dataset is to represent worldwide variability, this multi-source differences are negligible compared to the natural variability.

The synthetic dataset of downwelling irradiance was generated using the Second Simulation of a Satellite Signal in the Solar Spectrum, version 1 (6SV1) (Vermeote et al., 1997). The simulation was performed from 300 nm up to 2600 nm in steps of 1 nm (slightly below 6SV1 resolution). Above that spectral range up to 4000 nm, it was set to zero to reduce computing time since the irradiance can be considered negligible. The parameterisation of 6SV1 was specific for each biome in terms of aerosol optical thickness (AOT), water vapour (WV), altitude and sun zenith angle. AOT and WV maps from March 2019 to March 2020 and an altitude map were obtained from NASA Earth Observation (NEO, <https://neo.gsfc.nasa.gov/>) at a 0.1° spatial resolution. Viewing angles were set to nadir, ozone to 0.330 atm-cm, the atmosphere to mid-latitude summer and aerosol type to continental.

The spectral albedo and downwelling irradiance described above define both the simulated broadband albedo (a_s) and simulated spectral albedos in Sentinel-3 bands (a_{λ}). The latter require the further convolution of the spectral albedo and downwelling irradiance by the mean spectral response functions of OLCI (S3 CalVal Team, 2016a, 2016b) and SLSTR (Nightingale, 2015, 2017). Then, a linear regression between

them considering weights proportional to the land cover area in Table 7, defines the coefficients that represent a VIS/NIR/BB spectral region for both BSA and WSA albedos. The coefficients for Sentinel-3A and Sentinel-3B satellites (Table 9) include specific coefficients for the biome snow and for the rest of biomes (snow free, referred in the table as *glob*). Since the algorithm uses observations of both satellites, the mean value for each coefficient is used by the processing chain.

The fitting error represents the difference between the simulated broadband albedo, the broadband albedo reconstructed using the coefficients in Table 9 and the Sentinel-3 band-convolved albedo. Table 10 summarizes the fitting results. It contains the level of correlation (R^2) and the weighted standard deviation of the errors (i.e. STD, considers the weight for each biome). The levels of correlation are high ($R^2 > 0.99$) and the residual error is low (std < 0.01) for all cases. These values are in line with fitting results that can be found for other studies and missions (Liang, 2001; Van Leeuwen and Roujean, 2002).

4.1.5. Uncertainty propagation

The C3S SA products include an uncertainty estimate associated to the different broadband albedo values. This uncertainty is the result of propagation through the retrieval chain, taking as starting point the uncertainty of the BRDF retrieval module. This is explained as the Sentinel-3 input does not currently include uncertainty information. Then, we start from approximated (synthetic) surface reflectance uncertainties in the BRDF retrieval step (Leon-Tavares, 2020), which are taking into account the number of observations during the accumulation period, the radiometric values and the solar and view angles. BRDF descriptors are retrieved along with their variances, which are estimated assuming uncorrelated errors as the diagonal of the inverse problem of the BRDF inversion (Geiger et al., 2008).

As BRDF model parameters and spectral albedos have a linear relationship, the error covariance matrix of the model parameters is used for standard (“1-sigma”) error estimates of the spectral albedo quantities (Lucht and Lewis, 2000). Then, the uncertainty of the spectral albedos is estimated by propagating the BRDF retrievals variances through the spectral albedos polynomial computations. On the other hand, assuming that the errors of the narrow to broadband linear relationship are uncorrelated by the dependence of the spectral wavelength, the broadband albedo quantity error estimates can be expressed by the following expression:

Table 9

Sentinel-3 albedo narrowband to broadband coefficients in three predefined domains: visible (VI - [0.4 μm–0.7 μm]), near infra-red (NI - [0.7 μm–4 μm]) and total shortwave (BB - [0.3 μm–4 μm]). Channels out of the VI and NI predefined domains are not used.

Satellite / Land cover coverage / Albedo type		C _{0y} Interc.	C _{λy}									
			Oa03	Oa04	Oa07	Oa17	Oa21	S1	S2	S5	S6	
Sentinel-3 A	global	AL-DH-VI	0.0016	0.1732	0.2422	0.2755	0	0	0.1984	0.1048	0	0
		AL-DH-NI	0.0007	0	0	0	0.5630	0.0833	0	0	0.2530	0.0856
		AL-DH-BB	-0.0010	-0.0746	0.2793	0.8184	0.0721	0.2975	-0.0909	-0.4972	0.1174	0.0294
		AL-BH-VI	0.0016	0.2808	0.2334	0.2079	0	0	0.1700	0.0828	0	0
		AL-BH-NI	-0.0010	0	0	0	0.6620	0.0167	0	0	0.2425	0.0655
		AL-BH-BB	0.0002	-0.0127	0.0238	0.06372	0.1221	0.2202	-0.0357	-0.3567	0.1028	0.0351
	snow	AL-DH-VI	-0.0002	0.2060	0.1478	0.0438	0	0	0.2918	0.3111	0	0
		AL-DH-NI	0.0050	0	0	0	0.4469	0.2627	0	0	-0.0997	0.3323
		AL-DH-BB	-0.0010	-0.2862	0.6762	0.9336	0.2140	0.2121	-0.2979	-0.6213	0.0721	0.0943
		AL-BH-VI	-0.0004	0.3535	0.1462	-0.0284	0	0	0.2660	0.2633	0	0
		AL-BH-NI	0.0059	0	0	0	0.5288	0.2298	0	0	-0.1798	0.3542
		AL-BH-BB	-0.0014	-0.3631	0.9954	0.8732	0.2305	0.1757	-0.3820	-0.6845	0.0199	0.1206
	global	AL-DH-VI	0.0018	0.1630	0.2604	0.2871	0	0	0.1928	0.0908	0	0
		AL-DH-NI	0.0007	0	0	0	0.5616	0.0851	0	0	0.2527	0.0856
		AL-DH-BB	-0.0010	-0.0697	0.2722	0.8215	0.0722	0.2977	-0.0955	-0.4935	0.1172	0.0293
		AL-BH-VI	0.0018	0.2721	0.2496	0.2290	0	0	0.1609	0.0631	0	0
		AL-BH-NI	-0.0010	0	0	0	0.6605	0.0184	0	0	0.2427	0.0650
		AL-BH-BB	0.0002	-0.0105	0.2356	0.6439	0.1220	0.2207	-0.0411	-0.3579	0.1029	0.0348
Sentinel-3 B	global	AL-DH-VI	-0.0002	0.2093	0.1451	0.0460	0	0	0.2932	0.3068	0	0
		AL-DH-NI	0.0049	0	0	0	0.4476	0.2614	0	0	-0.0985	0.3311
		AL-DH-BB	-0.0011	-0.3046	0.7006	0.9201	0.2113	0.2141	-0.3096	-0.6007	0.0800	0.0876
	snow	AL-BH-VI	-0.0004	0.3569	0.1433	-0.0255	0	0	0.2668	0.2590	0	0
		AL-BH-NI	0.0057	0	0	0	0.5295	0.2285	0	0	-0.1786	0.3527
		AL-BH-BB	-0.0014	-0.3907	1.0381	0.9135	0.2276	0.1784	-0.4260	-0.6949	0.0306	0.1115

Table 10
Fitting error (STD) and correlation (R^2) of C3S Sentinel-3 narrowband to broadband albedo coefficients presented in Table 9.

Land cover	Param.	AL-DH-VI	AL-DH-NI	AL-DH-BB	AL-BH-VI	AL-BH-NI	AL-BH-BB
Global	R^2	0.9997	0.9962	0.9905	0.9975	0.9939	0.9961
	STD	0.0012	0.0049	0.0051	0.0038	0.0061	0.0030
Snow	R^2	1.0000	0.9996	0.9996	1.0000	0.9993	1.0000
	STD	0.0001	0.0056	0.0058	0.0007	0.0074	0.0018

$$\sigma[a_{\lambda}] = \sqrt{\sum_{\lambda} \left(\frac{\sigma_{a_{\lambda}}^2}{a_{\lambda}^2} + c_{\lambda\gamma}^2 \right) a_{\lambda}^2} \quad (4)$$

Where a_{λ} are the spectral albedo quantities; $\sigma_{a_{\lambda}}$ are the albedo errors for each spectral channel; $c_{\lambda\gamma}$ are the narrow to broadband coefficients for each channel (see Table 9); and $\sigma_{c_{\lambda\gamma}}$ are the fitting errors of these coefficients. The STD values (see Table 10) are used as an approximation

of the fitting error (Liang, 2001).

4.1.6. Output products

The output of the processing (see Fig. 4) consists in 4 sets of products distributed as separate files. Both directional-hemispherical reflectances (variables named DH) or bi-hemispherical reflectances (BH) are provided for both spectral (ALSP) and broadband (ALBB) albedos. Products

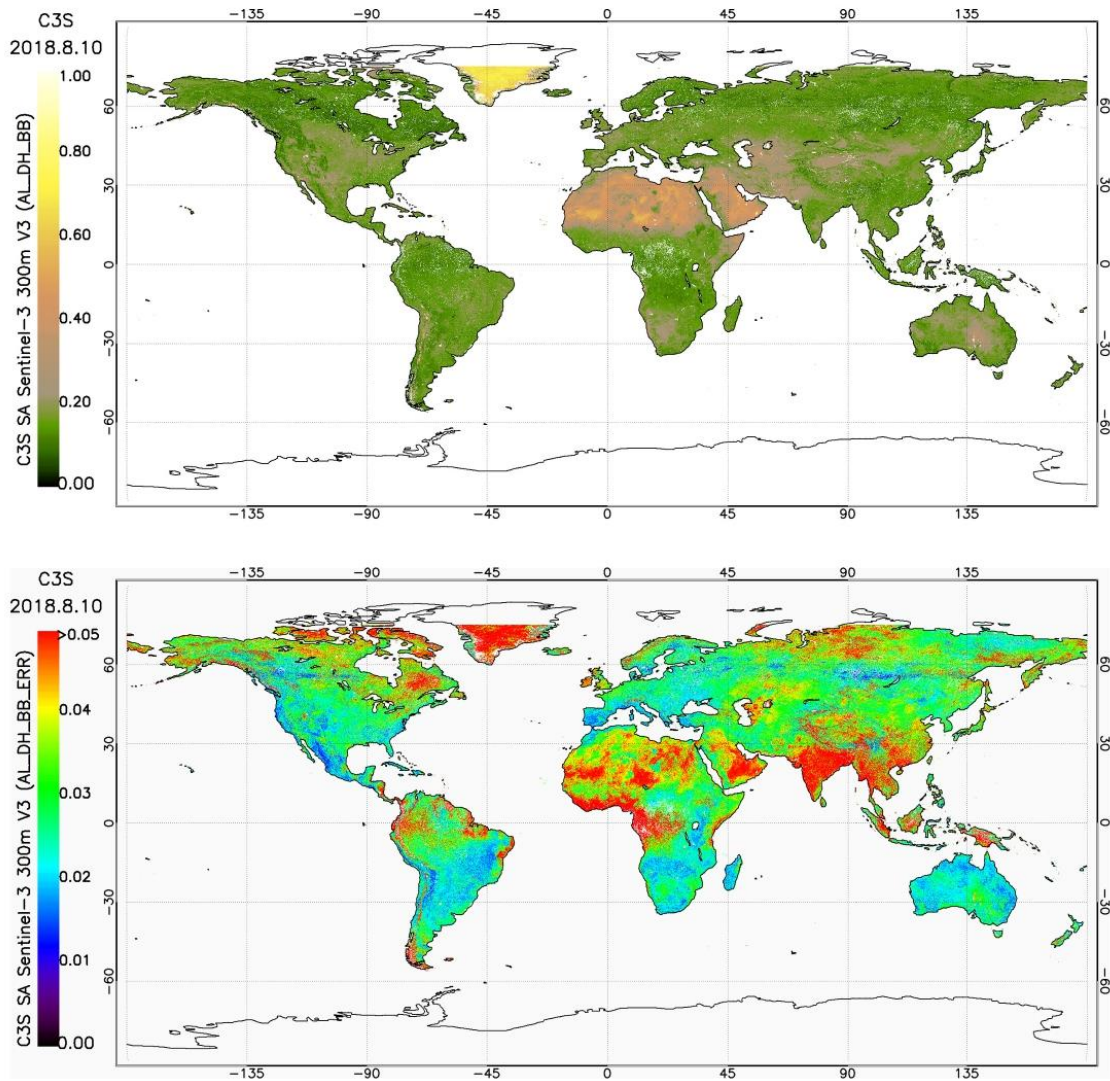


Fig. 4. Global maps of C3S Sentinel-3 SA v3.0 AL-DH-BB (top) for 10th August 2018 and associated uncertainty (bottom).

are almost globally produced over land covering longitudes from 180°E to 180°W and latitudes from 80°N to 60°S on Plate Carrée regular latitude/longitude projection (with the ellipsoid WGS 1984), as detailed in the coordinates reference system variable metadata. The resolution of the grid is 1/336°, giving respectively approximately 300 m of pixel extent at the equator. The files of version 3.0 of Surface Albedo products are generated in Network Common Data Form version 4 (NetCDF4) format, internally compressed. Metadata attributes are compliant with climate and forecast conventions.

The ALSP-DH and ALSP-BH products contain the spectral albedos and their corresponding uncertainties and quality flags (QFLAG), for each OLCI (Oa03, Oa04, Oa07, Oa17, Oa21) and SLSTR (S1, S2, S5, S6) channel. Spectral albedos are finally combined using narrow to broadband coefficients (Table 9) to produce the ALBB-DH and ALBB-BH products, containing the broadband albedos in the three spectral domains (VI, NI, BB) and their corresponding uncertainties and QFLAG. It should be noted that different nominal spatial resolutions are combined when using OLCI (~300 m) and SLSTR (~500 m). However, the combination of observations with different footprints for BRDF inversion is a current practice of existing albedo products based on wide FOV sensors (Carrer et al., 2021; Schaaf and Wang, 2015). This is consequence of the effect of effective pixel size growth at increasing the view angles (Campagnolo and Montano, 2014). More information about the product can be found in the product documentation (Sánchez-Zapero et al., 2021a).

5. Quality assessment results

5.1. Temporal consistency

Sentinel-3 SA v3.0 temporal variations are analysed over the globally representative LANDVAL network of sites for each main land cover, and qualitatively compared with the other satellite references (C3S PROBA-V SA v1.0, MCD43A3 C6). Fig. 5 illustrates the typical temporal trend of the albedo products for each main biome type.

Note that Sentinel-3 SA v3.0 quality flag information is displayed in the temporal profiles: dots represent pixels identified with 'probability' of snow, and crosses represent retrievals where no data is available during the composite period. Vertical bars of Sentinel-3 SA v3.0 correspond to associated error auxiliary layer. MCD43A3 C6 pixels classified as snow according to quality product dataset (MCD43A2) are also identified with dots.

For Evergreen Broadleaved Forest (EBF), typically located over equatorial areas, Sentinel-3 SA v3.0 shows remarkable stable temporal trajectories and noteworthy good completeness as a result of the use of BRDF prior information in the model inversion. The other satellite products (C3S SA v1.0, MCD43A3 C6) display larger number of missing values and noisier profiles. For the other forest cases, such as Needle-Leaf (NLF, which is mainly distributed at northern latitudes) and Deciduous Broadleaved (DBF) Forests, Sentinel-3 SA v3.0 fit temporally well with reference satellite products, properly reproducing the typical situations over these cases: periods with stable values, slight changes due to seasonality and rapid and large changes in magnitude due to snow events. Note that Sentinel-3 SA v3.0 algorithm tends to identify lower number of snow cases than MCD43A3 C6 during the common periods (see for instance December 2018 – April 2019 in LANDVAL#233), but it can deal with this issue providing reliable snow albedo values and improving the completeness due to persistent cloud coverage. For long periods with low availability of data in the transitions from snow-free to snow coverage (e.g., November–December 2018 in LANDVAL#564), Sentinel-3 tends to provide slower transition from low to high albedo values than the expected trend (rapid albedo changes). This can be explained by the low availability of input data. If observations are not available, the model cannot react immediately.

Close temporal patterns are noticed between sensors over cultivated areas and other biomes (herbaceous or shrublands), well reproducing

the phenology of the crops or variations due to natural vegetation. In case of bare areas targets, C3S Sentinel-3 SA v3.0 properly provides stable temporal trends.

5.2. Error evaluation (product intercomparison)

The overall error between C3S Sentinel-3 SA v3.0 was evaluated through product intercomparison with satellite references (C3S PROBA-V SA v1.0, MCD43A3 C6). LANDVAL network of sites was used for sampling global conditions, and the period of the study corresponds to the availability of Sentinel-3 demonstration dataset (July 2018–April 2019).

5.2.1. Overall consistency between C3S Sentinel-3 SA v3.0 vs C3S PROBA-V v1.0

Scatter-plots of total shortwave BSA with associated metrics are displayed in Fig. 6, as well as the box-plots of the difference per range albedo value (bottom). The performance figures for both BSA and WSA are summarized in Table 11 for the three broadband ranges.

Good correlations were found for visible domain ($R = 0.92$) with almost no bias for black-sky albedos ($MD \sim 0$) and negative MD of -4.2% for white-sky albedo. Box-plots show the slight median negative bias (Sentinel-3 < PROBA-V) for almost all SA ranges, except for the higher values (from 0.8 to 1, positive bias). In overall, negative bias (MD) (Sentinel-3 < PROBA-V) of around -5% was found for NIR, with RMSD of around 0.05 ($\sim 15\%$). Similarly, Sentinel-3 SA v3.0 have a tendency to display lower retrievals than PROBA-V SA v1.0 (MD of -5.7% for AL-DH-BB, and -8.4% for AL-BH-BB) for the total shortwave, with overall uncertainties (RMSD) of around 0.05 ($\sim 20\%$). The negative bias was found for most of the product ranges (with the exception of albedo values higher than 0.6 in NIR and 0.8 in total shortwave). Typically around 20% - 40% of cases are within the optimal (GCOS) uncertainty requirements, and typically around 50% considering the target level (C3S KPI).

5.2.2. Overall consistency between C3S Sentinel-3 SA v3.0 vs MCD43A3 C6

This section shows the overall comparison of C3S Sentinel-3 SA v3.0 vs MCD43A3 C6. Scatter-plots and analysis of bias per range albedo BSA total shortwave albedo value are displayed in Fig. 7. The summary of all performance statistics for both BSA and WSA in all broadband ranges (visible, NIR and total shortwave) is presented in Table 12.

Mean negative bias of -1.8% and -5.2% is observed for visible domain (AL-DH-VI, AL-BH-VI) with positive median value (MD) of 6% and 1.6%. Differences in the sign of the bias between mean and median values are due to outliers over snow cases (Sentinel-3 < MCD43A3 C6), and median values are more realistic to report the accuracy in those cases. These outliers are due to underestimation of snow albedo values in case of Sentinel-3 and to the slow transition between snow-free and snow-covered seasons, as observed in the temporal consistency analysis. For the near infrared, the accuracy of Sentinel-3 SA v3.0 compared with MCD43A3 C6 showed, in overall, positive sign with MD of 4.2% and 7.2% for BSA and WSA. For the total shortwave, in overall, positive MD of 6–7% was found. Box-plots clearly display the slight median positive bias (Sentinel-3 > MCD43A3 C6) for the lower albedo values (where most of pixels are located) and large negative for highest albedos (typically snow cases). Regardless the uncertainty requirements, typically between 20% and 30% of cases achieved optimal (GCOS) level of consistency, and >50% of cases within target level (C3S KPI).

5.2.3. Analysis per biome type

The Probability density function distributions of Sentinel-3 SA v3.0 (Fig. 8) albedo retrievals per main biome type are evaluated and qualitatively compared with reference products (MCD43A3 C6, C3S PROBA-V SA v1.0).

C3S Sentinel-3 SA v3.0 products showed similar distribution of

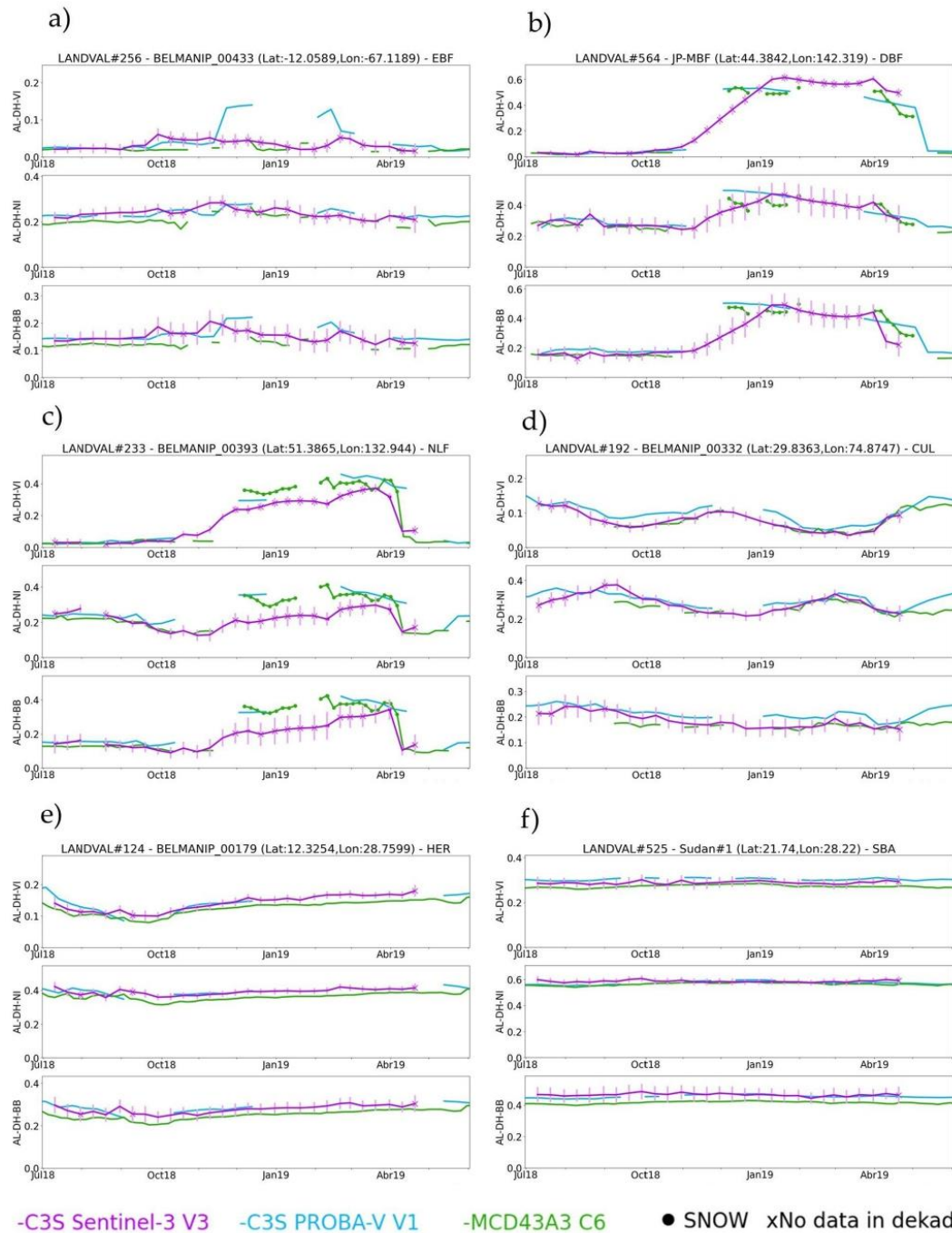


Fig. 5. Temporal profiles of C3S Sentinel-3 SA v3.0 (purple), C3S PROBA-V SA v1.0 (blue) and MCD43A3 C6 (green) for July 2018–June 2019 period. Examples over one selected LANDVAL site representing the main biome types (a) EBF, b) DBF, c) NLF, d) CUL, e) HER, f) SBA). For Sentinel-3 SA v3.0, dots and crosses represent pixels identified with ‘probability of snow’ and ‘no data available during the dekad’, respectively. In case of MCD43A3 C6, dots represent pixels classified as snow. (For interpretation of the references to colour in this figure legend, the reader is referred to the web version of this article.)

J. Sánchez-Zapero et al.

Remote Sensing of Environment 287 (2023) 113460

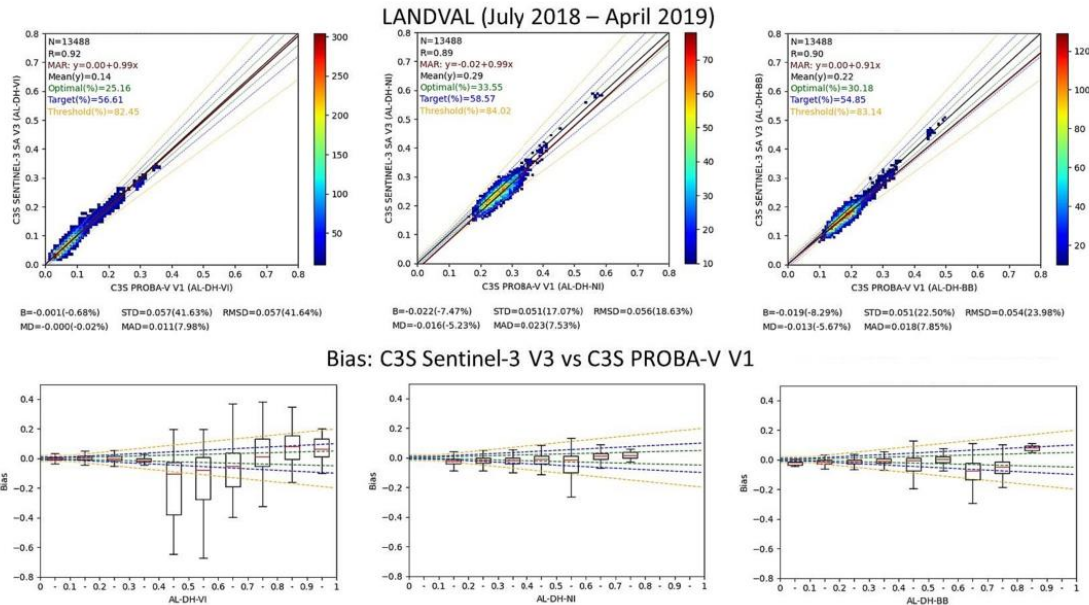


Fig. 6. Top: Scatter-plots (AL-DH-VI, AL-DH-NI, AL-DH-BB) between C3S Sentinel-3 SA v3.0 (average of 3 × 3 pixels) (Y-axis) versus C3S PROBA-V SA v1.0 (one high quality pixel) (X-axis) products from July 2018 to April 2019. Green, blue and orange dashed lines correspond to optimal, target and threshold predefined levels around continuous black 1:1 line. MAR is represented in Red line. Bottom: Box-plots bias per range albedo value. Red bars of boxes display median values, boxes stretch from the 25th to the 75th percentiles of the data and whiskers include 99.3% of the coverage data ($\pm 2.7 \sigma$). Outliers are not displayed. (For interpretation of the references to colour in this figure legend, the reader is referred to the web version of this article.)

Table 11

Performance statistics between C3S Sentinel-3 SA v3.0 versus C3S PROBA-V SA v1.0 products. Computation in July 2018 to April 2019 over LANDVAL.

	C3S Sentinel-3 SA v3.0 versus C3S PROBA-V SA v1.0					
	AL-DH-VI	AL-DH-NI	AL-DH-BB	AL-BH-VI	AL-BH-NI	AL-BH-BB
Correlation	0.92	0.89	0.90	0.92	0.92	0.92
Bias (%)	-0.001 (-0.7%)	-0.022 (-7.5%)	-0.019 (-8.3%)	-0.008 (-5.6%)	-0.013 (-4.0%)	-0.023 (-9.8%)
MD (%)	<-0.001 (0.0%)	-0.016 (-5.2%)	-0.013 (-5.7%)	-0.006 (-4.2%)	-0.009 (-2.8%)	-0.020 (-8.4%)
STD (%)	0.057 (41.6%)	0.051 (17.1%)	0.051 (22.5%)	0.056 (40.7%)	0.044 (13.8%)	0.044 (18.5%)
MAD (%)	0.011 (8.0%)	0.023 (7.5%)	0.018 (7.9%)	0.014 (10.2%)	0.021 (6.7%)	0.023 (9.6%)
RMSD (%)	0.057 (41.6%)	0.056 (18.6%)	0.054 (24.0%)	0.056 (41.1%)	0.046 (14.4%)	0.049 (20.9%)
MAR	y = 0.00 + 0.99x	y = -0.02 + 0.99x	y = 0.00 + 0.91x	y = 0.00 + 0.97x	y = -0.02 + 1.01x	y = -0.01 + 0.95x
%optimal (GCOS)	25.2	33.6	30.2	18.3	37.7	24.0
%target (C3S KPI)	56.6	58.6	55.9	45.5	63.1	48.0

retrievals than both satellite references for most biome types in all spectral broadband ranges, except over EBF biome type, where both C3S products tend show values toward higher values compared with MCD43A3 C6. Note that EBF biome type is typically mainly affected by cloud contamination. Both C3S products also tend to provide slight tendency to high albedo values than MCD43A3 C6 for DBF, NLF, cultivated and herbaceous for the total shortwave.

5.2.4. Analysis over snow

In order to better understand the uncertainties of C3S Sentinel-3 SA v3.0 values over snow targets, they have been compared with reference satellite PROBA-V SA v1.0 (Fig. 9, Table 13) and MCD43A3 C6 (Fig. 10, Table 14) products over pixels classified as snow. The analysis is

performed over LANDVAL sites, and the classification of snow covered pixels was performed using the ‘Snow BRDF Albedo’ flag of MCD43A2 C6 BRDF/albedo quality product.

The comparison with PROBA-V shows negative biases of around -5% for visible domain and large negative bias for NIR and total shortwave (around -25% for BSA and -10%/-14% for WSA). Overall uncertainties (RMSD) from 0.1 up to 0.18 are found depending of spectral domain. Similarly, Sentinel-3 SA v3.0 tends to provide systematically lower values than MCD43A3 C6, with negative biases from -14% (AL-BH-NI) to -35% (AL-DH-BB) and overall uncertainties (RMSD) ranging from 0.1 to 0.2. MCD43A3 albedo has demonstrated overall good quality during the snow-covered periods in previous works (Wang et al., 2012, 2014) with overall RMSD lower than 0.05 and bias

J. Sánchez-Zapero et al.

Remote Sensing of Environment 287 (2023) 113460

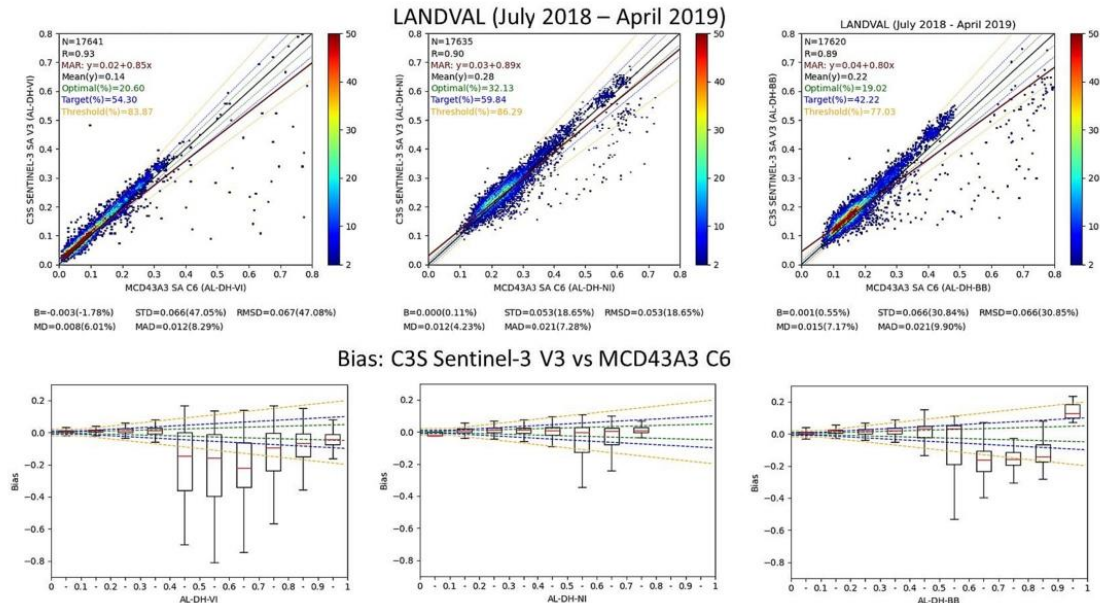


Fig. 7. Top: Scatter-plots (AL-DH-VI, AL-DH-NI, AL-DH-BB) between C3S Sentinel-3 SA v3.0 (average of 3×3 pixels) (Y-axis) versus MCD43A3 C6 (average of 2×2 good quality pixels) (X-axis) products from July 2018 to April 2019. Green, blue and orange dashed lines correspond to optimal, target and threshold predefined levels around continuous black 1:1 line. MAR is represented in Red line. Bottom: Box-plots of bias per range albedo value. Red bars of boxes display median values, boxes stretch from the 25th to the 75th percentiles of the data and whiskers include 99.3% of the coverage data ($\pm 2.7 \sigma$). Outliers are not displayed. (For interpretation of the references to colour in this figure legend, the reader is referred to the web version of this article.)

Table 12 Performance statistics between C3S Sentinel-3 SA v3.0 versus MCD43A3 C6 products. Computation in July 2018 to April 2019 over LANDVAL sites.

	C3S Sentinel-3 SA v3.0 versus MCD43A3 SA C6					
	AL-DH-VI	AL-DH-NI	AL-DH-BB	AL-BH-VI	AL-BH-NI	AL-BH-BB
Correlation	0.93	0.90	0.89	0.94	0.93	0.92
Bias (%)	-0.003 (-1.8%)	<0.001 (0.1%)	0.001 (0.6%)	-0.007 (-5.2%)	0.017 (5.7%)	0.003 (1.3%)
MD (%)	0.008 (6.0%)	0.012 (4.2%)	0.015 (7.2%)	0.002 (1.6%)	0.022 (7.2%)	0.013 (5.7%)
STD (%)	0.066 (47.1%)	0.053 (18.7%)	0.066 (30.8%)	0.063 (44.8%)	0.043 (14.4%)	0.056 (25.2%)
MAD (%)	0.012 (8.3%)	0.021 (7.3%)	0.021 (9.9%)	0.009 (6.1%)	0.026 (8.5%)	0.017 (7.6%)
RMSD (%)	0.067 (47.1%)	0.053 (18.7%)	0.066 (30.9%)	0.064 (45.1%)	0.046 (15.4%)	0.056 (25.3%)
MAR	$y = 0.02 + 0.85x$	$y = 0.03 + 0.89x$	$y = 0.04 + 0.80x$	$y = 0.01 + 0.85x$	$y = 0.04 + 0.92x$	$y = 0.04 + 0.83x$
%optimal (GCOS)	20.6	32.1	19.0	31.6	27.1	28.2
%target (C3S KPI)	54.3	59.8	42.2	66.2	53.2	55.7

close to zero in comparison with ground measurements. Large scattering of values were found for intermediate albedo ranges in Fig. 9 and Fig. 10, as expected, explained in the fact that this is consequence of the sub-pixel heterogeneity (Jin et al., 2003) (i.e., mixed of snow-free with snow covered areas) due to processes such as snowmelt. The different strategy of temporal composites and sampling between the two sensor systems is another reason of these discrepancies and large uncertainties over snow targets are expected for longer spanning composite windows (Wang et al., 2012).

5.3. Error evaluation (direct validation)

Fig. 11 shows the scatter-plots of the validation of satellite datasets

(C3S Sentinel-3 SA v3.0 and PROBA-V SA v1.0, and MCD43A3 C6) compared with measurements from 32 ground stations. The validation metrics are summarized in Table 15. The footprint of ground measurement is homogeneous at 1 km^2 area (see Annex II), and the comparison was performed using the primary resolution of PROBA-V based products, and average of 3×3 and 2×2 windows in case of Sentinel-3 and MODIS based products. Temporal trends of satellite products compared with ground measurements are displayed in Fig. 12 over a selection of different biome types.

Sentinel-3 SA v3.0 provides slightly worse accuracy than MCD43A3 C6, and opposite sign of differences: MD = 6.3% in case of Sentinel-3 SA v3.0, and MD = -3.3% in case of MCD43A3 C6. PROBA-V SA v1.0 provides larger positive systematic differences (MD = 15.8%), in line to that

J. Sánchez-Zapero et al.

Remote Sensing of Environment 287 (2023) 113460

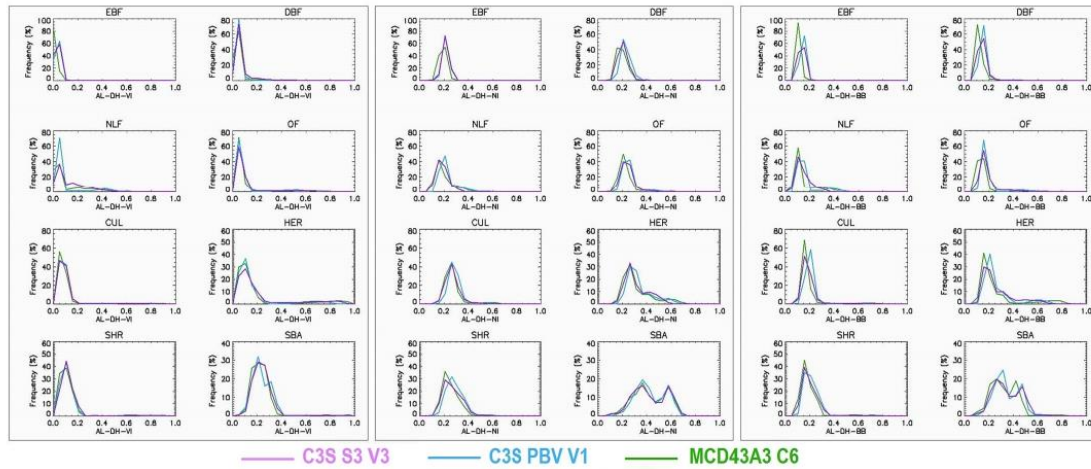


Fig. 8. Distribution of black-sky broadband albedo values for visible (left), NIR (center) and total shortwave (right) per main biome type. Comparison between C3S Sentinel-3 SA v3.0 (purple), C3S PROBA-V SA v1.0 (blue) and MCD43A3 C6 (green) products at 1km² resolution in July 2018 to April 2019 period over LANDVAL sites. (For interpretation of the references to colour in this figure legend, the reader is referred to the web version of this article.)

LANDVAL Snow pixels (July 2018 – April 2019)

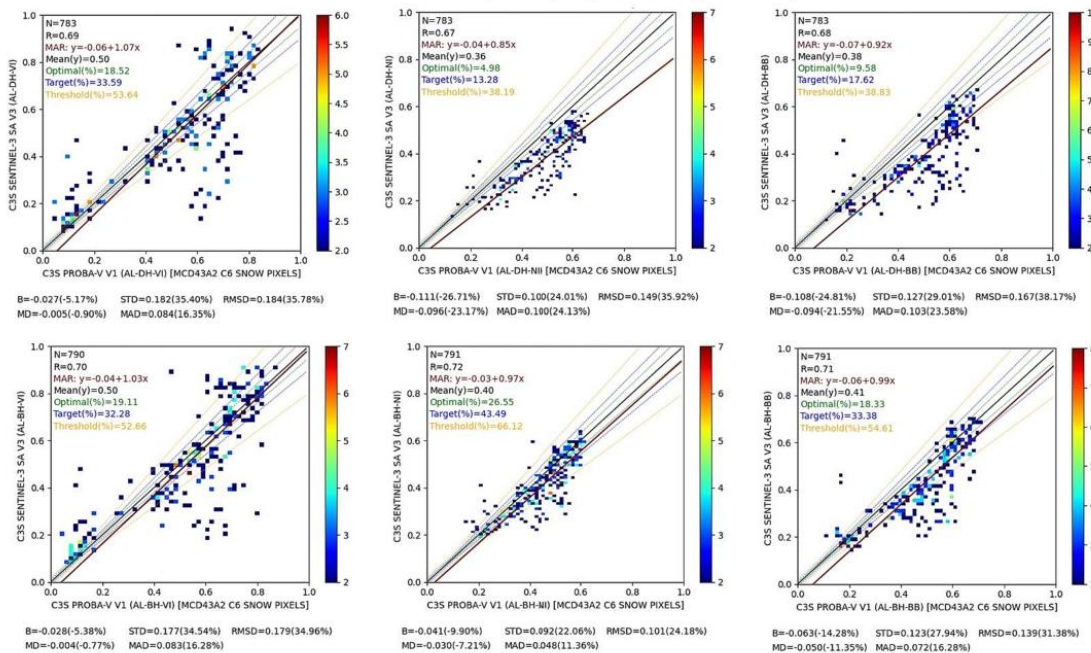


Fig. 9. Scatter-plots (Top: AL-DH-VI, AL-DH-NI, AL-DH-BB; Bottom: AL-DH-VI, AL-DH-NI, AL-DH-BB) between C3S Sentinel-3 SA v3.0 (average of 3 × 3 pixels) (Y-axis) versus C3S PROBA-V SA v1.0 (one high quality pixel) (X-axis) products from July 2018 to April 2019 over LANDVAL pixels classified as snow using MCD43A2 C6 snow flag. Green, blue and orange dashed lines correspond to optimal, target and threshold predefined levels around continuous black 1:1 line. MAR is represented in Red line. (For interpretation of the references to colour in this figure legend, the reader is referred to the web version of this article.)

found in previous exercises (Sánchez-Zapero et al., 2020).

The three satellite products provided similar results in terms of precision (STD, MAD) and overall uncertainty (RMSD). MCD43A3 C6

provided the best precision (MAD = 8.6%) and uncertainty (RMSD = 0.029). Worse agreement was found for PROBA-V SA v1.0 (MAD = 18.1%, RMSD = 0.037), whereas intermediate results were

Table 13
Performance statistics between C3S Sentinel-3 SA v3.0 versus C3S PROBA-V SA v1.0 products. Computation in July 2018 to April 2019 over LANDVAL pixels classified as snow using MCD43A2 C6 snow flag.

	C3S Sentinel-3 SA v3.0 versus C3S PROBA-V SA v1.0 (snow)					
	AL-DH-VI	AL-DH-NI	AL-DH-BB	AL-BH-VI	AL-BH-NI	AL-BH-BB
Correlation	0.69	0.67	0.68	0.70	0.72	0.71
Bias (%)	-0.027 (-5.1%)	-0.111 (-26.7%)	-0.108 (-24.8%)	-0.028 (-5.4%)	-0.041 (-9.9%)	-0.063 (-14.3%)
MD (%)	-0.005 (-0.9%)	-0.096 (-23.2%)	-0.094 (-21.6%)	-0.004 (-0.8%)	-0.030 (-7.2%)	-0.050 (-11.4%)
STD (%)	0.182 (35.4%)	0.100 (24.0%)	0.127 (29.0%)	0.177 (34.5%)	0.092 (22.1%)	0.123 (27.9%)
MAD (%)	0.084 (16.4%)	0.100 (24.1%)	0.103 (23.6%)	0.083 (16.3%)	0.048 (11.4%)	0.072 (16.3%)
RMSD (%)	0.184 (35.8%)	0.149 (35.9%)	0.167 (38.2%)	0.179 (35.0%)	0.101 (24.2%)	0.139 (31.4%)
MAR	$y = -0.06 + 1.07x$	$y = -0.024 + 0.85x$	$y = -0.07 + 0.92x$	$y = -0.04 + 1.03x$	$y = -0.03 + 0.97x$	$y = -0.06 + 0.99x$
%optimal (GCOS)	18.5	5.0	9.6	19.1	26.6	18.3
%target (C3S KPI)	33.6	13.3	17.6	32.3	43.5	33.4

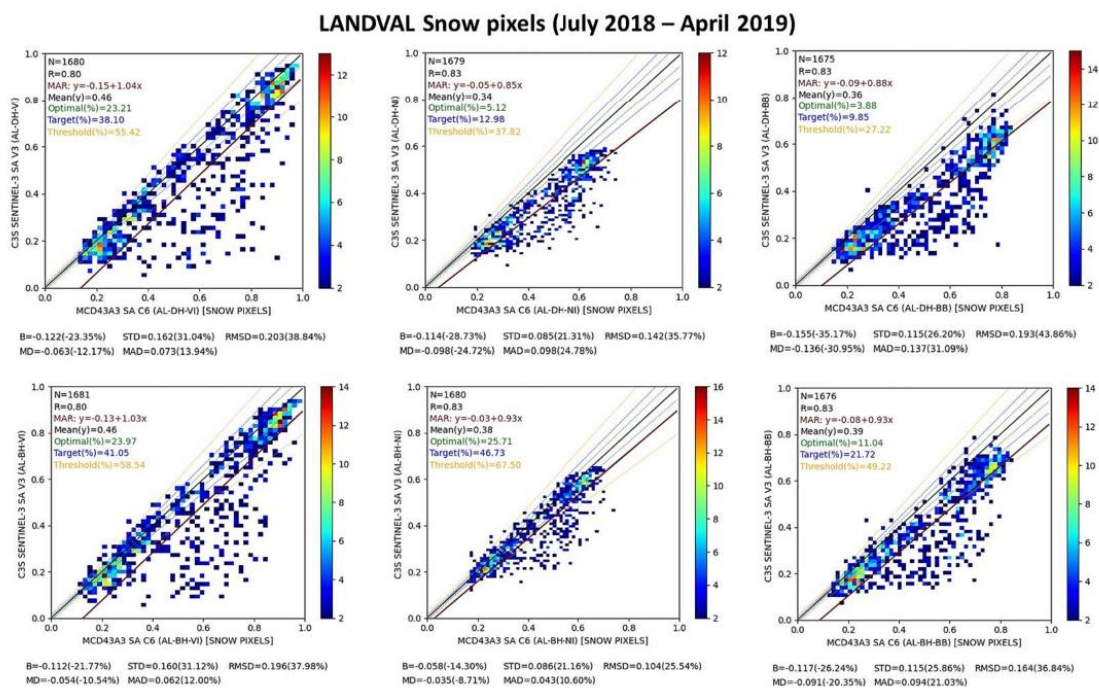


Fig. 10. Scatter-plots (Top: AL-DH-VI, AL-DH-NI, AL-DH-BB; Bottom: AL-DH-VI, AL-DH-NI, AL-DH-BB) between C3S Sentinel-3 SA v3.0 (average of 3 × 3 pixels) versus MCD43A3 C6 (average of 2 × 2 good quality pixels) (X-axis) products from July 2018 to April 2019 over LANDVAL pixels classified as snow using MCD43A2 C6 snow flag. Green, blue and orange dashed lines correspond to optimal, target and threshold predefined levels around continuous black 1:1 line. MAR is represented in Red line. (For interpretation of the references to colour in this figure legend, the reader is referred to the web version of this article.)

found for Sentinel-3 SA v3.0 (MAD = 13.9%, RMSD = 0.033). Overall, the correlation of Sentinel-3 SA v3.0 ($R = 0.61$) with ground values is similar than MCD43A3 C6 ($R = 0.68$) and PROBA-V SA v1.0 ($R = 0.58$). Per biome type, high correlation is found over crops ($R = 0.92$) but low correlations for desert ($R = 0.08$), forests ($R = 0.14$) and grassland/shrublands (0.05) as a consequence of the low variability of albedo values for these biome types. C3S Sentinel-3 SA v3.0 temporal trends, as the rest of satellite products under study, are efficient over stable targets like evergreen forests (e.g., TALL, AU_ASM, AU_RCR, AU_WSE) or shrublands (SRER).

Smooth albedo changes due to seasonality (e.g., NET_CABA grassland and LENO deciduous forest) are also well captured by C3S Sentinel-3 SA v3.0, ditto PROBA-V and MCD43A3 C6. The changes in albedo values due to snow events are generally well captured by C3S Sentinel-3 SA v3.0 (e.g., USA TEAK), however C3S tends to underestimate albedo snow measurements (e.g., USA SFSD). Moreover, for cases where spurious snow events of few days are observed (e.g., KONZ), C3S Sentinel-3 SA v3.0 (as PROBA-V v1.0) is not able to reproduce the snow albedo rapid surges unlike MCD43A3 C6. It is also noticeable that in some cases smooth snow transitions are observed (e.g., USA SFSD)

J. Sánchez-Zapero et al.

Remote Sensing of Environment 287 (2023) 113460

Table 14
Performance statistics between C3S Sentinel-3 SA v3.0 versus MCD43A3 C6 products. Computation in July 2018 to April 2019 over LANDVAL pixels classified as snow using MCD43A2 C6 snow flag.

	C3S Sentinel-3 SA v3.0 versus MCD43A3 SA C6 (snow)					
	AL-DH-VI	AL-DH-NI	AL-DH-BB	AL-BH-VI	AL-BH-NI	AL-BH-BB
Correlation	0.80	0.83	0.83	0.80	0.83	0.83
Bias (%)	-0.122 (-23.4%)	-0.114 (-28.7%)	-0.155 (-35.2%)	-0.112 (-21.8%)	-0.058 (-14.3%)	-0.117 (-26.2%)
MD (%)	-0.063 (-12.7%)	-0.098 (-24.7%)	-0.136 (-31.0%)	-0.054 (-10.5%)	-0.035 (-8.7%)	-0.091 (-20.4%)
STD (%)	0.162 (31.0%)	0.085 (21.3%)	0.115 (26.2%)	0.160 (31.1%)	0.086 (21.2%)	0.115 (25.9%)
MAD (%)	0.073 (13.9%)	0.098 (24.8%)	0.137 (31.1%)	0.062 (12.0%)	0.043 (10.6%)	0.094 (21.0%)
RMSD (%)	0.203 (38.8%)	0.142 (35.8%)	0.193 (43.9%)	0.196 (38.0%)	0.104 (25.5%)	0.164 (36.8%)
MAR	$y = -0.15 + 1.04x$	$y = -0.05 + 0.85x$	$y = -0.09 + 0.88x$	$y = -0.13 + 1.03x$	$y = -0.03 + 0.93x$	$y = -0.08 + 0.93x$
%optimal (GCOS)	20.6	5.1	3.9	24.0	25.7	11.0
%target (C3S KPI)	54.3	13.0	9.9	41.1	46.7	21.7

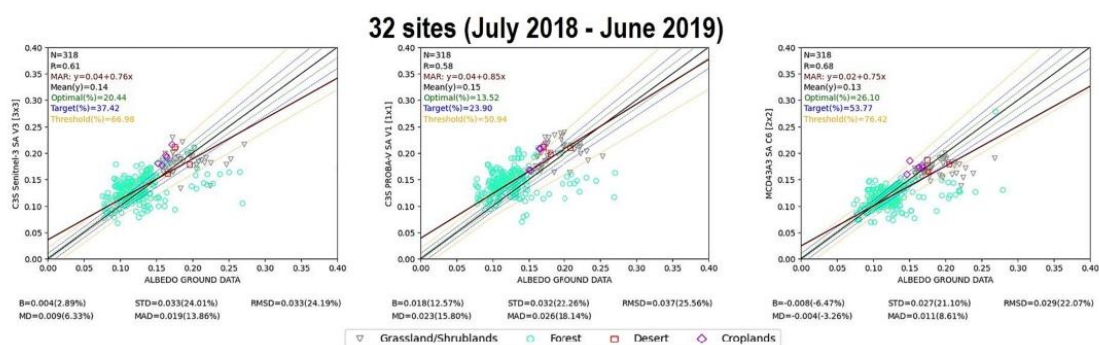


Fig. 11. Direct validation of satellite albedo products (from left to right: C3S Sentinel-3 SA v3.0, C3S PROBA-V SA v1.0, MCD43A3 C6) versus ground values from July 2018 to April 2019 at 1 km² of spatial resolution. Green, blue and orange dashed lines correspond to optimal (GCOS), target (C3S KP) and threshold predefined uncertainty levels around continuous black 1:1 line. MAR is represented in Red line. (For interpretation of the references to colour in this figure legend, the reader is referred to the web version of this article.)

Table 15
Direct validation relevant statistics of satellite albedo products (C3S Sentinel-3 SA v3.0, C3S PROBA-V SA v1.0 and MCD43A3 C6) products versus albedo ground values at 1 km² of spatial resolution during the July 2018–April 2019 period.

	C3S S-3 SA v3.0	C3S PBV SA v1.0	MCD43A3 C6
Stations (N)	33 (318)		
Correlation	0.61	0.58	0.68
Bias	0.004 (2.9%)	0.018 (12.6%)	-0.008 (-6.5%)
MD	0.009 (6.3%)	0.023 (15.8%)	-0.004 (-3.3%)
STD	0.033 (24.0%)	0.032 (22.3%)	0.027 (21.1%)
MAD	0.019 (13.9%)	0.026 (18.1%)	0.011 (8.6%)
RMSD	0.033 (24.2%)	0.037 (25.6%)	0.029 (22.1%)
Offset (MAR)	0.04	0.04	0.02
Slope (MAR)	0.76	0.85	0.75
%optimal (GCOS)	20.4	13.5	26.1
%target (C3S KPI)	37.4	23.9	53.8

whereas rapid transitions are observed in ground and MODIS albedo values. The main explanation for that is the lack of input data over snow which triggers the use of the prior (climatology) over some snow events.

It is important to note that only the satellite retrievals classified as the best quality, according to QFLAGS (Table 3), were used in the direct validation. As observed in the temporal consistency (Fig. 12), the use of QFLAGS removes most of the valid snow retrievals in the case of

Sentinel-3. Then, this exercise is almost equivalent to snow-free conditions.

6. Summary and conclusions

The Climate Change Service of Copernicus undertook an initiative with aim to provide operational global estimates of the surface albedo based on Sentinel-3 OLCI and SLSTR observations, which is implemented in the C3S Sentinel-3 SA v3.0 prototype. The SA C3S existing CDR continuity is ensured thanks to the switch to Surface Albedo v3.0 algorithm. In the past, C3S CDR is based on NOAA/AVHRR (September 1981–2005), SPOT/VGT (April 1998–May 2014) and PROBA-V (November 2013 – June 2020). C3S Sentinel-3 also provides improved spatial resolution (300m versus 1km and 4km for Vegetation and AHVRR sensors) and richer spectral information (nine spectral albedos versus four) compared to previous datasets. The SA v3.0 responds to the GCOS requirement for an improved spatial resolution (200/500m) of satellite-based EO products.

The quality assessment is performed over a limited demonstration test dataset covering 10 months (from July 2018 to April 2019). The validation is performed considering global conditions, expanding the spatial and temporal coverage of the quality assessment of initial developments of the prototype (Sanchez-Zapero et al., 2021). This preliminary scientific evaluation demonstrated that C3S Sentinel-3 SA v3.0 pre-operational product is good enough to guarantee continuation of

J. Sánchez-Zapero et al.

Remote Sensing of Environment 287 (2023) 113460

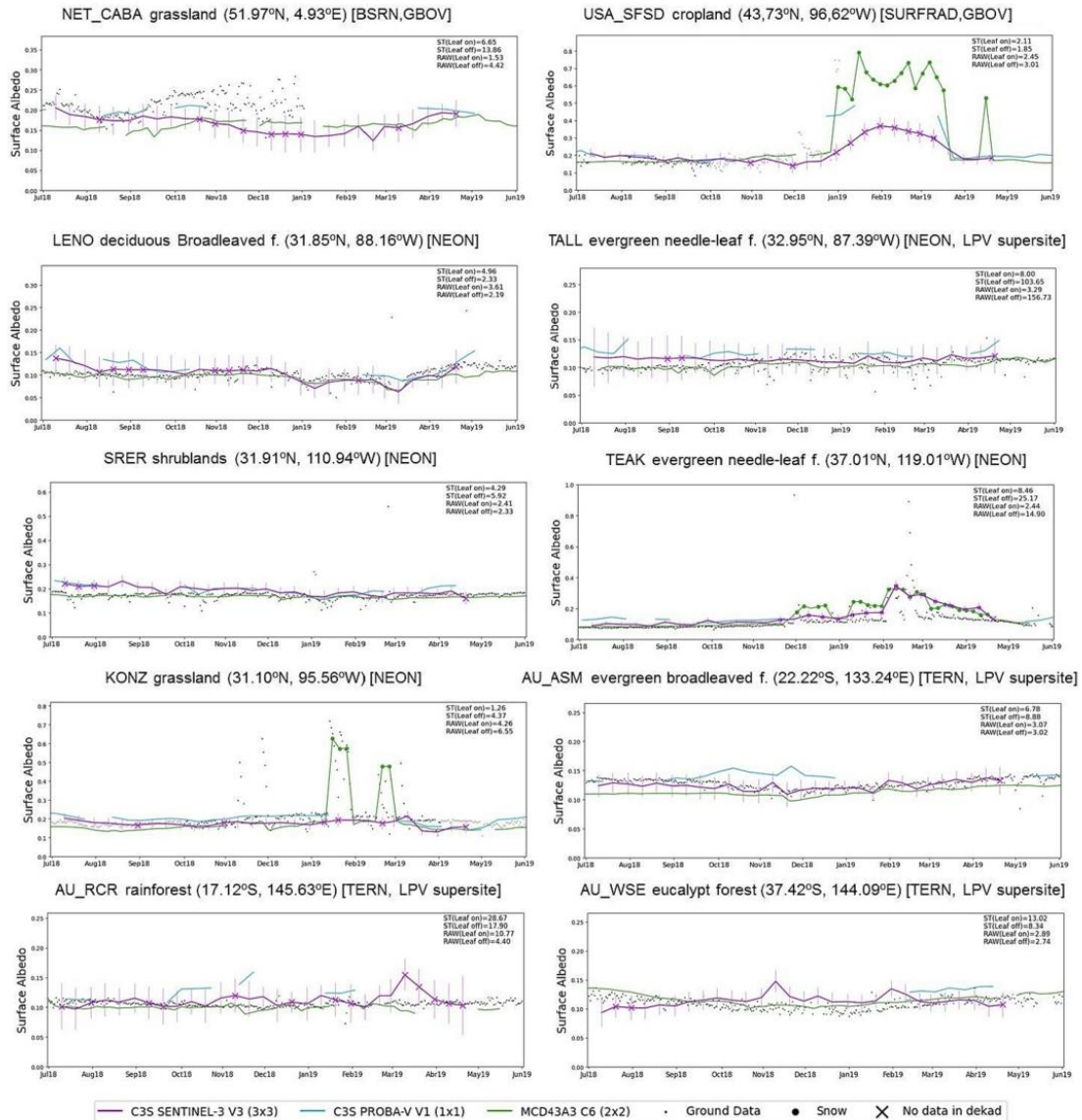


Fig. 12. Temporal profiles of C3S Sentinel-3 SA v3.0 (purple), C3S PROBA-V SA v1.0 (blue) and MCD43A3 C6 (green) for July2018-June2019 period over a selection of sites with availability of ground-based tower measurements (see black dots). ST and RAW scores, indicative of spatial representativeness, are displayed for each station. For Sentinel-3 SA v3.0, dots and crosses represent pixels identified with 'probability of snow' and 'no data available during the dekad', respectively. In case of MCD43A3 C6, dots represent pixels classified as snow. (For interpretation of the references to colour in this figure legend, the reader is referred to the web version of this article.)

PROBA-V time series, as it shows good overall consistency with other products and similar performance against in-situ observations. Time and space good agreements are noticed between C3S Sentinel-3 SA v3.0 and reference satellite datasets (C3S PROBA-V SA v1.0, MCD43A3 C6), with overall discrepancies (RMSD) of around 0.05. The comparison with ground data shows similar accuracy than MCD43A3 C6 but opposite sign of differences (slight positive in case of Sentinel-3), improving the accuracy of C3S products based on PROBA-V.

The main drawbacks are the underestimation of snow albedo values, the slow transition from snow-free to snow albedo values and the limited capability to reproduce spurious snow events. This is mainly explained due to the current limitation related to input data from the ESA Sentinel-3 mission. In particular IdePix processor, used in the CGLS pre-processing chain does not provide a correct identification of snow pixels. For that, Surface Albedo v3.0 algorithm incorporated and alternative decision rule in the prototype based on NDSI index, that was able

J. Sánchez-Zapero et al.

Remote Sensing of Environment 287 (2023) 113460

to identify large quantity of snow cases, but providing underestimation of snow albedo values (–14% to –35% compared to MCD43A3 C6). The consequence is the low quantity of good quality observations (based on IdePix) ingested as input data in the BRDF retrieval. The algorithm can deal with low availability of input data due to the use of BRDF prior information based on MODIS BRDF climatology. Another factor that could contribute to low accuracy over snow cases is the impact of topography, that complicates the modeling and land surface albedo retrieval due to shadow effects and the redistribution of incident radiation (Hao et al., 2018; Schaaf et al., 1994). Therefore, users dealing with cryosphere or hydrosphere applications (e.g., freezing/thaw, snowfall, snow water equivalent estimations or flood hazards) should use with caution the current version of C3S Sentinel-3 SA v3.0.

Additionally, vicarious TOA SLSTR calibration coefficients (S3_MPC, 2021b) were not used in the CGLS pre-processing chain to correct the systematic negative bias (mainly observed in S5 and S6 channels). We applied these calibration coefficients directly to spectral albedos, and corrected the bias compared with MCD43A3 C6 in >10 points in relative terms.

The shortcomings of the product (cloud/snow identification and calibration coefficients) can be overcome with future improved input data, which would justify the reprocessing of a new version. The current phase of C3S land satellite-based ECVs includes two main activities: i) the switch to new version (v2) of surface reflectances input dataset from CGLS using an evolution of IdePix; and ii) the full quality assessment evaluation of the products over an extended temporal coverage. The new input dataset will include two main improvements, a better cloud detection and snow identification due to use of new IdePix version and the application of the TOA SLSTR calibration coefficients. We expect that main issues related to snow albedo values will be partly solved with the switch to surface reflectances v2 in 2023. The data can be accessed through the CDS using this link: <https://cds.climate.copernicus.eu/cdsapp#!/dataset/satellite-albedo?tab=overview>

CRedit authorship contribution statement

Jorge Sánchez-Zapero: Conceptualization, Methodology, Validation, Software, Formal analysis, Writing – original draft. **Fernando Camacho:** Conceptualization, Supervision, Formal analysis, Writing – review & editing. **Enrique Martínez-Sánchez:** Validation, Software, Writing – review & editing. **Javier Gorroño:** Methodology, Writing – review & editing. **Jonathan León-Tavares:** Methodology, Writing – review & editing. **Iskander Benhadj:** Supervision, Project administration, Writing – review & editing. **Carolien Toté:** Writing – review & editing. **Else Swinnen:** Writing – review & editing. **Joaquín Muñoz-Sabater:** Funding acquisition, Project administration, Writing – review & editing.

Declaration of Competing Interest

The authors declare that they have no known competing financial interests or personal relationships that could have appeared to influence the work reported in this paper.

Data availability

C3S S-3 SA product is available in C3S climate data store (<https://cds.climate.copernicus.eu/#/home>). Data and documentation are available in C3S albedo ECV page: <https://cds.climate.copernicus.eu/cdsapp#!/dataset/satellite-albedo?tab=overview>

Acknowledgements

This work was developed in the framework of the Copernicus Climate Change Service (COP_059 contract). The Sentinel-3 Surface Albedo v3.0 algorithm was developed by EOLAB and the product is a data set produced by VITO. The product is based on Sentinel-3 surface reflectances, which are provided by Copernicus Global Land Service.

Annex I. Main characteristics of the 58 evaluated ground stations with availability of data during the 2018–2019 period

#	Site ID	Name	Country	Network	Land Cover	Lat	Lon
1	USA_BOND	Bondville	USA	SURFRAD	Croplands	40.052	–88.373
2	BEL_BRAD	Brasschaat	Belgium	GBOV/ICOS CEOS LPV SuperSite	Mixed Forest	51.309	4.521
3	NET_CABS	Cabauw	Netherlands	BSRN	Grasslands	51.971	4.927
4	AUS_CPRM	Calperum	Australia	GBOV/ICOS CEOS LPV SuperSite	Shrublands	–34.003	140.588
5	USA_DRK	Desert Rock	USA	GBOV	Bare Soil	36.624	–116.019
6	USA_FPRK	Fort Peck	USA	GBOV	Grasslands	48.308	–105.102
7	NAM_GOBA	Gobabeb	Namibia	GBOV/ICOS CEOS LPV SuperSite	Bare Soil	–23.561	15.042
8	USA_GCMK	Goodwin Creek	USA	GBOV	Deciduous Broadleaf	34.255	–89.873
9	FRA_GRIG	Grignon	France	GBOV	Croplands	48.844	1.952
10	FRA_GUYA	Guyanaflux	French Guyana	GBOV/ICOS CEOS LPV SuperSite	Evergreen Broadleaf	5.279	–52.925
11	GER_HAIN	Hainich	Germany	GBOV/ICOS CEOS LPV SuperSite	Mixed Forest	51.070	10.450
12	USA_NRFT	Niwot Ridge	USA	GBOV	Evergreen Needleleaf	40.033	–105.546
13	USA_PSSUS	Rock Springs	USA	GBOV	Deciduous Broadleaf	40.720	–77.931
14	USA_SFS	Sioux Falls	USA	SURFRAD	Croplands	43.730	–96.620
15	USA_SGP	Southern Great Plains	USA	GBOV	Croplands	36.606	–97.489
16	USA_TBLN	Table Mountain	USA	GBOV	Bare soil and Rocks	40.125	–105.237
17	AUS_TUMB	Tumbarumba	Australia	GBOV/ICOS CEOS LPV SuperSite	Evergreen Broadleaf	–35.657	148.152
18	LENO	Lenoir Landing	USA	NEON	Deciduous Broadleaf	31.854	–88.161
19	TALL	Talladega National Forest	USA	NEON/ICOS CEOS LPV SuperSite	Needle-Leaf	32.950	–87.393
20	BONA	Caribou-Poker	USA	NEON	Needle-Leaf	65.154	–147.503
21	DEJU	Delta Junction	USA	NEON	Needle-Leaf	63.881	–145.751
22	HEAL	Healy	USA	NEON	Shrublands	63.876	–149.213
23	TOOL	Toolik	USA	NEON	Shrublands	68.66109	–149.37047
24	SRER	Santa Rita Experimental Range	USA	NEON	Shrublands	31.911	–110.835
25	SOAP	Soaproot Saddle	USA	NEON	Needle-Leaf	37.033	–119.262
26	TEAK	Lower Teakettle	USA	NEON	Needle-Leaf	37.006	–119.006
27	CPER	Central Plains Experimental Range	USA	NEON/ICOS CEOS LPV SuperSite	Grasslands	40.816	–104.746
28	NIWO	Niwot Ridge Mountain Research Station	USA	NEON	Needle-Leaf	40.054	–105.582
29	STER	Sterling	USA	NEON	Croplands	40.462	–103.029
30	DSNY	Disney Wilderness Preserve	USA	NEON	Croplands	28.125	–81.436

(continued on next page)

J. Sánchez-Zapero et al.

Remote Sensing of Environment 287 (2023) 113460

(continued)

#	Site ID	Name	Country	Network	Land Cover	Lat	Lon
31	OSBS	Ordway-Swisher Biological Station	USA	NEON/ICOS CEOS LPV SuperSite	Needle-Leaf	29.689	-81.993
32	JERC	Jones Ecological Research Center	USA	NEON	Needle-Leaf	31.195	-84.469
33	KONA	Konza Prairie Biological Station – Relocatable	USA	NEON	Grasslands	39.110	-96.613
34	KONZ	Konza Prairie Biological Station	USA	NEON	Grasslands	39.10077	-96.56309
35	HARV	Harvard Forest	USA	NEON/ICOS CEOS LPV SuperSite	Deciduous Broadleaf	42.537	-72.173
36	BART	Barlett Experimental Forest	USA	NEON	Deciduous Broadleaf	44.064	-71.287
37	GUAN	Guanica Forest	USA	NEON/ICOS CEOS LPV SuperSite	Evergreen Broadleaf	17.970	-66.869
38	ORNL	Oak Ridge	USA	NEON/ICOS CEOS LPV SuperSite	Deciduous Broadleaf	35.964	-84.28
39	MOAB	Moab	USA	NEON/ICOS SuperSite	Shrublands	38.248	-109.388
40	MLBS	Mountain Lake Biological Station	USA	NEON/ICOS CEOS LPV SuperSite	Deciduous Broadleaf	37.378	-80.525
41	SCBI	Smithsonian Conservatory Biology Institute	USA	NEON/ICOS CEOS LPV SuperSite	Deciduous Broadleaf	38.893	-78.140
42	STEI	Steigerwaldt Land Services	USA	NEON/ICOS CEOS LPV SuperSite	Deciduous Broadleaf	45.509	-89.586
43	DE-HoH	Hohes Holz	Germany	ICOS/ICOS CEOS LPV SuperSite	Deciduous Broadleaf	52.087	11.222
44	SE-Svb	Svartberget	Sweden	ICOS/ICOS CEOS LPV SuperSite	Needle-Leaf	64.256	19.775
45	FI-Hyy	Hyytiälä	Finland	ICOS/ICOS CEOS LPV SuperSite	Needle-Leaf	61.847	24.295
46	DE-RuS	Selhausen Juelich	Germany	ICOS/ICOS CEOS LPV SuperSite	Croplands	50.866	6.447
47	AU_ASM*	Alice Spring Meller	Australia	TERN/ICOS CEOS LPV SuperSite	Forest	-22.283	133.249
48	AU_BOY*	Boyanginj Wandoo Woodland	Australia	TERN/ICOS CEOS LPV SuperSite	Forest	-32.477	116.939
49	AU_Cum*	Cumberland Plain	Australia	TERN/ICOS CEOS LPV SuperSite	Forest	-33.615	150.724
50	AU_DRP*	Deintree Rainforest	Australia	TERN/ICOS CEOS LPV SuperSite	Forest	-16.238	145.427
51	AU_Gin*	Gingin Banksia Woodland	Australia	TERN/ICOS CEOS LPV SuperSite	Forest	-31.376	115.713
52	AU_GWW*	Great Western Woodlands	Australia	TERN/ICOS CEOS LPV SuperSite	Forest	-30.191	120.654
53	AU_LIS*	Litchfield Savanna	Australia	TERN/ICOS CEOS LPV SuperSite	Forest	-13.179	130.795
54	AU_RCR*	Robson Creek Rainforest	Australia	TERN/ICOS CEOS LPV SuperSite	Forest	-17.117	145.630
55	AU_SPU*	Samford Peri-Urban	Australia	TERN/ICOS CEOS LPV SuperSite	Forest	-27.388	152.878
56	AU_Wrr*	Warra Tall Eucalypt	Australia	TERN/ICOS CEOS LPV SuperSite	Forest	-43.095	146.655
57	AU_WSE*	Wombat Stringbark Eucalypt	Australia	TERN/ICOS CEOS LPV SuperSite	Forest	-37.422	144.094
58	AU_WDE*	Whroo Dry Eucalypt	Australia	TERN/ICOS CEOS LPV SuperSite	Forest	-36.673	145.029

* sites where diffuse fraction was not available for the period under study.

Annex II. Geostatistical information of the selected sites at 1 km resolution

Note: R_{CV} , R_{SE} , R_{ST} and R_{SV} stand for relative coefficient of variation, scale requirement index, relative strength of the spatial correlation and relative proportion of structural variation. ST_{SCORE} and RAW_{SCORE} represent standard and first order scores for the spatial representativeness. Footprint is calculated as 'footprint = 2Htan (FOV)' (Román et al., 2009), where H is the height of the field albedometer.

#	Site ID	Footprint(m) /tower height (m)	Seasonal Period	R_{CV} (%)	R_{SE} (%)	R_{ST} (%)	R_{CV} (%)	ST_{SCORE}	RAW_{SCORE}
2	BEL_BRAS	505 / 40	Leaf-off	11.81	0.01	0.29	-3.38	19.36	4.23
			Leaf-on	11.99	0.06	-0.58	-16.03	10.42	4.17
3	NET_CABA	580.9 / 46	Leaf-off	11.31	0.20	-2.61	7.13	13.86	4.42
			Leaf-on	32.62	0.01	0.74	11.70	6.65	1.53
4	USA_CPRM	253 / 20	Leaf-off	-5.83	31.92	4.15	-4.62	2.72	8.58
			Leaf-on	-11.07	29.70	2.53	-3.13	2.83	4.52
12	USA_NRFT	322 / 26	Leaf-off*	-	-	-	-	-	-
			Leaf-on	-2.63	21.72	-3.30	2.81	4.06	19.03
13	USA_PSUS	126 / 10	Leaf-off	81.60	27.49	11.72	113.98	1.04	0.61
			Leaf-on	1.57	24.88	2.89	-22.24	2.96	31.82
14	USA_SFSD	126 / 10	Leaf-off	-16.59	40.51	-0.95	23.19	1.85	3.01
			Leaf-on	-20.44	35.53	1.82	13.35	2.11	2.45
16	USA_TBLN	126 / 10	1-Season	-22.36	79.12	NaN	13.11	NaN	2.24
17	AUS_TUMB	884 / 70	1-Season	18.41	0.00	0.01	7.27	11.6539	2.7152
18	LENO	593 / 47	Leaf-off	22.88	0.95	6.82	96.36	2.33	2.19
			Leaf-on	-13.85	12.95	0.14	-7.65	4.96	3.61
19	TALL	442 / 35	Leaf-off	-0.32	0.02	-2.30	-0.22	103.65	156.73
			Leaf-on	15.21	0.31	-0.22	21.13	8.00	3.29
20	BONA	240 / 19	Leaf-off*	-	-	-	-	-	-
			Leaf-on	16.61	21.70	2.05	24.31	2.78	3.01
21	DEJU	278 / 22	Leaf-off*	-	-	-	-	-	-
			Leaf-on	4.96	15.05	-1.17	28.27	3.77	10.07
24	SRER	101 / 8	Leaf-off	21.43	9.26	1.47	-0.02	5.92	2.33
			Leaf-on	20.72	14.20	1.87	4.77	4.29	2.41
25	SOAP	404 / 32	Leaf-off	-11.18	0.00	-0.90	-3.32	19.48	4.47
			Leaf-on	-15.21	0.15	-2.50	-1.17	10.58	3.29
26	TEAK	745 / 59	Leaf-off	-3.35	0.00	-0.96	-7.64	25.17	14.90
			Leaf-on	-20.48	0.00	6.85	-8.13	8.46	2.44
32	JERC	530 / 42	Leaf-off	7.01	0.00	4.74	11.34	12.99	7.13
			Leaf-on	6.82	0.04	10.21	44.92	4.83	7.33
34	KONZ	101 / 8	Leaf-off	7.63	17.19	0.37	9.14	4.37	6.55
			Leaf-on	-11.73	69.09	4.85	-14.35	1.26	4.26

(continued on next page)

J. Sánchez-Zapero et al.

Remote Sensing of Environment 287 (2023) 113460

(continued)

#	Site ID	Footprint(m) /tower height (m)	Seasonal Period	R _{CV} (%)	R _{SE} (%)	R _{ST} (%)	R _{CV} (%)	ST _{SCORE}	RAW _{SCORE}
35	HARV	492 / 39	Leaf-off	0.59	0.00	3.41	-3.50	40.01	84.78
			Leaf-on	-12.45	2.82	3.29	23.25	6.32	4.02
36	BART	442 / 35	Leaf-off	10.23	0.00	8.58	27.31	6.50	4.89
			Leaf-on	28.10	0.27	0.36	69.25	3.04	1.78
37	GUAN	290 / 23	1-Season	10.84	0.95	4.87	12.22	9.7502	4.611
38	ORNL	492 / 39	Leaf-off	16.77	0.09	0.48	-5.35	13.12	2.98
			Leaf-on	91.14	0.03	6.68	107.14	1.46	0.55
40	MLBS	366 / 29	Leaf-off	-9.88	0.03	0.14	30.37	7.41	5.06
			Leaf-on	13.81	3.61	1.70	167.03	1.55	3.62
41	SCBI	657 / 52	Leaf-off	61.67	0.00	1.66	56.04	2.51	0.81
			Leaf-on	14.73	0.00	0.74	6.17	13.86	3.39
42	STEI	278 / 22	Leaf-off	10.92	0.09	6.13	29.27	6.44	4.58
			Leaf-on	47.38	0.96	14.20	98.54	1.84	1.06
43	DE-HoH	631 / 50	Leaf-off	23.67	0.10	-0.36	18.84	6.95	2.11
			Leaf-on	-7.43	5.24	-4.59	-29.11	5.28	6.73
47	AU_ASM	146 / 12	Leaf-off	-16.55	2.35	4.84	-5.35	8.88	3.02
			Leaf-on	-16.27	4.58	-4.58	-9.66	6.78	3.07
49	AU_Cum	379 / 30	Leaf-off	20.11	0.07	5.31	22.96	6.18	2.49
			Leaf-on	109.66	4.68	3.43	160.25	1.04	0.46
50	AU_DRF	442 / 35	Leaf-off	14.79	0.03	-3.95	3.96	13.17	3.38
			Leaf-on	18.93	0.00	8.12	39.16	4.53	2.64
53	AU_Lis	505 / 40	Leaf-off	-0.07	0.00	2.14	6.42	34.74	667.25
			Leaf-on	0.74	4.30	-6.45	19.08	7.66	67.63
54	AU_RCR	505 / 40	Leaf-off	11.37	0.00	-0.05	5.34	17.90	4.40
			Leaf-on	4.64	0.00	1.27	4.56	28.67	10.77
56	AU_Wrr	1010 / 80	Leaf-off	-2.75	0.00	9.07	67.96	3.76	18.16
			Leaf-on	13.28	0.00	5.60	72.04	3.30	3.77
57	AU_WSE	379 / 30	Leaf-off	18.23	0.00	6.75	11.00	8.34	2.74
			Leaf-on	17.28	0.00	1.37	4.39	13.02	2.89

* Not clear high resolution images were found to evaluate representativeness in the period.

References

- Amut, A., Gong, L., Yuan, Z., 2007. Spatial distributions of surface albedo from satellite data in arid oasis, pp. 550–555. <https://doi.org/10.1117/12.746119>, 6679.
- Bacour, C., Jacquemoud, S., Tourbier, Y., Dechambre, M., Frangi, J.P., 2002. Design and analysis of numerical experiments to compare four canopy reflectance models. *Remote Sens. Environ.* 79, 72–83. [https://doi.org/10.1016/S0034-4257\(01\)00240-1](https://doi.org/10.1016/S0034-4257(01)00240-1).
- Baret, F., Weiss, M., Lacaze, R., Camacho, F., Makhmara, H., Pacholczyk, P., Smets, B., 2013. GEOV1: LAI and FAPAR essential climate variables and FCOVER global time series capitalizing over existing products. Part I: principles of development and production. *Remote Sens. Environ.* 137, 299–309. <https://doi.org/10.1016/j.rse.2012.12.027>.
- Barnsley, M.J., Strahler, A.H., Morris, K.P., Muller, J.P., 1994. Sampling the surface bidirectional reflectance distribution function (BRDF): 1. Evaluation of current and future satellite sensors. *Remote Sens. Rev.* 8, 271–311. <https://doi.org/10.1080/02757259409532205>.
- Bartholome, E., Belward, A., 2005. GLC2000: a new approach to global land cover mapping from earth observation data. *Int. J. Remote Sens.* 26, 1959–1977. <https://doi.org/10.1080/01431160412331291297>.
- Betts, A.K., 2009. Land-surface-atmosphere coupling in observations and models. *J. Adv. Model. Earth Syst.* 1, n/a/n/a. <https://doi.org/10.3894/JAMES.2009.1.4>.
- Breon, F.-M., Maignan, F., 2017. A BRDF-BPDF database for the analysis of Earth target reflectances. *Earth Syst. Sci. Data* 9, 31–45. <https://doi.org/10.5194/essd-9-31-2017>.
- Bréon, F.-M., Vermote, E., 2012. Correction of MODIS surface reflectance time series for BRDF effects. *Remote Sens. Environ.* 125, 1–9. <https://doi.org/10.1016/j.rse.2012.06.025>.
- Campagnolo, M.L., Montano, E.L., 2014. Estimation of effective resolution for daily modis gridded surface reflectance products. *IEEE Trans. Geosci. Remote Sens.* 52, 5622–5632. <https://doi.org/10.1109/TGRS.2013.2291496>.
- Carrer, D., Ceamanos, X., Pinault, F., Benhadj, I., Toté, C., 2019. Algorithm Theoretical Basis Document (ATBD) of PROBA-V CDR and ICDR Surface Albedo v1.0 (Official reference number service contract: 2018/C3S_312b_Lot5_VITO/SCI). [WWW Document]. Tech. Rep. Prep. Copernicus Clim. Chang. Serv. URL (accessed 5.2.22). https://datastore.copernicus-climate.eu/documents/satellite-albedo/D1.3.3-v1.0_ATBD_CDR-ICDR_SA_PROBAV_v1.0_PRODUCTS_v1.0.2.pdf.
- Carrer, D., Pinault, F., Lellouche, G., Trigo, I.F., Benhadj, I., Camacho, F., Ceamanos, X., Moparth, S., Muñoz-Sabater, J., Schüller, L., Sánchez-Zapero, J., 2021. Surface albedo retrieval from 40-years of Earth observations through the EUMETSAT/LSA SAF and EU/C3S programmes: the versatile algorithm of PYALUS. *Remote Sens.* 13, 372. <https://doi.org/10.3390/rs13030372>.
- Carrer, D., Roujean, J.L., Meurey, C., 2010. Comparing operational MSG/SEVIRI land surface albedo products from land SAF with ground measurements and MODIS. *IEEE Trans. Geosci. Remote Sens.* 48, 1714–1728. <https://doi.org/10.1109/TGRS.2009.2034530>.
- Cescatti, A., Marcolla, B., Santhana Vannan, S.K., Pan, J.Y., Román, M.O., Yang, X., Clais, P., Cook, R.B., Law, B.E., Matteucci, G., Migliavacca, M., Moors, E., Richardson, A.D., Seufert, G., Schaaf, C.B., 2012. Intercomparison of MODIS albedo retrievals and in situ measurements across the global FLUXNET network. *Remote Sens. Environ.* 121, 323–334. <https://doi.org/10.1016/j.rse.2012.02.019>.
- Claverie, M., Vermote, E., Franch, B., He, T., Hagolle, O., Kadiri, M., Masek, J., 2015. Evaluation of medium spatial resolution BRDF-adjustment techniques using multi-angular SPOT4 (Take5) acquisitions. *Remote Sens.* 7, 12057–12075. <https://doi.org/10.3390/rs70912057>.
- Dickinson, R.E., 1995. Land processes in climate models. *Remote Sens. Environ.* 51, 27–38. [https://doi.org/10.1016/0034-4257\(94\)00062-R](https://doi.org/10.1016/0034-4257(94)00062-R).
- Diner, D.J., Beckert, J.C., Reilly, T.H., Bruegge, C.J., Conel, J.E., Kahn, R.A., Martonchik, J.V., Ackerman, T.P., Davies, R., Gerst, S.A.W., Gordon, H.R., Muller, J.P., Myneni, R.B., Sellers, P.J., Pinty, B., Verstraete, M.M., 1998. Multi-angle imaging spectroradiometer (MISR) instrument description and experiment overview. *IEEE Trans. Geosci. Remote Sens.* 36, 1072–1087. <https://doi.org/10.1109/36.700992>.
- Diner, D.J., Martonchik, J.V., Borel, C., Gerst, S.A.W., Gordon, H.R., Knyazikhin, Y., Myneni, R., Pinty, B., Verstraete, M.M., 2008. Level 2 surface retrieval algorithm theoretical basis level 2 surface retrieval algorithm theoretical basis approval.
- Doxani, G., Vermote, E., Roger, J.-C., Gascon, F., Adriaensens, S., Frantz, D., Hagolle, O., Hollstein, A., Kirches, G., Li, F., Louis, J., Mangin, A., Pahlevan, N., Pflug, B., Vanhellemont, Q., 2018. Atmospheric correction inter-comparison exercise. *Remote Sens.* 10, 352. <https://doi.org/10.3390/rs10020352>.
- Franch, B., Vermote, E.F., Sobrino, J.A., Julien, Y., 2014. Retrieval of surface albedo on a daily basis: application to MODIS data. *IEEE Trans. Geosci. Remote Sens.* 52 <https://doi.org/10.1109/TGRS.2014.2313842>.
- Fuster, B., Sánchez-Zapero, J., Camacho, F., García-Santos, V., Verger, A., Lacaze, R., Weiss, M., Baret, F., Smets, B., 2020. Quality assessment of PROBA-V LAI, FAPAR and FCOVER collection 300 m products of copernicus global land service. *Remote Sens.* 12, 1017. <https://doi.org/10.3390/rs12061017>.
- GCOS-154, 2011. Systematic observation requirements for satellite-based data products for climate. Supplemental details to the satellite-based component of the "Implementation Plan for the GCOS in Support of the UNFCCC" [WWW Document]. URL (accessed 4.10.22). https://library.wmo.int/doc_num.php?explnum_id=3710.
- GCOS-200, 2016. Space agency response to GCOS implementation plan [WWW Document] accessed 5.2.22. <https://gcos.wmo.int/en/gcos-implementation-plan>.
- Geiger, B., Carrer, D., Franchistéguy, L., Roujean, J.L., Meurey, C., 2008. Land surface albedo derived on a daily basis from meteosat second generation observations. *IEEE Trans. Geosci. Remote Sens.* 46, 3841–3856. <https://doi.org/10.1109/TGRS.2008.2001798>.
- Govaerts, Y.M., Lattanzio, A., Taberner, M., Pinty, B., 2008. Generating global surface albedo products from multiple geostationary satellites. *Remote Sens. Environ.* 112, 2804–2816. <https://doi.org/10.1016/j.rse.2008.01.012>.

J. Sánchez-Zapero et al.

Remote Sensing of Environment 287 (2023) 113460

- Gueymard, C.A., Lara-Fanego, V., Sengupta, M., Xie, Y., 2019. Surface albedo and reflectance: review of definitions, angular and spectral effects, and intercomparison of major data sources in support of advanced solar irradiance modeling over the Americas. *Sol. Energy*. <https://doi.org/10.1016/j.solener.2019.02.040>.
- Hao, D., Wen, J., Xiao, Q., Wu, S., Lin, X., Dou, B., You, D., Tang, Y., 2018. Simulation and analysis of the topographic effects on snow-free albedo over rugged terrain., 2018 *Remote Sens.* 10. <https://doi.org/10.3390/RS10020278>. Page 278 10, 278.
- Harper, W.V., 2014. Reduced major Axis regression: teaching alternatives to least squares. *Proc. Ninth Int. Conf. Teach. Stat.* 1-4 <https://doi.org/10.1016/B978-0-12-420228-3.00013-0>.
- Henderson-Sellers, A., Wilson, M.F., 1983. Surface albedo data for climatic modeling. *Rev. Geophys.* 21, 1743-1778. <https://doi.org/10.1029/RG021i008P01743>.
- Hu, B., Lucht, W., Li, X., Strahler, A.H., 1997. Validation of kernel-driven semiempirical models for the surface bidirectional reflectance distribution function of land surfaces. *Remote Sens. Environ.* 62, 201-214. [https://doi.org/10.1016/S0034-4257\(97\)00082-5](https://doi.org/10.1016/S0034-4257(97)00082-5).
- Huemmerich, K.F., 2013. Simulations of seasonal and latitudinal variations in leaf inclination angle distribution: implications for remote sensing. *Adv. Remote Sens.* 2, 93-101. <https://doi.org/10.4236/ARS.2013.2.2013>.
- Jacquemoud, S., Baret, F., 1990. PROSPECT: a model of leaf optical properties spectra. *Remote Sens. Environ.* 34, 75-91. [https://doi.org/10.1016/0034-4257\(90\)90100-2](https://doi.org/10.1016/0034-4257(90)90100-2).
- JCGM-GUM, 2008. Joint Committee for Guides in Metrology (JCGM) - Guides to the expression of Uncertainty in Measurement (GUM). [ISO/IEC Guide 98 - Part 3, 2008]. [WWW Document]. URL (accessed 11.10.22). <https://www.iso.org/sites/JCGM/GUM-introduction.htm>.
- Jin, Y., Schaaf, C.B., Woodcock, C.E., Gao, F., Li, X., Strahler, A.H., Lucht, W., Liang, S., 2003. Consistency of MODIS surface bidirectional reflectance distribution function and albedo retrievals: 1. Validation. *J. Geophys. Res. D Atmos.* 108, 1-15. <https://doi.org/10.1029/2002JD002804>.
- Jolivet, D., 2021. "CGLOPS-1" Framework Service Contract N° 199494 (JRC). Quality Assessment Report of Atmospheric Correction for Sentinel-3 OLCI and SLSTR products [WWW Document]. URL (accessed 11.28.22). https://land.copernicus.eu/global/sites/cgls.vito.be/files/products/CGLOPS1_QAR_S3-AC_V1_20.pdf.
- Justice, C., Belward, A., Morisette, J., Lewis, P., Privette, J., Baret, F., 2000. Developments in the validation of satellite sensor products for the study of the land surface. *Int. J. Remote Sens.* 21, 3383-3390.
- Kokaly, R.F., Clark, R.N., Swayze, G.A., Livo, K.E., Hoefen, T.M., Pearson, N.C., Wise, R.A., Benzel, W.M., Lowery, H.A., Driscoll, R.L., Klein, A.J., 2017. USGS spectral library version 7 Data Series. <https://doi.org/10.3133/DS1035>.
- Lacherade, S., Fagnie, B., Henry, P., Gamet, P., 2013. Cross calibration over desert sites: description, methodology, and operational implementation. *IEEE Trans. Geosci. Remote Sens.* 51, 1098-1113. <https://doi.org/10.1109/TGRS.2012.2227061>.
- le Maire, G., François, C., Soudani, K., Berville, D., Pontailier, J.Y., Bréda, N., Genet, H., Davi, H., Dufrene, E., 2008. Calibration and validation of hyperspectral indices for the estimation of broadleaved forest leaf chlorophyll content, leaf mass per area, leaf area index and leaf canopy biomass. *Remote Sens. Environ.* 112, 3846-3864. <https://doi.org/10.1016/j.rse.2008.06.005>.
- Lellouch, G., Carrer, D., Vincent, C., Paré, M.C., Frietas, S., Trigo, I.F., 2020. Evaluation of two global land surface albedo datasets distributed by the copernicus climate change service and the EUMETSAT LSA-SAF. *Remote Sens.* 12, 1888. <https://doi.org/10.3390/rs12111888>.
- Leon-Tavares, J., 2020. Copernicus Global Land Operations "Vegetation and Energy". "CGLOPS-1" Framework Service Contract N° 199494 (JRC) Algorithm Theoretical Basis Document BRDF Model retrieval from Sentinel-3 Collection 300 m Version 1. Issue 11.00 [WWW Document]. URL (accessed 5.24.22). https://land.copernicus.eu/global/sites/cgls.vito.be/files/products/CGLOPS1_ATBD_BRDFCorrection300m-V1_11.10.pdf.
- Leroy, M., Deuzé, J.L., Bréon, F.M., Hautecoeur, O., Herman, M., Buriez, J.C., Tanré, D., Bouffies, S., Chazette, P., Roujean, J.L., 1997. Retrieval of atmospheric properties and surface bidirectional reflectances over land from POLDER/ADEOS. *J. Geophys. Res. Atmos.* 102, 17023-17037. <https://doi.org/10.1029/96JD02662>.
- Lewis, P., Barnsley, M., 1994. In: Influence of the sky radiance distribution on various formulations of the earth surface albedo. *Proc. Conf. Phys. Meas. Signatures Remote Sens.*, pp. 707-715.
- Liang, S., 2003. A direct algorithm for estimating land surface broadband albedos from MODIS imagery. *IEEE Trans. Geosci. Remote Sens.* 41, 136-145. <https://doi.org/10.1109/TGRS.2002.807751>.
- Liang, S., 2001. Narrowband to broadband conversions of land surface albedo I algorithms. *Remote Sens. Environ.* 76, 213-238. [https://doi.org/10.1016/S0034-4257\(00\)0205-4](https://doi.org/10.1016/S0034-4257(00)0205-4).
- Liang, S., Shuey, C.J., Russ, A.L., Fang, H., Chen, M., Walthall, C.L., Daughtry, C.S.T., Hunt, R., 2003. Narrowband to broadband conversions of land surface albedo: II. Validation. *Remote Sens. Environ.* 84, 25-41. [https://doi.org/10.1016/S0034-4257\(02\)00068-8](https://doi.org/10.1016/S0034-4257(02)00068-8).
- Los, S.O., North, P.R.J., Grey, W.M.F., Barnsley, M.J., 2005. A method to convert AVHRR normalized difference vegetation index time series to a standard viewing and illumination geometry. *Remote Sens. Environ.* 99, 400-411. <https://doi.org/10.1016/j.rse.2005.08.017>.
- Lucht, W., Lewis, P., 2000. Theoretical noise sensitivity of BRDF and albedo retrieval from the EOS-MODIS and MISR sensors with respect to angular sampling. *Int. J. Remote Sens.* 21, 81-98. <https://doi.org/10.1080/014311600211000>.
- Lucht, W., Schaaf, C.B., Strahler, A.H., 2000. An algorithm for the retrieval of albedo from space using semiempirical BRDF models. *IEEE Trans. Geosci. Remote Sens.* 38, 977-998. <https://doi.org/10.1109/36.841980>.
- Mayr, S., Kuenzer, C., Gessner, U., Klein, I., Rutzinger, M., 2019. Validation of earth observation time-series: a review for large-area and temporally dense land surface products. *Remote Sens.* 11, 2616. <https://doi.org/10.3390/rs11222616>.
- Mecklenburg, S., Dransfeld, S., Gascon, F., Nieve, J., Donlon, C., Drusch, M., Schüttemeyer, D., Berruti, B., 2018. In: ESA's sentinel-3 mission - Status and performance. *Int. Geosci. Remote Sens. Symp.* 2018-July, pp. 3917-3919. <https://doi.org/10.1109/IGARSS.2018.8518877>.
- Meerdink, S.K., Hook, S.J., Roberts, D.A., Abbott, E.A., 2019. The ECOSTRESS spectral library version 1.0. *Remote Sens. Environ.* 230, 111196 <https://doi.org/10.1016/j.rse.2019.05.015>.
- Müller, J.-P., Lewis, Philip, Fischer, Jurgen, North, P., Frammer, U., López, G., Kennedy, T., Lewis, Philip, Fischer, Jürgen, Guanter, L., Preusker, R., Heckel, A., Krämer, U., Danne, O., Brockmann, C., Lewis, P., 2011. The ESA GlobAlbedo Project for mapping the Earth's land surface albedo for 15 years from European sensors, Geophysical Research Abstracts.
- Nicodemus, F., Richmond, J., Hsia, J., Ginsberg, I., Limperis, T., 1977. Geometrical considerations and nomenclature for reflectance. National Bureau of Standards, U.S. Department 333 of Commerce, Washington, DC. Technical Report October.
- Nightingale, J., Mitzag, J.P.D., Douglas, S., Dee, D., Ryder, J., Taylor, M., Old, C., Dieval, C., Fouron, C., Duveau, G., Merchant, C., 2019. Ten priority science gaps in assessing climate data record quality. *Remote Sens.* 11, 986. <https://doi.org/10.3390/rs11080986>.
- Nightingale, T., 2017. Sentinel-3 SLSTR PFM FPA Spectral Calibration Report [WWW Document]. URL (accessed 5.2.22). <https://sentinel.esa.int/documents/247904/3347387/Sentinel-3-SLSTR-Spectral-Calibration-Report>.
- Nightingale, T., 2015. Sentinel-3 SLSTR B FPA Spectral Calibration Report [WWW Document]. URL (accessed 5.2.22). <https://sentinel.esa.int/documents/247904/322305/SLSTR+Spectral+Calibration+Function>.
- Ollinger, S.V., Richardson, A.D., Martin, M.E., Hollinger, D.Y., Frolking, S.E., Reich, P.B., Plourde, L.C., Katul, G.G., Munger, J.W., Oren, R., Smith, M.L., Paw, U.K.T., Bolta, P.V., Cook, B.D., Day, M.C., Martin, T.A., Monson, R.K., Schmid, H.P., 2008. Canopy nitrogen, carbon assimilation, and albedo in temperate and boreal forests: Functional relations and potential climate feedbacks. *Proc. Natl. Acad. Sci. U. S. A.* 105, 19336-19341. https://doi.org/10.1073/PNAS.0810021105/SUPPL_FILE/0810021105SI.PDF.
- Pdgs, 2016. GSC Sentinel-3 PDGS products definition - sentinel online [WWW Document] accessed 5.2.22. https://sentinel.esa.int/documents/247904/351187/GSC_Sentinel-3_Products_Definition.
- Pinty, B., Laverne, T., Dickinson, R.E., Widlowski, J.-L., Gobron, N., Verstraete, M.M., 2006. Simplifying the interaction of land surfaces with radiation for relating remote sensing products to climate models. *J. Geophys. Res.* 111, D02116. <https://doi.org/10.1029/2005JD005952>.
- Pinty, B., Roveda, F., Verstraete, M.M., Gobron, N., Govaerts, Y., Martonchik, J.V., Diner, D.J., Kahn, R.A., 2000a. Surface albedo retrieval from meteosat 1 Theory. *J. Geophys. Res. Atmos.* 105, 18099-18112. <https://doi.org/10.1029/2000JD900113>.
- Pinty, B., Roveda, F., Verstraete, M.M., Gobron, N., Govaerts, Y., Martonchik, J.V., Diner, D.J., Kahn, R.A., 2000b. Surface albedo retrieval from meteosat 2. Applications. *J. Geophys. Res. Atmos.* 105, 18113-18134. <https://doi.org/10.1029/2000JD900114>.
- Pirazzini, R., 2004. Surface albedo measurements over Antarctic sites in summer. *J. Geophys. Res.* 109, D20118. <https://doi.org/10.1029/2004JD004617>.
- Pirazzini, R., Vihma, T., Granskog, M.A., Cheng, B., 2006. Surface albedo measurements over sea ice in the Baltic Sea during the spring snowmelt period. *Ann. Glaciol.* 44, 7-14. <https://doi.org/10.3189/172756406781811565>.
- Pokrovsky, I., Pokrovsky, O., Roujean, J.L., 2003. Development of an operational procedure to estimate surface albedo from the SEVIRI/MSG observing system by using POLDER BRDF measurements II. Comparison of several inversion techniques and uncertainty in albedo estimates. *Remote Sens. Environ.* 87, 215-242. [https://doi.org/10.1016/S0034-4257\(03\)00166-4](https://doi.org/10.1016/S0034-4257(03)00166-4).
- Quaife, T., Lewis, P., 2010. Temporal constraints on linear BRDF model parameters. *IEEE Trans. Geosci. Remote Sens.* 48, 2445-2450. <https://doi.org/10.1109/TGRS.2009.2038901>.
- Rahman, H., Dedieu, G., 1994. SMAC: a simplified method for the atmospheric correction of satellite measurements in the solar spectrum. *Int. J. Remote Sens.* 15, 123-143. <https://doi.org/10.1080/01431169408954055>.
- Ramon, D., Jolivet, D., Compiègne, M., 2021. "CGLOPS-1" Framework Service Contract N° 199494 (JRC). Algorithm Theoretical Basis Document Atmospheric Correction for Sentinel-3 OLCI and SLSTR products. Version 1.0 Issue 11.20 [WWW Document]. URL (accessed 5.2.22). https://land.copernicus.eu/global/sites/cgls.vito.be/files/products/CGLOPS1_ATBD_S3-AC-V1_11.20.pdf.
- Roman, M.O., Schaaf, C.B., Lewis, P., Gao, F., Anderson, G.P., Privette, J.L., Strahler, A.H., Woodcock, C.E., Barnsley, M., 2010. Assessing the coupling between surface albedo derived from MODIS and the fraction of diffuse skylight over spatially-characterized landscapes. *Remote Sens. Environ.* 114, 738-760. <https://doi.org/10.1016/j.rse.2009.11.014>.
- Roman, M.O., Schaaf, C.B., Woodcock, C.E., Strahler, A.H., Yang, X., Branswell, R.H., Curtis, P.S., Davis, K.J., Dragoni, D., Goulden, M.L., Gu, L., Hollinger, D.Y., Kolb, T.E., Meyers, T.P., Munger, J.W., Privette, J.L., Richardson, A.D., Wilson, T.B., Wofsy, S.C., 2009. The MODIS (Collection V005) BRDF/albedo product assessment of spatial representativeness over forested landscapes. *Remote Sens. Environ.* 113, 2476-2498. <https://doi.org/10.1016/j.rse.2009.07.009>.
- Roujean, J.-L., Leroy, M., Deschamps, P.-Y., 1992. A bidirectional reflectance model of the Earth's surface for the correction of remote sensing data. *J. Geophys. Res.* 97, 20455. <https://doi.org/10.1029/92JD01411>.

J. Sánchez-Zapero et al.

Remote Sensing of Environment 287 (2023) 113460

- Roujean, J.L., 2017. Inversion of lumped parameters using BRDF kernels. In: *Comprehensive Remote Sensing*. Elsevier, pp. 23–34. <https://doi.org/10.1016/B978-0-12-409548-9.10346-X>.
- Roujean, J.L., Leon-Tavares, J., Smets, B., Claes, P., Camacho De Coca, F., Sanchez-Zapero, J., 2018. Surface albedo and toc-r 300 m products from PROBA-V instrument in the framework of copernicus global land service. *Remote Sens. Environ.* 215, 57–73. <https://doi.org/10.1016/j.rse.2018.05.015>.
- Roy, D.P., Zhang, H.K., Ju, J., Gomez-Dans, J.L., Lewis, P.E., Schaaf, C.B., Sun, Q., Li, J., Huang, H., Kovalsky, V., 2016. A general method to normalize Landsat reflectance data to nadir BRDF adjusted reflectance. *Remote Sens. Environ.* 176, 255–271. <https://doi.org/10.1016/j.rse.2016.01.023>.
- S3_MPC, 2021. Sentinel-3 SLSTR Product Data Format Specification - Level 1 products - Sentinel Online [WWW Document]. URL (accessed 5.2.22). https://sentinels.copernicus.eu/web/sentinel/user-guides/sentinel-3-slstr/document-library/-/asset_publisher/fgRuiak1n39/content/id/3402065.
- S3_MPC, 2021. Sentinel-3 Optical Annual Performance Report - 2020 - Sentinel Online [WWW Document]. URL (accessed 5.2.22). https://sentinels.copernicus.eu/web/sentinel/user-guides/sentinel-3-olci/document-library/-/asset_publisher/hkf7sg9Ny1d5/content/sentinel-3-optical-annual-performance-report-2020.
- S3_MPC, 2019. Sentinel-3 OLCI Product Data Format Specification - Level 1 products - Sentinel Online [WWW Document]. URL (accessed 5.2.22). https://sentinels.copernicus.eu/web/sentinel/user-guides/sentinel-3-olci/document-library/-/asset_publisher/hkf7sg9Ny1d5/content/id/34020157_com_lifery_asset_publisher_web_portlet_AsetPublisherPortlet_INSTANCE_hkf7sg9Ny1d5_redirect=https%3A%2F%2Fsentinel.
- S3 CalVal Team, 2016a. Technical note: Sentinel-3 OLCI-A spectral response functions [WWW Document] accessed 5.2.22. <https://sentinels.copernicus.eu/documents/247904/2700436/Sentinel-3-OLCI-A-spectral-response-functions>.
- S3 CalVal Team, 2016b. Technical note: Sentinel-3 OLCI-B spectral response functions from pre-flight characterisation [WWW Document] accessed 5.2.22. <https://sentinels.copernicus.eu/documents/247904/2700436/Sentinel-3-OLCI-B-spectral-response-functions>.
- Samain, O., Geiger, B., Roujean, J.L., 2006. Spectral normalization and fusion of optical sensors for the retrieval of BRDF and albedo: application to VEGETATION, MODIS, and MERIS data sets. *IEEE Trans. Geosci. Remote Sens.* 44, 3166–3178. <https://doi.org/10.1109/TGRS.2006.879545>.
- Sánchez-Zapero, J., Camacho, F., 2019. Product Quality Assessment Report (PQAR) of CDR and ICDR Surface Albedo v1.0 based on PROBA-V (Official reference number service contract: 2018/C3S_312b_Lot5_VITO/SCI). [WWW Document]. URL (accessed 4.9.22). <https://cds.climate.copernicus.eu/cdsapp#/dataset/satellite-albedo?tab=doc>.
- Sánchez-Zapero, J., Camacho, F., Leon-Tavares, J., Martínez-Sánchez, E., Gorroño, J., Benhadj, I., Tote, C., Swinnen, E., Muñoz-Sabater, J., 2021. Prototype for surface albedo retrieval based on Sentinel-3 OLCI and SLSTR data in the framework of copernicus climate change. 2021 IEEE Int. Geosci. Remote Sens. Symp. IGARSS 2377–2380. <https://doi.org/10.1109/IGARSS47720.2021.9555099>.
- Sánchez-Zapero, J., Camacho, F., Martínez-Sánchez, E., Lacaize, R., Carrer, D., Pinault, F., Benhadj, I., Muñoz-Sabater, J., 2020. Quality Assessment of PROBA-V Surface Albedo V1 for the Continuity of the Copernicus Climate Change Service. *Remote Sens.* 2020, Vol. 12, Page 2596 12, 2596. <https://doi.org/10.3390/rs12162596>.
- Sánchez-Zapero, J., Gorroño, J., Martínez-Sánchez, E., Camacho, F., Leon-Tavares, J., Benhadj, I., Tote, C., 2021. Algorithm Theoretical Basis Document CDR/ICDR Sentinel-3 Surface Albedo v3.0. Official reference number service contract: 2020/COP_059_VITO.Albedo. [WWW Document]. URL (accessed 5.2.22). https://datastore.copernicus-climate.eu/documents/satellite-albedo/C3S_COP_059_D-02_ATBD_CDR-ICDR_SA_SENTINEL3_v3.0_PRODUCTS_v1.1.pdf.
- Sánchez-Zapero, J., Martínez-Sánchez, E., Camacho, F., 2021. Copernicus Global Land Operations “Vegetation and Energy”. “CGLOPS-1” Framework Service Contract N° 199494 (JRC) Quality Assessment Report Sentinel-3 Top Of Canopy (TOC) reflectance Collection 300m Version 1 Issue 1.00 [WWW Document]. URL (accessed 5.2.22). https://land.copernicus.eu/global/sites/cgls.vito.be/files/products/CGLOPS1_QAR_S3-TOC_300m-v1.1.00.pdf.
- Schaaf, C., Wang, Z., 2015. MCD43A3 MODIS/Terra+Aqua BRDF/Albedo Daily L3 Global - 500m V006 [Data set]. NASA EOSDIS Land Processes DAAC. [WWW Document]. USGS. <https://doi.org/10.5067/MODIS>.
- Schaaf, C.B., Gao, F., Strahler, A.H., Lucht, W., Li, X., Tsang, T., Strugnell, N.C., Zhang, X., Jin, Y., Muller, J.P., Lewis, P., Barnsley, M., Hobson, P., Disney, M., Roberts, G., Dunderdale, M., Doll, C., D’Entremont, R.P., Hu, B., Liang, S., Privette, J.L., Roy, D., 2002. First operational BRDF, albedo nadir reflectance products from MODIS. *Remote Sens. Environ.* 83, 135–148. [https://doi.org/10.1016/S0034-4257\(02\)00091-3](https://doi.org/10.1016/S0034-4257(02)00091-3).
- Schaaf, C.B., Li, X., Strahler, A.H., 1994. Topographic effects on bidirectional and hemispherical reflectances calculated with a geometric-optical canopy model. *IEEE Trans. Geosci. Remote Sens.* 32, 1186–1193. <https://doi.org/10.1109/36.338367>.
- Schaepman-Strub, G., Schaepman, M.E., Painter, T.H., Dangel, S., Martonchik, J.V., 2006. Reflectance quantities in optical remote sensing—definitions and case studies. *Remote Sens. Environ.* 103, 27–42. <https://doi.org/10.1016/j.rse.2006.03.002>.
- Sellers, P.J., Meeson, B.W., Hall, F.G., Asrar, G., Murphy, R.E., Schiffer, R.A., Bretherton, F.P., Dickinson, R.E., Ellingson, R.G., Field, C.B., Huemrich, K.F., Justice, C.O., Melack, J.M., Roulet, N.T., Schimel, D.S., Try, P.D., 1995. Remote sensing of the land surface for studies of global change: models — algorithms — experiments. *Remote Sens. Environ.* 51, 3–26. [https://doi.org/10.1016/0034-4257\(94\)00061-Q](https://doi.org/10.1016/0034-4257(94)00061-Q).
- Shuai, Y., Tuerhanjiang, L., Shao, C., Gao, F., Zhou, Y., Xie, D., Liu, T., Liang, J., Chu, N., 2020. In: Re-understanding of land surface albedo and related terms in satellite-based retrievals, 4, pp. 45–67. <https://doi.org/10.1080/20964471.2020.1716561>.
- Stephens, G.L., O’Brien, D., Webster, P.J., Pilewski, P., Kato, S., Li, J.L., 2015. The albedo of Earth. *Rev. Geophys.* 53, 141–163. <https://doi.org/10.1002/2014RG000449>.
- Strahler, A.H., Muller, J.-P., Members, M.S.T., 1999. MODIS BRDF/Albedo product: algorithm theoretical basis document version 5.0.
- Toté, C., 2020. Copernicus Global Land Operations “Vegetation and Energy”. “CGLOPS-1” Evaluation Report of OLCI and SLSTR cloud, cloud shadow and snow detection. Issue 11.00 [WWW Document]. URL (accessed 5.2.22). https://land.copernicus.eu/global/sites/cgls.vito.be/files/products/CGLOPS1_QAR_S3-CloudMask_11.00.pdf.
- Van Leeuwen, W.J.D., Roujean, J.L., 2002. Land surface albedo from the synergistic use of polar (EPS) and geo-stationary (MSG) observing systems: an assessment of physical uncertainties. *Remote Sens. Environ.* 81, 273–289. [https://doi.org/10.1016/S0034-4257\(02\)00005-6](https://doi.org/10.1016/S0034-4257(02)00005-6).
- Verhoef, W., 1984. Light scattering by leaf layers with application to canopy reflectance modeling: the SAIL model. *Remote Sens. Environ.* 16, 125–141. [https://doi.org/10.1016/0034-4257\(84\)90057-9](https://doi.org/10.1016/0034-4257(84)90057-9).
- Vermote, E., Justice, C.O., Bréon, F.M., 2009. Towards a generalized approach for correction of the BRDF effect in MODIS directional reflectances. *IEEE Trans. Geosci. Remote Sens.* 47, 898–908. <https://doi.org/10.1109/TGRS.2008.2005977>.
- Vermote, E.F., Tanré, D., Deuzé, J.L., Herman, M., Morcrette, J.J., 1997. Second simulation of the satellite signal in the solar spectrum, 6s: an overview. *IEEE Trans. Geosci. Remote Sens.* 35, 675–686. <https://doi.org/10.1109/36.581987>.
- Wang, Z., Schaaf, C., Lattanzio, A., Carrer, D., Grant, I., Roman, M., Camacho, F., Yang, Y., Sánchez-Zapero, J., 2019. Global surface albedo product validation best practices protocol. Version 1.0. In: Wang, Z., Nickeson, J., Román, M. (Eds.), *Good Practices for Satellite-Derived Land Product Validation* (p. 45): Land Product Validation Subgroup (WGCV/CEOS). [WWW Document]. <https://doi.org/10.5067/DOC/CEOSWGCV/LPV/ALBEDO.001>.
- Wang, Z., Schaaf, C.B., Chopping, M.J., Strahler, A.H., Wang, J., Román, M.O., Rocha, A.V., Woodcock, C.E., Shuai, Y., 2012. Evaluation of moderate-resolution imaging spectroradiometer (MODIS) snow albedo product (MCD43A). *Remote Sens. Environ.* 117, 264–280. <https://doi.org/10.1016/j.rse.2011.10.002>.
- Wang, Z., Schaaf, C.B., Strahler, A.H., Chopping, M.J., Román, M.O., Shuai, Y., Woodcock, C.E., Hollinger, D.Y., Fitzjarrald, D.R., 2014. Evaluation of MODIS albedo product (MCD43A) over grassland, agriculture and forest surface types during dormant and snow-covered periods. *Remote Sens. Environ.* 140, 60–77. <https://doi.org/10.1016/j.rse.2013.08.025>.
- Wang, Z., Schaaf, C.B., Sun, Q., Shuai, Y., Román, M.O., 2018. Capturing rapid land surface dynamics with collection V006 MODIS BRDF/NBAR/Albedo (MCD43) products. *Remote Sens. Environ.* 207, 50–64. <https://doi.org/10.1016/j.rse.2018.02.001>.
- Wanner, W., Li, X., Strahler, A.H., 1995. On the derivation of kernels for kernel-driven models of bidirectional reflectance. *J. Geophys. Res.* 100, 21077–21089. <https://doi.org/10.1029/95jd02371>.

